

Quantitative Characterization of Dynamic Sitting Control during
Continuous Multi-Directional Perturbations

by

Fatemeh Gholibeigian

A thesis submitted in partial fulfillment of the requirements for the degree of Master of Science

Department of Mechanical Engineering
University of Alberta

© Fatemeh Gholibeigian, 2017

Abstract

Facilitating trunk stability is one of the most important objectives in human balance control. This is especially evident in individuals with spinal cord injury (SCI) who are typically not able to control seated balance on their own. As a consequence of their injury, they often suffer under a reduction of strength and control of their trunk muscles and, hence, under reduced independence during daily activities. One of the top priorities for individuals with SCI is therefore to improve their trunk control and, consequently, quality of life. To enhance existing therapies and/or develop bio-inspired assistive technologies that can facilitate dynamic trunk stability in these individuals, a more comprehensive, quantitative understanding of the neuromechanical mechanisms of dynamic sitting control in non-disabled individuals is needed. The objective of this study was therefore twofold: (1) to quantify the effect of varying levels of seat instability as well as of visual information elimination on postural efficiency during continuous, multi-directional perturbations using a wobble board paradigm; and (2) to quantify the temporal and spatial relationship between muscle activity and wobble board motion during the perturbations. 15 non-disabled individuals were asked to sit on a wobble board inducing continuous, multi-directional perturbations and maintain an upright sitting posture as closely as possible. Five different hemispheres with decreasing diameter were attached to the bottom of the wobble board to induce five different levels of seat instability. Sitting tasks were performed with eyes open and eyes closed. A motion capture system was used to collect trunk and pelvis kinematics as well as those of the wobble board. The activity of fourteen major superficial trunk and upper leg muscles was recorded via an electromyography system. Wobble board kinematics and muscle electromyography were then used to characterize trunk control and stability during dynamic sitting. In a first step,

posturographic analyses in time and frequency domain were performed to assess postural proficiency. In a second step, cross-correlation analysis was applied to identify temporal and spatial determinants of muscle activation and, hence, reactive trunk control for the wobble board task. For the posturographic analyses, our findings revealed that time-domain measures were generally increased and frequency-domain measures generally decreased when task difficulty was increased. Similarly, time-domain measures were generally increased and frequency-domain measures generally decreased when visual information was eliminated. For the cross-correlation analysis, our findings indicate the existence of a relation between phasic muscle activation/deactivation and wobble board motion, which increased in intensity with higher levels of seat instability, irrespective of eye condition. Spatial features revealed that the rectus abdominis, erector spinae, biceps femoris, and rectus femoris muscles were correlated with anterior-posterior wobble board displacement, whereas the external oblique muscles were correlated with medial-lateral wobble board displacement. Moreover, temporal features revealed that, regardless of base, eye condition, and wobble board displacement direction, muscle activation/deactivation preceded the wobble board displacement. On the one hand, the posturographic findings suggest that, by increasing seat instability or eliminating vision, the control effort increases and the degree of stability decreases. On the other hand, the cross-correlation results indicate that the dynamic balancing task is accomplished with significant contributions from active control mechanisms that originate from the central nervous system (CNS). More specifically, the spatial characterization suggests that the CNS modulates the phasic muscle activity levels to break the upcoming wobble board motion. For sagittal plane motion, this is done by increasing the effective stiffness between the human body and the wobble board. For frontal plane motion, further work is needed to confirm or dispute the use of such CNS-based stiffness control strategy. The temporal characterization

suggests that the CNS takes advantage of the velocity information of the body and/or wobble board to generate the required motor command in advance of an imminent displacement. These interpretations demonstrate that the performed work has made significant contributions to our fundamental understanding of human balance control in general and of wobble board stabilization more specifically. The gained knowledge may be beneficial for enhancing existing therapies and quantitative assessments, but also for developing bio-inspired assistive technologies that can facilitate trunk stability in individuals with SCI.

Preface

This thesis is an original work by Fatemeh Gholibeigian. The research project, of which this thesis is a part, received research ethics approval from the Health Research Ethics Board of the University of Alberta, Project Name “Use of Stochastic Resonance for Improving Postural Control in the Elderly and Individuals Post-Stroke”, No. Pro00039437, June 24, 2013.

Dedicated to Amir, my love.

Acknowledgments

I would like to express my sincere gratitude to my supervisor, Dr. Albert Vette. For his encouragement, patience, motivation, and immense knowledge. His guidance helped me tremendously in all the time of research and writing this thesis.

I would like to thank my lab colleagues for their contribution. I would like to especially thank Andy Williams for assisting me during the experiments, for being my pilot participant numerous times, and for his assistance with motion data analysis. Many thanks also go to Alireza Noamani for always being there for me when I needed him and for offering his help whenever I needed assistance. I would also like to thank Justin Lewicke for lending his expertise and answering many questions that I had about the motion capture system. My thanks also go to Dhruv Prakash for his assistance with data analysis. I am extremely grateful to Joel Winterhalt, Quinton Rebke, and Chris Wayne for helping me in designing the experiment and for being my pilot participants countless times. I could always count on Milad Nazarahari, Hooman Bahari, and Niloufar Ahmadian to help me whenever I needed assistance.

I would like to thank all my family and friends who have been extremely supportive throughout the process. And finally, I would like to thank my love, and husband, Amir Sajedian, for his love, patience, and endurance. None of this could have been possible without your support.

This project was made possible through the generous support from the Faculty of Engineering, University of Alberta; the Faculty of Graduate Studies and Research, University of Alberta; the Glenrose Rehabilitation Hospital Foundation, Alberta Health Services; and the Natural Sciences and Engineering Research Council of Canada.

Table of Contents

Acknowledgments.....	vii
Table of Contents.....	viii
List of Tables	xiii
List of Figures.....	xvi
Nomenclature.....	xxvi
1 Introduction.....	1
1.1 Trunk Stability in Individuals with Spinal Cord Injury.....	1
1.2 Approaches for Enhancing Trunk Stability	2
1.3 Thesis Objectives.....	3
1.4 Organization of the Thesis.....	4
2 Literature Review.....	5
2.1 Trunk Stability and Instability	5
2.1.1 Introduction.....	5
2.1.2 Muscles Involved in Trunk Stabilization.....	6
2.1.3 Trunk Stability in Non-Disabled Individuals.....	7
2.1.4 Trunk Instability in Individuals with Spinal Cord Injury	7
2.2 Electromyography.....	9
2.2.1 Introduction.....	9

2.2.2	EMG Signal Processing	10
2.2.3	Issues with Surface EMG Recordings	13
2.3	Human Motion Capture	13
2.3.1	Introduction.....	13
2.3.2	Stereophotogrammetric Systems	14
2.3.3	Kinematic Data Acquisition and Processing.....	15
2.3.4	Limitations of Stereophotogrammetric Systems.....	20
2.4	Wobble Board Studies	21
3	Preliminary Studies	24
3.1	Technical Validation of Time Synchronization of Recording Systems.....	24
3.1.1	Background and Rationale.....	24
3.1.2	Objective.....	24
3.1.3	Experimental Setup.....	24
3.1.4	Participants and Experimental Procedure	25
3.1.5	Experimental Data Processing and Analysis	27
3.1.6	Results and Discussion	28
3.1.7	Conclusion and Limitations	30
3.2	Evaluation of MVC Exercises and MVC Value Identification Methods	31
3.2.1	Background and Rationale.....	31
3.2.2	Objective.....	32

3.2.3	Experimental Setup.....	32
3.2.4	Participants and Experimental Procedure.....	32
3.2.5	Data Processing and Analysis.....	34
3.2.6	Results and Discussion.....	35
3.2.7	Conclusion.....	40
4	Materials and Methods.....	41
4.1	Overview.....	41
4.2	Participants.....	41
4.3	Experimental Setup.....	41
4.4	Experimental Procedure.....	45
4.4.1	EMG Setup and Recordings.....	45
4.4.2	Wobble Board Practice Trials.....	49
4.4.3	MoCap Setup and Recordings.....	49
4.4.4	Experimental Tasks.....	51
4.5	Experimental Data Processing.....	52
4.5.1	Processing of EMG Data.....	52
4.5.2	Processing of MoCap Data.....	53
4.6	Data Analysis.....	60
4.6.1	Posturographic Measures.....	61
4.6.2	Cross-Correlation.....	64

5	Results.....	67
5.1	Participants.....	67
5.2	Wobble Board Base Selection	68
5.3	MVC Results.....	69
5.4	Main Experiment Results.....	75
5.4.1	Normalized EMG.....	75
5.4.2	Posturographic Measures	79
5.4.3	Cross-Correlation.....	87
6	Discussion	105
6.1	Adequacy of Using Wobble Board Kinematics to Quantify Postural Control During Unstable Sitting.....	105
6.2	Postural Control Effort and Output are Affected by Seat Instability Level.....	106
6.3	Visual Input Improves Stability During Unstable Seated Balance.....	107
6.4	How Does the Human Body Control Upright Sitting While Balancing on a Wobble Board?.....	109
6.4.1	Correlation Between Muscle Activation/Deactivation and Wobble Board Motion Confirms the Presence of Active Control	109
6.4.2	Spatial Configuration of Trunk and Upper Leg Muscles is a Key Influencer of Active Control.....	110
6.4.3	Temporal and Spatial Determinants of Trunk and Upper Leg Muscle Activation/Deactivation Provide Insights into the Underlying Type of Active Control	111
6.5	Limitations of This Thesis Research.....	114

7	Conclusions.....	115
7.1	Recommendations for Future Work.....	117
8	References.....	119
9	Appendices.....	142
9.1	Appendix A – Figures for Validation of Time Synchronization Procedure.....	142
9.2	Appendix B – MVC Values Obtained via Four Different Calculation Methods.....	150
9.3	Appendix C – Health Screening Form.....	153
9.4	Appendix D – Consent Form.....	155
9.5	Appendix E – Wobble Board and Bases Drawings.....	160
9.6	Appendix F – Group-Ensemble Average Levels of Muscle Activity for Each Participant	162
9.7	Appendix G – Group-Ensemble Posturographic Measures for Each Participant.....	177
9.8	Appendix H – Number of Participants for Calculating the Group-Ensemble CC Functions.....	192

List of Tables

Table 1. The sampling frequencies of the MoCap, EMG, and push button signals.	27
Table 2. The MVC values of the two exercises for the right rectus abdominis. All values are presented as mean \pm SD across three trials. All values are in mV.....	37
Table 3. The MVC values of the two exercises for the right external oblique. All values are presented as mean \pm SD across three trials. All values are in mV.....	37
Table 4. The MVC values of the two exercises for the right latissimus dorsi. All values are presented as mean \pm SD across three trials. All values are in mV.....	38
Table 5. The MVC values for all muscles and the two chosen MVC exercises, calculated via 4 MVC value identification methods. All values are in mV and presented as mean \pm SD. In light of the participant-specific EMG normalization procedure, the standard deviations are presented as the means of the within-participant standard deviations, assessing the group-ensemble MVC value variability across participant trials.	39
Table 6. The spherical radii and curved heights of the wobble board bases as well as their associated levels of difficulty (level 1: very easy to level 5: very difficult).	44
Table 7. Participant characteristics.	67
Table 8. Selection of wobble board bases for each participant and eye condition.	68
Table 9. Overall wobble board base coverage across trials and participants.....	69
Table 10. MVC values for each participant and the following muscles: right rectus abdominis, left rectus abdominis, right external oblique, and left external oblique. All values are presented as mean \pm SD across three trials and given in millivolts (mV).	72

Table 11. MVC values for each participant and the following muscles: right thoracic erector spinae, left thoracic erector spinae, right lumbar erector spinae, left lumbar erector spinae, right latissimus dorsi, and left latissimus dorsi. All values are presented as mean \pm SD across three trials and given in millivolts (mV)..... 73

Table 12. MVC values for each participant and the following muscles: right rectus femoris, left rectus femoris, right biceps femoris, and left biceps femoris. All values are presented as mean \pm SD across three trials and given in millivolts (mV)..... 74

Table 13. MVC values across participants for each muscle being studied. All values are in mV. 74

Table 14. Average values of the normalized EMG activity across participants for all muscles and conditions. Values are presented as mean \pm SD across participants. All values are given as a percentage of MVC (%). 78

Table 15. Analysis of the AP, ML, TM, and TD fluctuations. Posturographic measures were calculated for Base #1 and #2 under EC condition. Shown are the mean \pm SD across participants for MA, RMSA, MV, RMSV, RANGE, CFREQ, and FREQD. A Wilcoxon signed rank test was used to identify potential differences between Base #1 and Base #2 when eyes are closed. 81

Table 16. Analysis of the AP, ML, TM, and TD fluctuations. Posturographic measures were calculated for Base #3 and #4 under eyes open condition. Shown are the mean \pm SD across participants for MA, RMSA, MV, RMSV, RANGE, CFREQ, and FREQD. A Wilcoxon signed rank test was used to identify potential differences between Base #3 and Base #4 when eyes were open..... 84

Table 17. Analysis of the AP, ML, TM, and TD fluctuations. Posturographic measures were calculated for Base #2 under EO and EC conditions. Shown are the mean \pm SD across participants for MA, RMSA, MV, RMSV, RANGE, CFREQ, and FREQD. A Wilcoxon signed rank test was used to identify potential differences between EO and EC with Base #2. 86

Table 18. Correlation coefficient and time lag values for ANT and POST under Base #2/EC and Base #4/EO conditions for the following muscles: right rectus abdominis, left rectus abdominis, right thoracic erector spinae, left thoracic erector spinae, right lumbar erector spinae, left lumbar erector spinae, right biceps femoris, left biceps femoris, right rectus femoris, and left rectus femoris. All values are presented as mean \pm SD. 101

Table 19. Correlation coefficient and time lag values for LEFT and RIGHT under Base #2/EC and Base #4/EO conditions for RExO and LExO. All values are presented as mean \pm SD..... 104

List of Figures

- Figure 1. The position vectors of the markers (d_1 , d_2 , and d_3) in the global coordinate system (X_g, Y_g, Z_g) that are used to define the local coordinate system (X_l, Y_l, Z_l). 17
- Figure 2. To obtain the rotation matrix between coordinate systems {A} and {B}, a set of rotations around the fixed axes can be performed. Rotations are performed in the order of $RZ(\gamma)$, $RY\beta$, $RX(\alpha)$ 19
- Figure 3. The schematic of the push button setup (left) and a picture of the experimental setup (right). The push button is connected to both motion capture and EMG systems via two BNC cables. A Tee connector was utilized to connect the BNC cables. 25
- Figure 4. Identifying the synchronized start time in Signal #2 (A) and in Signal #4 (B). The synchronized start times (time = 0 seconds) in the MoCap and EMG signals (Signal #1 and Signal #3) are t_1 and t_2 , respectively. $\Delta *$ is equal to or greater than zero and smaller than 1 ms. 28
- Figure 5. Exemplary experimental data from the third trial of Participant #1. The top subplot (PB MoCap) shows the MoCap Push Button signal; the second subplot (PB EMG) the EMG Push Button signal; the third subplot (Biceps Brachii) the rectified EMG signal of the left biceps brachii; and the bottom subplot (Vertical Disp.) the vertical displacement of the left wrist as an average of the two wrist markers (with respect to the laboratory floor). 29
- Figure 6. Exemplary experimental data from the first trial of Participant #4. The top subplot (PB MoCap) shows the MoCap Push Button signal; the second subplot (PB EMG) the EMG Push Button signal; the third subplot (Biceps Brachii) the rectified EMG signal of the left biceps brachii; and the bottom subplot (Vertical Disp.) the vertical displacement of the left wrist as an average of the two wrist markers (with respect to the laboratory floor). 29
- Figure 7. Exemplary push button signals for the MoCap and EMG systems after time synchronization, when focusing on the first rise in both systems (zoomed-in version of Figure 6).

Since the sampling frequencies of the MoCap and EMG systems were different, a between-system time shift and, hence, synchronization error of up to 1 ms could be observed (this trial: 0 ms).. 30

Figure 8. Exemplary rectified muscle activity for right rectus abdominis. Shown is the second MVC trial for Participant #1..... 35

Figure 9. Exemplary rectified muscle activity for right external oblique. Shown is the third MVC trial for Participant #1..... 36

Figure 10. Exemplary rectified muscle activity for right latissimus dorsi. Shown is the third MVC trial for Participant #1..... 36

Figure 11. The utilized EMG setup. Left: Powerlab 16/35 data acquisition system, the LabChart data acquisition software, and the EMG electrodes; right: the Bagnoli-16 EMG system amplifier. 42

Figure 12. An eight-camera motion capture system was used to capture the motion of the trunk, pelvis and wobble board. The capture volume was: 6.10 m (length) × 1.83 m (width) × 1.83 m (height)..... 43

Figure 13. Models of the custom-made wobble board and stool as well as a photograph of the 5 different bases of the wobble board. Top left: the 3D model of the custom-made wobble board with a sitting surface of 0.185 m² (diameter of 48.5 cm); top right: the 3D model of the wobble board on the stool; bottom: a photograph of the five different bases of the wobble board. From left to right, Base #1 to Base #5 are shown. One of five hemispheres of different diameters could be attached to the bottom of the wobble board..... 44

Figure 14. Back (left) and front (right) views of the location of the EMG electrodes. EMG electrodes were placed bilaterally on the muscles being studied. RA: rectus abdominis; ExO: external oblique; LD: latissimus dorsi; TES: thoracic erector spinae; LES: lumbar erector spinae; RF: rectus femoris; and BF: biceps femoris. 46

Figure 15. Photographs of the MVC exercises performed for the muscles being studied: (1) RA; (2) ExO; (3) LD; (4) TES and LES; (5) RF; and (6) BF..... 48

Figure 16. Back (left) and front (right) views of the location of MoCap markers. The markers were placed on the following anatomical landmarks: the seventh cervical vertebra (C7), the eighth thoracic vertebra (T8), the deepest point of the incisura jugularis (IJ), the processus xiphoideus (PX), and bilaterally on the anterior superior iliac spine (ASIS) and posterior superior iliac spine (PSIS)..... 50

Figure 17. The location of the markers on the wobble board, with the participant facing the reader and the negative direction of the Y-axis of the laboratory coordinate system. BFR: board front right side; BBR: board back right side; BBL: board back left side; and BFL: board front left side. 51

Figure 18. The orientation of the LCS of the wobble board using three markers: (1) using the BFR, BFL, and BBL markers; (2) using the BBR, BBL, and BFR markers; (3) using the BFR, BFL, and BBR markers; and (4) using the BBR, BBL, and BFL markers..... 54

Figure 19. The orientation of the LCS for the pelvis (left) and trunk (right) segments. For the pelvis LCS (left): the origin was located at RASIS, with the x-axis pointing medially from RASIS to LASIS, the z-axis pointing superiorly when defined as a vector perpendicular to the plane spanned by the x-axis and an auxiliary vector from RASIS to RPSIS, and the y-axis pointing posteriorly when defined as the cross-product of the z- and x-axes. For the trunk LCS (right): the origin was located at PX, with the y-axis pointing posteriorly from PX to T8, the x-axis pointing left when defined as a vector perpendicular to the plane spanned by the y-axis and an auxiliary vector from PX to C7, and the z-axis pointing superiorly when defined as the cross-product of the x- and y-axes. Figures obtained from “Essential Skeleton 4” mobile application software. 56

Figure 20. The AP tilt angle (α) and ML tilt angle (β) were calculated by using the z-component of the local y- and x-unit vectors in the laboratory coordinate system, respectively..... 57

Figure 21. The wobble board tilt in AP (left) and ML (right) directions. Left: side view of the participant on the wobble board. A positive AP tilt angle represents a wobble board rotation to the front; Right: back view of the participant on the wobble board. A positive ML tilt angle represents a wobble board rotation to the left of the participant. 58

Figure 22. The wobble board’s tilt direction (TD). The left-hand side of the wobble board represents the negative angles (ranging from -179° to 0°), and the right-hand side of the wobble board represents the positive angles (ranging from 0° to 180°). 59

Figure 23. The cross-correlation analysis: first, the three largest peaks in the MoCap signal were identified. Second, a 4-second window centered at each peak was created. Third, corresponding 4-second windows were created in the down-sampled EMG signal. Then, each of these segments (i.e., the 4-second window centered at each peak in the MoCap signal and its time-matched 4-second window in the down-sampled EMG signal) was demeaned and cross-correlated. Finally, the obtained CC functions were averaged for each trial. 65

Figure 24. Exemplary abdominal muscle activity during respective MVC exercises for the first trial of Participant #5. The top subplot (RRA) shows the filtered muscle activity for the right rectus abdominis; the second subplot (LRA) the filtered muscle activity for the left rectus abdominis; the third subplot (RExO) the filtered muscle activity for the right external oblique; and the bottom subplot (LExO) the filtered muscle activity for left external oblique. 69

Figure 25. Exemplary back muscle activity during respective MVC exercises for the first trial of Participant #5. The top subplot (RTES) shows the filtered muscle activity for the right thoracic erector spinae; the second subplot (LTES) the filtered muscle activity for the left thoracic erector spinae; the third subplot (RLES) the filtered muscle activity for the right lumbar erector spinae; the fourth subplot (LLES) the filtered muscle activity for the left lumbar erector spinae; the fifth subplot (RLD) the filtered muscle activity for the right latissimus dorsi; and the bottom subplot (LLD) the filtered muscle activity for the left latissimus dorsi. 70

Figure 26. Exemplary upper leg muscle activity during respective MVC exercises for the first trial of Participant #5. The top subplot (RRF) shows the filtered muscle activity for the right rectus femoris; the second subplot (LRF) the filtered muscle activity for the left rectus femoris; the third subplot (RBF) the filtered muscle activity for the right biceps femoris; and the bottom subplot (LBF) the filtered muscle activity for the left biceps femoris. 71

Figure 27. Exemplary normalized EMG time series for the abdominal muscles and the first trial of Participant #5, using Base #5 with eyes open. The top subplot (RRA) shows the normalized EMG time series for the right rectus abdominis; the second subplot (LRA) the normalized EMG for the left rectus abdominis; the third subplot (RExO) the normalized EMG for the right external oblique; and the bottom subplot (LExO) the normalized EMG for the left external oblique..... 75

Figure 28. Exemplary normalized EMG time series for the back muscles and the first trial of Participant #5, using Base #5 with eyes open. The top subplot (RTES) shows the normalized EMG for the right thoracic erector spinae; the second subplot (LTES) the normalized EMG for the left thoracic erector spinae; the third subplot (RLES) the normalized EMG for the right lumbar erector spinae; the fourth subplot (LLES) the normalized EMG for the left lumbar erector spinae; the fifth subplot (RLD) the normalized EMG for the right latissimus dorsi; and the bottom subplot (LLD) the normalized EMG for the left latissimus dorsi. 76

Figure 29. Exemplary normalized EMG time series for the upper leg muscles and the first trial of Participant #5, using Base #5 with eyes open. The top subplot (RRF) shows the normalized EMG for the right rectus femoris; the second subplot (LRF) the normalized EMG for the left rectus femoris; the third subplot (RBF) the normalized EMG for the right biceps femoris; and the bottom subplot (LBF) the normalized EMG for the left biceps femoris..... 77

Figure 30. Examples of the wobble board kinematics in AP and ML directions. A: The AP (top) and ML (bottom) time series during sitting on the wobble board with Base #1 (left) and Base #2 (right) for the EC condition. B: The planar phase plots of the wobble board kinematics during sitting with Base #1 (top) and Base #2 (bottom) for the EC condition. Shown is the third trial for Participant #15. 80

Figure 31. Examples of the wobble board kinematics in AP and ML directions. A: The AP (top) and ML (bottom) time series during sitting on the wobble board with Base #3 (left) and Base #4 (right) for the EO condition. B: The planar phase plots of the wobble board kinematics during sitting with Base #3 (top) and Base #4 (bottom) for the EO condition. Shown is the third trial for Participant #15. 82

Figure 32. Examples of the wobble board kinematics in AP and ML directions. A: The AP (top) and ML (bottom) time series during sitting on the wobble board with Base #2 for EO (left) and EC (right) conditions. B: The planar phase plots of the wobble board kinematics during sitting with Base #2 for EO (top) and EC (bottom) conditions. Shown is the third trial for Participant #15.. 85

Figure 33. Exemplary wobble board kinematics in the AP direction (top subplot) and the down-sampled, normalized EMG signal for LBF (bottom subplot) for Participant #13 with Base #1 and EC. The top subplot shows the three largest peaks in the anterior tilt of the wobble board as well as the 4-second windows centered at each peak. The bottom subplot shows the time-matched, corresponding 4-second windows created in the EMG time series. 87

Figure 34. The averaged CC function (from three segments) between LBF and ANT for Participant #13 under Base #1 and EC condition. The positive correlation peak indicates LBF muscle activation during ANT wobble board displacements. The negative time lag for that peak suggests that the LBF time series preceded the wobble board displacement in the anterior direction. 88

Figure 35. The averaged CC functions across participants between RExO and RIGHT for Bases #2, #3, #4, and #5 when eyes were open. The activation of RExO preceded RIGHT: Base #2: $r = 0.36 \pm 0.10$, $\tau = -0.15 \pm 0.09$; Base #3: $r = 0.43 \pm 0.12$, $\tau = -0.18 \pm 0.06$; Base #4: $r = 0.55 \pm 0.17$, $\tau = -0.17 \pm 0.05$; Base #5: $r = 0.68 \pm 0.09$, $\tau = -0.15 \pm 0.02$ 89

Figure 36. A schematic summary of findings during anterior-posterior wobble board displacements [264]–[266]. The CC results indicate the activation and deactivation of RA and BF muscles, during ANT and POST wobble board displacements respectively. In addition, the results indicate the

deactivation and activation of TES, LES, and RF muscles, during ANT and POST wobble board displacements respectively..... 90

Figure 37. The averaged CC functions across participants between RRA and ANT (left); and the averaged CC functions between RRA and POST (right). Results are shown for Base #2 when eyes were closed (top), and Base #4 when eyes were open (bottom). Left: the largest peaks had a positive r and a negative time lag (EC: $r = 0.33 \pm 0.09$, $\tau = -0.16 \pm 0.04$; EO: $r = 0.39 \pm 0.12$, $\tau = -0.18 \pm 0.04$), suggesting that, regardless of eye condition, RRA activation preceded ANT; Right: the largest peaks had a negative r and a negative time lag (EC: $r = -0.24 \pm 0.07$, $\tau = -0.11 \pm 0.07$; EO: $r = -0.34 \pm 0.11$, $\tau = -0.17 \pm 0.04$), suggesting that, regardless of eye condition, RRA deactivation preceded POST..... 91

Figure 38. The averaged CC functions across participants between LRA and ANT (left); and the averaged CC functions between LRA and POST (right). Results are shown for Base #2 when eyes were closed (top), and Base #4 when eyes were open (bottom). Left: the largest peaks had a positive r and a negative time lag (EC: $r = 0.30 \pm 0.09$, $\tau = -0.14 \pm 0.04$; EO: $r = 0.40 \pm 0.14$, $\tau = -0.18 \pm 0.05$), suggesting that, regardless of eye condition, LRA activation preceded ANT; Right: the largest peaks had a negative r and a negative time lag (EC: $r = -0.24 \pm 0.07$, $\tau = -0.16 \pm 0.06$; EO: $r = -0.30 \pm 0.06$, $\tau = -0.17 \pm 0.05$), suggesting that, regardless of eye condition, LRA deactivation preceded POST..... 92

Figure 39. The averaged CC functions across participants between RTES and ANT (left); and the averaged CC functions between RTES and POST (right). Results are shown for Base #2 when eyes were closed (top), and Base #4 when eyes were open (bottom). Left: the largest peaks had a negative r and a negative time lag (EC: $r = -0.21 \pm 0.06$, $\tau = -0.45 \pm 0.41$; EO: $r = -0.29 \pm 0.07$, $\tau = -0.19 \pm 0.10$), suggesting that, regardless of eye condition, RTES deactivation preceded ANT; Right: the largest peaks had a positive r and a negative time lag (EC: $r = 0.27 \pm 0.06$, $\tau = -0.17 \pm 0.09$; EO: $r = 0.31 \pm 0.10$, $\tau = -0.20 \pm 0.09$), suggesting that, regardless of eye condition, RTES activation preceded POST..... 93

Figure 40. The averaged CC functions across participants between LTES and ANT (left); and the averaged CC functions between LTES and POST (right). Results are shown for Base #2 when eyes were closed (top), and Base #4 when eyes were open (bottom). Left: the largest peaks had a negative r and a negative time lag (EC: $r = -0.23 \pm 0.06$, $\tau = -0.39 \pm 0.25$; EO: $r = -0.28 \pm 0.08$, $\tau = -0.24 \pm 0.06$), suggesting that, regardless of eye condition, LTES deactivation preceded ANT; Right: the largest peaks had a positive r and a negative time lag (EC: $r = 0.26 \pm 0.09$, $\tau = -0.25 \pm 0.08$; EO: $r = 0.29 \pm 0.10$, $\tau = -0.25 \pm 0.08$), suggesting that, regardless of eye condition, LTES activation preceded POST..... 94

Figure 41. The averaged CC functions across participants between RLES and ANT (left); and the averaged CC functions between RLES and POST (right). Results are shown for Base #2 when eyes were closed (top), and Base #4 when eyes were open (bottom). Left: the largest peaks had a negative r and a negative time lag (EC: $r = -0.31 \pm 0.09$, $\tau = -0.29 \pm 0.05$; EO: $r = -0.31 \pm 0.07$, $\tau = -0.22 \pm 0.10$), suggesting that, regardless of eye condition, RLES deactivation preceded ANT; Right: the largest peaks had a positive r and a negative time lag (EC: $r = 0.23 \pm 0.09$, $\tau = -0.24 \pm 0.08$; EO: $r = 0.27 \pm 0.09$, $\tau = -0.23 \pm 0.07$), suggesting that, regardless of eye condition, RLES activation preceded POST..... 95

Figure 42. The averaged CC functions across participants between LLES and ANT (left); and the averaged CC functions between LLES and POST (right). Results are shown for Base #2 when eyes were closed (top), and Base #4 when eyes were open (bottom). Left: the largest peaks had a negative r and a negative time lag (EC: $r = -0.31 \pm 0.09$, $\tau = -0.25 \pm 0.08$; EO: $r = -0.27 \pm 0.09$, $\tau = -0.16 \pm 0.07$), suggesting that, regardless of eye condition, RLES deactivation preceded ANT; Right: the largest peaks had a positive r and a negative time lag (EC: $r = 0.28 \pm 0.10$, $\tau = -0.17 \pm 0.16$; EO: $r = 0.28 \pm 0.09$, $\tau = -0.18 \pm 0.11$), suggesting that, regardless of eye condition, RLES activation preceded POST..... 96

Figure 43. The averaged CC functions across participants between RBF and ANT (left); and the averaged CC functions between RBF and POST (right). Results are shown for Base #2 when eyes were closed (top), and Base #4 when eyes were open (bottom). Left: the largest peaks had a positive r and a negative time lag (EC: $r = 0.54 \pm 0.11$, $\tau = -0.19 \pm 0.04$; EO: $r = 0.47 \pm 0.12$, $\tau =$

-0.18 ± 0.05), suggesting that, regardless of eye condition, RBF activation preceded ANT; Right: the largest peaks had a negative r and a negative time lag (EC: $r = -0.46 \pm 0.16$, $\tau = -0.18 \pm 0.07$; EO: $r = -0.38 \pm 0.17$, $\tau = -0.20 \pm 0.06$), suggesting that, regardless of eye condition, RBF deactivation preceded POST..... 97

Figure 44. The averaged CC functions across participants between LBF and ANT (left); and the averaged CC functions between LBF and POST (right). Results are shown for Base #2 when eyes were closed (top), and Base #4 when eyes were open (bottom). Left: the largest peaks had a positive r and a negative time lag (EC: $r = 0.53 \pm 0.12$, $\tau = -0.18 \pm 0.06$; EO: $r = 0.52 \pm 0.11$, $\tau = -0.18 \pm 0.06$), suggesting that, regardless of eye condition, RBF activation preceded ANT; Right: the largest peaks had a negative r and a negative time lag (EC: $r = -0.45 \pm 0.13$, $\tau = -0.19 \pm 0.07$; EO: $r = -0.43 \pm 0.16$, $\tau = -0.19 \pm 0.09$), suggesting that, regardless of eye condition, RBF deactivation preceded POST..... 98

Figure 45. The averaged CC functions across participants between RRF and ANT (left); and the averaged CC functions between RRF and POST (right). Results are shown for Base #2 when eyes were closed (top), and Base #4 when eyes were open (bottom). Left: the largest peaks had a negative r and a negative time lag (EC: $r = -0.35 \pm 0.10$, $\tau = -0.21 \pm 0.10$; EO: $r = -0.41 \pm 0.15$, $\tau = -0.20 \pm 0.09$), suggesting that, regardless of eye condition, RRF deactivation preceded ANT; Right: the largest peaks had a positive r and a negative time lag (EC: $r = 0.39 \pm 0.15$, $\tau = -0.22 \pm 0.08$; EO: $r = 0.44 \pm 0.14$, $\tau = -0.18 \pm 0.08$), suggesting that, regardless of eye condition, RRF activation preceded POST..... 99

Figure 46. The averaged CC functions across participants between LRF and ANT (left); and the averaged CC functions between LRF and POST (right). Results are shown for Base #2 when eyes were closed (top), and Base #4 when eyes were open (bottom). Left: the largest peaks had a negative r and a negative time lag (EC: $r = -0.40 \pm 0.14$, $\tau = -0.25 \pm 0.17$; EO: $r = -0.39 \pm 0.18$, $\tau = -0.17 \pm 0.12$), suggesting that, regardless of eye condition, LRF deactivation preceded ANT; Right: the largest peaks had a positive r and a negative time lag (EC: $r = 0.49 \pm 0.14$, $\tau = -0.18 \pm 0.09$; EO: $r = 0.47 \pm 0.15$, $\tau = -0.17 \pm 0.07$), suggesting that, regardless of eye condition, LRF activation preceded POST..... 100

Figure 47. A schematic summary of findings during medial-lateral wobble board displacements [266]. The CC results indicate the activation and deactivation of RExO during RIGHT and LEFT wobble board displacements, respectively. Moreover, they indicate the deactivation and activation of LExO during RIGHT and LEFT wobble board displacements, respectively..... 102

Figure 48. The averaged CC functions across participants between RExO and LEFT (left); and the averaged CC functions between RExO and RIGHT (right). Results are shown for Base #2 when eyes were closed (top), and Base #4 when eyes were open (bottom). Left: the largest peaks had a negative r and a negative time lag (EC: $r = -0.42 \pm 0.13$, $\tau = -0.19 \pm 0.09$; EO: $r = -0.50 \pm 0.14$, $\tau = -0.16 \pm 0.08$), suggesting that, regardless of eye condition, RExO deactivation preceded LEFT; Right: the largest peaks had a positive r and a negative time lag (EC: $r = 0.43 \pm 0.16$, $\tau = -0.17 \pm 0.09$; EO: $r = 0.55 \pm 0.17$, $\tau = -0.17 \pm 0.05$), suggesting that, regardless of eye condition, RExO activation preceded RIGHT. 103

Figure 49. The averaged CC functions across participants between LExO and LEFT (left); and the averaged CC functions between LExO and RIGHT (right). Results are shown for Base #2 when eyes were closed (top), and Base #4 when eyes were open (bottom). Left: the largest peaks had a positive r and a negative time lag (EC: $r = 0.46 \pm 0.16$, $\tau = -0.18 \pm 0.06$; EO: $r = 0.61 \pm 0.12$, $\tau = -0.18 \pm 0.04$), suggesting that, regardless of eye condition, LExO activation preceded LEFT; Right: the largest peaks had a negative r and a negative time lag (EC: $r = -0.38 \pm 0.15$, $\tau = -0.19 \pm 0.04$; EO: $r = -0.55 \pm 0.10$, $\tau = -0.16 \pm 0.06$), suggesting that, regardless of eye condition, LExO deactivation preceded RIGHT. 104

Nomenclature

3D	Three-dimensional
ADLs	Activities of daily living
ANT	Anterior direction of the board tilt
AP	Anterior-posterior
APAs	Anticipatory postural adjustments
ASIS	Anterior superior iliac spine
BBL	Board back left side
BBR	Board back right side
BF	Biceps femoris
BFL	Board front left side
BFR	Board front right side
C7	Seventh cervical vertebra
CC	Cross-correlation
CCF	Cross-correlation function
CFREQ	Centroidal frequency

CNS	Central nervous system
COM	Center of mass
COP	Center of pressure
CPAs	Compensatory postural adjustments
EC	Eyes closed
EMG	Electromyogram
EO	Eyes open
ES	Erector spinae
ExO	External oblique
FES	Functional electrical stimulation
FREQD	Frequency dispersion
IJ	Deepest point of the incisura jugularis
IO	Internal oblique
LBF	Left biceps femoris
LBP	Low back pain
LCS	Local coordinate system

LD	Latissimus dorsi
LEDs	Light-emitting diodes
LEFT	Left direction of the board tilt
LES	Lumbar erector spinae
LExO	Left external oblique
LLD	Left latissimus dorsi
LLES	Left lumbar erector spinae
LRA	Left rectus abdominis
LRF	Left rectus femoris
LTES	Left thoracic erector spinae
MA	Mean angle
MAV	mean absolute value
ML	Medial-lateral
MoCap	Motion capture
MV	Absolute angular velocity
MVC	Maximum voluntary contraction

POST	Posterior direction of the board tilt
PSIS	Posterior superior iliac spine
PX	Processus xiphoideus
RA	Rectus abdominis
RANGE	Range
RBF	Right biceps femoris
RExO	Right external oblique
RF	Rectus femoris
RIGHT	Right direction of the board tilt
RLD	Right latissimus dorsi
RLES	Right lumbar erector spinae
RMS	root mean square
RMSA	Root mean square amplitude of the angle
RMSV	Root mean square amplitude of the angular velocity
RRA	Right rectus abdominis
RRF	Right rectus femoris

RTES	Right thoracic erector spinae
SCI	Spinal cord injury
sub-MVC	sub-maximal voluntary contraction
T8	Eighth thoracic vertebra
TES	Thoracic erector spinae

Chapter 1

1 Introduction

1.1 Trunk Stability in Individuals with Spinal Cord Injury

Postural stability is defined as the ability of a system to return to an equilibrium position following a perturbation [1], and is achieved when the projection of the system's center of mass (COM) is located within the base of support [2]. Trunk stability is one of the most critical prerequisites of human function and mobility, and this independent of the movement or task performed. This is not surprising considering that over half of the body's mass is located above the pelvis [3]. Consequently, fundamental activities of daily living (ADLs) – such as sitting, standing, walking, and reaching – cannot be accomplished unless the trunk is being successfully stabilized [4]. In individuals who experience neuromuscular impairments affecting trunk control and stability, the consequences are oftentimes highly detrimental and can be easily recognized. For example, individuals who have suffered complete or incomplete spinal cord injury (SCI) between the head and 10th thoracic vertebra (T10) usually experience at least some degree of trunk function impairment [5]. As a result, affected individuals are usually not able to control seated balance on their own, leading to trunk muscle atrophy, reduced independence in ADLs, and, ultimately, a lower quality of life [6], [7].

In order to compensate for neuromuscular deficiencies and facilitate sitting balance, individuals with SCI frequently tilt their pelvis further backward than non-disabled individuals, which increases stability in the anterior direction [8]. In addition, to artificially anchor the upper body's center of mass and prevent the trunk from falling forward irrepressibly when reaching with one arm, they often need to hinge the other arm over the back of their chair. Using this form of compensation, it is literally impossible for affected individuals to perform bilateral reaching and grasping tasks, and larger or heavier objects have to be conveniently placed in their lap or on a close-by table [9]. Although such compensational sitting arrangements allow individuals with SCI to perform a range of upper extremity tasks during sitting, they can also cause or aggravate

secondary health complications such as respiratory dysfunction (reducing respiratory capacity) [10], [11], pressure sores [12], and kyphosis [13]–[15]. Therefore one of the highest priorities for individuals with SCI is to improve their trunk control [16]. In fact, in light of the described characteristics and consequences of impaired trunk control, it is not surprising that restoring trunk stability is of higher priority for individuals with SCI than restoring walking function [17] – highlighting the fundamental importance of trunk control in human mobility.

1.2 Approaches for Enhancing Trunk Stability

Several attempts have been made to improve sitting stability in individuals with SCI during functional upper extremity tasks such as reaching and grasping. Customizing the configurations of the wheelchair itself by changing its inclination angle [18], attaching footrests or chest straps [19], [20], or making use of novel seat cushions [21] have been shown to improve sitting stability for individuals with SCI. One limitation of these *passive* modifications is, however, that they: (1) support the trunk solely in the *anterior* direction; and (2) do not take dynamic demands into account that depend on the particular functional and/or environmental context. As a consequence, the ability to stabilize the trunk in the medial-lateral and posterior directions – as required, for example, during a bus ride – and to dynamically regulate such stability is oftentimes still compromised when using these solutions.

In this light, recent developments suggest that neuroprostheses utilizing functional electrical stimulation (FES) may be able to facilitate or restore trunk stability during sitting, standing, and other tasks involving postural control. FES is an electromechanical technique delivering pre-programmed (open-loop) or feedback-based (closed-loop) trains of short electrical pulses to specific muscles that contract to facilitate a desired posture or movement by generating the required forces and/or torques. To accomplish this objective, three different types of FES systems – or neuroprostheses – can be used: Implantable FES systems, percutaneous FES systems, and transcutaneous FES systems. Implantable FES systems are the most invasive option as the stimulator and electrodes need to be implanted in the body via surgery [22], [23]. Percutaneous FES systems are less invasive, but still require the stimulation electrodes to penetrate the user’s skin to allow fixation to the muscles of interest [23], [24]. Transcutaneous FES systems are the

only non-invasive option for which the stimulation electrodes are placed above the muscles of interest on the surface of the skin [23], [25]. Since the electrodes for transcutaneous FES systems can be removed easily, they are suitable for many assistive and rehabilitative applications [9].

Using transcutaneous FES systems in open- or closed-loop control schemes, functions such as grasping and reaching have been shown to be restorable in individuals with SCI that present with a range of injury severities [26]. Preliminary results indicate that FES has the potential to also assist in the completion of more complex tasks such as sitting, standing, and walking (e.g., [27]–[29]). These tasks, however, have larger gravitational compensation demands, calling for higher overall stimulation intensities that accelerate the onset of muscle fatigue [30] and increase the risk of malfunction of the given FES system [28]. In addition, such postural and mobility tasks require the many involved muscles to be contracted synergistically, adhering to well-defined spatial and temporal activation patterns.

For seated trunk stability, a solution to the first challenge – the reduction or prevention of FES-induced muscle fatigue – is to apply low-intensity, open-loop FES, which has been suggested to facilitate fatigue-resistant *static trunk stability* by increasing overall trunk stiffness and damping [27]. Such low-intensity, or base level of FES can then be paired with intermittent, closed-loop FES that ensures *dynamic trunk stability* as needed for the completion of many ADLs. To define the required spatial and temporal muscle activation patterns – the second challenge for seated trunk stability – one approach is to mimic trunk muscle activation patterns that non-disabled individuals use to regulate trunk stability. The use of such bio-inspired, closed-loop stimulation schemes promises to not only generate natural movements and postures, but also to minimize energy expenditure and, hence, muscle fatigue during sitting.

1.3 Thesis Objectives

To improve trunk stability during sitting and, consequently, functional independence of individuals with SCI, more advanced, active approaches are needed that enhance stability not only in the anterior, but also in the posterior and medial-lateral directions. One potential solution is to use transcutaneous FES that combines a low-intensity, open-loop FES component (increasing trunk

stiffness and damping) with a bio-inspired, closed-loop FES component (rejecting postural disturbances and facilitating functional tasks). However, to realize a bio-inspired FES component that mimics healthy trunk stabilization during dynamic sitting while minimizing the occurrence of muscle fatigue, a more comprehensive understanding of the relation between muscle activity and multi-directional trunk motion during healthy, reactive balance control is needed.

Based on these considerations, the overall goal of this research project was to obtain a more comprehensive, quantitative understanding of the neuromechanical mechanisms of dynamic sitting control during continuous multi-directional perturbations. Using a wobble board paradigm that induces continuous tilt perturbations about the continuum of horizontal axes, specific operational objectives were to quantify: (1) the effect of varying levels of wobble board instability on postural proficiency; (2) the effect of visual information on postural proficiency; (3) spatial determinants of trunk muscle activation; and (4) temporal determinants of trunk muscle activation. For the utilized unstable sitting paradigm, postural proficiency was assessed using a range of kinematic measures obtained from the wobble board kinematics. Future work will design closed-loop FES control schemes that can elicit muscle activation patterns as well as wobble board and trunk kinematics that mimic those obtained in the present study. For this purpose, principals of classical control (as in [31]) and system identification (as in [32]) will be applied.

1.4 Organization of the Thesis

Chapter 2 presents reviews of the literature that are relevant to this thesis: a review of trunk stability studies; an overview of electromyography in trunk and upper leg muscles; an overview of kinematic models and kinematic analysis using motion capture systems; and a review of wobble board studies. Chapter 3 describes the preliminary studies conducted to: (1) validate the time synchronization procedure, and (2) determine the most adequate “activation exercise” for eliciting maximum voluntary contractions of a given muscle. Chapter 4 describes the experiment conducted (i.e., material and methods, wobble board tasks, and analyses). Chapter 5 presents the results and findings. Chapter 6 discusses the results and the limitation of this study. Chapter 7 summarizes the findings and provides concluding remarks and recommendations for future work.

Chapter 2

2 Literature Review

2.1 Trunk Stability and Instability

2.1.1 Introduction

When stabilizing the trunk during functional activities such as sitting, standing, or reaching, the central nervous system (CNS) primarily applies two postural strategies [33], [34]: *Anticipatory postural adjustments* (APAs) and *compensatory postural adjustments* (CPAs). On the one hand, APAs activate the trunk and leg muscles *prior to* an external or self-induced disturbance (such as leaning for the purpose of reaching an object) to prepare the body for upcoming, predictable perturbations [35]. Note that these APAs oftentimes imply co-contraction of antagonist muscles, which presumably increases the stiffness of the upper body [16], [27] and further stabilizes its COM location. On the other hand, CPAs act *following* a disturbance and are used to return the upper body to the upright equilibrium position based on the rich information provided by sensory modalities including vision and proprioception [34], [36]. This sensory drive initiates the CPAs, which are accomplished via short-latency automatic postural responses [37] that are fine-tuned via long-latency, feedback-based responses [37].

Both APAs and CPAs are neurally-driven – or active – control mechanisms that, as described earlier, originate in the central nervous system. They are complemented by biomechanical – or passive – control mechanisms that take advantage of intraabdominal pressure [38], [39] and intrinsic mechanical properties of the spine, joints, and tissue [40], [41] to increase the overall stiffness and damping of the system [16], [27]. Since this research study is focused on spatial and temporal determinants of trunk muscle activation during unstable sitting, the literature review will primarily focus on active mechanisms of trunk control and particularly on the trunk muscles involved in trunk stabilization.

2.1.2 Muscles Involved in Trunk Stabilization

It is well known that the large and superficial trunk muscles whose activity can be measured via surface electromyography (*see Section 2.2*) can be broadly categorized into *trunk flexors* and *trunk extensors*. Among the trunk flexors, the rectus abdominis muscle (RA) [42]–[45] as well as the internal and external oblique muscles (IO & ExO) [42]–[47] have been found to play an important role in trunk stabilization. On the one hand, RA contractions cause the trunk to flex (e.g., when bending down to pick something up from the ground) or to resist posterior trunk displacements (e.g., during sudden forward accelerations) [48]. On the other hand, IO and ExO contractions allow an individual to bend in both lateral and anterior directions (e.g., during diagonal reaching) as well as to axially rotate to one of the two body sides (e.g., when grasping the seatbelt prior to buckling up in a car) [48]. Among the trunk extensors, the erector spinae muscle (ES) has been found to significantly contribute to trunk stabilization [48], which is not surprising considering that it spans the entire length of the back. ES consists of three groups of muscles called the longissimus, spinalis, and iliocostalis muscles [48], which are used to stabilize the trunk against continuous gravitational forces that intrinsically rotate the trunk forward due to the anterior location of the trunk's COM [49], [50]. Moreover, these muscle groups have been shown to also act differentially and synergistically to resist forward trunk displacements, e.g., during a sudden stop when sitting on a bus [51]–[53]. In this context, it is important to note that, in individuals with SCI, paralysis of the left and right ES is highly detrimental as they lose their ability to compensate for gravity, which is a prerequisite for executing many functional activities during sitting [54].

In addition to the trunk flexors and trunk extensors described above, there are several other large superficial muscles that directly or indirectly contribute to trunk stability. While the latissimus dorsi muscle (LD) – a larger, flat muscle on the dorsolateral side of the trunk – is primarily responsible for arm and shoulder movement [48], it also contributes to lateral flexion and extension of the lower trunk [48]. Finally, the biceps femoris (BF) and rectus femoris (RF) – two of the primary actors in the upper leg – stabilize the pelvis via hip extension [55]–[58] and hip flexion [55], [57], [59]–[61], respectively, indirectly promoting trunk stabilization as well.

2.1.3 Trunk Stability in Non-Disabled Individuals

Numerous studies have investigated neuromuscular mechanisms that contribute to human trunk stabilization. For example, recent work has characterized the role of anticipation in trunk muscle activation and trunk stabilization [62], which relates to the previously described APAs. In addition, researchers have studied the effect of fatigue on spinal stability [63], whereas others have quantified the contribution of trunk and/or spinal stiffness to trunk stabilization [16], [27], [64], [65]. Furthermore, driven by the alarming number of individuals being affected by low back pain (LBP), the use of exercises in the prevention or treatment of this impairment has been studied [46], [64]–[74]. In the immediate context of the described thesis work, many studies have also reported on neuromuscular mechanisms underlying trunk loading [46], [64]–[66], [68]–[70], [73]–[75] and functional tasks involving the trunk, including reaching [21], [19], [76], rotating [77]–[81], pointing [82], lifting [77], [83]–[85], hand loading [62], [86]–[88], balancing on a wobble board [89]–[96], and performing stability exercises [71], [72], [97]–[103].

In most human trunk studies, the trunk was perturbed using different methodologies. The perturbation could be applied to the participant's body externally (i.e., representing an external perturbation), using a perturbation platform, a cable or a pulley system [46], [63]–[65], [69], [95], or could be self-initiated (i.e., representing an intrinsic perturbation), using, for example, voluntary motion or a posture-challenging environment such as a wobble board [93], [94], [96], [104]–[107].

2.1.4 Trunk Instability in Individuals with Spinal Cord Injury

As mentioned earlier, facilitating trunk stability is one of the most important objectives in postural control, allowing humans to set the stage for successful completion of many ADLs [4]. The critical role of trunk stability is especially evident in individuals with SCI who are frequently not able to control seated balance, which, in turn, compromises their independence in many everyday situations [5], [7]. The inability to control seated balance is caused by the fact that affected individuals lose complete or partial control over their trunk muscles. Such active control, however, is critical considering the previously described role of especially the ES – to counteract the so-called gravity toppling torque of the upper body during sitting.

Two factors associated with SCI have a significant influence on the degree of trunk control impairment affected individuals experience: the severity and level of the injury. The *severity of injury* can be broadly categorized into complete and incomplete SCI [108]. On the one hand, complete SCI is characterized by (close to) complete loss of neural connectivity between the central and peripheral nervous systems, resulting in a (close to) complete loss of controllability of the muscles below the site of injury [109]. On the other hand, incomplete SCI results in only a partial loss of that connectivity, allowing a certain, yet variable degree of controllability of the muscles below the site of injury [109], [110]. In addition to SCI severity, also the *level of injury* plays an important role in trunk instability, with especially those individuals affected by an injury between the head and the 10th thoracic vertebra experiencing difficulties with maintaining seated balance [6], [21].

As a direct consequence of their inability to adequately stabilize the trunk, individuals with SCI use non-postural muscles including the neck and shoulder muscles to facilitate compensatory movements or postures that allow them to maintain their balance during sitting and wheeling [91]. To reach an object in front of them, they usually put one arm over the back of the wheelchair to ensure the necessary forces to prevent the body from moving forward uncontrollably [9]. In addition, they tilt their pelvis backward as described earlier, resulting in a posterior shift of the body's COM and an increase in overall trunk stability [111].

It is important to note that trunk instability and the utilized compensatory strategies can lead to health complications such as pressure sores [16], shoulder pain [14], kyphosis [13], and respiratory dysfunction reducing respiratory capacity [16]. Primary causes of these secondary consequences include a suboptimal spine posture during sitting, an unequal weight distribution on the seat cushion and back rest [9] as well as non-physiological use of intact muscles and joints (e.g., in the shoulder) required for compensatory movements [6], [112], [113]. Due to both the functional and secondary health implications of trunk instability, it is not surprising that recovering trunk stability is one of the highest priorities for individuals with SCI [17].

Several attempts have been made to improve sitting stability in individuals with SCI during upright – or quiet – sitting, wheeling, and reaching. Customizing the configurations of the wheelchair such

as using different types of seat cushions [21], using footrests or chest straps are some of the ways to improve sitting stability in individuals with SCI [114]. As mentioned earlier, these modifications have been shown, however, to only passively increase sitting stability in individuals with SCI, and this in the anterior direction only.

2.2 Electromyography

2.2.1 Introduction

A motor unit, the smallest functional unit of muscle, consists of a motoneuron and a group of individual muscle fibers innervated by it [115]. The number of muscle fibers within each unit can vary, ranging from 3 to 2000 [115]. When an impulse reaches the neuromuscular junction, a synapse between the motoneuron and muscle fibers, motoneurons release a neurotransmitter called acetylcholine [116]. Acetylcholine then binds to its receptors on the muscle fibers; as a result, the electro-chemical balance of the muscle fiber membranes changes, which triggers a muscle fiber action potential that spreads along the muscle fiber [116]. An electromyogram (EMG) represents the summation of motor unit action potentials that can be detected via electrodes [117]. The underlying technique that is used to measure EMG signals and determine overall levels of muscle activity is called electromyography [115].

Two different types of electrodes can be used to measure EMG signals: surface and indwelling electrodes. Surface electrodes, non-invasive and relatively inexpensive [118], can be attached above the targeted muscle [1] and used to record EMG activities from the skin surface overlying superficial muscles [119], [120]. Indwelling electrodes can be inserted into the muscles [115]; therefore, they are more suitable when studying deep muscles [119]. They can also be used when the potential for measuring a signal from nearby muscles, known as cross-talk, is high [118]. These electrodes are more expensive, invasive, and may cause pain [118].

The location of electrodes, which are generally placed over the belly of the muscle [119], can be different for each study. By aligning the direction of the EMG electrodes with that of the muscle fibers, the EMG electrodes provide the best signal to noise ratio [52]. The reference or ground

electrode, usually placed over a bony prominence [119], is used to eliminate environmental electrical noise [121].

After choosing the location of electrodes, skin preparation is needed to reduce the impedance at the electrode-skin interface [3]. Based on Ohm's law, in a circuit, impedance is the resistance to current flow and is directly proportional to the voltage [122]. Impedance consistency is an issue in measuring muscles activity [121]. Therefore, minimizing the EMG voltage variability caused by superficial skin resistance is important. To alleviate this effect, skin preparation is usually employed, which results in minimizing the EMG voltage variations that is not due to muscle activity [3]. There are different techniques for preparing the skin: shaving [123], using sandpaper [123], cleaning with ethanol [123], or cleaning with alcohol [123].

2.2.2 EMG Signal Processing

The raw signals that are collected from the muscles are often processed to determine the level of muscle activity, to quantify muscle activation profiles, and/or to detect muscle activation onsets [124]. A series of processing steps can be applied to the raw signals to reduce any undesired variability [125].

In the first step, any direct current components are removed to reduce equipment noise in form of constant voltage shifts. An optional high-pass filter [68], [117], [126]–[128] or band-pass filter [129]–[134] can be used to reduce the effects of cross-talk, heart rate, and/or low-frequency motion artifacts. Note that bandpass filters include a low-pass filter and a high-pass filter [130]. The cutoff frequency of high-pass and band-pass filters varies from study to study. High-pass filters have been using cut-off frequencies of 10 Hz [126], [127], 30 Hz [68], [127], 60 Hz [127], and 50 Hz [126], whereas band-pass filters have been using frequency ranges of 20-500 Hz [135], 8-300 Hz [136], 20-450 Hz [137], 5-490 Hz [138], and 25-500 Hz [129]. EMG signals are then full-wave rectified [120], [139].

The next step in EMG signal processing is to use a smoothing procedure for estimating EMG amplitude and, hence, the level of muscle activation [127]. The most commonly used methods for smoothing and creating a linear envelope are root-mean-square (RMS) processing [131], [132],

mean-absolute-value (MAV) processing and low-pass filtering [124], [127], [131] (such as via a low-pass Butterworth filter at 500 Hz [130], 2 Hz [134], 2.5Hz [46], [140] or 6 Hz [47], [141]). Note that a time window needs to be defined when calculating RMS (over 50 ms [131], [142] or 1000 ms [132]) and MAV (over 100-200 ms [143], [144]).

In addition to smoothing the EMG signals, they are oftentimes normalized. EMG is a highly variable signal, with its magnitude being affected by many different factors such as the thickness of subcutaneous tissue, electrode size and placement, skin impedance, and temperature [145]. To eliminate such factors [146], [147] and reduce variability, a normalization procedure is used that enhances the reliability of the EMG signals [123]. The normalization technique quantifies muscle activity as a percentage of a reference EMG value recorded during an exercise that qualifies as a reference test [124], [143], [147], [148]. EMG normalization allows for comparison to be made between participants, muscles, days, or studies [124], [143], [147]. Among many different methods to normalize EMG signals, the maximum voluntary contraction (MVC) and sub-maximal voluntary contraction (sub-MVC) tests are the most common [45], [119], [123], [146], [148]. For both methods and each muscle being studied, the participants perform a set of MVC exercises. For the MVC method, the maximum value of the EMG signal collected during the MVC exercises is used, in one way or another (see below), in the process of normalization [40], [41]. However, for the sub-MVC method, different percentages of the MVC value are used as target levels for the sub-MVC trials [78], and the maximum value of the EMG signal recorded during the sub-MVC trials is used, in one way or another (see below), for normalization.

For eliciting MVCs from each muscle being studied, one or more exercises are performed [143]. The resistance required to elicit MVCs is applied by either a researcher manually or a machine such as a dynamometer [70], [78], [151]. In contrast to sub-MVC normalization, MVC normalization has the advantage of having a physiological meaning since the level of muscle activity is expressed relative to its maximum [147], [148]. However, since the MVC method can be mostly used in healthy study participants who are able to perform respective MVC exercises, it also has some disadvantages. Eliciting MVCs in individuals who experience pain or in the elderly is not always feasible [124], [146], [147]. Therefore, for comparing two groups of study participants for which the MVC method does not yield reliable results, the sub-MVC method (see

below) or other methods are used [146]. For example, some studies show that individuals with low back pain have lower MVC values than healthy individuals [152], [153]. Moreover, fatigue [154] and a lack of motivation have been shown to potentially affect the MVC results [119], [124]. It should also be noted that performing MVC exercises can be very time-consuming and that acquiring MVCs may not be anatomically possible for some muscles as nearby muscles or other anatomical structures may prevent maximum contractions [139].

In case the MVC method is appropriate and chosen for normalization, normalization values are calculated after performing MVC exercises. For quantifying muscle activity levels, all EMG signals are normalized based on the value selected for normalization [124], [147], [148]. Different methods can be used for calculating this value: the root mean square over a specific time period [155]–[158], the peak amplitude [159], [160], a moving average window [145], the average of the signal over a fixed window, centered at the peak [161]–[163].

The sub-MVC method is another commonly used method to normalize EMG signals. One of the concerns regarding the previously described MVC technique is the reliability of EMG data. Motivated by this limitation, a recent study has compared the MVC and sub-MVC techniques, suggesting that, for normalization purposes, the sub-MVC method is more reliable [146]. In this context, it has also been shown that the sub-MVC method can be used to evaluate low levels of muscle activity with greater sensitivity [44], [119], [164]. However, establishing equivalent sub-maximal loads – as needed for the sub-MVC method – may be difficult [123].

In addition to the previously described steps in EMG processing, it is also sometimes necessary to determine the onset of muscle activity. Among different techniques used for this purpose, two methods are most common: (1) *Visual onset detection* [76], [165]: the onset of EMG activity is determined by an experienced analyst, or operator. This method is highly dependent on the expertise of the operator and is considered to provide highly accurate onset estimates [165]–[167]. However, this method is very time-consuming as the analyst has to investigate each EMG recording separately [166]. In addition, several researchers have criticized this method for its subjectivity and poor reproducibility [166]. (2) *Computer-based onset detection* [168]: single or double threshold criteria in algorithm-based methods can be used. The single threshold algorithm

involves identification of the point in time where the processed EMG signal deviates from the average baseline signal by a specified number of standard deviations [166], [167], [169]. The double threshold method detects onset when at least r_0 out of m consecutive samples exceed the threshold used in the single threshold method. The additional parameters (r_0 and m) used in the double threshold method allow for a more robust detection of onsets [170], [171]. Two different types of error can occur in algorithm-based methods [167]: Type I error occurs when the threshold is low and factual inactivity of muscle is identified as muscle activity [167]. Type II error occurs when the utilized threshold method fails to identify the onset of factual muscle activity [167]. The double threshold method minimizes the occurrence of Type I errors [166].

2.2.3 Issues with Surface EMG Recordings

There are different factors that can affect the recording and analysis of EMG signals. Physical, anatomical, and/or geometrical factors of the tested individual can affect the amount of noise in EMG signals [120], [172]. In addition, noise artifacts from the EMG collection system itself, including wires, electrodes, and amplifiers, can affect the recordings of EMG muscle activities [173], [172]. These artifacts are oftentimes eliminated or minimized using post-recording (offline) signal processing techniques (such as low-pass filtering etc. [46], [140], [174]). Finally, when recording the activity of trunk muscles, electrical cross-talk from the heart is a major concern in light of the heart's vicinity to several trunk muscles [172], [175].

2.3 Human Motion Capture

2.3.1 Introduction

Human movement analysis aims to produce quantitative information that can be used to assess and analyze the movements of the human musculoskeletal system [3]. This information is oftentimes associated with body kinematics, which are used to describe the relative movements between adjacent body parts, or segments [3]. Dependent on the task or movement being studied, this form of analysis may consider all segments of the body or a certain subset of body segments. The first step in using this method is to capture the three-dimensional (3D) movements of each body

segment. In a second step, the collected data is used to calculate kinematic variables such as linear displacements and velocities or angular displacements, velocities, and accelerations [3].

Various techniques can be used to measure the 3D movements of the body segments of interest: electromagnetic tracking systems [176]–[178], stereoradiography [179], optoelectronic stereophotogrammetry [180], [181], wearable inertial measurement units (IMUs) [182]–[187], and markerless motion capture systems [188]–[190]. Among these techniques, stereophotogrammetry is still considered the gold-standard and remains the most commonly used in fundamental scientific research [181].

2.3.2 Stereophotogrammetric Systems

An optoelectronic stereophotogrammetric system is used to reconstruct 3D landmark coordinates from radiographs [191], [192], photographs [193], or video images [194]. Video-based optoelectronic systems, also called motion capture systems, are the most popular systems in human movement analysis since they are less expensive and more time efficient than other established techniques [195]. It should be noted at this point that new emerging techniques such as IMU-based and markerless systems are gaining more and more attention, especially due to their lower cost and enhanced ease-of-use [182], [189], [196]. However, their accuracy and reliability do not yet meet those of gold-standard motion capture systems [190], [196], [197].

When using video-based optoelectronic systems, a minimum of three markers are placed on the skin above each segment of interest, and their instantaneous 3D positions are measured [181]. For the purpose of capturing multi-body kinematics, each set of markers is assumed to represent a rigid portion of the human body. Note that, in many cases, a fourth marker is added to a given segment [31], [180], [198], increasing the robustness of the acquired data, e.g., when losing points or segments of data due to marker occlusion (see below).

The markers that are used in motion capture systems can be either retroreflective (passive) or light-emitting (active) [195]. On the one hand, retroreflective passive markers are illuminated by infrared light generated via an array of light-emitting diodes (LEDs) mounted around the lens of each stationary camera [199], [200]. Pattern recognition software or dedicated hardware circuits

are then used to recognize the passive markers in the video frames [199], [200]. On the other hand, active markers emit LED light themselves, with the system being able to automatically detect each marker by virtue of the markers' sequential pulse timing [195]. The absence of batteries, wires, and pulsing circuitry on the body of study participants is an advantage of passive marker systems; however, higher possible sampling rates and accuracy in detecting 3D marker locations are advantages of active marker systems [195], [201].

2.3.3 Kinematic Data Acquisition and Processing

Independent of the system used, kinematic data are captured by attaching markers onto body segments and recording the markers' movement [202]. Markers are placed individually (anatomical markers), usually on bony landmarks [31], [203]–[206], or in clusters of at least three markers (e.g., on cluster plates) [31], [207]. The location and type of markers vary widely from study to study [22]–[29]. Each marker must be seen by at least two cameras simultaneously for reconstructing the movement of different body segments [209]. During the experiment, markers may be obscured from camera views because of body movements such as arm swinging and participant rotation; therefore, using more than two cameras is recommended [209].

In general, kinematic variables can describe the movements of different body segments that took place during an experiment [9] and can be obtained mathematically using a kinematic model. This model consists of a chain of segments and can vary from study to study [31], [203], [204], [206], [207]. In the context of the human trunk, the simplest kinematic model consists of a single trunk segment, i.e., of all the body parts between the base of the neck and the hip except the upper limbs [180], when treated as a single rigid body. This model considers the angles of the entire trunk with respect to the hip [198], [205]. While the advantage of using such model is that only 3 to 4 markers are needed to measure overall trunk movement, it implies that relative motion between different levels of the trunk is ignored [210]. More complex kinematic models divide the trunk into two [181], [211] or more segments [212], [213]. By increasing the number of trunk segments, the accuracy of reconstructing actual trunk motion is increased [181], [212], [213]. However, as a trunk model increases in complexity, also the computational cost increases. In contrast to the trunk,

the pelvis is generally treated as a single rigid body or segment. Nevertheless, the location of utilized landmarks can still vary from study to study [206], [208], [214].

The location of the segment under analysis can be referenced with respect to either a local or global coordinate system [3]. The global coordinate system is defined based on the movement analysis laboratory, whereas the local coordinate system, for each segment, is defined using the instantaneous positions of the markers placed on the segment [3]. To define a local coordinate system, the instantaneous 3D positions of the markers are first captured with respect to the global coordinate system. Associated position vectors d_1 , d_2 , and d_3 of the markers in the global coordinate system are shown in Figure 1.

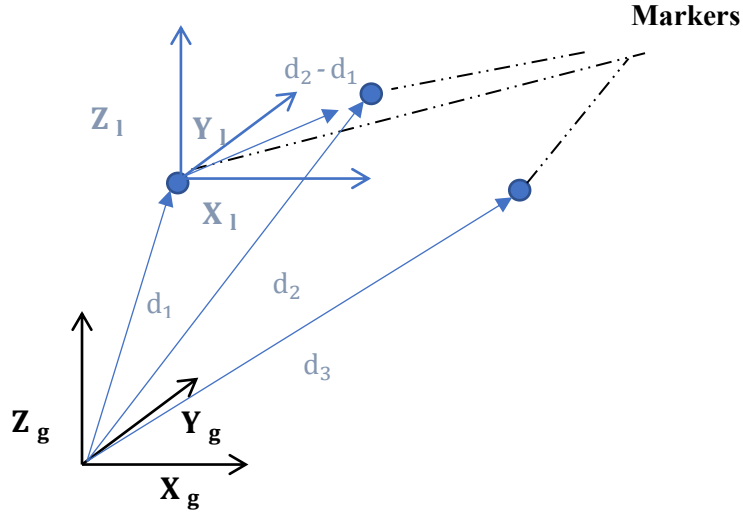


Figure 1. The position vectors of the markers (d_1 , d_2 , and d_3) in the global coordinate system (X_g, Y_g, Z_g) that are used to define the local coordinate system (X_1, Y_1, Z_1).

Using the definitions in Figure 1 above, the local coordinate system is then defined using the following calculation:

$$X_1 = \frac{d_3 - d_1}{\|d_3 - d_1\|}, y' = \frac{d_2 - d_1}{\|d_2 - d_1\|}, Z_1 = X_1 \times y', Y_1 = Z_1 \times X_1 \quad (\text{Eq. 1})$$

To describe the orientation and position of a given segment, we apply a coordinate transformation via the following equation:

$${}^gP = {}^gR_1 P + {}^gO \quad (\text{Eq. 2})$$

where

$${}^gR_1 = \begin{bmatrix} \cos\theta_{x_g x_1} & \cos\theta_{x_g y_1} & \cos\theta_{x_g z_1} \\ \cos\theta_{y_g x_1} & \cos\theta_{y_g y_1} & \cos\theta_{y_g z_1} \\ \cos\theta_{z_g x_1} & \cos\theta_{z_g y_1} & \cos\theta_{z_g z_1} \end{bmatrix} \quad (\text{Eq. 3})$$

is referred to as the rotation matrix defining the orientation of the local coordinate system relative to the global coordinate system. P and gP are the position vectors of the segment under analysis relative to the local and global coordinate systems, respectively. gO is the position vector of the origin of the local coordinate system relative to the global coordinate system and, hence, defines the position of the local coordinate system relative to the global coordinate system [181].

Extracting the 3D angles – flexion/extension, lateral bending and axial rotation in the case of the trunk – from the rotation matrix is often of interest [215]. The rotation matrix, derived from the orientation of the local coordinate system relative to the global coordinate system, can also be obtained by an ordered rotation sequence about the axes of a fixed (i.e., nonmoving) or a moving coordinate system [216]. The rotation could be either performed about three different axes (e.g., X, Y, Z), called Cardan sequence, or about the same axis more than once (e.g., Z, Y, Z), called Euler sequence [216]. One possible way to then derive the rotation matrix, e.g., between $\{A\}$ and $\{B\}$, is to first rotate $\{B\}$ about the fixed Z_A axis by an angle γ , then about the fixed Y_A axis by an angle β , and finally about the fixed X_A axis by an angle of α [215]. This set of rotations around the fixed axes, shown in Figure 2 (from left to right), can be used to isolate the 3D angles between the two coordinate systems.

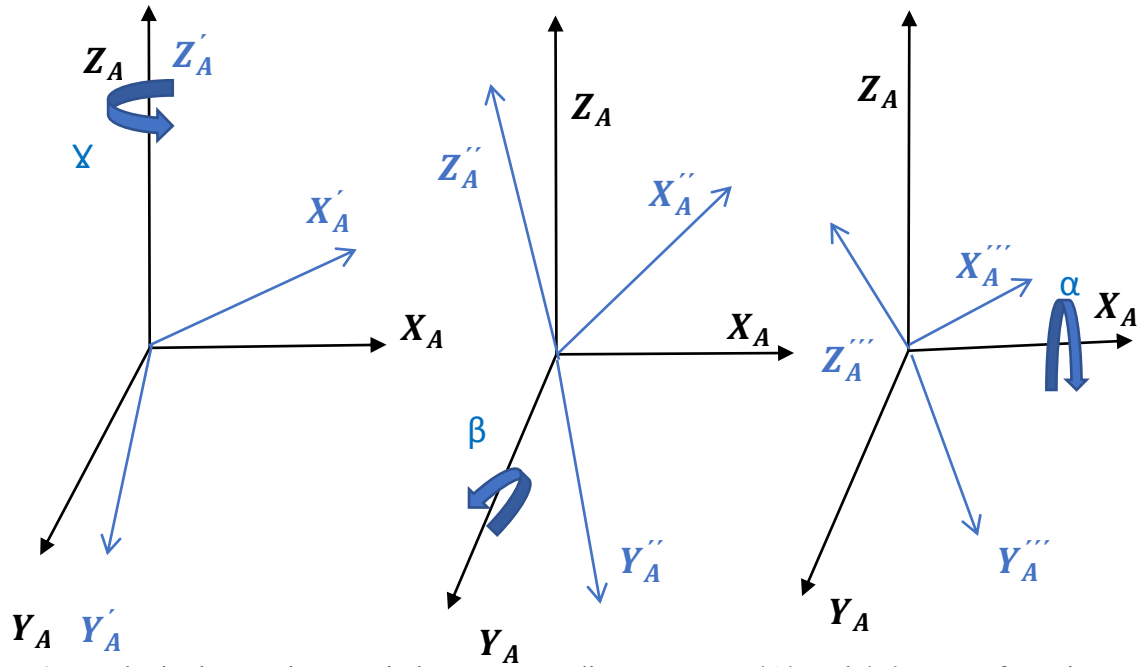


Figure 2. To obtain the rotation matrix between coordinate systems {A} and {B}, a set of rotations around the fixed axes can be performed. Rotations are performed in the order of $R_Z(\gamma)$, $R_Y(\beta)$, $R_X(\alpha)$.

The corresponding rotation matrix is:

$$\begin{aligned}
 R_{ZYX}(\gamma, \beta, \alpha) &= R_X R_Y R_Z \\
 &= \begin{bmatrix} 1 & 0 & 0 \\ 0 & \cos\alpha & -\sin\alpha \\ 0 & \sin\alpha & \cos\alpha \end{bmatrix} \begin{bmatrix} \cos\beta & 0 & \sin\beta \\ 0 & 1 & 0 \\ -\sin\beta & 0 & \cos\beta \end{bmatrix} \begin{bmatrix} \cos\gamma & -\sin\gamma & 0 \\ \sin\gamma & \cos\gamma & 0 \\ 0 & 0 & 1 \end{bmatrix} \quad (\text{Eq. 4})
 \end{aligned}$$

Multiplying out, we obtain:

$$\begin{aligned}
 R_{ZYX}(\gamma, \beta, \alpha) &= \begin{bmatrix} \cos\beta\cos\gamma & -\cos\beta\sin\gamma & \sin\beta \\ \sin\alpha\sin\beta\cos\gamma + \cos\alpha\sin\gamma & -\sin\alpha\sin\beta\sin\gamma + \cos\alpha\cos\gamma & -\sin\alpha\cos\beta \\ -\cos\alpha\sin\beta\cos\gamma + \sin\alpha\sin\gamma & \cos\alpha\sin\beta\sin\gamma + \sin\alpha\cos\gamma & \cos\alpha\cos\beta \end{bmatrix} \quad (\text{Eq. 5})
 \end{aligned}$$

Let

$$R_{ZYX}(\gamma, \beta, \alpha) = \begin{bmatrix} r_{11} & r_{12} & r_{13} \\ r_{21} & r_{22} & r_{23} \\ r_{31} & r_{32} & r_{33} \end{bmatrix} \quad (\text{Eq. 6})$$

Then, the angles (γ, β, α) can be derived as:

$$\begin{aligned} \beta &= \text{Atan2}(r_{13}, \sqrt{r_{23}^2 + r_{33}^2}) \\ \alpha &= \text{Atan2}(-r_{23}/\cos\beta, r_{33}/\cos\beta) \\ \gamma &= \text{Atan2}(-r_{12}/\cos\beta, r_{11}/\cos\beta) \end{aligned} \quad (\text{Eq. 7})$$

where $\text{Atan2}(y, x)$ computes $\tan^{-1}(y/x)$, but uses the signs of both x and y to determine in which quadrant the angle falls [215].

2.3.4 Limitations of Stereophotogrammetric Systems

There are various types of errors that can affect photogrammetric measurements: instrumental errors [195], [217], soft tissue artifacts [218], and anatomical landmark displacement errors [219]. Instrumental errors can be further classified as either random or systematic errors [12]. On the one hand, random errors may be due to marker flickering and/or electronic noise [195], [209]. On the other hand, systematic errors may occur due to improper lens and camera assembly or photogrammetric calibration inaccuracies [195]. Note that camera calibrations determine the optical and geometric characteristics of the cameras as well as the orientation and position of the camera frame with respect to a certain laboratory frame [195].

Errors originating at the interface between the bony segment of interest and the motion capture marker are classified as anatomical landmark displacement errors [219] as well as soft tissue artifacts [218]. The identification of anatomical landmarks depends on the level of expertise of the researcher, the palpation procedure, and the shape of the anatomical markers [220], [221]. The latter error, soft tissue artifacts, may occur due to skin movement or deformation during body

motion. Common direct causes of such soft tissue artifacts are muscle contractions and/or skin sliding, which happens mainly in areas that are closer to the joints [218].

2.4 Wobble Board Studies

Several studies have employed a wobble chair, or wobble board, as a tool to investigate balance control of the trunk in response to perturbations during unstable sitting [89], [90], [92]–[96], [104]–[107], [222]–[236]. In some of these studies, the wobble board had been restricted to swing in the sagittal and/or frontal plane only [89], [90], [92], [95], [222], [225], [227], [230], [232]. The swinging mechanism was provided by attaching a hemisphere to the bottom of the board [93], [94], [96], [104]–[107], [222]–[224], [228], [230]–[233], [236] or using a low-friction ball and socket joints [89], [90], [92], [95], [225]–[227], [229], [234], [235]. Task difficulty was also modulated by decreasing the diameter of the hemisphere attached to the bottom of the seat [94], [105], [228], changing the height of the seat [104], or changing the position of the springs [229], [233]–[235]. In addition, a foot rest, to limit the influence of lower extremities [89], [90], [92]–[96], [104], [105], [107], [222]–[227], [230]–[232], [236] and/or a safety bar, to grasp in case of balance loss [92]–[94], [96], [105], [107], [222]–[224], [226], [230]–[232], [236] may have been used. Finally, three types of measures were used to quantify postural proficiency: (1) center of pressure (COP) measures obtained via a force plate attached underneath the wobble board [93], [94], [96], [104], [105], [107]; (2) trunk kinematics measures obtained via a motion capture system [90], [92], [93], [106], [225], [229]; and/or (3) wobble board kinematics measures obtained via a motion capture system [90], [92], [225], [229].

Using these wobble board paradigms, a number of research questions were investigated. Trunk motor control strategy differences between individuals with LBP and non-disabled participants have been explored in several studies [89], [90], [92], [93], [96], [105]–[107], [225], [226], [232], [236]. While Van Dieen et al. [107] found no significant postural sway differences between these two groups, Van Daele et al. [106] reported a higher postural sway in individuals with LBP when compared to non-disabled individuals. Freddolini et al. [225] also compared kinematics of the trunk and hip between the two populations. Their results suggest that individuals with LBP show increased hip joint motion and decreased spine motion, which may be a compensatory strategy to

reduce the risk of further injury and/or pain. Furthermore, in another study [90], they investigated the activity of the trunk muscles during unstable sitting. They found that co-contraction (i.e., the simultaneous activation of agonist and antagonist muscles) increased in individuals with LBP compared to non-disabled individuals. Willigenburg et al. [93] assessed trunk control by measuring COP, trunk kinematics, and trunk muscle EMG in non-disabled individuals and those with LBP, revealing differences in muscle activation between the two groups. Furthermore, they found that the LBP group exhibited larger thoraco-lumbar movements than the non-disabled individuals. Lariviere et al. [92] investigated the effect of sex in non-disabled individuals and those with LBP, finding that females utilized different movement patterns to achieve a similar performance as males.

The reliability of COP, trunk, or wobble board kinematics measures during unstable sitting have been investigated in several studies [223], [226], [227]. Lee and Granta [227] investigated the reliability of wobble board kinematics measures in non-disabled participants, suggesting eight 30-second trials to achieve acceptable reliability results. Lariviere et al. [226] also assessed the reliability of the COP and wobble board kinematics measures in non-disabled individuals and those with LBP. They suggested that three 60-second trials are required to obtain the desired reliability. Moreover, Barbado et al. [223] investigated the reliability of COP and kinematic parameters and a potential learning effect, reporting that the reliability improved when the average or best outcome of multiple trials were used. Moreover, they suggested that a practice session should be performed to get familiar with the wobble board and to overcome learning effects.

Several studies have also examined the effect of sensory manipulations, i.e., of the visual, vestibular, and proprioceptive sensory systems, on trunk control during unstable sitting [96], [104], [105], [222], [231]. Andreopoulou et al. [222] investigated the effect of visual (eyes open/closed), vestibular (with or without galvanic vestibular stimulation), and proprioceptive (with or without muscle-tendon vibration) systems during unstable sitting. Their results suggest that postural sway increased with the lack of visual and/or vestibular inputs during stable sitting and more so during unstable sitting. They also found that proprioceptive manipulation influenced unstable sitting. Moreover, Silfies et al. [104] evaluated the effect of visual input and different seat instability levels. They found that postural sway increased when task difficulty increased or when the eyes

were closed. Sung et al. [96] also investigated the effect of visual manipulation in non-disabled individuals and those with LBP, finding that postural sway increased in the LBP group when eyes were closed compared to non-disabled individuals. Moreover, the effect of whole-body vibration on postural control of the trunk was investigated in a study by Slota et al. [233]. Their findings suggest that non-disabled individuals are less stable when whole-body vibration is applied.

Chapter 3

3 Preliminary Studies

3.1 Technical Validation of Time Synchronization of Recording Systems

3.1.1 Background and Rationale

In the main experiments of this study, a motion capture (MoCap) system was used to measure the angular kinematics of the wobble board and of different trunk segments. In addition, an EMG system was used to measure the activity of the large, superficial trunk muscles via surface electrodes. Since both systems were connected to independent, stand-alone data acquisition systems, a time synchronization procedure was required to align the time series data from the MoCap and EMG systems in time. In order to do so, a push button providing a voltage rise and connected to both systems was utilized. Before applying the synchronization procedure to the experimental data of the main experiment, a technical validation of the approach was required.

3.1.2 Objective

The objective of this study was to technically validate the time synchronization of the MoCap and EMG data acquisition systems. For this purpose, we decided to collect both MoCap and single-channel EMG data for a simple upper limb task in a group of participants and verify time synchronization across the MoCap and EMG recordings.

3.1.3 Experimental Setup

Two data acquisition systems were used in this study. Kinematic data for the upper limb task were recorded using an eight-camera motion capture system (Eagle Digital Camera, Motion Analysis Corporation, Santa Rosa, USA) with a sampling rate of 120 Hz. Muscle activity data for the upper

limb task were recorded via a 16-channel Bagnoli™ EMG system (Delsys Inc., Natick, USA) and a PowerLab 16/35 data acquisition system (ADInstruments, Sydney, Australia). The acquired analog EMG signal was amplified by a Bagnoli-16 EMG System amplifier (Delsys Inc.) and digitized at 1,000 Hz using the LabChart (ADInstruments) data acquisition software. For the purpose of time synchronization, an MLA92 Push Button Switch (ADInstruments) was utilized. The push button was connected to both the MoCap and EMG systems via a Tee connector and two BNC cables. The schematic of the push button setup is shown in Figure 3. The push button produced an approximate 6 V output signal when the button was pressed. The MoCap Push Button signal was sampled at 1,200 Hz, whereas the EMG Push Button signal was sampled at 1,000 Hz. MATLAB 2014a software was used to analyze the data.

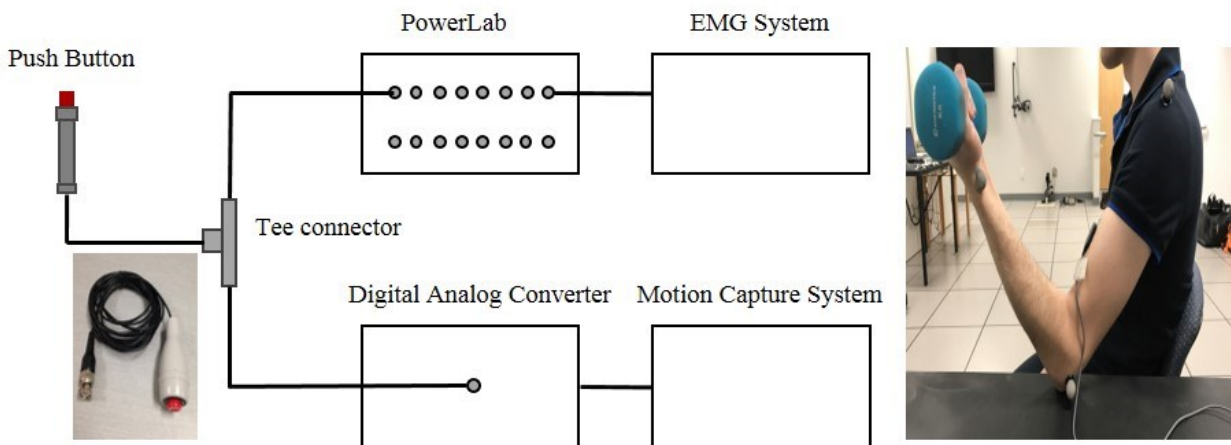


Figure 3. The schematic of the push button setup (left) and a picture of the experimental setup (right). The push button is connected to both motion capture and EMG systems via two BNC cables. A Tee connector was utilized to connect the BNC cables.

3.1.4 Participants and Experimental Procedure

Five non-disabled male individuals were recruited to participate in this study (age: 24 ± 3.9 ; weight: 80.6 ± 7.5 ; height: 180.3 ± 2.8). For each participant, four MoCap markers (Motion Analysis Corporation, Santa Rosa, USA) were placed on the skin of the left upper limb via plastic marker bases and double-sided adhesive tape (VICON Corporation, Denver, USA): one marker on

the acromion, one marker on the lateral epicondyle, and one marker each on the medial (radial) and lateral (ulnar) sides of the wrist. Note that the locations of the markers were specifically chosen for this sub-study. To ensure stable marker attachment throughout the experiments, the marker bases were further secured using Durapore™ tape. Following MoCap marker attachment, the target location for the EMG electrode, the center of the muscle belly of the left biceps brachii, was first identified with a felt pen. Then, the skin above the muscle was shaved (if needed), cleaned with an alcohol swap, and gently abraded with sand paper. A surface EMG electrode (Bagnoli™ 2-bar surface EMG sensors) was placed on the prepared skin using an adhesive interface for 2-bar sensors (Delsys Inc.). In addition, one self-adhesive reference electrode (Dermatode, Delsys Inc.) was placed over the olecranon (i.e., the bony prominence at the very tip of the elbow). To ensure stable electrode attachment throughout the experiments, the EMG electrode was further secured using 3M Transpore™ tape.

Each participant was asked to sit on a chair and place his left elbow and wrist on a table and hold a 5 kg dumbbell with the left hand and its palm facing up (Figure 3). The experimenter then started the data acquisition for both the MoCap and EMG systems and pressed the push button after visually confirming that both systems were collecting respective data. Once the button was pressed, the researcher asked the participant to perform a periodic movement by repeatedly raising the dumbbell to shoulder height and lowering it again to bring it back to the starting position (table height). A metronome was used to initiate and pace the speed of the movement, with beats occurring in 2-second intervals at both the table and shoulder heights. As such, the participant was instructed to adjust his movement speed so that the minimum (table height) and maximum (shoulder height) elevations were aligned with the metronome beats (resulting in a movement period of 4 seconds). Note that, every time the weight was returned to the starting position (table height), the researcher pressed the push button again. The experimental task lasted for approximately eight cycles and was repeated three times for each participant.

3.1.5 Experimental Data Processing and Analysis

For each trial, the recorded EMG signal was first demeaned, to eliminate any DC components, and then rectified. For referencing purposes, the sampling frequencies of the MoCap, EMG, and push button signals are again shown in Table 1.

Table 1. The sampling frequencies of the MoCap, EMG, and push button signals.

Signal #	Signal	Sampling Frequency
1	MoCap	120 Hz
2	Push Button – MoCap	1,200 Hz
3	EMG	1,000 Hz
4	Push Button – EMG	1,000 Hz

The synchronized start time (time = 0 seconds) for each system (MoCap, EMG) was identified as follows (Figure 4).

1. The MoCap system time (in seconds) corresponding to the first rise in the MoCap Push Button signal (*Signal #2*) was identified (t_{p_1}).
2. Since the MoCap signal (*Signal #1*) was sampled at a lower frequency, the time of the sample in the MoCap signal that occurred at or just prior to t_{p_1} was found (t_{m_1}). This time was defined as the synchronized start time t_1 in the MoCap signal (time = 0 seconds).
3. The time difference between the time when the rise occurred (t_{p_1}) in the MoCap Push Button signal (*Signal #2*) and the synchronized start time $t_1 = t_{m_1}$ in the MoCap signal (*Signal #1*) was calculated ($\Delta = t_{p_1} - t_1$).
4. The EMG system time (in seconds) corresponding to the first rise in the EMG Push Button signal (*Signal #4*) was identified (t_{p_2}).
5. The *theoretical* synchronized start time t_2^* in the EMG signal (*Signal #3*) was identified via $t_2^* = t_{p_2} - \Delta$. However, since the MoCap and EMG systems obeyed different sampling frequencies (*see Table 1*), the *actual* synchronized start time t_2 in the EMG signal (time = 0 seconds) was chosen as the sampled time in the EMG signal that occurred at or just after

t_2^* . Considering the sampling frequency of 1,000 Hz for the EMG data, this resulted in a maximum synchronization error, $t_2 - t_1$, of 1 ms.

- All MoCap and EMG signals were finally cropped to start at t_1 and t_2 , respectively, when set to 0 seconds.

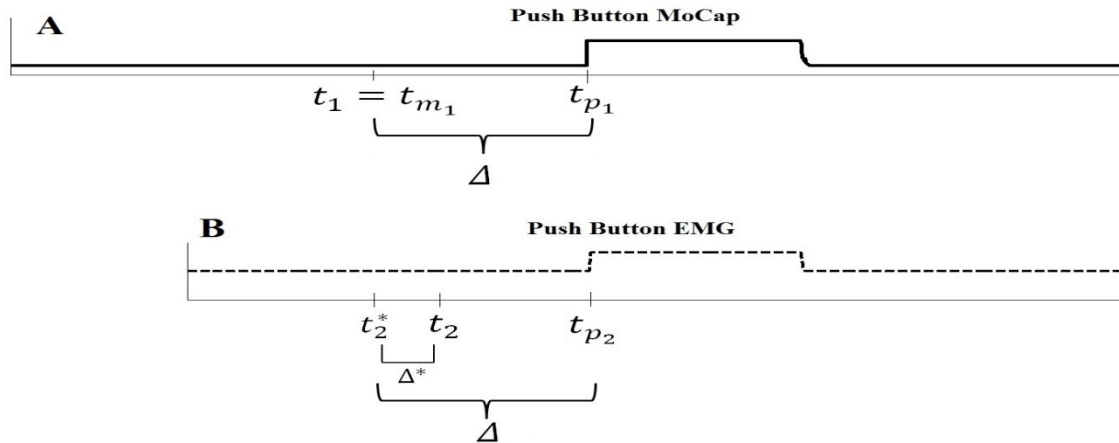


Figure 4. Identifying the synchronized start time in Signal #2 (A) and in Signal #4 (B). The synchronized start times (time = 0 seconds) in the MoCap and EMG signals (Signal #1 and Signal #3) are t_1 and t_2 , respectively. Δ^* is equal to or greater than zero and smaller than 1 ms.

3.1.6 Results and Discussion

All six participants completed the upper limb task. Exemplary acquired signals for Participant #1 and Participant #4 are shown in Figure 5 and Figure 6, respectively. Each of these figures shows: the MoCap Push Button signal (top plot); the EMG Push Button signal (second plot); the demeaned and rectified EMG signal of the left biceps brachii (third plot); and the vertical displacement of the left wrist as an average of the two wrist markers, with respect to the laboratory floor (bottom plot). The results for other participants are given in Appendix A.

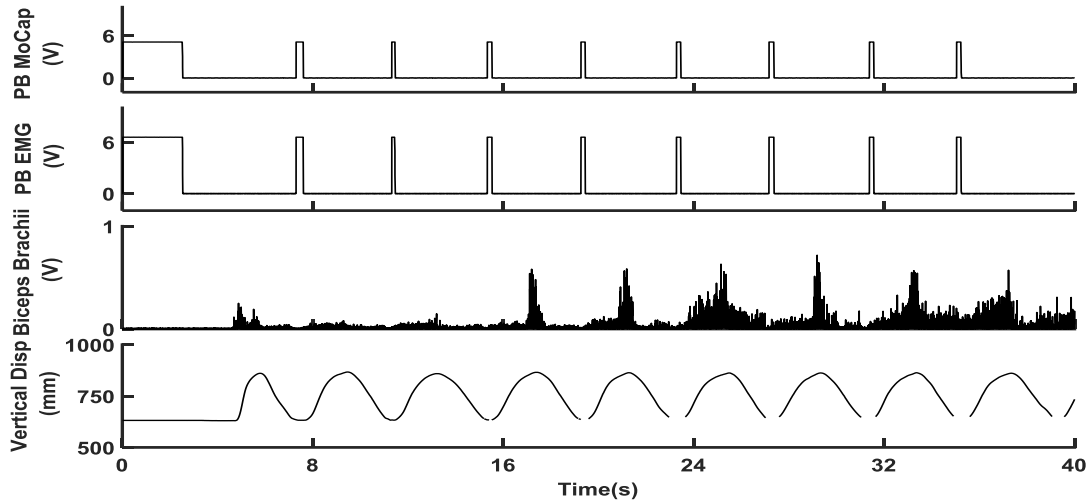


Figure 5. Exemplary experimental data from the third trial of Participant #1. The top subplot (PB MoCap) shows the MoCap Push Button signal; the second subplot (PB EMG) the EMG Push Button signal; the third subplot (Biceps Brachii) the rectified EMG signal of the left biceps brachii; and the bottom subplot (Vertical Disp.) the vertical displacement of the left wrist as an average of the two wrist markers (with respect to the laboratory floor).

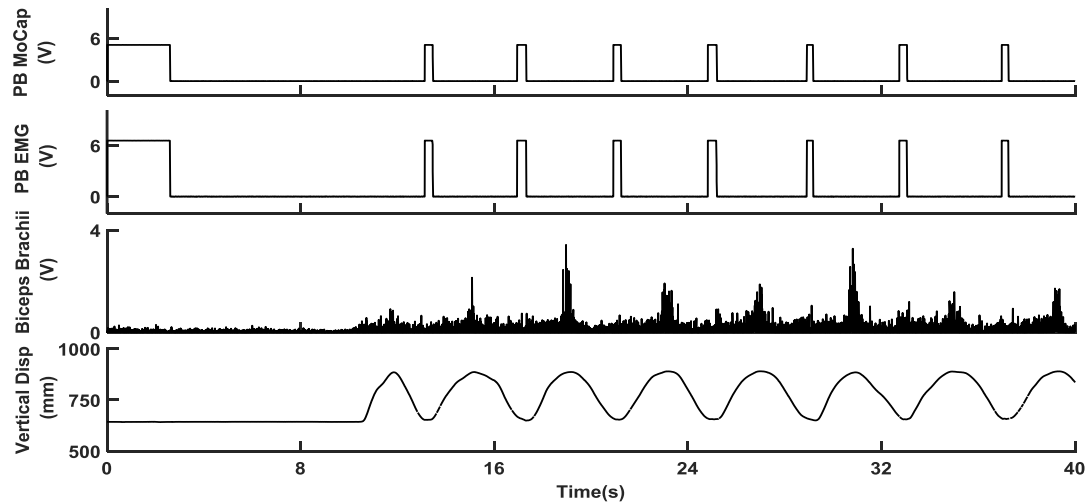


Figure 6. Exemplary experimental data from the first trial of Participant #4. The top subplot (PB MoCap) shows the MoCap Push Button signal; the second subplot (PB EMG) the EMG Push Button signal; the third subplot (Biceps Brachii) the rectified EMG signal of the left biceps brachii; and the bottom subplot (Vertical Disp.) the vertical displacement of the left wrist as an average of the two wrist markers (with respect to the laboratory floor).

A visual inspection was performed to evaluate the time synchronization procedure: exemplary rises in the push button signals (Signal #2 and Signal #4) after time synchronization are shown for the first trial of Participant #4 in Figure 7 (zoomed-in version of Figure 6). Since the sampling frequencies of the MoCap and EMG systems were different, a time shift of up to 1 ms was possible between the two signals (*see above*). The fact that the two rises occurred within 1 ms for all participants and trials (the maximum error) suggests that the synchronization procedure was implemented accurately. Furthermore, it was expected and verified that: (1) the push button signals *during* trial execution were aligned across the two systems (see Figure 5 and Figure 6; first and second subplots); (2) the push button signals occurred around the lowest vertical wrist position, i.e., at table height (see Figure 5 and Figure 6; first, second, and fourth subplots); and (3) the muscle activity increased when the dumbbell approached and reached the shoulder height (see Figure 5 and Figure 6; third and fourth subplots).

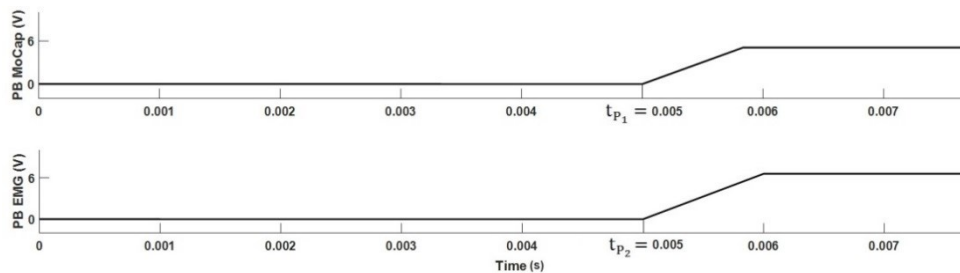


Figure 7. Exemplary push button signals for the MoCap and EMG systems after time synchronization, when focusing on the first rise in both systems (zoomed-in version of Figure 6). Since the sampling frequencies of the MoCap and EMG systems were different, a between-system time shift and, hence, synchronization error of up to 1 ms could be observed (this trial: 0 ms).

3.1.7 Conclusion and Limitations

The time synchronization procedure of the MoCap and EMG systems was technically validated, with the results from all participants and trials confirming its reliability. Therefore, the described synchronization procedure was applied to the data collected in the main experiment. It should be noted, however, that the push button signals of the two systems being sampled at different frequencies was a minor limitation (MoCap Push Button signal: 1,200 Hz; EMG Push Button

signal: 1,000 Hz). As a result, a small synchronization error of up to 1 ms could be present in spite of performing the correct time synchronization. Considering the nature of the obtained data in both this sub-study and the main experiments, a maximum potential error of 1 ms is negligible. Nonetheless, we decided to optimize the recording systems by changing the sampling frequencies for the motion capture and MoCap Push Button data to 100 Hz and 1,000 Hz, respectively, in the main experiments. As a consequence, no delay was introduced when the described synchronization procedure was applied to the experimental data of the main study (ultimately implying $t_1 = t_2$ in Figure 4).

3.2 Evaluation of MVC Exercises and MVC Value Identification Methods

3.2.1 Background and Rationale

As mentioned in Section 2.2.2, MVC is the most frequently used method to normalize EMG signals [147], [149], [150]. For eliciting maximum voluntary contractions in each trunk muscle being studied, various exercises have been reported. For example, the MVC exercises for the rectus abdominis and external oblique muscles can be grouped into sit-ups [46], [71], [75], [123], [140], [145], [161], [237]–[241], twist to the right and left [46], [71], [75], [98], [145], [140], [240], [161], [242]–[244], and right and left lateral bend [46], [98], [123], [140], [145], [161], [238], [245]. Trunk extensions are performed for back muscles such as the latissimus dorsi and erector spinae [46], [71], [123], [140], [145], [161], [237], [239]–[242], [244], [245]. MVC exercises are usually repeated 2 to 5 times, and EMG data from respective muscles are recorded for 3 to 5 seconds [68], [119], [130]. Resting breaks in between trials usually last for 30 to 120 seconds [72], [237], [246]. The maximum value of the EMG MVC signal as obtained via a chosen MVC identification method [145], [161], [163], [247] is then used for normalizing the participant-specific time series EMG data of a given experiment (*as described in detail in Section 2.2.2*).

Preliminary tests conducted in our laboratory suggest that there are multiple MVC exercise candidates for some of the muscles being targeted in the main experiment of this study. In addition, although several methods for identifying the actual MVC value from the EMG time series have

been reported in the literature [145], [161], [163], [247], their reliability (associated with low MVC variability across trials) has not been compared between methods. Therefore, conducting a preliminary study was required to evaluate the adequacy of different MVC exercise candidates and to determine the most reliable MVC value identification method.

3.2.2 Objective

The goal of this study was twofold: (1) to evaluate novel or secondary MVC exercise candidates *[EX1]* for the rectus abdominis, external oblique, and latissimus dorsi muscles against established MVC exercise candidates *[EX2]*, in terms of the elicited EMG magnitudes; and (2) to determine the most appropriate method for calculating the MVC value, in terms of its within-participant variability across different MVC trials.

3.2.3 Experimental Setup

Muscle activity data for the MVC exercises were recorded via a 16-channel Bagnoli™ EMG system (Delsys Inc., Natick, USA) and the standalone PowerLab 16/35 data acquisition system (ADInstruments, Sydney, Australia). The acquired analog EMG signals were amplified by a Bagnoli-16 EMG System amplifier (Delsys Inc.) and digitized at 1,000 Hz using the LabChart (ADInstruments) data acquisition software. MATLAB R2016a software was used to analyze the data.

3.2.4 Participants and Experimental Procedure

Six non-disabled male individuals were recruited to participate in this study (age: 29.3 ± 5.1 ; weight: 70.3 ± 10.3 ; height: 176.2 ± 5.7). For each participant and muscle being studied, the target location for each EMG electrode was first identified with a marker. Then, the skin above the selected muscles was shaved (if needed), cleaned with an alcohol swap, and then gently abraded with sand paper. Using adhesive interfaces for 2-bar sensors (Delsys Inc.), six surface EMG electrodes (Bagnoli™ 2-bar surface EMG sensors, Delsys Inc.) were placed bilaterally on the skin over the following muscles: (1) RA – 3 cm lateral of the umbilicus [42], [45]–[47], [239]; (2) ExO – 15 cm lateral of the umbilicus, aligned at 45 degrees off the vertical [42], [45]–[47], [239]; and

(3) LD – lateral of T9 (the ninth thoracic vertebra) over the muscle belly [42], [46], [47], [239]. Right muscles are denoted as RRA, RExO, and RLD, whereas left muscles are denoted as LRA, LExO, and LLD. In addition, two self-adhesive reference electrodes (Dermatode, Delsys Inc.) were placed on the left and right olecranon (the bony prominence at the very tip of the elbow). Note that the two references were pooled across the two subject-worn EMG boxes, serving as a single reference for all recorded muscle activities (as recommended by the manufacturer). To ensure stable electrode attachment throughout the experiments, the EMG electrodes were further secured using 3M Transpore™ tape.

Participants were asked to perform two different MVC exercises for each muscle according to a set of exercise-specific instructions. In addition, an instructor demonstrated how to perform each MVC exercise correctly. Three trials, each three seconds in length, were performed for each MVC exercise, and a resting break of 30 seconds [246] was given in between trials. The muscle-specific MVC exercises were as follows:

(1) Rectus Abdominis: *[EX1]* – The participant lied in supine position, with his hands behind the head and raised legs that were parallel and flexed at 45° at the hip joints, maintaining a knee joint angle of 90°. One assistant braced the trunk, keeping the chest aligned with the bench (supine), while another assistant applied resistance to the legs by pushing down just above the ankle joints. In this condition, the participant was instructed to maximally counter the trunk resistance while keeping his legs in starting position. *[EX2]* – The participant adopted a sit-up position on a bench with his hands positioned behind the head. The participant's torso was to be flexed to approximately 45° from the horizontal, with the knees and hips flexed at 90°. While one assistant braced his legs and ankles, another assistant applied manual resistance backwards at the participant's sternum. In this condition, the participant was instructed to maximally counter the trunk resistance [145], [241], [161], [243], [245].

(2) External Oblique: *[EX1]* – The participant adopted a sit-up position on a bench, with his hands positioned behind the head and an assistant bracing his ankles and legs. The participant was instructed to twist, with maximal effort, right (left) by flexing his trunk to approximately 45° and concurrently bringing his left (right) elbow to the right (left) knee. Another assistant resisted

this twisting motion by pulling the participant's left (right) shoulder backwards towards the bench [241], [243], [244]. **[EX2]** – The participant adopted a side plank position, placing his free arm across the chest, with the wrist on the opposite shoulder. One assistant was to secure the participant's feet, while another assistant was to apply a downward force at the participant's hip. In this condition, the participant bent his trunk upwards with maximal effort [245].

(3) Latissimus Dorsi: **[EX1]** – Two chairs were positioned a couple feet apart. The participant sat between them on the floor, with his shoulder abducted by 90° and the elbows flexed at 90°. The participant was instructed to raise his body with the arms with maximal effort (adducting the shoulder) while an assistant pushed down on his shoulders **[EX2]** – The participant lay supine, abducted his shoulder to 90°, and flexed his elbow to 90°. The participant then attempted to maximally adduct and internally rotate while holding to the edge of the bench with his opposite hand. An assistant resisted the targeted movement [145].

Note that, dependent on the muscle and exercise, EMGs were recorded from both body sides simultaneously (RA for both exercises and LD for *EX1*) or separately (ExO for both exercises and LD for *EX2*).

3.2.5 Data Processing and Analysis

For each MVC trial, the recorded EMG signal was first demeaned, to eliminate any DC components, and then rectified. The rectified EMG signal was then filtered using a 4th order, low-pass Butterworth filter at a cutoff frequency of 2.5 Hz [46], [140], [174]. The MVC activation level was calculated via four methods: (1) the maximum value of the rectified, unfiltered EMG signal was selected as the MVC value [248]; (2) the maximum value of the rectified, filtered EMG signal was selected as the MVC value [161]; (3) the average of the rectified, filtered EMG signal over a 0.5 second window centered at the signal peak was selected as the MVC value [161], [247], [163]; and (4) a 0.5 second moving average window was applied to the rectified, filtered EMG signal, and the largest mean value was selected as the MVC value [145]. For each method, the mean and standard deviation (SD) for three MVC trials were calculated.

A Wilcoxon signed-rank test was used to identify significant differences in the group means between the two MVC exercises for a given MVC identification method. In light of the small sample size ($n = 6$), a non-parametric test was chosen as we cannot be certain that the data are normally distributed. The significance level was set at 0.05 to prevent excessive false-positive results.

3.2.6 Results and Discussion

All six participants completed all required MVC exercises as described above. Exemplary EMG results for the right muscles – RRA, RExO, and RLD – are shown in Figure 8, Figure 9, and Figure 10, respectively (Participant #1). A visual inspection of the time series data suggests that MVC exercise #1 elicited higher EMG activities for RExO and RLD, whereas MVC exercise #2 elicited higher EMG activities for RRA.

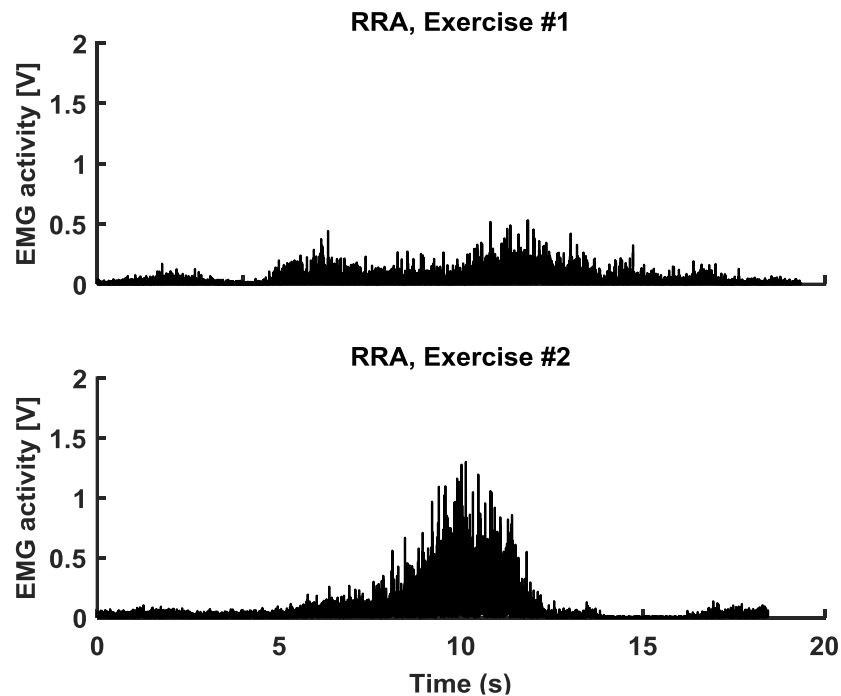


Figure 8. Exemplary rectified muscle activity for right rectus abdominis. Shown is the second MVC trial for Participant #1.

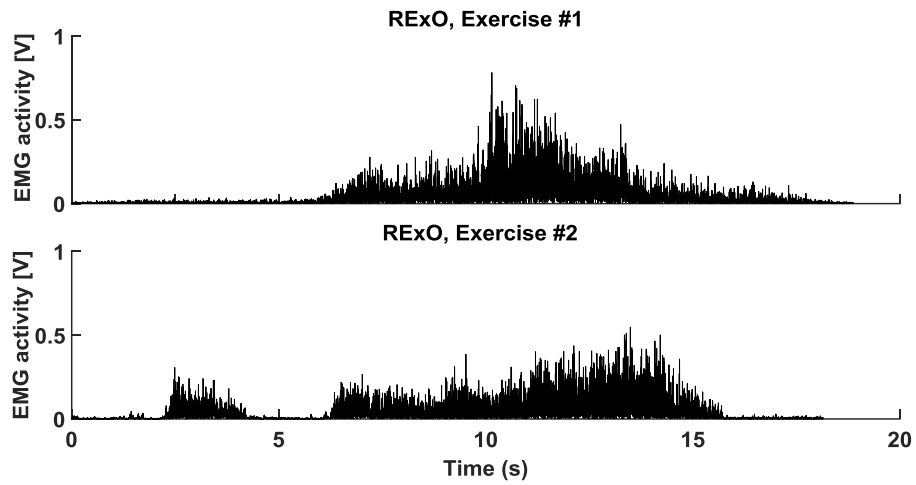


Figure 9. Exemplary rectified muscle activity for right external oblique. Shown is the third MVC trial for Participant #1.

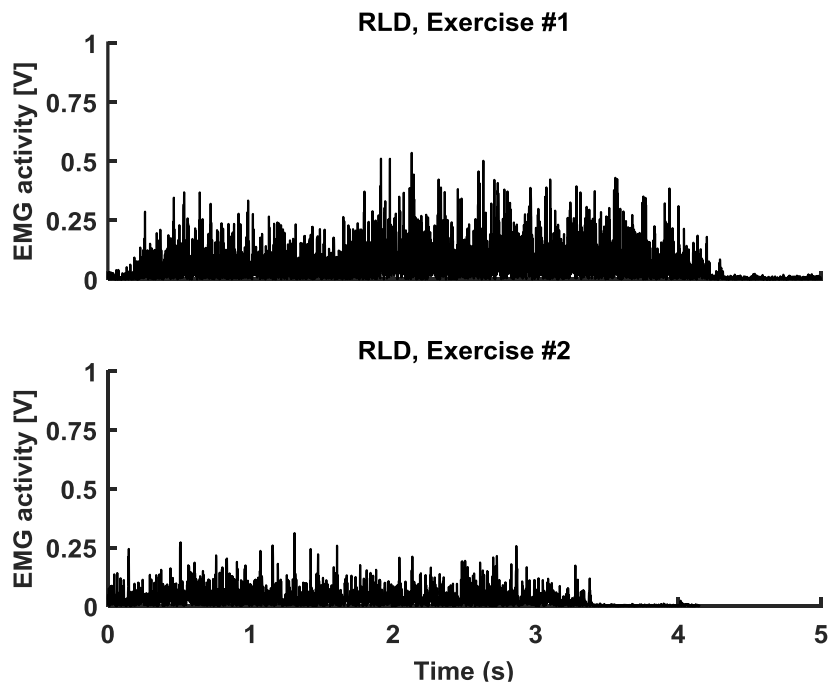


Figure 10. Exemplary rectified muscle activity for right latissimus dorsi. Shown is the third MVC trial for Participant #1.

Respective MVC values for Participant #1 (mean \pm SD for 3 trials), obtained via the four different calculation methods, are shown in Table 2 (RRA), Table 3 (RExO), and Table 4 (RLD). Note that the results for other participants and muscles are given in Appendix B.

Table 2. The MVC values of the two exercises for the right rectus abdominis. All values are presented as mean \pm SD across three trials. All values are in mV.

Right Rectus Abdominis (RRA)				
Participant #1	Method 1 (mV)	Method 2 (mV)	Method 3 (mV)	Method 4 (mV)
Exercise #1	578 \pm 162	102 \pm 8	91 \pm 8	92 \pm 8
Exercise #2	1,506 \pm 291	375 \pm 14	322 \pm 26	333 \pm 11

Table 3. The MVC values of the two exercises for the right external oblique. All values are presented as mean \pm SD across three trials. All values are in mV.

Right External Oblique (RExO)				
Participant #1	Method 1 (mV)	Method 2 (mV)	Method 3 (mV)	Method 4 (mV)
Exercise #1	815 \pm 28	218 \pm 18	194 \pm 13	197 \pm 16
Exercise #2	601 \pm 152	155 \pm 29	132 \pm 22	143 \pm 32

Table 4. The MVC values of the two exercises for the right latissimus dorsi. All values are presented as mean \pm SD across three trials. All values are in mV.

Right Latissimus Dorsi (RLD)				
Participant #1	Method 1 (mV)	Method 2 (mV)	Method 3 (mV)	Method 4 (mV)
Exercise #1	597 \pm 92	149 \pm 34	132 \pm 26	134 \pm 25
Exercise #2	301 \pm 57	60 \pm 8	52 \pm 9	55 \pm 9

Table 5 shows the group-ensemble results for all muscles, both muscle-specific MVC exercises, and all four MVC identification methods. Three main observations can be made: (1) for a given MVC identification method, the MVC magnitudes were comparable across the two exercises for some muscles (e.g., RRA), but not for others (e.g., RLD); (2) independent of the choice of muscle, the variability of MVC values across trials was in most cases comparable for both exercises and a given MVC identification method (except for RRA and LRA, Method 1; RExO, Method 2; and LExO, Method 4); and (3) independent of the choice of exercise and muscle, the MVC magnitude and the variability of MVC identification method 1 were generally larger than for the other three methods. However, for RExO and LExO (exercise #1), the variability for one other MVC identification method (RExO: Method 2; LExO: Method 4) was comparable to or larger than the one for MVC identification method 1.

The Wilcoxon signed-rank test revealed no significant differences between the two MVC exercises for both RRA and LRA and all MVC identification methods (Right – Method 1: $p = 0.688$; Method 2: $p = 0.844$; Method 3: $p = 0.844$; Method 4: $p = 0.844$; Left – Method 1: $p = 1.00$; Method 2: $p = 1.00$; Method 3: $p = 1.00$; Method 4: $p = 0.844$). Similarly, no significant differences between the two exercises were found for RExO and LExO and all MVC identification methods (Right – Method 1: $p = 0.219$; Method 2: $p = 0.094$; Method 3: $p = 0.219$; Method 4: $p = 0.313$; Left – Method 1: $p = 0.875$; Method 2: $p = 0.875$; Method 3: $p = 0.875$; Method 4: $p = 0.250$). For RLD, exercise #1 elicited significantly larger MVC values than exercise #2, and this for all MVC identification methods (Method 1: $p = 0.031$; Method 2: $p = 0.031$; Method 3: $p = 0.031$; Method 4: $p = 0.031$). For LLD, exercise #1 elicited significantly larger MVC values than exercise #2 for

Methods 1, 2, and 4 only (Method 1: $p = 0.031$; Method 2: $p = 0.031$; Method 3: $p = 0.063$; Method 4: $p = 0.031$).

Table 5. The MVC values for all muscles and the two chosen MVC exercises, calculated via 4 MVC value identification methods. All values are in mV and presented as mean \pm SD. In light of the participant-specific EMG normalization procedure, the standard deviations are presented as the means of the within-participant standard deviations, assessing the group-ensemble MVC value variability across participant trials.

Muscle	Exercise #1 (all in mV)				Exercise #2 (all in mV)			
	Method 1	Method 2	Method 3	Method 4	Method 1	Method 2	Method 3	Method 4
RRA	739 \pm 172	189 \pm 21	155 \pm 12	165 \pm 12	682 \pm 101	191 \pm 14	159 \pm 13	167 \pm 10
LRA	409 \pm 89	101 \pm 8	85 \pm 11	88 \pm 9	463 \pm 35	121 \pm 12	103 \pm 6	107 \pm 9
RExO	546 \pm 95	202 \pm 110	134 \pm 24	138 \pm 25	453 \pm 104	129 \pm 24	110 \pm 20	115 \pm 21
LExO	513 \pm 60	151 \pm 20	128 \pm 18	189 \pm 95	538 \pm 60	154 \pm 12	134 \pm 9	138 \pm 9
RLD	514 \pm 67	124 \pm 18	106 \pm 14	109 \pm 13	242 \pm 50	52 \pm 10	46 \pm 9	48 \pm 10
LLD	472 \pm 58	113 \pm 10	95 \pm 15	99 \pm 0.13	246 \pm 62	62 \pm 13	53 \pm 10	55 \pm 10

As mentioned above, Table 5 also suggests that, generally, MVC values obtained via MVC identification method 1 had greater variability in comparison to the other three methods – and this independent of the choice of MVC exercise and muscle. This can be explained by the fact that Method 1 selects the maximum peak of the *unfiltered* MVC time series as the MVC value; such unfiltered signal contains larger fluctuations due to noise than the *filtered* signal, which is used as a basis for MVC value identification in Methods 2 to 4. In other words, the signal used for Methods 1 may not reliably represent the underlying muscle activity, and intermittent spikes will likely have a significant effect on a given trial’s MVC value and its variability across trials. In addition, it can be seen that, regardless of MVC exercise and muscle, Methods 3 and 4 agree well with each other in terms of MVC magnitude and variability. This may be due to the fact that, for both methods,

the average of a 0.5 s window was used to calculate the MVC values from the filtered EMG signal: in one case, the window is centered at the signal peak (Method 3); in the other case, that particular window is chosen which gives the maximum MVC value (Method 4). With both methods reporting similar MVC values and variabilities, it can be speculated that Method 4 may choose a final window that is positioned close to the window in Method 3 (i.e., with the center of the window in Method 4 being close to the signal peak).

3.2.7 Conclusion

In this study, two different MVC exercises were performed for each of RA, ExO, and LD. In addition, four different methods were investigated for identifying the MVC value used for EMG data normalization. Since, for RA and ExO, no significant differences between the two respective MVC exercises were found, MVC exercises were selected based on previous use in the literature as well as ease-of-use and comfort. That is, for RA and ExO, exercise #2 and exercise #1 were chosen, respectively. In addition, exercise #1 was chosen for LD as it elicited larger MVC values than exercise #2 (see Table 5). To calculate final MVC values, MVC identification Method 4 was chosen due to its robustness across trials, its comparability with Method 3, and its previous use in the literature [145].

Chapter 4

4 Materials and Methods

4.1 Overview

Two sitting tasks with two different eye conditions (eyes open (EO) and eyes closed (EC)) were performed in this study. For the first task, “Perturbed Sitting”, postural perturbations were applied to the seated study participant using an unstable wobble board. For the second task, “Quiet Sitting”, the study participant was asked to maintain an upright posture during unperturbed sitting.

4.2 Participants

Fifteen non-disabled male individuals were recruited to participate in this study (age: 25 ± 5.2 years; height: 179.6 ± 6.7 cm; and weight: 75.1 ± 13.0 kg). Based on self-report, none of the participants had any history of neurological or musculoskeletal impairments or pain, gait or balance difficulties, or used a walking aid. All participants gave their written informed consent (see Appendices C and D) to participate in the study, whose experimental procedures were approved by the Health Research Ethics Board of the University of Alberta (Study ID: Pro00039437).

4.3 Experimental Setup

Two data acquisition systems were used in this study. Muscle activity data were recorded via a 16-channel Bagnoli™ EMG system (Delsys Inc., Natick, USA) and a PowerLab 16/35 data acquisition system (ADInstruments, Sydney, Australia). The acquired analog EMG signals were amplified by a Bagnoli-16 EMG System amplifier (Delsys Inc.) and digitized at 1,000 Hz using the LabChart (ADInstruments) data acquisition software. The EMG setup is shown in Figure 11.



Figure 11. The utilized EMG setup. Left: Powerlab 16/35 data acquisition system, the LabChart data acquisition software, and the EMG electrodes; right: the Bagnoli-16 EMG system amplifier.

Kinematic data were recorded using an eight-camera motion capture system (Eagle Digital Camera, Motion Analysis Corporation, Santa Rosa, USA) with a sampling rate of 100 Hz. The space in which the eight-camera motion capture system could capture was: 6.10 m (length) \times 1.83 m (width) \times 1.83 m (height). The locations of the cameras are shown in Figure 12.

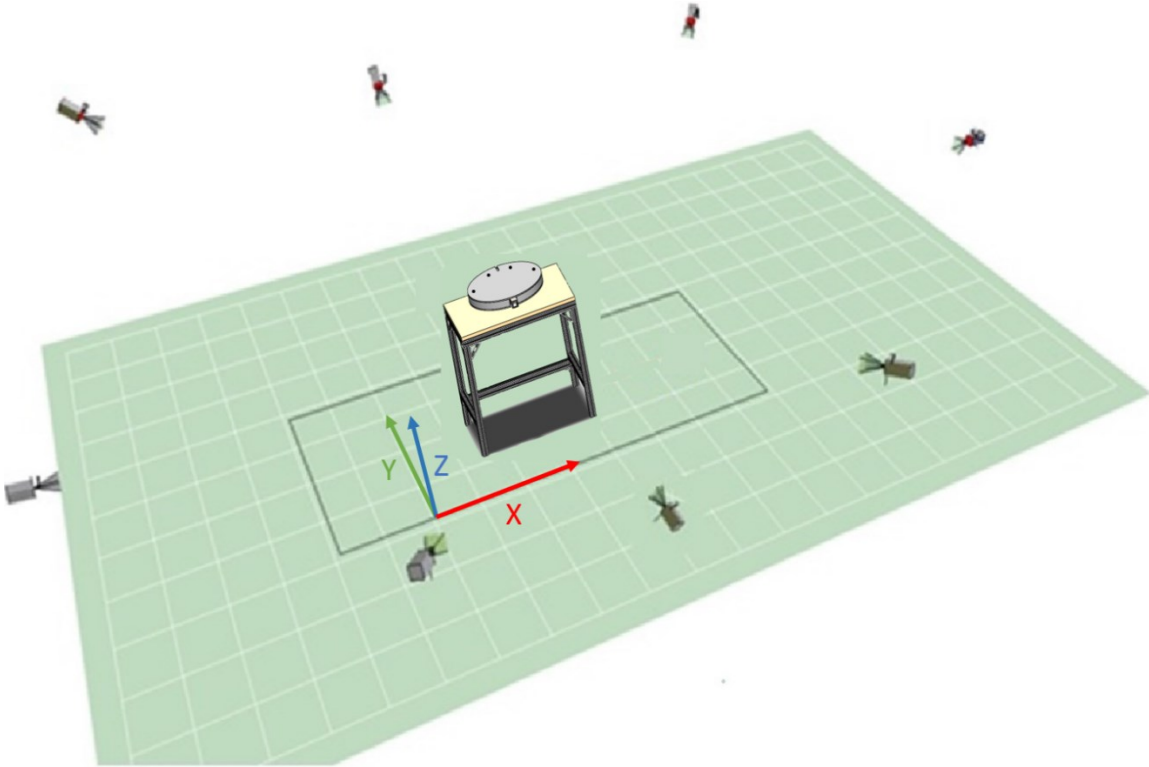


Figure 12. An eight-camera motion capture system was used to capture the motion of the trunk, pelvis and wobble board. The capture volume was: 6.10 m (length) \times 1.83 m (width) \times 1.83 m (height).

For the purpose of time synchronization, an MLA92 Push Button Switch (ADIInstruments) connected to both the MoCap and EMG systems was utilized. The push button produced an approximate 6 V output signal when the button was pressed (*see Section 3.1.3 for details*). A custom-made wobble board with a sitting surface of 0.185 m² (diameter of 48.5 cm) and a height of 5.08 cm was utilized to induce multi-directional, intrinsic perturbations. When using the term “perturbation” in this thesis document, we refer to such multi-directional, intrinsic perturbations that are elicited by the challenging postural environment induced by the wobble board. One of five hemispheres of different diameters could be attached to the bottom of the wobble board, inducing five different levels of seat instability. The spherical radii, curved heights and total height of the bases as well as their associated levels of difficulty are listed in Table 6.

Table 6. The spherical radii and curved heights of the wobble board bases as well as their associated levels of difficulty (level 1: very easy to level 5: very difficult).

Base	Spherical Radius (cm)	Curved Height (cm)	Total Height (cm)	Level of difficulty
Base #1	25	1.19	6.25	1
Base #2	20	1.51	6.25	2
Base #3	15	2.08	6.25	3
Base #4	13	2.47	6.25	4
Base #5	11	3.07	6.25	5

The wobble board was placed on a stool (width: 76.2 cm; depth: 55.9 cm; height: 71.0 cm). Figure 13 shows a model of the custom-made wobble board and stool as well as a photograph of the five different bases of the wobble board. The wobble board and base drawings used for machining are provided in Appendix E.

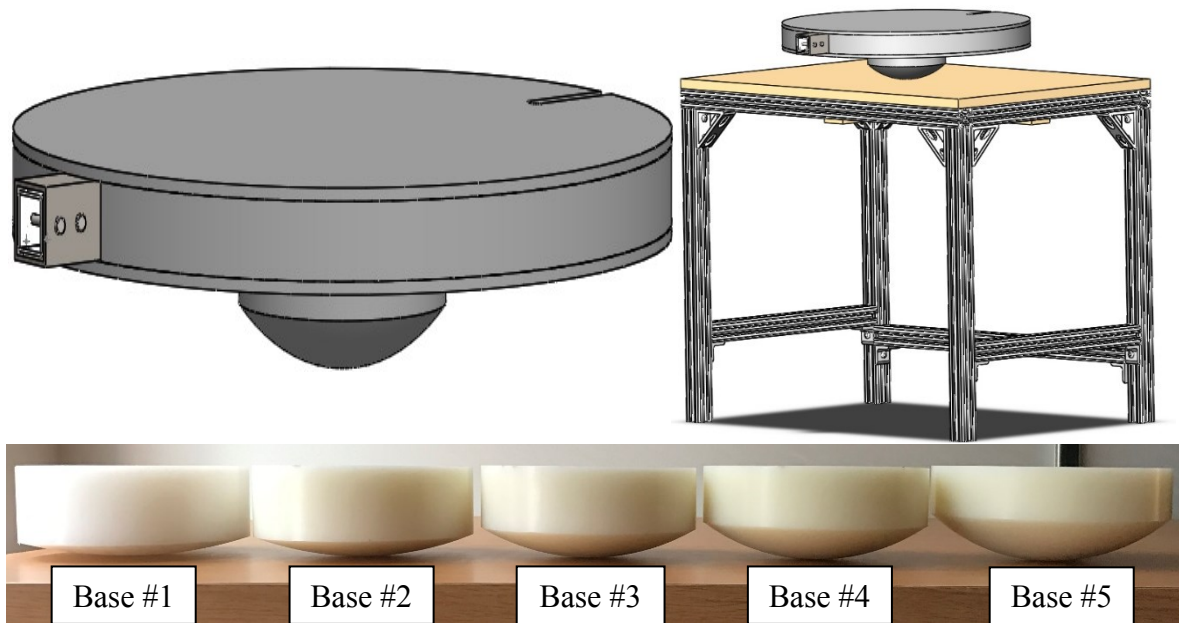


Figure 13. Models of the custom-made wobble board and stool as well as a photograph of the 5 different bases of the wobble board. Top left: the 3D model of the custom-made wobble board with a sitting surface of 0.185 m² (diameter of 48.5 cm); top right: the 3D model of the wobble board on the stool; bottom: a photograph of the five different bases of the wobble board. From left to right, Base #1 to Base #5 are shown. One of five hemispheres of different diameters could be attached to the bottom of the wobble board.

4.4 Experimental Procedure

4.4.1 EMG Setup and Recordings

For each participant and muscle being studied, the target location for each EMG electrode was first identified with a black marker. Then, the skin above the selected muscles was shaved if needed, cleaned with an alcohol swap, and then gently abraded with sand paper. Using adhesive interfaces for 2-bar sensors (Delsys Inc.), fourteen surface EMG electrodes (Bagnoli™ 2-bar surface EMG sensors, Delsys Inc.) were placed bilaterally on the skin over the following muscles: (1) RA – 3 cm lateral of the umbilicus, aligned vertically [42], [45]–[47], [239]; (2) ExO – 15 cm lateral of the umbilicus, aligned at 45 degrees off the vertical [42], [45]–[47], [239]; (3) LD – lateral of T9 (the ninth thoracic vertebra) over the muscle belly [42], [46], [47], [239]; (4) thoracic erector spinae (TES) – 5 cm lateral of T9, aligned vertically [42], [44], [47], [239]; (5) lumbar erector spinae (LES) – 3 cm lateral of L3 (the third lumbar vertebra), aligned vertically [42], [45], [47], [239], [249], [250]; (6) RF – at 50% on the line from the anterior superior iliac spine (ASIS) to the superior part of the patella [251]–[254]; and (7) BF – at 50% on the line between the ischial tuberosity and the lateral epicondyle of the tibia [253], [254]. Right muscles are denoted as RRA, RExO, RLD, RTES, RLES, RRF, and RBF, whereas left muscles are denoted as LRA, LExO, LLD, LTES, LLES, LRF, and LBF. In addition, two self-adhesive reference electrodes (Dermatode, Delsys Inc.) were placed on the left and right olecranon (the bony prominence at the very tip of the elbow). Note that the two references were pooled across the two participant-worn EMG boxes, serving as a single reference for all recorded muscle activities (as recommended by the manufacturer). To ensure stable electrode attachment throughout the experiments, the EMG electrodes were further secured using 3M Transpore™ tape. The location of the surface electrodes is shown in Figure 14.

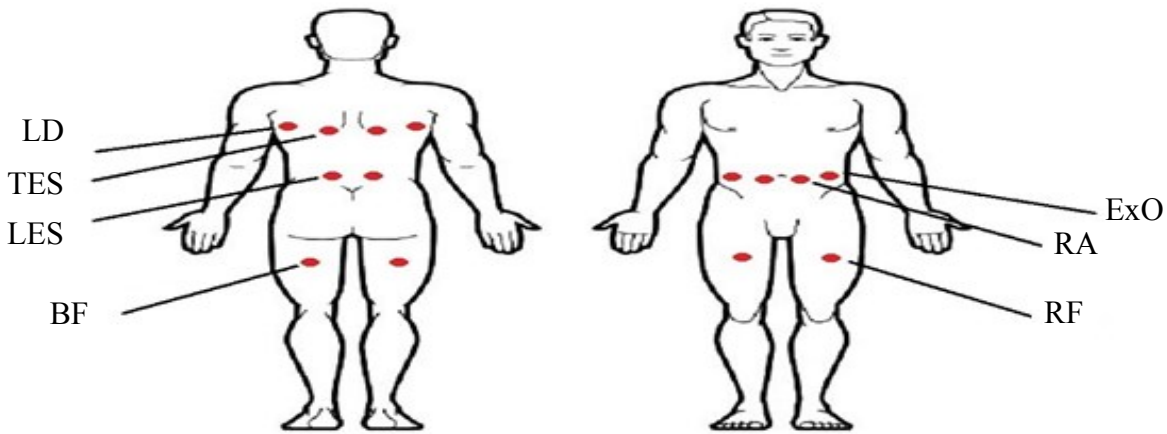


Figure 14. Back (left) and front (right) views of the location of the EMG electrodes. EMG electrodes were placed bilaterally on the muscles being studied. RA: rectus abdominis; ExO: external oblique; LD: latissimus dorsi; TES: thoracic erector spinae; LES: lumbar erector spinae; RF: rectus femoris; and BF: biceps femoris.

After fixating the EMG electrodes, each participant was given a tight t-shirt and shorts to wear. For collecting resting levels of muscle activity, the participant was then asked to “lie down on a bench in a supine position, with their eyes open, and to relax and not talk for 5 seconds”. Then, the participant was asked to perform an MVC exercise for each muscle according to a set of exercise-specific instructions. Three trials, each three seconds in length, were performed for each exercise, and a resting break of 30 seconds [246] was given in between trials. During and after each trial, the recorded EMG activity was monitored to confirm the quality of the signals.

The muscle-specific MVC exercises were as follows: (1) RA: The participant adopted a sit-up position on a bench with his hands positioned behind the head. The participant’s torso was to be flexed to approximately 45° from the horizontal, with the knees and hips flexed at 90° . While one assistant braced his legs and ankles, another assistant applied manual resistance backwards at the participant’s sternum. In this condition, the participant was instructed to maximally counter the trunk resistance [145], [241], [161], [243], [245]; (2) ExO: The participant adopted a sit-up position on a bench, with his hands positioned behind the head and an assistant bracing his ankles and legs. The participant was instructed to twist, with maximal effort, right (left) by flexing his trunk to approximately 45° and concurrently bringing his left (right) elbow to the right (left) knee.

Another assistant resisted this twisting motion by pulling the participant's left (right) shoulder backwards towards the bench [241], [243], [244]; (3) LD: Two chairs were positioned a couple feet apart. The participant sat between them on the floor, with his shoulder abducted and the elbows flexed at 90°. The participant was instructed to raise his body with the arms with maximal effort (adducting the shoulder) while an assistant pushed down on his shoulders; (4) TES and LES: the participant adopted the Biering-Sorenson position (prone with the iliac crests aligned at the edge of the bench so that the trunk was hanging off the edge), with his arms crossed over the chest. An assistant secured the legs and feet to the bench. The participant was instructed to maximally extend the trunk against a manual force applied by an assistant near the inferior border of the scapula [145], [161], [245], [255]; (5) RF: the participant sat on the bench with the edge of the bench lining up with his knee joint. The participant was to hold onto the edge of the bench and attempt to extend his knee by maximally contracting the quadriceps while an assistant held his lower leg in starting position (by holding it just superior of the ankle joint) [158]; (6) BF: the participant lied prone with one leg flexed at 45° while holding onto the edge of the bench with outstretched arms. One assistant braced the participant's pelvis while the other attempted to straighten the leg by pulling just superior of the ankle joint. The participant was to resist this attempt by maximally contracting the hamstrings [158]. The researcher provided verbal encouragement during MVC exercises. Figure 15 shows the MVC exercise performed for each muscle being studied.

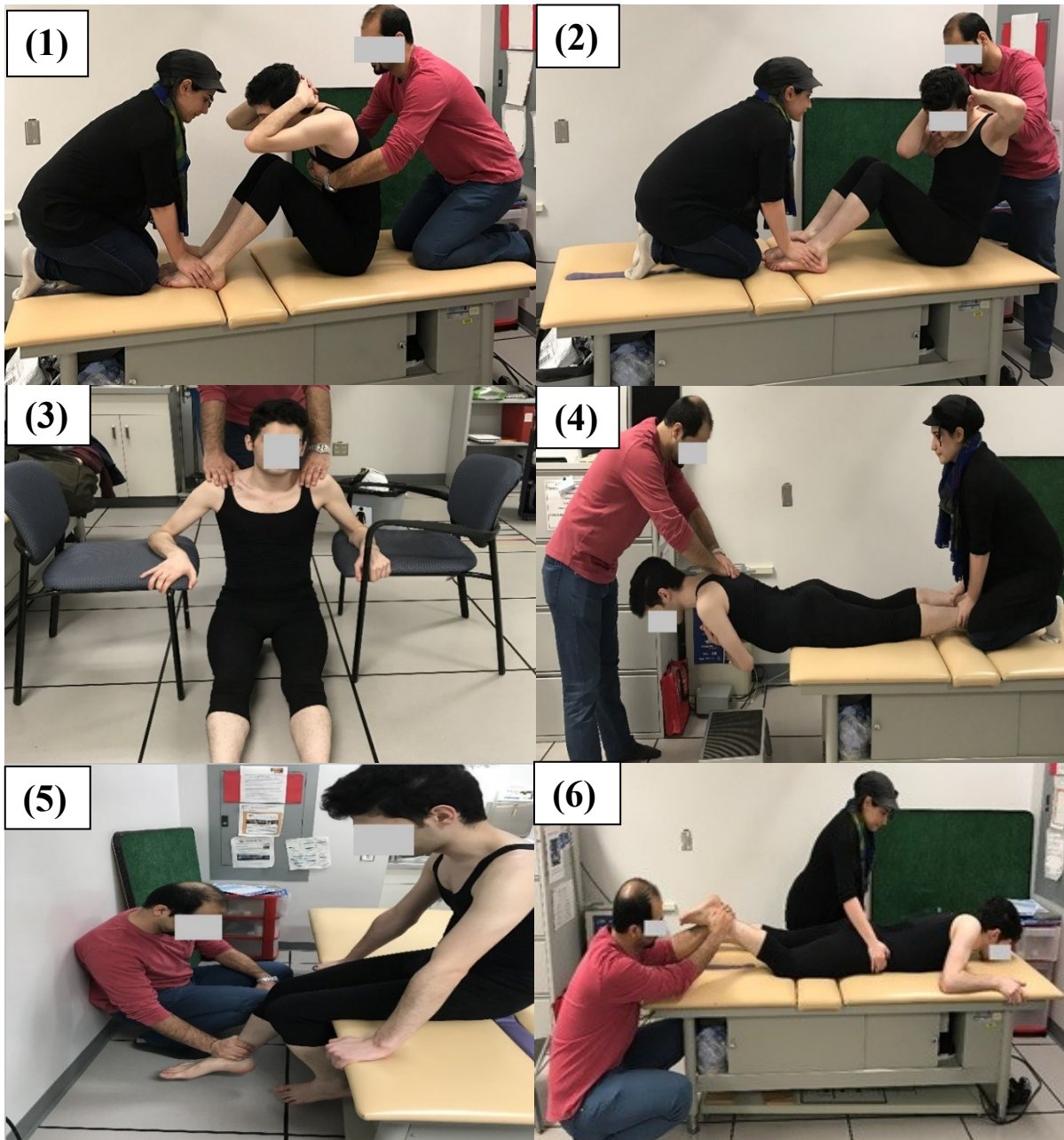


Figure 15. Photographs of the MVC exercises performed for the muscles being studied: (1) RA; (2) ExO; (3) LD; (4) TES and LES; (5) RF; and (6) BF.

4.4.2 Wobble Board Practice Trials

After performing the MVC exercises, the participant was asked to relax and lightly stretch his muscles. During this time, the wobble board was set up. The participant was then brought to the wobble board set up and was asked to practice balancing on the board. The purpose of this practice was threefold: (1) to allow the participant to familiarize himself with wobble board balancing; (2) to assess how well the participant balances on the wobble board with different bases; and (3) to reduce potential learning effects. As mentioned above, five different bases, attached to the bottom of the wobble board, were used to induce five different levels of difficulty (from Base #1: very easy to Base #5: very difficult).

The specific practice procedure was as follows: First, the participant was asked to sit on the wobble board with Base #1, put his hands on his stomach, and try to balance with eyes open for one minute. Then, he was asked to repeat the task with eyes closed. After performing the task for both eye conditions, Base #1 was replaced by Base #2 and the task repeated for each eye condition. While this procedure was repeated up until Base #5, preliminary tests found that it was not safe to use Base #4 and Base #5 with eyes closed. Therefore, these bases were not considered for the EC condition. Based on how well the participant balanced on the wobble board for each eye condition, the bases for the main study were chosen as follows: For EC, Base #1, Base #2, and potentially Base #3 (if the participant was able to balance on the board with this base) were used. For EO, Base #3, Base #4, and potentially Base #5 were used. If the participant was not able to balance well on the board with Base #5 and EO, Base #2 was used instead.

4.4.3 MoCap Setup and Recordings

After the practice procedure, eight MoCap markers (Motion Analysis Corporation, Santa Rosa, USA) were placed, using plastic marker bases and double-sided adhesive tape (VICON Corporation, Denver, USA), on the following anatomical landmarks: the seventh cervical vertebra (C7), the eighth thoracic vertebra (T8), the deepest point of the incisura jugularis (IJ), the processus xiphoideus (PX) [205], and bilaterally on the ASIS and posterior superior iliac spine (PSIS) [208]. The locations of the markers on the body as shown in Figure 16 were used to capture the kinematics of the trunk and pelvis during balancing.

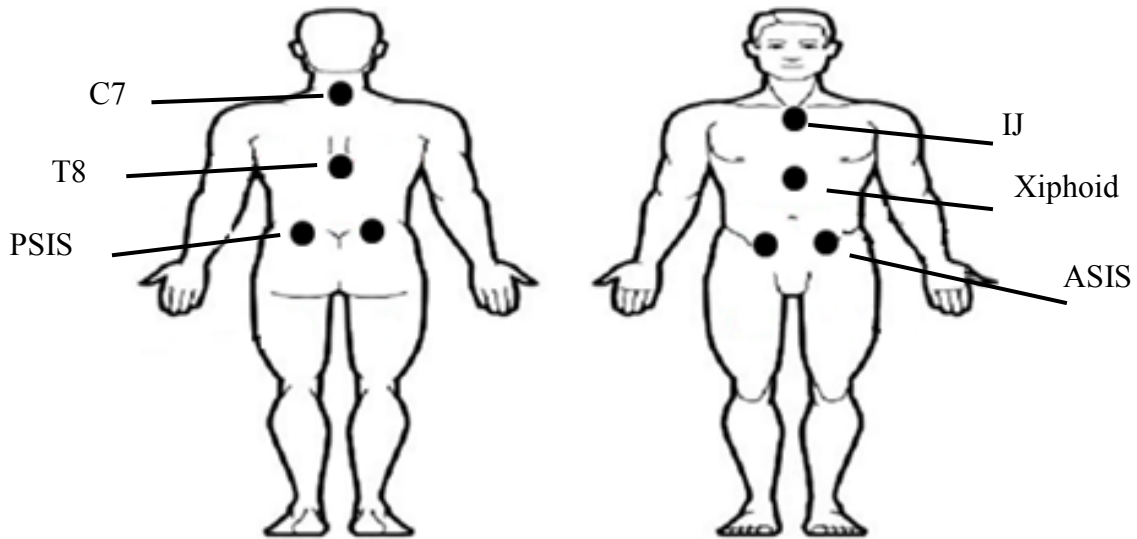


Figure 16. Back (left) and front (right) views of the location of MoCap markers. The markers were placed on the following anatomical landmarks: the seventh cervical vertebra (C7), the eighth thoracic vertebra (T8), the deepest point of the incisura jugularis (IJ), the processus xiphoideus (PX), and bilaterally on the anterior superior iliac spine (ASIS) and posterior superior iliac spine (PSIS).

Moreover, four markers were placed on the wobble board. The locations of the markers on the wobble board to capture the kinematics of the wobble board are shown in Figure 17. To ensure stable attachment of all markers throughout the experiments, the marker bases were further secured using Durapore™ tape.

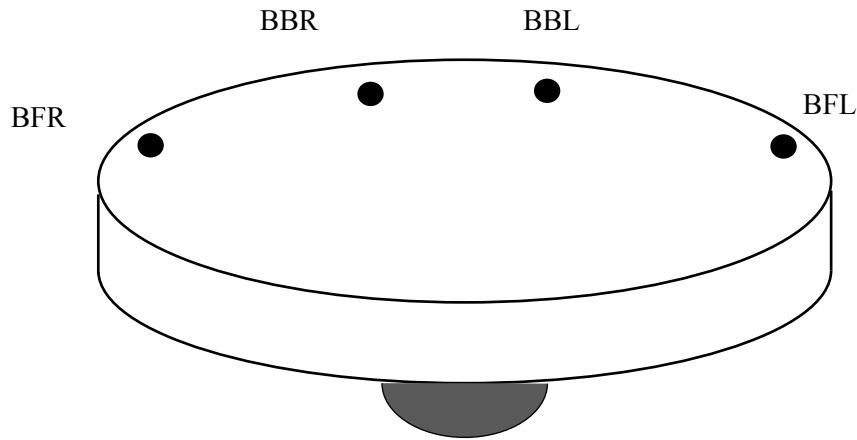


Figure 17. The location of the markers on the wobble board, with the participant facing the reader and the negative direction of the Y-axis of the laboratory coordinate system. BFR: board front right side; BBR: board back right side; BBL: board back left side; and BFL: board front left side.

4.4.4 Experimental Tasks

In the main experimental component of the study, each participant was asked to complete two tasks – a perturbation task and a quiet sitting task. For the perturbation task, each participant was instructed to sit on the wobble board and to “place the hands on the stomach, and try to maintain stability while keeping an upright posture”. The task was performed for both eye conditions, EC and EO, and the wobble board bases for each eye condition were chosen based on the practice trials described above. Four trials, each approximately 35 seconds in length, were performed for each base and eye condition, and a resting break of 30 seconds [246] was given in between trials. The order of performing the task with EO and EC was randomized such that some participants started with EC and some with EO.

For the quiet sitting task, each participant was instructed to sit on the wobble board without base attached, to “place the hands on the stomach and try to maintain stability while keeping an upright posture”. Note that sitting on the wobble board without base equals to quiet upright sitting on a stool. Two trials, each 60 seconds in length [91], were performed for each eye condition. A resting break of 30 seconds was given in between trials. For both the perturbation and quiet sitting tasks, the EMG and MoCap data were recorded at the previously specified sampling frequencies and time-stamped via the MLA92 Push Button Switch.

4.5 Experimental Data Processing

Using the push button signal, the EMG and MoCap signals were synchronized as described in Section 3.2. MATLAB R2016a and the SPSS software (SPSS Inc., Chicago, USA) were then used to process and analyze the synchronized EMG and MoCap signals (as described below).

4.5.1 Processing of EMG Data

For each MVC trial for a given muscle, the EMG signal collected from the MVC exercise was demeaned, rectified and then filtered using a 4th order, low-pass Butterworth filter with a cut-off frequency of 2.5 Hz [46], [140], [174]. A 200 ms moving average window was applied to the rectified and filtered EMG signal, and the largest mean value was selected as the MVC value [145]. The average MVC value from three MVC trials was then used to normalize the EMG data for a given muscle. This procedure was applied to all 14 muscles investigated in this study.

The synchronized EMG signals, collected during the wobble board study, were demeaned, rectified and then filtered as the MVC EMG data [46], [140], [174]. For subsequent analyses, a 30 second data segment was isolated for each trial, starting 1 second after the time stamp of the push button switch. The filtered EMG signals were then normalized for all muscles and trials using the following equation [168], [256]:

$$EMG_{NK} = \frac{EMG_{FK}}{Max_K} \times 100 \quad [\%] \quad (\text{Eq. 8})$$

where EMG_{NK} is the normalized EMG signal for muscle K, EMG_{FK} the filtered EMG signal for muscle K, and Max_K the MVC value for muscle K.

4.5.2 Processing of MoCap Data

4.5.2.1 Laboratory Coordinate System

Figure 12 above shows the orientation of the laboratory coordinate system. In relation to the experimental setup, the X-axis points to the left of the participant, the Y-axis points to the back of the participant, and the Z-axis points upward.

4.5.2.2 Wobble Board Local Coordinate System

Four markers were placed on the wobble board (Figure 17). The position of each marker over time was captured using the motion capture system. Since it was assumed that all four markers lie in the same plane and that the line between the front markers and the line between the back markers were parallel, any three markers may be used (Figure 18) to create a Local Coordinate System (LCS): (1) using the BBL, BFL, and BFR markers: the origin of the LCS was located at BFR, with the x-axis pointing medially from BFR to BFL, the z-axis pointing superiorly when defined as a vector perpendicular to the plane spanned by the x-axis and an auxiliary vector from BFR to BBL, and the y-axis pointing posteriorly when defined as the cross-product of the z- and x-axes; (2) using the BBR, BBL, and BFR markers: the origin of the LCS was located at BBR, with the x-axis pointing medially from BBR to BBL, the z-axis pointing superiorly when defined as a vector perpendicular to the plane spanned by an auxiliary vector from BBR to BFR and the x-axis, and the y-axis pointing posteriorly when defined as the cross-product of the z- and x-axes; (3) using the BFR, BFL, and BBR markers: the origin of the LCS was located at BFR, with the x-axis pointing medially from BFR to BFL, the z-axis pointing superiorly when defined as a vector perpendicular to the plane spanned by the x-axis and an auxiliary vector from BFR to BBR, and the y-axis pointing posteriorly when defined as the cross-product of the z- and x-axes; and (4) using the BBR, BBL, and BFL markers: the origin of the LCS was located at BBR, with the x-axis pointing medially from BBR to BBL, the z-axis pointing superiorly when defined as a vector perpendicular to the plane spanned by an auxiliary vector from BBR to BFL and the x-axis, and the y-axis pointing posteriorly when defined as the cross-product of the z- and x-axes. The locations and coinciding orientations of the LCSs of the wobble board are shown in Figure 18.

During experimental data recording, there may be instances when a single marker was visible by less than two cameras; as such, a procedure for reconstructing missing data had to be developed.

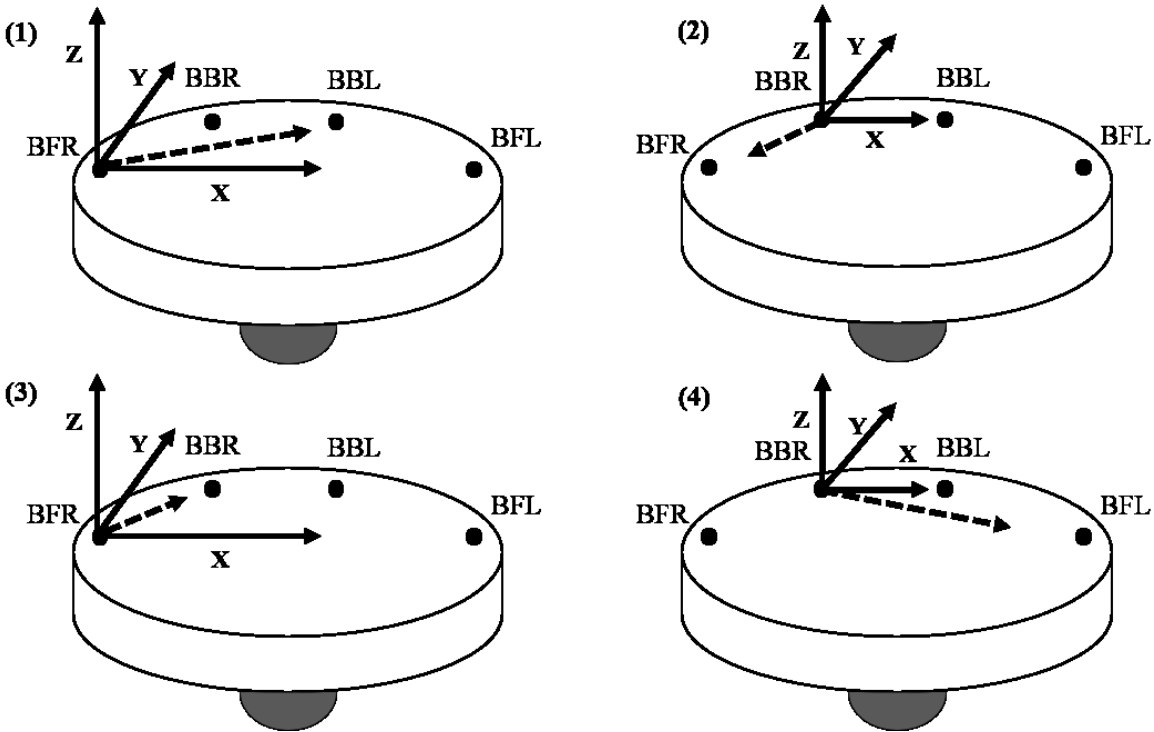


Figure 18. The orientation of the LCS of the wobble board using three markers: (1) using the BFR, BFL, and BBL markers; (2) using the BBR, BBL, and BFR markers; (3) using the BFR, BFL, and BBR markers; and (4) using the BBR, BBL, and BFL markers.

4.5.2.3 Reconstruction of Missing Markers

For reconstructing the missing data, a combination of three methods was used: (1) SELECT: selecting the three markers with the fewest missing samples; (2) INTERP: using cubic spline interpolation; and/or (3) SWITCH: using the 4th marker.

First, the three markers with the fewest missing samples throughout a given trial were selected to create the LCS (SELECT). Then, if remaining gaps for a given marker were shorter than five consecutive samples, cubic spline interpolation was employed to recover missing frames

(INTERP). The values of the missing samples can be estimated by fitting a cubic spline, constructed of a piecewise third-order polynomial, through the set of data points (samples) [257]. However, based on Nyquist's sampling theorem, a limit exists for the maximum number of consecutively missing samples that can be recovered via this method, without losing accurate information [258]. This theorem states that a signal should be sampled at a frequency that is at least twice as high as the maximum meaningful frequency component within that signal [3], [257]. Moreover, in agreement with the literature [259], the largest frequency component present in the MoCap signal was less than 10 Hz. Therefore, theoretically, the MoCap signal must be sampled at a minimum of 20 Hz. Since, in this study, the MoCap signal was sampled at 100 Hz (i.e., five times larger than the theoretical sampling frequency), the true signal can be reconstructed, via interpolation, if four or less consecutive samples were missing. Finally, if any remaining gap for a given marker was larger than four frames, the 4th marker was used to create the LCS for those frames (SWITCH).

It should be noted that, practically, 4 markers may almost never lie in the same plane; therefore, switching to the 4th marker may introduce some fluctuation in the kinematics. Moreover, frequent switching between default and redundant markers could slightly change the frequency spectrum of the signal. Furthermore, SWITCH cannot be used if there are two markers missing simultaneously. Therefore, INTERP was used before SWITCH whenever possible.

4.5.2.4 Pelvis and Trunk Local Coordinate Systems

In order to obtain the angle kinematics of the trunk and pelvis, two LCSs were defined (Figure 19). For the pelvis segment, the pelvis LCS was defined using the right ASIS (RASIS), the left ASIS (LASIS), and the right PSIS (RPSIS) markers: the origin was located at RASIS, with the x-axis pointing medially from RASIS to LASIS, the z-axis pointing superiorly when defined as a vector perpendicular to the plane spanned by the x-axis and an auxiliary vector from RASIS to RPSIS, and the y-axis pointing posteriorly when defined as the cross-product of the z- and x-axes.

For the trunk segment, the trunk LCS was defined using the T8, C7, and xiphoid markers: the origin was located at PX, with the y-axis pointing posteriorly from PX to T8, the x-axis pointing

left when defined as a vector perpendicular to the plane spanned by the y-axis and an auxiliary vector from PX to C7, and the z-axis pointing superiorly when defined as the cross-product of the x- and y-axes. The locations and orientations of the pelvis LCS and trunk LCS are shown in Figure 19.

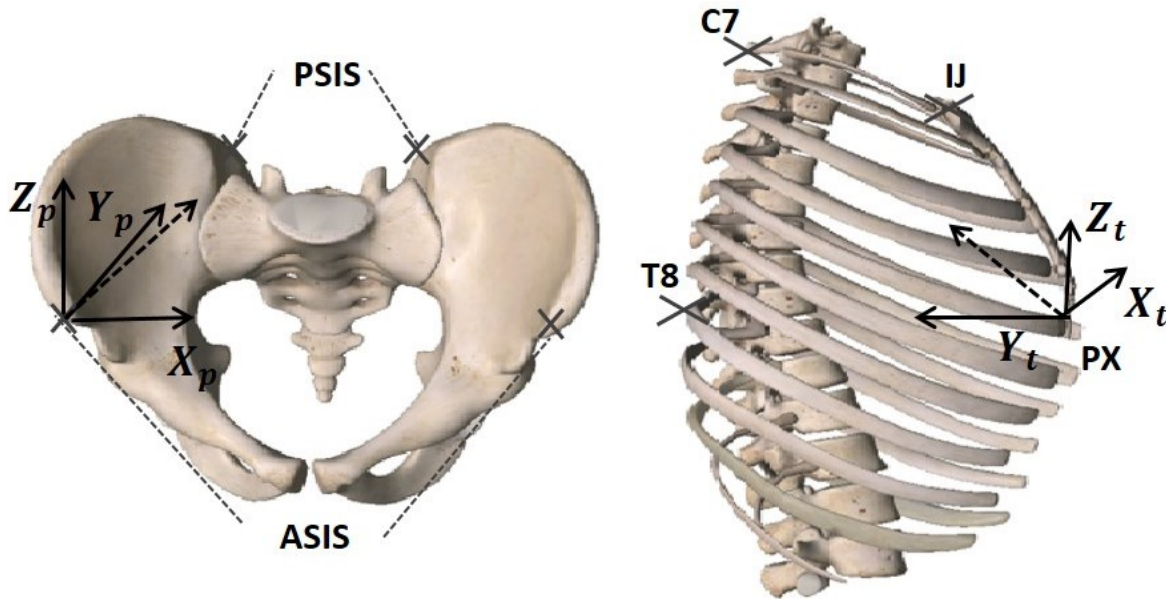


Figure 19. The orientation of the LCS for the pelvis (left) and trunk (right) segments. For the pelvis LCS (left): the origin was located at RASIS, with the x-axis pointing medially from RASIS to LASIS, the z-axis pointing superiorly when defined as a vector perpendicular to the plane spanned by the x-axis and an auxiliary vector from RASIS to RPSIS, and the y-axis pointing posteriorly when defined as the cross-product of the z- and x-axes. For the trunk LCS (right): the origin was located at PX, with the y-axis pointing posteriorly from PX to T8, the x-axis pointing left when defined as a vector perpendicular to the plane spanned by the y-axis and an auxiliary vector from PX to C7, and the z-axis pointing superiorly when defined as the cross-product of the x- and y-axes. Figures obtained from “Essential Skeleton 4” mobile application software.

4.5.2.5 Wobble Board Angular Kinematics

After constructing local coordinate systems for each segment, the wobble board angles in the anterior-posterior (AP) and medial-lateral (ML) directions with respect to the lab coordinate

system were calculated. The AP tilt angle (α) and ML tilt angle (β) were derived from the z-component of the local y- and x-unit vectors in the laboratory coordinate system, respectively (Figure 20).

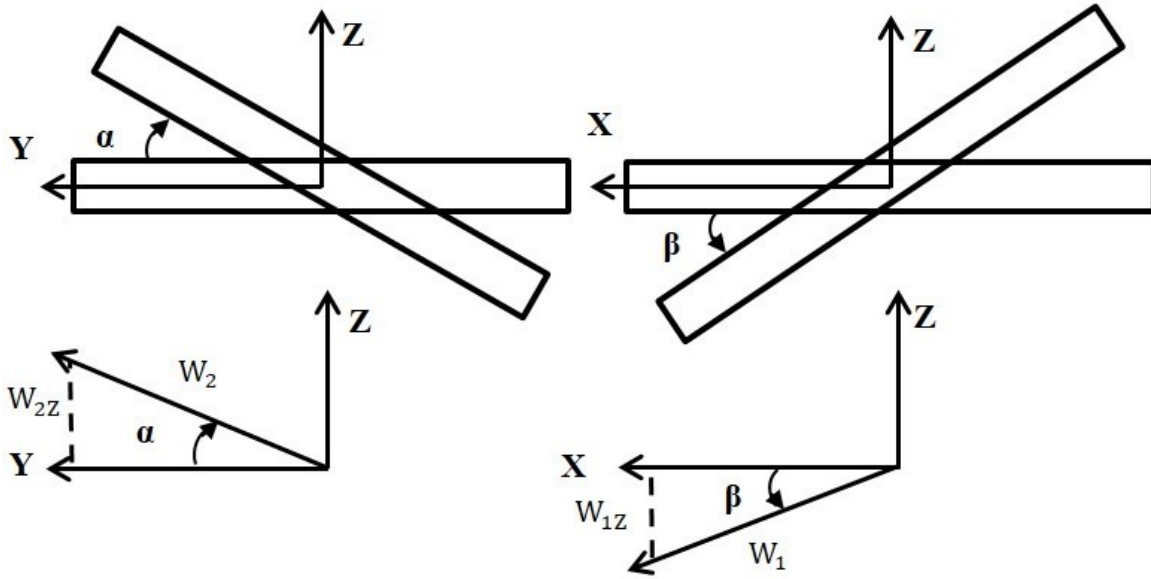


Figure 20. The AP tilt angle (α) and ML tilt angle (β) were calculated by using the z-component of the local y- and x-unit vectors in the laboratory coordinate system, respectively.

The z-component of the local y-unit vector was geometrically associated with the AP tilt (Eq. 9), whereas the z-component of the local x-unit vector was geometrically associated with the ML tilt (Eq. 10):

$$\alpha = \arcsin\left(\frac{W_{2Z}}{W_2}\right) = \arcsin\left(\frac{W_{2Z}}{1}\right) \quad (\text{Eq. 9})$$

$$\beta = -\arcsin\left(\frac{W_{1Z}}{W_1}\right) = -\arcsin\left(\frac{W_{1Z}}{1}\right) \quad (\text{Eq. 10})$$

Positive AP tilt (α) represents a wobble board rotation to the front, and positive ML tilt (β) represents a wobble board rotation to the left of the participant. The AP and ML tilt angles (i.e., α and β , respectively) are shown in Figure 21.

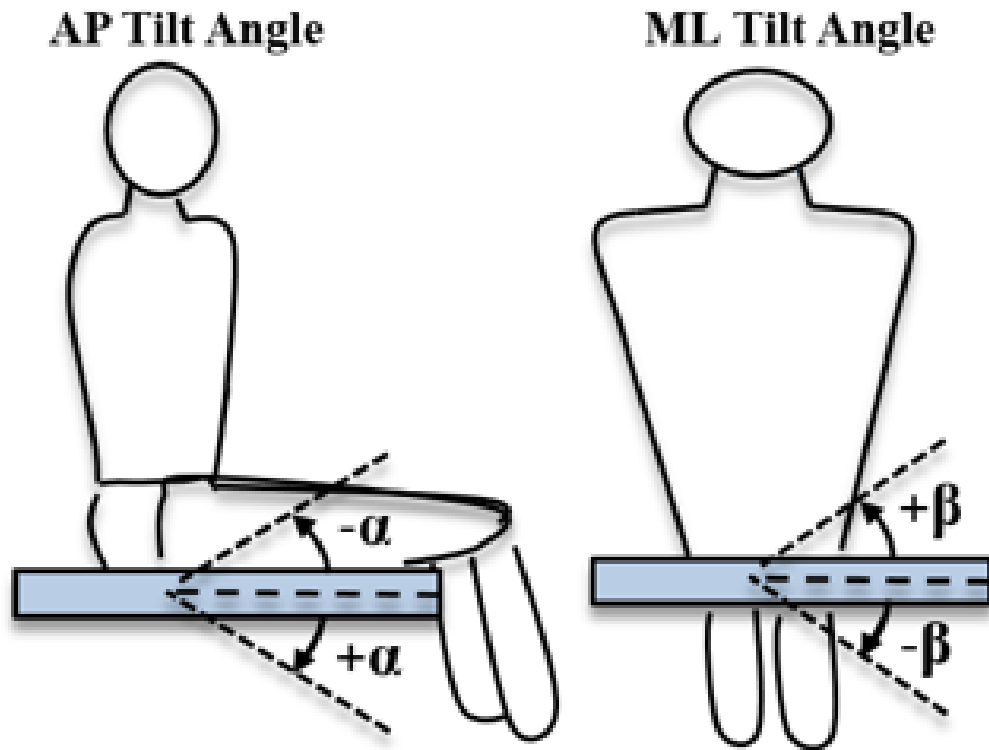


Figure 21. The wobble board tilt in AP (left) and ML (right) directions. Left: side view of the participant on the wobble board. A positive AP tilt angle represents a wobble board rotation to the front; Right: back view of the participant on the wobble board. A positive ML tilt angle represents a wobble board rotation to the left of the participant.

AP and ML wobble board tilt time series were then filtered using a 4th-order, low-pass Butterworth filter with a cut-off frequency of 2.5 Hz [93]. Moreover, the overall board tilt magnitude (TM) and the overall wobble board tilt direction (TD), shown in Figure 22, were calculated.

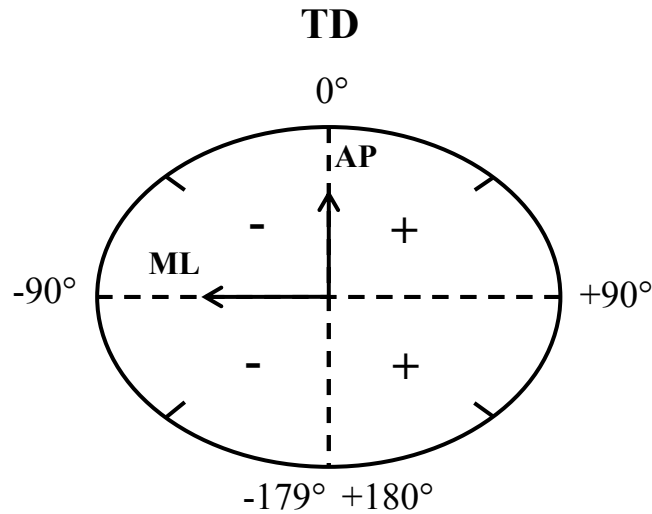


Figure 22. The wobble board's tilt direction (TD). The left-hand side of the wobble board represents the negative angles (ranging from -179° to 0°), and the right-hand side of the wobble board represents the positive angles (ranging from 0° to 180°).

The following equations were used to calculate TM and TD from the filtered AP and ML wobble board tilt time series:

$$\begin{aligned}
 TM &= \sqrt{AP^2 + ML^2} \\
 TD &= \text{Atan2}(-ML, AP)
 \end{aligned}
 \tag{Eq. 11}$$

For subsequent analyses, a 30-second data segment (from 1 to 31 seconds) was isolated for each trial.

4.5.2.6 Trunk and Pelvis Angular Kinematics

The pelvis and trunk data were first calibrated to align the local coordinate systems of the pelvis and trunk with the laboratory coordinate system [260]: first, two calibration matrices describing the orientation of the pelvis and trunk local coordinate systems during quiet sitting with respect to the laboratory were calculated. Then, for each time sample of the pelvis and trunk time series data,

the original LCS were designated the provisional coordinate systems. Finally, the pelvis and trunk coordinate systems were calculated by multiplying their provisional coordinate systems with their calibration matrices for each time sample. These pelvis and trunk coordinate systems were then the final LCSs of the pelvis and trunk segments, respectively, and were used for subsequent calculations [260].

After the calibration, the 3D pelvis angles, relative to the wobble board, were extracted using a Cardan rotation sequence: axial rotation (Υ) – lateral bending (β) – flexion/extension (α) (yaw, roll, and pitch) about the fixed axes of wobble board coordinate system; or flexion/extension – lateral bending – axial rotation (pitch, roll, and yaw) about the moving axes of pelvis coordinate system (Eq. 12) [261]. Similarly, the 3D trunk angles, relative to the pelvis, were extracted using a Cardan rotation sequence: axial rotation – lateral bending – flexion/extension (yaw, roll, and pitch) about the fixed axes of the pelvis coordinate system; or flexion/extension – lateral bending – axial rotation (pitch, roll, and yaw) about the moving axes of the trunk coordinate system (Eq. 12) [261].

$$\begin{aligned}
 \alpha &= \text{Atan2}\left(\frac{-r_{23}}{\cos\beta}, \frac{r_{33}}{\cos\beta}\right) \\
 \beta &= \text{Atan2}(r_{13}, \sqrt{r_{23}^2 + r_{33}^2}) \\
 \Upsilon &= \text{Atan2}\left(\frac{-r_{12}}{\cos\beta}, \frac{r_{11}}{\cos\beta}\right)
 \end{aligned}
 \tag{Eq. 12}$$

where $\text{Atan2}(y, x)$ computes $\tan^{-1}(y/x)$, but uses the signs of both x and y to determine in which quadrant the angle falls [215].

4.6 Data Analysis

Only the wobble EMG recordings and wobble board kinematics were analyzed as the analysis and interpretation of the trunk and pelvis kinematics was outside the scope of this thesis research. Analyses were performed, as described below, using the MATLAB R2016a software.

4.6.1 Posturographic Measures

The AP, ML, TM, and TD time series were quantified using time and frequency-domain measures: the mean angle (MA), which is the mean absolute value of each time series; the root mean square amplitude of the angle (RMSA); the mean of the absolute angular velocity (MV); the root mean square amplitude of the angular velocity (RMSV); the range (RANGE); the centroidal frequency (CFREQ), which is the frequency at which the spectral mass is concentrated; and the frequency dispersion (FREQD), which is a unit-less measure of the variability in the frequency content [262], [263]. The time series (i.e., AP, ML, TM, and TD) were first demeaned [262] using the following calculations:

$$\begin{aligned}
 AP_{[n]} &= AP_{0[n]} - \frac{1}{N} \sum AP_{0[n]} \\
 ML_{[n]} &= ML_{0[n]} - \frac{1}{N} \sum ML_{0[n]} \\
 TM_{[n]} &= TM_{0[n]} - \frac{1}{N} \sum TM_{0[n]} \\
 TD_{[n]} &= TD_{0[n]} - \frac{1}{N} \sum TD_{0[n]}
 \end{aligned} \tag{Eq. 13}$$

where AP_0 , ML_0 , TM_0 , and TD_0 are the filtered time series and N is the number of data points. All summations are from 1 to N . Then, MA was calculated using the following equations [262]:

$$\begin{aligned}
 MA_{AP} &= \frac{1}{N} \sum |AP_{[n]}| \\
 MA_{ML} &= \frac{1}{N} \sum |ML_{[n]}| \\
 MA_{TM} &= \frac{1}{N} \sum |TM_{[n]}| \\
 MA_{TD} &= \frac{1}{N} \sum |TD_{[n]}|
 \end{aligned} \tag{Eq. 14}$$

RMSA, which is the standard deviation of each time series, was calculated using the equations below [262]:

$$RMSA_{AP} = \sqrt{\frac{1}{N} \sum AP_{[n]}^2}$$

$$\text{RMSA}_{\text{ML}} = \sqrt{\frac{1}{N} \sum \text{ML}_{[n]}^2} \quad (\text{Eq. 15})$$

$$\text{RMSA}_{\text{TM}} = \sqrt{\frac{1}{N} \sum \text{TM}_{[n]}^2}$$

$$\text{RMSA}_{\text{TD}} = \sqrt{\frac{1}{N} \sum \text{TD}_{[n]}^2}$$

MV is the mean of the absolute angular velocity of each time series and is calculated using the following expressions [262]:

$$\begin{aligned} \text{MV}_{\text{AP}} &= \frac{\sum_{n=1}^{N-1} |\text{AP}_{[n+1]} - \text{AP}_{[n]}|}{T} \\ \text{MV}_{\text{ML}} &= \frac{\sum_{n=1}^{N-1} |\text{ML}_{[n+1]} - \text{ML}_{[n]}|}{T} \\ \text{MV}_{\text{TM}} &= \frac{\sum_{n=1}^{N-1} |\text{TM}_{[n+1]} - \text{TM}_{[n]}|}{T} \\ \text{MV}_{\text{TD}} &= \frac{\sum_{n=1}^{N-1} |\text{TD}_{[n+1]} - \text{TD}_{[n]}|}{T} \end{aligned} \quad (\text{Eq. 16})$$

where T is the time length of the experiment. RMSV, which is the standard deviation of the angular velocity for each time series, is calculated using the equations below [262]:

$$\begin{aligned} \text{RMSV}_{\text{AP}} &= \sqrt{\frac{1}{N} \sum \text{MV}_{\text{AP}}^2} \\ \text{RMSV}_{\text{ML}} &= \sqrt{\frac{1}{N} \sum \text{MV}_{\text{ML}}^2} \\ \text{RMSV}_{\text{TM}} &= \sqrt{\frac{1}{N} \sum \text{MV}_{\text{TM}}^2} \\ \text{RMSV}_{\text{TD}} &= \sqrt{\frac{1}{N} \sum \text{MV}_{\text{TD}}^2} \end{aligned} \quad (\text{Eq. 17})$$

RANGE, which is the difference between the largest and the smallest values in each time series, is calculated using the following expression:

$$\begin{aligned}
\text{RANGE}_{\text{AP}} &= \max_{\text{AP}} - \min_{\text{AP}} \\
\text{RANGE}_{\text{ML}} &= \max_{\text{ML}} - \min_{\text{ML}} \\
\text{RANGE}_{\text{TM}} &= \max_{\text{TM}} - \min_{\text{TM}} \\
\text{RANGE}_{\text{TD}} &= \max_{\text{TD}} - \min_{\text{TD}}
\end{aligned} \tag{Eq. 18}$$

The frequency-domain measures (i.e., CFREQ and FREQD) were calculated for all time series (i.e., AP, ML, TM, and TD). The measures were calculated for the frequency range from 0.01 to 5 Hz, with i and j in Eq. 19 providing these limits. Δf is the frequency increment in the discrete power spectral density estimate, $G[m]$. These measures were calculated based on the spectral moment, u_k , using the following equation:

$$\begin{aligned}
u_{k,\text{AP}} &= \sum_{m=i}^j (m\Delta f)^k G_{\text{AP}}[m] \\
u_{k,\text{ML}} &= \sum_{m=i}^j (m\Delta f)^k G_{\text{ML}}[m] \\
u_{k,\text{TM}} &= \sum_{m=i}^j (m\Delta f)^k G_{\text{TM}}[m] \\
u_{k,\text{TD}} &= \sum_{m=i}^j (m\Delta f)^k G_{\text{TD}}[m]
\end{aligned} \tag{Eq. 19}$$

where $k = 0,1,2$. Finally, CFREQ and FREQD were calculated using the following calculations:

$$\begin{aligned}
\text{CFREQ}_{\text{AP}} &= \sqrt{\frac{u_{2,\text{AP}}}{u_{0,\text{AP}}}} \\
\text{CFREQ}_{\text{ML}} &= \sqrt{\frac{u_{2,\text{ML}}}{u_{0,\text{ML}}}} \\
\text{CFREQ}_{\text{TM}} &= \sqrt{\frac{u_{2,\text{TM}}}{u_{0,\text{TM}}}} \\
\text{CFREQ}_{\text{TD}} &= \sqrt{\frac{u_{2,\text{TD}}}{u_{0,\text{TD}}}}
\end{aligned} \tag{Eq. 20}$$

$$\begin{aligned}
\text{FREQD}_{\text{AP}} &= \sqrt{1 - \frac{u_{1,\text{AP}}^2}{u_{0,\text{AP}} u_{2,\text{AP}}}} \\
\text{FREQD}_{\text{ML}} &= \sqrt{1 - \frac{u_{1,\text{ML}}^2}{u_{0,\text{ML}} u_{2,\text{ML}}}} \\
\text{FREQD}_{\text{TM}} &= \sqrt{1 - \frac{u_{1,\text{TM}}^2}{u_{0,\text{TM}} u_{2,\text{TM}}}} \\
\text{FREQD}_{\text{TD}} &= \sqrt{1 - \frac{u_{1,\text{TD}}^2}{u_{0,\text{TD}} u_{2,\text{TD}}}}
\end{aligned} \tag{Eq. 21}$$

For each participant and time series (i.e., AP, ML, TM, and TD), all measures were calculated and averaged across four trials (same eye condition and wobble board base). Then, for each measure, a Wilcoxon signed-rank test was used to assess whether there are any significant differences in the group means between: (1) Base #1 and Base #2 for EC; (2) Base #3 and Base #4 for EO; and (3) EC and EO for Base #2. The significance level was set at 0.05 to prevent excessive false-positive results. A non-parametric test (Wilcoxon signed-rank) was chosen over the equivalent parametric test since the Shapiro-Wilk test revealed that not all identified measures were normally distributed.

4.6.2 Cross-Correlation

Cross-correlation (CC) analysis between EMG and MoCap was performed to quantify the relationship between trunk muscle activity and wobble board motion. This analysis required that MoCap and EMG signals had the same sampling rate. Therefore, the sampling rate of the filtered EMG signals was down-sampled to 100 Hz. The CC analysis was performed in four steps (Figure 23): first, for each direction of the board tilt (i.e., anterior (ANT) *or* posterior (POST) for AP; right (RIGHT) *or* left (LEFT) for ML), the three largest peaks in the MoCap signal were identified. Second, a 4-second window centered at each peak was created. Third, time-matched, corresponding 4-second windows were created in the down-sampled EMG signal. These windows were centered at the same time samples where the largest MoCap peaks occurred. Then, each of these segments (i.e., the 4-second window centered at each peak in the MoCap signal and its time-matched 4-second window in the down-sampled EMG signal) was demeaned and cross-correlated. Finally, the obtained cross-correlation functions (CCF) were averaged for each trial.

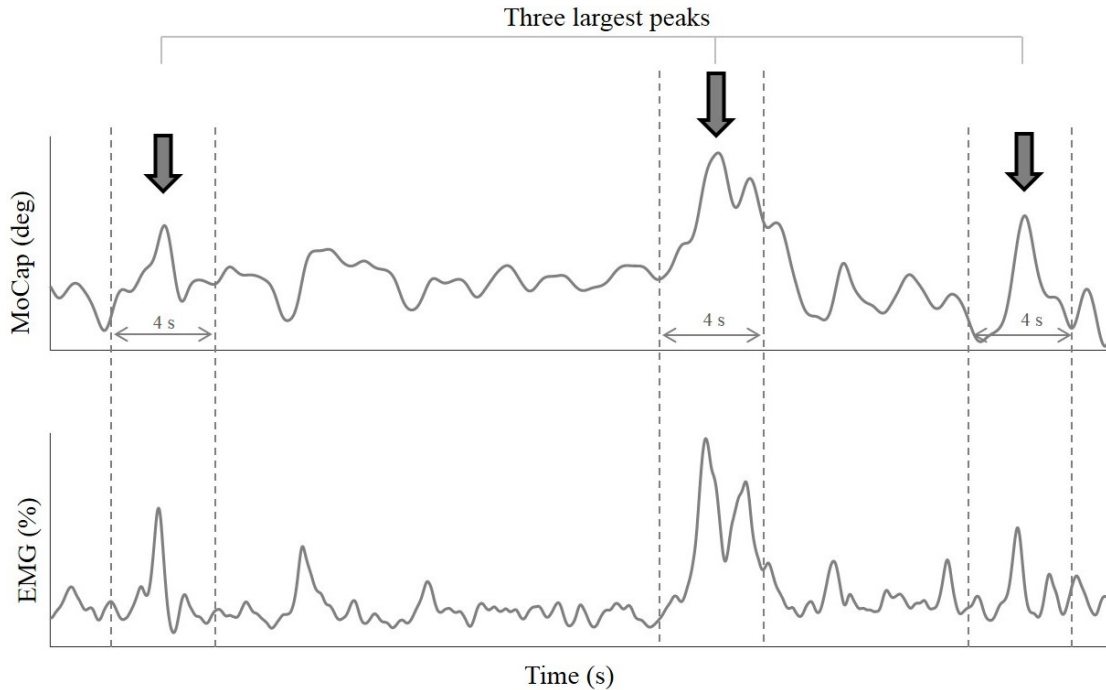


Figure 23. The cross-correlation analysis: first, the three largest peaks in the MoCap signal were identified. Second, a 4-second window centered at each peak was created. Third, corresponding 4-second windows were created in the down-sampled EMG signal. Then, each of these segments (i.e., the 4-second window centered at each peak in the MoCap signal and its time-matched 4-second window in the down-sampled EMG signal) was demeaned and cross-correlated. Finally, the obtained CC functions were averaged for each trial.

The CC coefficient threshold at which the CC coefficient value becomes statistically different from zero is ± 0.15 ($P < 0.01$, $n = 400$) [264], [265]. If the CC peak was above this threshold, there was said to be a correlation between EMG and board angle.

The CCF results were investigated at four different levels. For each level (described below), several factors were considered to decide whether the results are consistent: (1) the averages of r and τ for the largest peak (termed CCF metrics from here on); (2) the standard deviations of the CCF metrics; (3) the signs of the CCF metrics; and (4) the number of trials and participants that exhibited correlations above the defined threshold ($|r| = 0.15$). First, for each muscle being studied (i.e., RA, ExO, LD, TES, LES, RF, and BF) and each direction, the CCF metrics were compared

between different wobble board bases and eye conditions. Second, for each muscle being studied, the CCF metrics were compared between different directions (i.e., between ANT and POST; and between LEFT and RIGHT). Third, for each muscle being studied, the CCF metrics were compared between the right and left body sides. Finally, the CCF metrics were compared between different muscles.

Moreover, the average of the CC functions across 4 trials for a given participant as well as the group-ensemble CC functions across participants were calculated. Subsequently, the group mean value and standard deviation of the correlation coefficients, r , and the corresponding time lags, τ , were obtained for each participant separately as well as across participants. Data from a participant were excluded if the magnitude of the largest CC peak across 4 trials was below the determined threshold of significance ($|r|= 0.15$) and/or if the sign of the correlation coefficient, r , or time lag, τ , was not consistent. It should be noted that CC functions were mirrored with respect to the x-axis for the POST and RIGHT directions so that positive and negative r values always imply muscle activation and deactivation, respectively. This procedure was performed on the MoCap time series, i.e., the AP and ML time series, and 14 EMG signals to quantify the relationship between muscle activation and wobble board motion. For example, cross-correlations were performed between AP and RRA, ML and RRA, AP and LRA, and so on.

Chapter 5

5 Results

5.1 Participants

Fifteen non-disabled male individuals in the age range of 20 to 33 years were recruited to participate in this study. None of the participants had any history of neurological or musculoskeletal impairments or pain, gait or balance issues, or made use of a walking aid. The age, weight, height, hand dominance, and date of experiment for each participant are presented in Table 7.

Table 7. Participant characteristics.

Participant #	Age (years)	Weight (kg)	Height (cm)	Dominant Hand	Date of Experiment
1	24	78	178	right	Dec. 11/2015
2	32	71	170	right	Jan. 22/2016
3	22	80	178	right	Jan. 28/2016
4	32	70	177	right	Jan. 29/2016
5	21	100	188	right	Feb. 02/2016
6	20	70	177	left	Feb. 04/2016
7	32	58	178	right	Feb. 09/2016
8	23	86	185	right	Feb. 16/2016
9	23	82	186	right	Feb. 22/2016
10	20	60	173	right	Feb. 25/2016
11	23	95	195	right	Mar. 04/2016
12	21	54	173	right	Mar. 09/2016
13	32	70	178	right	Mar. 16/2016
14	22	69	174	right	Mar. 31/2016
15	33	84	184	right	Apr. 22/2016

5.2 Wobble Board Base Selection

Based on how well a given participant balanced, for each eye condition, on the wobble board, the bases for the main study were chosen. The bases used in the main study are shown, for each participant and eye condition, in Table 8.

Table 8. Selection of wobble board bases for each participant and eye condition.

Participant #	Base #1		Base #2		Base #3		Base #4		Base #5	
	EC	EO								
1	✓	-	✓	✓	-	✓	-	✓	-	-
2	✓	-	✓	-	✓	✓	-	✓	-	✓
3	✓	-	✓	-	✓	✓	-	✓	-	✓
4	✓	-	✓	✓	-	✓	-	✓	-	-
5	✓	-	✓	✓	-	✓	-	✓	-	✓
6	✓	-	✓	✓	-	✓	-	✓	-	-
7	✓	-	✓	✓	-	✓	-	✓	-	-
8	✓	-	✓	-	✓	✓	-	✓	-	✓
9	✓	-	✓	✓	-	✓	-	✓	-	-
10	✓	-	✓	✓	-	✓	-	✓	-	-
11	✓	-	✓	✓	-	✓	-	✓	-	-
12	✓	-	✓	✓	-	✓	-	✓	-	-
13	✓	-	✓	✓	-	✓	-	✓	-	-
14	✓	-	✓	✓	-	✓	-	✓	-	-
15	✓	-	✓	✓	-	✓	-	✓	-	-

The total number of participants that used each base, for each eye condition, and the total number of trials for each base and eye condition are shown in Table 9.

Table 9. Overall wobble board base coverage across trials and participants.

	Base #1		Base #2		Base #3		Base #4		Base #5	
	Trials	Participants								
EO	0	0	48	12	59	15	59	15	16	4
EC	60	15	60	15	12	3	0	0	0	0

5.3 MVC Results

All participants completed all required MVC exercises. Exemplary MVC results for the abdominal muscles – RRA, LRA, RExO, and LExO – are shown in Figure 24.

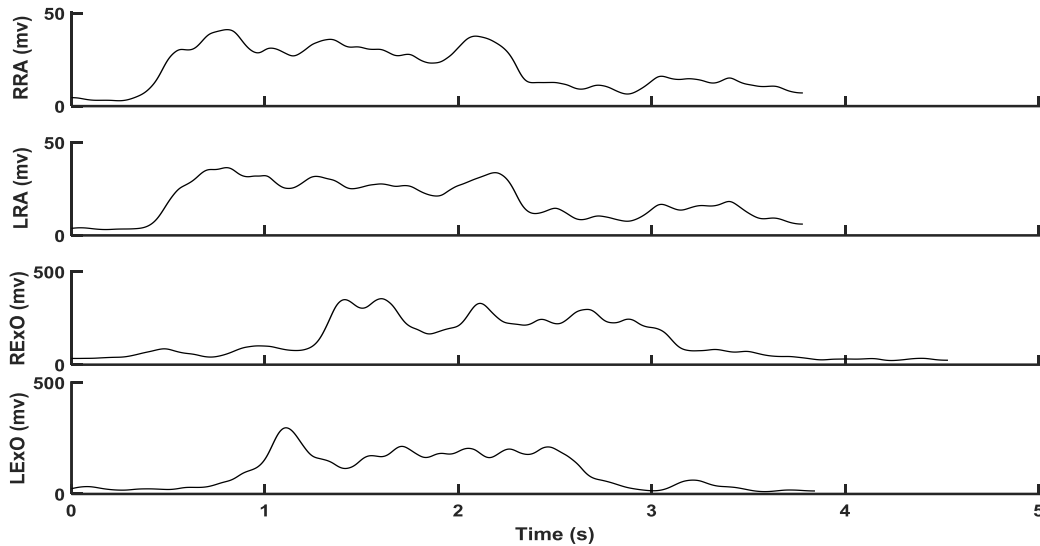


Figure 24. Exemplary abdominal muscle activity during respective MVC exercises for the first trial of Participant #5. The top subplot (RRA) shows the filtered muscle activity for the right rectus abdominis; the second subplot (LRA) the filtered muscle activity for the left rectus abdominis; the third subplot (RExO) the filtered muscle activity for the right external oblique; and the bottom subplot (LExO) the filtered muscle activity for left external oblique.

Exemplary MVC results for the back muscles – RTES, LTES, RLES, LLES, RLD, and LLD – are shown in Figure 25. Exemplary MVC results for the upper leg muscles – RRF, LRF, RBF and LBF – are shown in Figure 26.

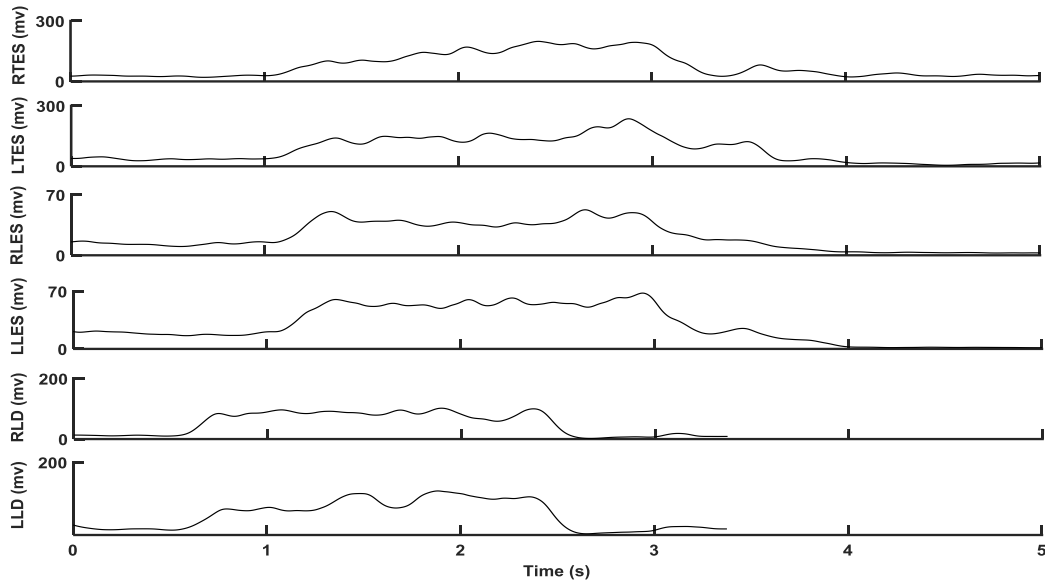


Figure 25. Exemplary back muscle activity during respective MVC exercises for the first trial of Participant #5. The top subplot (RTES) shows the filtered muscle activity for the right thoracic erector spinae; the second subplot (LTES) the filtered muscle activity for the left thoracic erector spinae; the third subplot (RLES) the filtered muscle activity for the right lumbar erector spinae; the fourth subplot (LLES) the filtered muscle activity for the left lumbar erector spinae; the fifth subplot (RLD) the filtered muscle activity for the right latissimus dorsi; and the bottom subplot (LLD) the filtered muscle activity for the left latissimus dorsi.

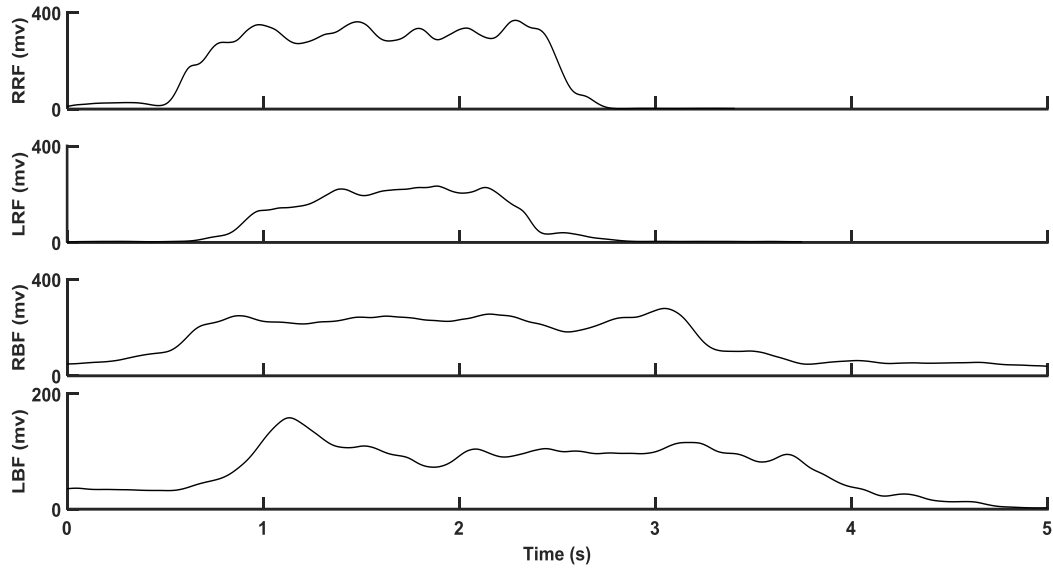


Figure 26. Exemplary upper leg muscle activity during respective MVC exercises for the first trial of Participant #5. The top subplot (RRF) shows the filtered muscle activity for the right rectus femoris; the second subplot (LRF) the filtered muscle activity for the left rectus femoris; the third subplot (RBF) the filtered muscle activity for the right biceps femoris; and the bottom subplot (LBF) the filtered muscle activity for the left biceps femoris.

MVC values for the abdominal (RRA, LRA, RExO, and LExO), back (RTES, LTES, RLES, LLES, RLD and LLD), and upper leg (RRF, LRF, RBF, and LBF) muscles are shown for each participant in Table 10, Table 11, and Table 12, respectively (mean \pm SD for 3 trials).

Table 10. MVC values for each participant and the following muscles: right rectus abdominis, left rectus abdominis, right external oblique, and left external oblique. All values are presented as mean \pm SD across three trials and given in millivolts (mV).

Participant #	RRA (mV)	LRA (mV)	RExO (mV)	LExO (mV)
1	119 \pm 2	86 \pm 1	258 \pm 52	363 \pm 55
2	33 \pm 3	42 \pm 3	115 \pm 23	113 \pm 20
3	56 \pm 15	37 \pm 12	195 \pm 43	281 \pm 31
4	31 \pm 14	29 \pm 6	183 \pm 27	34 \pm 7
5	42 \pm 5	37 \pm 6	315 \pm 39	273 \pm 7
6	105 \pm 5	105 \pm 5	280 \pm 12	354 \pm 16
7	28 \pm 3	44 \pm 8	312 \pm 35	221 \pm 34
8	43 \pm 4	34 \pm 3	277 \pm 19	187 \pm 18
9	94 \pm 43	174 \pm 99	502 \pm 8	314 \pm 32
10	63 \pm 2	93 \pm 16	239 \pm 14	264 \pm 35
11	26 \pm 9	29 \pm 10	128 \pm 6	131 \pm 40
12	104 \pm 11	163 \pm 37	115 \pm 6	172 \pm 11
13	21 \pm 8	19 \pm 8	119 \pm 4	126 \pm 17
14	24 \pm 1	24 \pm 3	73 \pm 10	54 \pm 13
15	34 \pm 6	48 \pm 13	85 \pm 16	61 \pm 11

Table 11. MVC values for each participant and the following muscles: right thoracic erector spinae, left thoracic erector spinae, right lumbar erector spinae, left lumbar erector spinae, right latissimus dorsi, and left latissimus dorsi. All values are presented as mean \pm SD across three trials and given in millivolts (mV).

Participant #	RTES (mV)	LTES (mV)	RLES (mV)	LLES (mV)	RLD (mV)	LLD (mV)
1	222 \pm 33	145 \pm 18	206 \pm 22	150 \pm 8	98 \pm 33	112 \pm 23
2	42 \pm 6	78 \pm 27	74 \pm 4	63 \pm 5	24 \pm 21	18 \pm 12
3	119 \pm 15	125 \pm 37	86 \pm 8	107 \pm 9	177 \pm 18	262 \pm 52
4	70 \pm 5	48 \pm 2	101 \pm 11	92 \pm 14	69 \pm 5	117 \pm 8
5	199 \pm 43	230 \pm 6	51 \pm 2	66 \pm 1	103 \pm 6	108 \pm 14
6	149 \pm 12	121 \pm 5	191 \pm 14	143 \pm 36	87 \pm 8	168 \pm 19
7	111 \pm 3	80 \pm 9	117 \pm 7	146 \pm 12	61 \pm 16	76 \pm 9
8	151 \pm 17	195 \pm 15	89 \pm 14	92 \pm 9	86 \pm 2	114 \pm 4
9	415 \pm 388	203 \pm 6	229 \pm 23	169 \pm 19	187 \pm 29	180 \pm 28
10	106 \pm 8	84 \pm 8	155 \pm 4	124 \pm 6	135 \pm 7	166 \pm 7
11	141 \pm 13	107 \pm 4	73 \pm 5	79 \pm 1	160 \pm 12	197 \pm 6
12	121 \pm 11	125 \pm 27	161 \pm 14	182 \pm 14	146 \pm 18	94 \pm 8
13	47 \pm 2	43 \pm 2	66 \pm 3	67 \pm 5	114 \pm 12	77 \pm 17
14	81 \pm 33	71 \pm 10	69 \pm 18	68 \pm 15	29 \pm 18	50 \pm 53
15	33 \pm 2	32 \pm 2	45 \pm 4	40 \pm 6	30 \pm 6	69 \pm 16

Table 12. MVC values for each participant and the following muscles: right rectus femoris, left rectus femoris, right biceps femoris, and left biceps femoris. All values are presented as mean \pm SD across three trials and given in millivolts (mV).

Participant #	RRF (mV)	LRF (mV)	RBF (mV)	LBF (mV)
1	132 \pm 13	96 \pm 16	170 \pm 20	117 \pm 5
2	42 \pm 11	55 \pm 6	144 \pm 10	136 \pm 23
3	73 \pm 11	117 \pm 5	142 \pm 19	170 \pm 19
4	78 \pm 5	67 \pm 3	118 \pm 7	98 \pm 13
5	95 \pm 5	72 \pm 1	120 \pm 15	144 \pm 15
6	164 \pm 20	88 \pm 8	333 \pm 25	294 \pm 51
7	79 \pm 12	96 \pm 6	240 \pm 25	274 \pm 31
8	87 \pm 70	157 \pm 5	223 \pm 17	118 \pm 25
9	420 \pm 62	233 \pm 7	248 \pm 41	188 \pm 65
10	115 \pm 6	88 \pm 9	224 \pm 23	143 \pm 18
11	70 \pm 15	90 \pm 14	230 \pm 10	123 \pm 4
12	148 \pm 34	131 \pm 26	304 \pm 26	361 \pm 73
13	47 \pm 12	46 \pm 17	154 \pm 11	160 \pm 10
14	53 \pm 13	81 \pm 38	98 \pm 6	71 \pm 6
15	75 \pm 31	86 \pm 9	207 \pm 41	200 \pm 9

The group-ensemble MVC values across participants (mean and SD) are shown, for each muscle studied, in Table 13.

Table 13. MVC values across participants for each muscle being studied. All values are in mV.

	RRA	LRA	RExO	LExO	RTES	LTES	RLES	LLS	RLD	LLD	RRF	LRF	RBF	LBF
Mean	55	64	213	196	134	113	114	106	100	121	112	100	197	173
SD	34	50	116	109	95	60	59	44	53	64	92	46	69	80

5.4 Main Experiment Results

5.4.1 Normalized EMG

Exemplary normalized EMG time series for the abdominal muscles – RRA, LRA, RExO, and LExO – and the first trial of Participant #5, using Base #5 with eyes open, are shown in Figure 27.

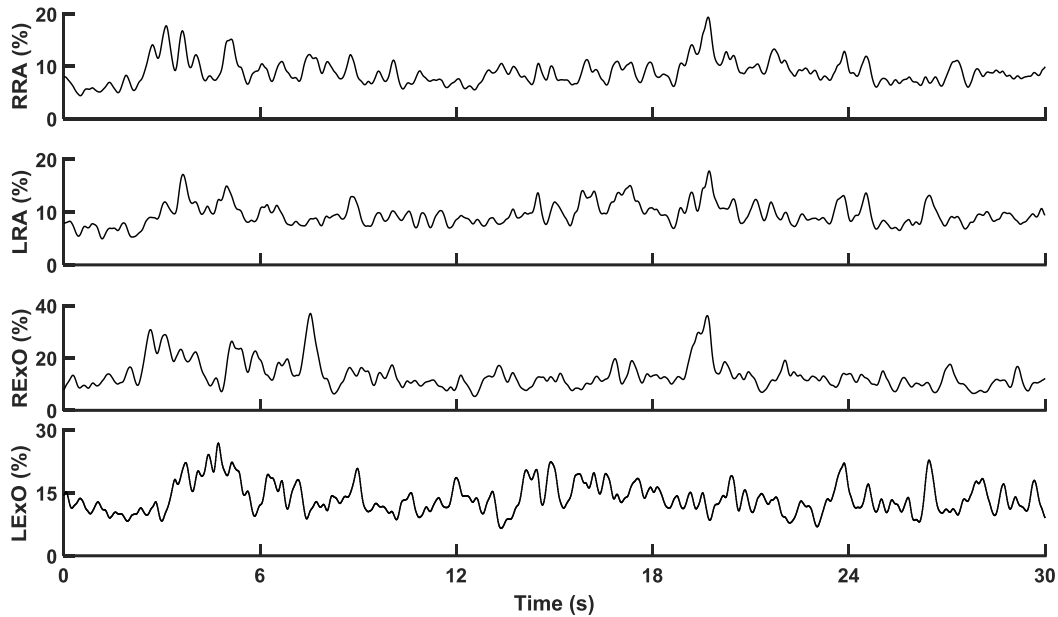


Figure 27. Exemplary normalized EMG time series for the abdominal muscles and the first trial of Participant #5, using Base #5 with eyes open. The top subplot (RRA) shows the normalized EMG time series for the right rectus abdominis; the second subplot (LRA) the normalized EMG for the left rectus abdominis; the third subplot (RExO) the normalized EMG for the right external oblique; and the bottom subplot (LExO) the normalized EMG for the left external oblique.

Exemplary normalized EMG time series for the back muscles – RTES, LTES, RLES, LLES, RLD and LLD – and the first trial of Participant #5, using Base #5 with eyes open, are shown in Figure 28.

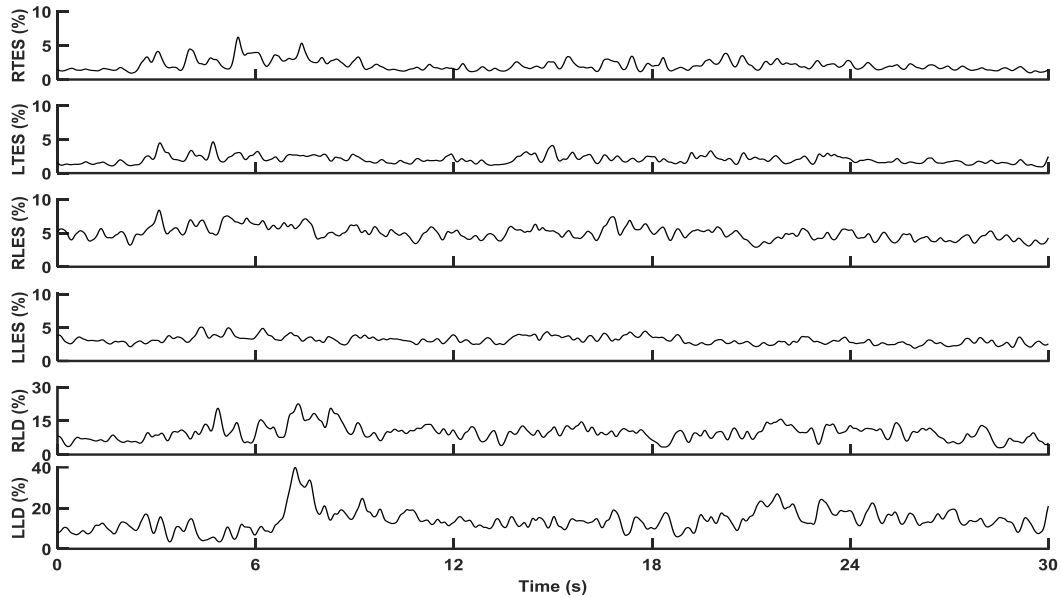


Figure 28. Exemplary normalized EMG time series for the back muscles and the first trial of Participant #5, using Base #5 with eyes open. The top subplot (RTES) shows the normalized EMG for the right thoracic erector spinae; the second subplot (LTES) the normalized EMG for the left thoracic erector spinae; the third subplot (RLES) the normalized EMG for the right lumbar erector spinae; the fourth subplot (LLES) the normalized EMG for the left lumbar erector spinae; the fifth subplot (RLD) the normalized EMG for the right latissimus dorsi; and the bottom subplot (LLD) the normalized EMG for the left latissimus dorsi.

Exemplary normalized EMG time series for the upper leg muscles – RRF, LRF, RBF, and LBF – and the first trial of Participant #5, using Base #5 with eyes open, are shown in Figure 29.

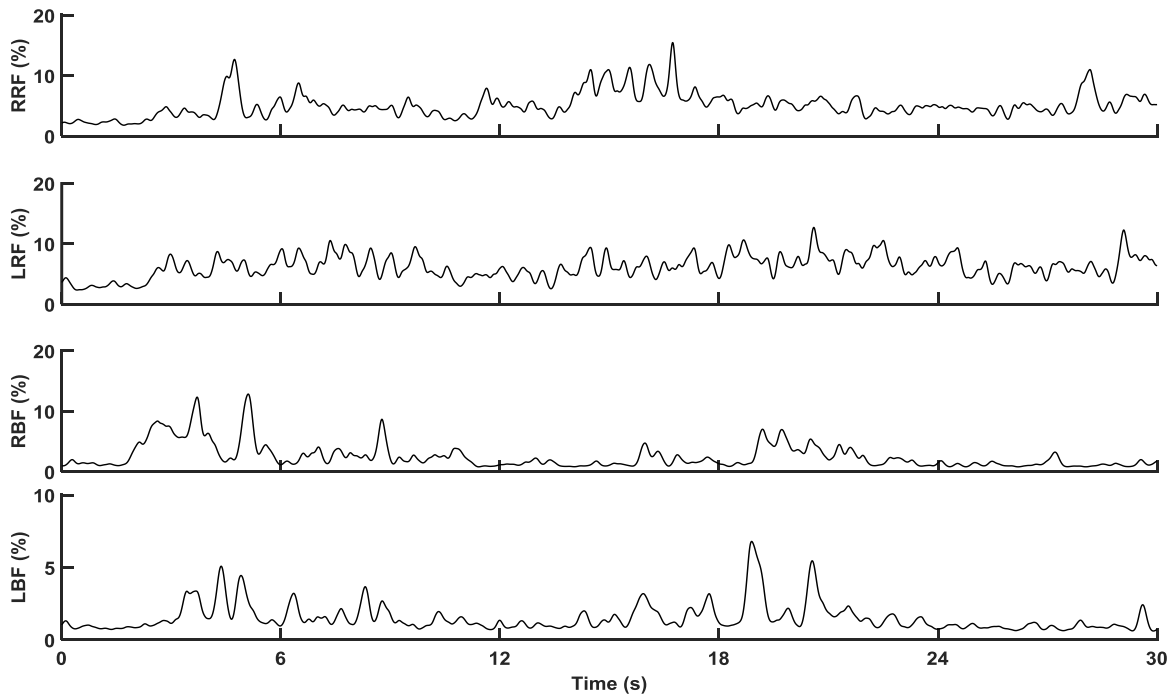


Figure 29. Exemplary normalized EMG time series for the upper leg muscles and the first trial of Participant #5, using Base #5 with eyes open. The top subplot (RRF) shows the normalized EMG for the right rectus femoris; the second subplot (LRF) the normalized EMG for the left rectus femoris; the third subplot (RBF) the normalized EMG for the right biceps femoris; and the bottom subplot (LBF) the normalized EMG for the left biceps femoris.

The group-ensemble average levels of muscle activity (%EMG) for all muscles and all conditions (i.e., different levels of difficulty under both eye conditions) are shown in Table 14. It can be seen that, independent of muscle choice and eye condition, an increase in seat instability (higher wobble board base number) results in an increase in muscle activity. The average levels of muscle activity (%EMG) for all muscles and all conditions for each participant can be found in Appendix F.

Table 14. Average values of the normalized EMG activity across participants for all muscles and conditions. Values are presented as mean \pm SD across participants. All values are given as a percentage of MVC (%).

Muscle	B #1, EC	B #2, EC	B #3, EC	B #2, EO	B #3, EO	B #4, EO	B #5, EO
RRA (%)	5.81 \pm 4.60	6.79 \pm 5.53	12.46 \pm 13.16	5.32 \pm 3.71	6.19 \pm 4.27	7.82 \pm 6.02	12.51 \pm 14.47
LRA (%)	6.03 \pm 5.50	7.03 \pm 7.09	10.97 \pm 5.21	5.27 \pm 4.04	6.72 \pm 5.81	7.73 \pm 6.75	11.53 \pm 8.74
RExO (%)	5.38 \pm 4.29	6.81 \pm 5.27	12.65 \pm 9.84	5.00 \pm 5.42	6.86 \pm 5.57	8.25 \pm 7.24	11.44 \pm 9.46
LExO (%)	5.55 \pm 4.23	6.14 \pm 4.77	9.67 \pm 6.75	5.04 \pm 4.55	7.34 \pm 5.47	8.66 \pm 7.58	10.74 \pm 7.67
RTES (%)	3.61 \pm 2.12	4.50 \pm 2.88	7.09 \pm 4.01	3.99 \pm 2.65	3.83 \pm 2.45	4.91 \pm 3.67	6.03 \pm 3.73
LTES (%)	4.87 \pm 2.34	5.27 \pm 2.80	7.81 \pm 3.76	4.87 \pm 2.86	4.95 \pm 3.41	6.32 \pm 6.10	6.99 \pm 4.74
RLES (%)	2.34 \pm 1.20	2.65 \pm 1.45	2.61 \pm 0.98	2.50 \pm 1.26	2.63 \pm 1.49	3.14 \pm 2.24	3.24 \pm 1.57
LLES (%)	2.11 \pm 1.00	2.30 \pm 1.28	2.42 \pm 1.28	2.19 \pm 1.02	2.25 \pm 1.29	2.67 \pm 1.87	2.64 \pm 1.59
RLD (%)	5.59 \pm 3.38	6.82 \pm 4.88	11.52 \pm 11.65	5.19 \pm 3.71	5.80 \pm 4.12	7.57 \pm 5.66	10.51 \pm 8.17
LLD (%)	5.47 \pm 6.86	5.47 \pm 6.30	15.79 \pm 20.45	5.43 \pm 7.88	6.20 \pm 10.47	6.57 \pm 8.71	19.39 \pm 29.21
RRF (%)	5.00 \pm 5.33	5.05 \pm 5.24	5.19 \pm 4.23	4.90 \pm 5.51	5.61 \pm 6.77	7.32 \pm 8.69	5.77 \pm 5.21
LRF (%)	4.14 \pm 3.68	4.16 \pm 3.84	4.49 \pm 5.51	4.34 \pm 3.69	4.65 \pm 4.16	6.53 \pm 8.18	5.14 \pm 3.77
RBF (%)	1.88 \pm 1.78	2.18 \pm 3.19	2.68 \pm 2.87	1.29 \pm 1.15	4.04 \pm 7.71	2.63 \pm 4.99	3.12 \pm 3.10
LBF (%)	1.46 \pm 1.40	1.64 \pm 2.09	2.37 \pm 2.08	0.99 \pm 0.67	1.43 \pm 1.81	1.80 \pm 2.03	2.02 \pm 1.98

5.4.2 Posturographic Measures

To quantify the postural proficiency during unstable sitting, the time-domain (i.e., MA, RMSA, MV, RMSV, and RANGE) and frequency-domain (i.e., CFREQ, and FREQD) measures described above were calculated. As a result, a total 28 measures were calculated (seven for each of the AP, ML, TM and TD time series). All posturographic measures (mean \pm SD) for all conditions and each participant can be found in Appendix G.

5.4.2.1 Bases #1 and #2 under Eyes Closed Condition

Figure 30 shows examples of the filtered AP and ML wobble board kinematics during unstable sitting for the third trial of Participant #15 under EC condition. Figure 30A shows the filtered AP (top) and ML (bottom) times series during sitting on the board with Base #1 (left) and Base #2 (right), whereas Figure 30B depicts the planar phase plots of the wobble board kinematics during sitting with Base #1 (top) and Base #2 (bottom). A visual inspection of the time series data suggests larger wobble board displacements for Base #2 when compared to Base #1 in both AP and ML directions.

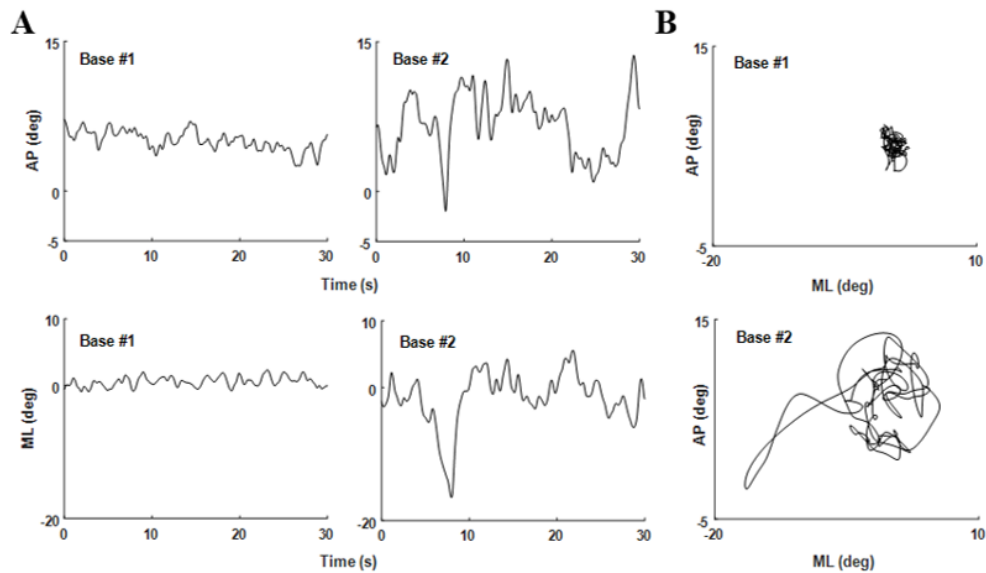


Figure 30. Examples of the wobble board kinematics in AP and ML directions. A: The AP (top) and ML (bottom) time series during sitting on the wobble board with Base #1 (left) and Base #2 (right) for the EC condition. B: The planar phase plots of the wobble board kinematics during sitting with Base #1 (top) and Base #2 (bottom) for the EC condition. Shown is the third trial for Participant #15.

All posturographic measures when comparing wobble board kinematics between Base #1 and Base #2 during EC are shown in Table 15 (mean \pm SD across participants). The Wilcoxon signed rank test revealed that the magnitudes of MA and RMSA significantly increased for Base #2 in comparison to Base #1 for all of AP, ML, TM, and TD (MA – AP: $p < 0.001$; ML: $p < 0.001$; TM: $p < 0.001$; TD: $p = 0.018$; RMSA – AP: $p < 0.001$; ML: $p < 0.001$; TM: $p < 0.001$; TD: $p = 0.018$). In addition, the magnitudes of MV and RMSV significantly increased for Base #2 when compared to Base #1 for AP, ML, and TM only (MV – AP: $p < 0.001$; ML: $p < 0.001$; TM: $p < 0.001$; TD: $p = 0.095$; RMSV – AP: $p < 0.001$; ML: $p < 0.001$; TM: $p < 0.001$; TD: $p = 0.083$). The magnitude of RANGE significantly increased for Base #2 for all of AP, ML, TM, and TD in comparison with Base #1 (RANGE – AP: $p < 0.001$; ML: $p < 0.001$; TM: $p < 0.001$; TD: $p < 0.001$). The magnitude of CFREQ decreased for Base #2 when compared to Base #1 for AP, ML, and TM only (CFREQ – AP: $p = 0.018$; ML: $p < 0.001$; TM: $p = 0.015$; TD: $p = 0.389$). The magnitude of FREQD

increased significantly for Base #2 in comparison with Base #1 for ML, TM, and TD only (FREQD – AP: $p = 0.208$; ML: $p = 0.030$; TM: $p = 0.015$; TD: $p = 0.003$).

Table 15. Analysis of the AP, ML, TM, and TD fluctuations. Posturographic measures were calculated for Base #1 and #2 under EC condition. Shown are the mean \pm SD across participants for MA, RMSA, MV, RMSV, RANGE, CFREQ, and FREQD. A Wilcoxon signed rank test was used to identify potential differences between Base #1 and Base #2 when eyes are closed.

Measure	Base #1, EC	Base #2, EC	P-values
MA (AP) (deg)	0.70 \pm 0.22	1.25 \pm 0.45	0.000
MA (ML) (deg)	0.55 \pm 0.17	1.17 \pm 0.54	0.000
MA (TM) (deg)	0.64 \pm 0.20	1.20 \pm 0.50	0.000
MA (TD) (deg)	25.69 \pm 28.68	39.69 \pm 34.24	0.018
RMSA (AP) (deg)	0.89 \pm 0.27	1.56 \pm 0.54	0.000
RMSA (ML) (deg)	0.70 \pm 0.22	1.51 \pm 0.72	0.000
RMSA (TM) (deg)	0.81 \pm 0.24	1.50 \pm 0.62	0.000
RMSA (TD) (deg)	32.25 \pm 33.45	48.64 \pm 36.20	0.018
MV (AP) (deg/s)	1.59 \pm 0.58	2.51 \pm 0.83	0.000
MV (ML) (deg/s)	1.54 \pm 0.55	2.57 \pm 0.76	0.000
MV (TM) (deg/s)	1.67 \pm 0.55	2.66 \pm 0.78	0.000
MV (TD) (deg/s)	84.57 \pm 116.01	107.43 \pm 105.74	0.095
RMSV (AP) (deg/s)	2.08 \pm 0.76	3.31 \pm 1.10	0.000
RMSV (ML) (deg/s)	2.04 \pm 0.68	3.43 \pm 0.99	0.000
RMSV (TM) (deg/s)	2.19 \pm 0.71	3.52 \pm 1.04	0.000
RMSV (TD) (deg/s)	593.90 \pm 921.62	815.75 \pm 950.87	0.083
RANGE (AP) (deg)	4.54 \pm 1.42	7.78 \pm 2.63	0.000
RANGE (ML) (deg)	3.85 \pm 1.09	8.04 \pm 3.83	0.000
RANGE (TM) (deg)	4.15 \pm 1.17	7.34 \pm 2.81	0.000
RANGE (TD) (deg)	154.89 \pm 121.92	235.15 \pm 103.03	0.000
CFREQ (AP) (Hz)	0.48 \pm 0.06	0.45 \pm 0.06	0.018
CFREQ (ML) (Hz)	0.54 \pm 0.08	0.46 \pm 0.06	0.000
CFREQ (TM) (Hz)	0.54 \pm 0.09	0.48 \pm 0.08	0.015
CFREQ (TD) (Hz)	0.71 \pm 0.28	0.79 \pm 0.28	0.389
FREQD (AP) (–)	0.56 \pm 0.04	0.57 \pm 0.03	0.208
FREQD (ML) (–)	0.54 \pm 0.04	0.56 \pm 0.03	0.030
FREQD (TM) (–)	0.56 \pm 0.03	0.58 \pm 0.03	0.015
FREQD (TD) (–)	0.61 \pm 0.05	0.66 \pm 0.07	0.003

5.4.2.2 Bases #3 and #4 under Eyes Open Condition

Figure 31 shows examples of the filtered AP and ML wobble board kinematics during unstable sitting for Participant #15 under EO condition. Figure 31A shows the AP (top) and ML (bottom) wobble board kinematics during sitting on the board with Base #3 (left) and Base #4 (right), whereas Figure 31B depicts the planar phase plots of the wobble board kinematics during sitting with Base #3 (top) and Base #4 (bottom). A visual inspection of the time series data suggests larger wobble board displacements for Base #4 when compared to Base #3 in both AP and ML directions.

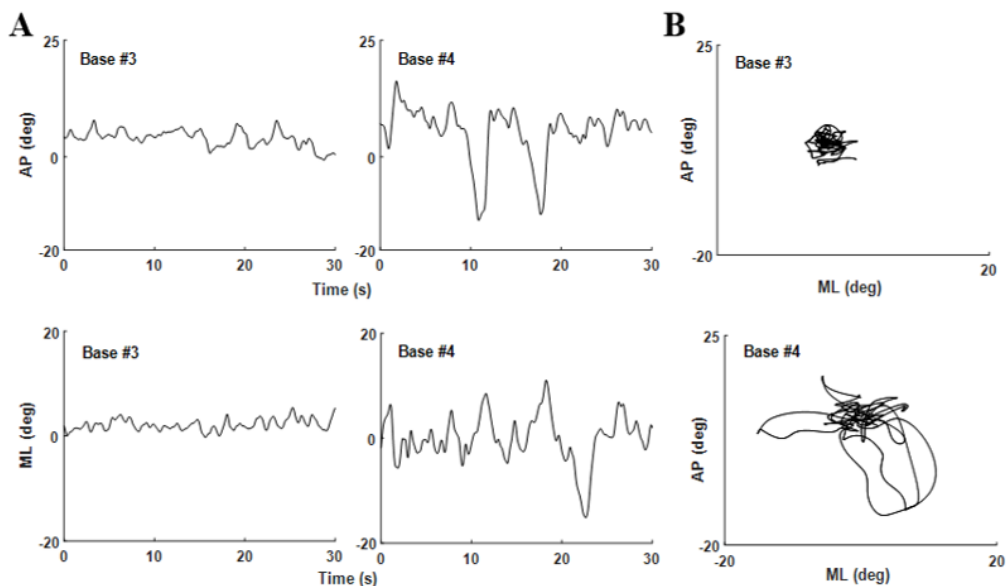


Figure 31. Examples of the wobble board kinematics in AP and ML directions. A: The AP (top) and ML (bottom) time series during sitting on the wobble board with Base #3 (left) and Base #4 (right) for the EO condition. B: The planar phase plots of the wobble board kinematics during sitting with Base #3 (top) and Base #4 (bottom) for the EO condition. Shown is the third trial for Participant #15.

All posturographic measures when comparing wobble board kinematics between Base #3 and Base #4 during EO are shown in Table 16 (mean \pm SD across participants). The Wilcoxon signed rank test revealed that MA and RMSA magnitudes significantly increased for Base #4 in comparison

to Base #3 for all of AP, ML, TM, and TD (MA – AP: $p < 0.001$; ML: $p < 0.001$; TM: $p < 0.001$; TD: $p = 0.015$; RMSA – AP: $p < 0.001$; ML: $p < 0.001$; TM: $p < 0.001$; TD: $p = 0.010$). The magnitude of MV significantly increased for Base #4 when compared to Base #3 for all of AP, ML, TM, and TD (MV – AP: $p < 0.001$; ML: $p < 0.001$; TM: $p < 0.001$; TD: $p = 0.041$). The magnitude of RMSV significantly increased for Base #4 in comparison with Base #3 for AP, ML, and TM only (RMSV – AP: $p < 0.001$; ML: $p < 0.001$; TM: $p < 0.001$; TD: $p = 0.055$). RANGE magnitude increased significantly for Base #4 when compared to Base #3 for all of AP, ML, TM, and TD (RANGE – AP: $p < 0.001$; ML: $p < 0.001$; TM: $p < 0.001$; TD: $p = 0.008$). No significant differences between Base #3 and Base #4 were found for the CFREQ and FREQD measures (CFREQ – AP: $p = 0.804$; ML: $p = 0.934$; TM: $p = 0.073$; TD: $p = 0.252$; FREQD – AP: $p = 0.107$; ML: $p = 0.524$; TM: $p = 0.679$; TD: $p = 0.135$).

Table 16. Analysis of the AP, ML, TM, and TD fluctuations. Posturographic measures were calculated for Base #3 and #4 under eyes open condition. Shown are the mean \pm SD across participants for MA, RMSA, MV, RMSV, RANGE, CFREQ, and FREQD. A Wilcoxon signed rank test was used to identify potential differences between Base #3 and Base #4 when eyes were open.

Measure	B #3, EO	B #4, EO	P-values
MA (AP) (deg)	1.19 \pm 0.57	1.94 \pm 0.94	0.000
MA (ML) (deg)	1.20 \pm 0.60	2.09 \pm 1.08	0.000
MA (TM) (deg)	1.14 \pm 0.46	1.71 \pm 0.65	0.000
MA (TD) (deg)	52.46 \pm 39.61	63.04 \pm 40.05	0.015
RMSA (AP) (deg)	1.51 \pm 0.70	2.48 \pm 1.20	0.000
RMSA (ML) (deg)	1.61 \pm 0.79	2.74 \pm 1.38	0.000
RMSA (TM) (deg)	1.45 \pm 0.55	2.15 \pm 0.79	0.000
RMSA (TD) (deg)	63.60 \pm 43.34	75.08 \pm 42.63	0.010
MV (AP) (deg/s)	2.23 \pm 1.18	3.77 \pm 1.81	0.000
MV (ML) (deg/s)	2.53 \pm 0.99	4.56 \pm 1.74	0.000
MV (TM) (deg/s)	2.47 \pm 1.08	4.09 \pm 1.67	0.000
MV (TD) (deg/s)	142.95 \pm 123.87	174.38 \pm 121.72	0.041
RMSV (AP) (deg/s)	2.96 \pm 1.57	5.01 \pm 2.37	0.000
RMSV (ML) (deg/s)	3.45 \pm 1.25	6.15 \pm 2.27	0.000
RMSV (TM) (deg/s)	3.35 \pm 1.41	5.52 \pm 2.19	0.000
RMSV (TD) (deg/s)	1227.80 \pm 1070.28	1475.05 \pm 1108.91	0.055
RANGE (AP) (deg)	7.60 \pm 3.64	12.52 \pm 5.86	0.000
RANGE (ML) (deg)	8.81 \pm 3.75	14.66 \pm 5.90	0.000
RANGE (TM) (deg)	7.09 \pm 2.58	10.24 \pm 2.89	0.000
RANGE (TD) (deg)	251.11 \pm 121.12	291.25 \pm 97.88	0.008
CFREQ (AP) (Hz)	0.45 \pm 0.08	0.45 \pm 0.07	0.804
CFREQ (ML) (Hz)	0.48 \pm 0.07	0.47 \pm 0.08	0.934
CFREQ (TM) (Hz)	0.50 \pm 0.08	0.53 \pm 0.09	0.073
CFREQ (TD) (Hz)	0.91 \pm 0.28	0.96 \pm 0.27	0.252
FREQD (AP) (-)	0.57 \pm 0.03	0.56 \pm 0.03	0.107
FREQD (ML) (-)	0.58 \pm 0.03	0.57 \pm 0.02	0.524
FREQD (TM) (-)	0.60 \pm 0.03	0.60 \pm 0.02	0.679
FREQD (TD) (-)	0.67 \pm 0.07	0.69 \pm 0.06	0.135

5.4.2.3 EO and EC Conditions with Base #2

Examples of the filtered AP and ML wobble board kinematics during unstable sitting for Participant #15 with Base #2 are shown in Figure 32. Figure 32A shows the AP (top) and ML (bottom) wobble board kinematics during sitting on the board with Base #2 for EO (left) and EC (right) conditions, whereas Figure 32B depicts the planar phase plots of the wobble board kinematics during sitting for EO (top) and EC (bottom) conditions with Base #2. A visual

inspection of the time series data suggests larger wobble board kinematics for EC in comparison to EO in both AP and ML directions.

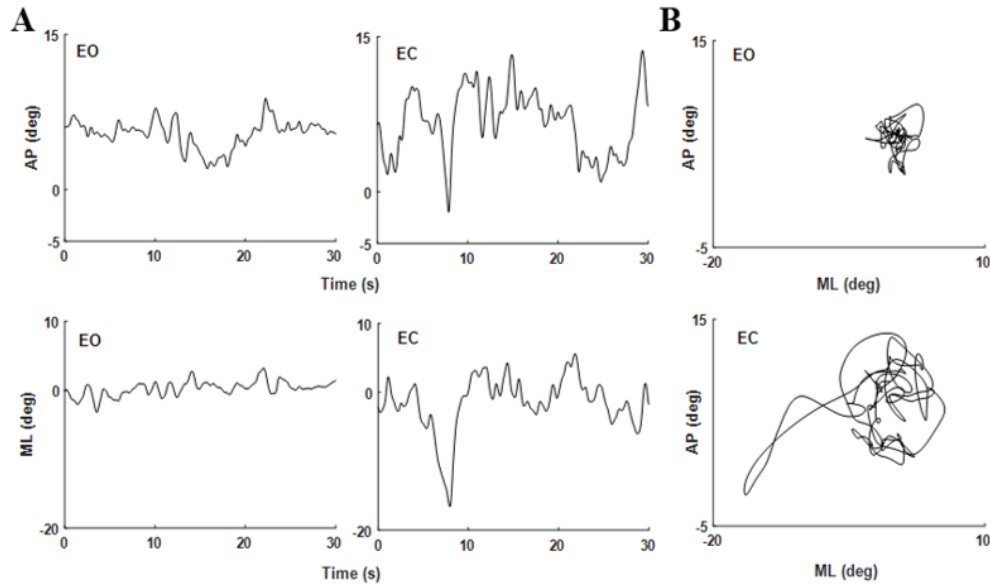


Figure 32. Examples of the wobble board kinematics in AP and ML directions. A: The AP (top) and ML (bottom) time series during sitting on the wobble board with Base #2 for EO (left) and EC (right) conditions. B: The planar phase plots of the wobble board kinematics during sitting with Base #2 for EO (top) and EC (bottom) conditions. Shown is the third trial for Participant #15.

All posturographic measures when comparing wobble board kinematics between EO and EC for Base #2 are shown in Table 17 (mean \pm SD across participants). The Wilcoxon signed rank test revealed that the magnitude of MA magnitude significantly increased for EC when compared to EO for all of AP, ML, TM, and TD (MA – AP: $p < 0.001$; ML: $p < 0.001$; TM: $p < 0.001$; TD: $p = 0.042$). RMSA magnitude increased for EC in comparison with EO for AP, ML, and TM only (RMSA – AP: $p < 0.001$; ML: $p < 0.001$; TM: $p < 0.001$; TD: $p = 0.052$). The magnitudes of MV and RMSV significantly increased for EC when compared to EO for all of AP, ML, TM, and TD (MV – AP: $p < 0.001$; ML: $p < 0.001$; TM: $p < 0.001$; TD: $p = 0.012$; RMSV – AP: $p < 0.001$; ML: $p < 0.001$; TM: $p < 0.001$; TD: $p = 0.042$). Similarly, RANGE magnitude significantly increased for EC in comparison with EO for all of AP, ML, TM, and TD (RANGE – AP: $p <$

0.001; ML: $p = 0.001$; TM: $p < 0.001$; TD: $p = 0.042$). No significant differences were found between EC and EO for the CFREQ measure (CFREQ – AP: $p = 0.910$; ML: $p = 0.339$; TM: $p = 0.569$; TD: $p = 0.266$). Moreover, FREQD magnitude significantly increased for EC when compared to EO for AP and ML only (FREQD – AP: $p = 0.042$; ML: $p = 0.034$; TM: $p = 0.176$; TD: $p = 0.204$).

Table 17. Analysis of the AP, ML, TM, and TD fluctuations. Posturographic measures were calculated for Base #2 under EO and EC conditions. Shown are the mean \pm SD across participants for MA, RMSA, MV, RMSV, RANGE, CFREQ, and FREQD. A Wilcoxon signed rank test was used to identify potential differences between EO and EC with Base #2.

Measure	B #2, EO	B #2, EC	P-value
MA (AP) (deg)	0.75 \pm 0.33	1.29 \pm 0.50	0.000
MA (ML) (deg)	0.55 \pm 0.19	1.22 \pm 0.59	0.000
MA (TM) (deg)	0.70 \pm 0.28	1.24 \pm 0.56	0.000
MA (TD) (deg)	26.78 \pm 30.74	40.82 \pm 36.36	0.042
RMSA (AP) (deg)	0.94 \pm 0.40	1.61 \pm 0.60	0.000
RMSA (ML) (deg)	0.70 \pm 0.24	1.58 \pm 0.79	0.000
RMSA (TM) (deg)	0.88 \pm 0.35	1.54 \pm 0.69	0.000
RMSA (TD) (deg)	34.35 \pm 33.36	49.57 \pm 37.72	0.052
MV (AP) (deg/s)	1.19 \pm 0.52	2.52 \pm 0.92	0.000
MV (ML) (deg/s)	1.13 \pm 0.46	2.62 \pm 0.85	0.000
MV (TM) (deg/s)	1.22 \pm 0.50	2.70 \pm 0.87	0.000
MV (TD) (deg/s)	69.41 \pm 92.73	109.80 \pm 114.30	0.012
RMSV (AP) (deg/s)	1.58 \pm 0.68	3.33 \pm 1.22	0.000
RMSV (ML) (deg/s)	1.55 \pm 0.63	3.49 \pm 1.11	0.000
RMSV (TM) (deg/s)	1.62 \pm 0.65	3.57 \pm 1.16	0.000
RMSV (TD) (deg/s)	548.06 \pm 831.93	825.30 \pm 992.42	0.042
RANGE (AP) (deg)	4.50 \pm 1.80	7.98 \pm 2.92	0.000
RANGE (ML) (deg)	3.70 \pm 1.41	8.42 \pm 4.20	0.001
RANGE (TM) (deg)	4.22 \pm 1.68	7.54 \pm 3.11	0.000
RANGE (TD) (deg)	170.08 \pm 114.78	234.39 \pm 103.68	0.042
CFREQ (AP) (Hz)	0.44 \pm 0.08	0.44 \pm 0.06	0.910
CFREQ (ML) (Hz)	0.48 \pm 0.06	0.45 \pm 0.07	0.339
CFREQ (TM) (Hz)	0.46 \pm 0.09	0.47 \pm 0.09	0.569
CFREQ (TD) (Hz)	0.68 \pm 0.28	0.77 \pm 0.29	0.266
FREQD (AP) (–)	0.59 \pm 0.03	0.56 \pm 0.02	0.042
FREQD (ML) (–)	0.58 \pm 0.04	0.55 \pm 0.03	0.034
FREQD (TM) (–)	0.59 \pm 0.03	0.57 \pm 0.03	0.176
FREQD (TD) (–)	0.63 \pm 0.06	0.66 \pm 0.07	0.204

5.4.3 Cross-Correlation

Figure 33 shows an example of the wobble board kinematics in AP direction and of the corresponding, down-sampled normalized EMG time series for LBF for Participant #13 under Base #1 and EC conditions. In this figure, the three largest peaks in the anterior tilt of the wobble board as well as the 4-second windows centered at each peak (top) and their time-matched corresponding 4-second windows in the EMG time series are indicated (bottom).

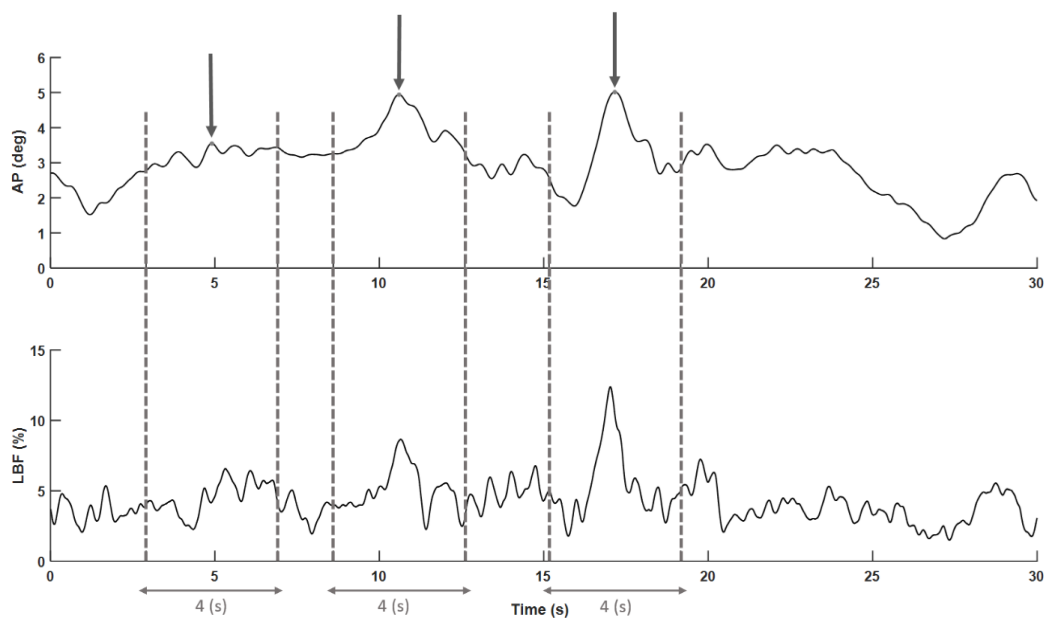


Figure 33. Exemplary wobble board kinematics in the AP direction (top subplot) and the down-sampled, normalized EMG signal for LBF (bottom subplot) for Participant #13 with Base #1 and EC. The top subplot shows the three largest peaks in the anterior tilt of the wobble board as well as the 4-second windows centered at each peak. The bottom subplot shows the time-matched, corresponding 4-second windows created in the EMG time series.

The averaged CC function (from three segments) between the LBF and ANT time series shown in Figure 33 is given in Figure 34. It can be seen that the averaged CC functions between LBF and ANT has a positive peak (indicating positive correlation) with a negative time lag ($r = 0.78$, $\tau =$

-0.12 s). The positive correlation coefficient indicates LBF muscle activation during ANT wobble board displacements. Moreover, the negative time lag for that peak suggests that the LBF time series preceded the wobble board displacement in the anterior direction. It should be noted that correlation coefficients (r) were normalized such that +1, 0, -1 represent perfect positive correlation, no correlation, and perfect negative correlation, respectively.

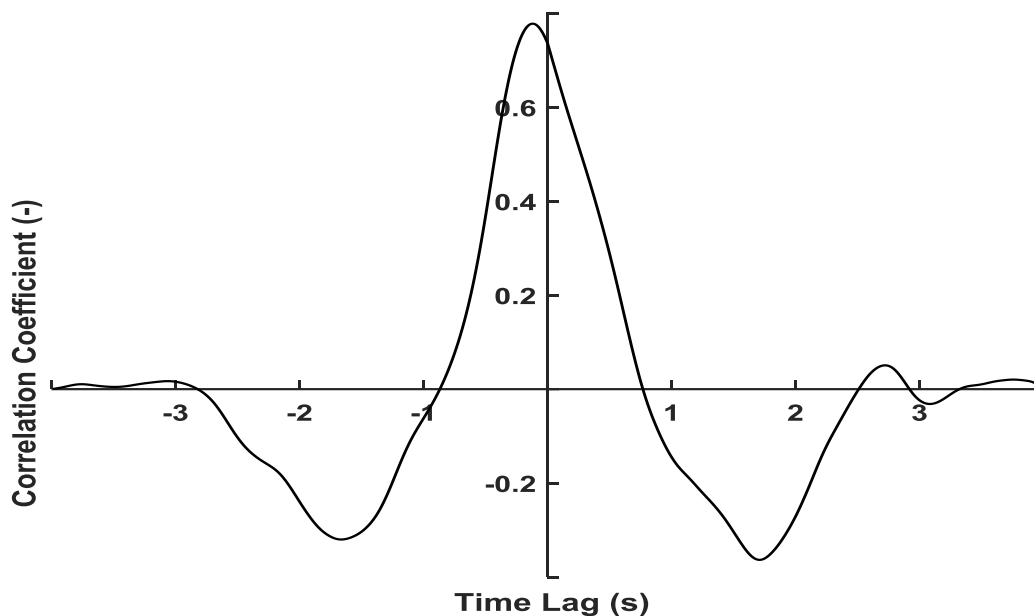


Figure 34. The averaged CC function (from three segments) between LBF and ANT for Participant #13 under Base #1 and EC condition. The positive correlation peak indicates LBF muscle activation during ANT wobble board displacements. The negative time lag for that peak suggests that the LBF time series preceded the wobble board displacement in the anterior direction.

Our overall results demonstrate that the magnitude of correlation becomes larger with increasing seat instability level (except for the magnitude of correlation coefficients for ES vs ANT/POST). For example, Figure 35 shows the averaged CC functions across participants between RExO and RIGHT for different levels of difficulty (i.e., Bases #2, #3, #4, and #5) when eyes were open. It can be seen that, regardless of the wobble board bases, the activation of RExO preceded RIGHT. Moreover, a visual inspection suggests that the correlation coefficient increases when decreasing the diameter hemisphere (Base #2: $r = 0.36 \pm 0.10$, $\tau = -0.15 \pm 0.09$; Base #3: $r = 0.43 \pm 0.12$, $\tau =$

-0.18 ± 0.06 ; Base #4: $r = 0.55 \pm 0.17$, $\tau = -0.17 \pm 0.05$; Base #5: $r = 0.68 \pm 0.09$, $\tau = -0.15 \pm 0.02$). The number of participants that were used to calculate the group-ensemble CC functions (across participants) is given in Appendix H.

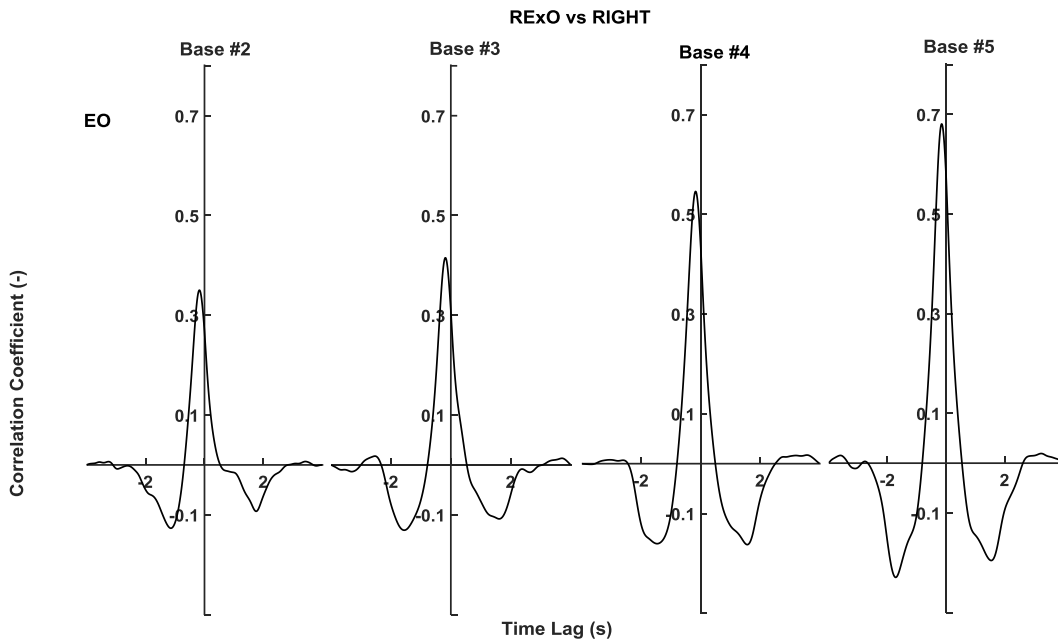


Figure 35. The averaged CC functions across participants between RExO and RIGHT for Bases #2, #3, #4, and #5 when eyes were open. The activation of RExO preceded RIGHT: Base #2: $r = 0.36 \pm 0.10$, $\tau = -0.15 \pm 0.09$; Base #3: $r = 0.43 \pm 0.12$, $\tau = -0.18 \pm 0.06$; Base #4: $r = 0.55 \pm 0.17$, $\tau = -0.17 \pm 0.05$; Base #5: $r = 0.68 \pm 0.09$, $\tau = -0.15 \pm 0.02$.

5.4.3.1 Anterior-Posterior Wobble Board Displacements

The CC results show that, in general, ANT and POST correlated with RA, BF, RF, TES, and LES. However, they did not show any correlation with ExO and LD. The activation and deactivation of RA and BF preceded ANT and POST, respectively (Figure 36; right). In addition, the deactivation and activation of TES, LES, and RF preceded ANT and POST, respectively (Figure 36; left).

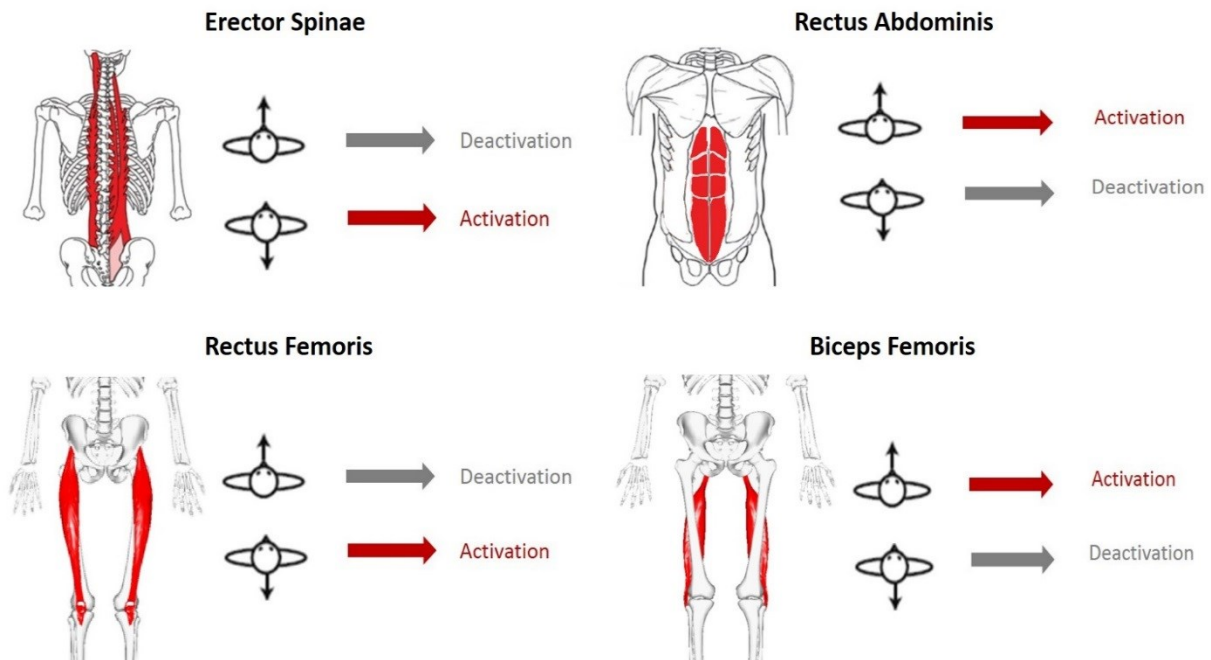


Figure 36. A schematic summary of findings during anterior-posterior wobble board displacements [266]–[268]. The CC results indicate the activation and deactivation of RA and BF muscles, during ANT and POST wobble board displacements respectively. In addition, the results indicate the deactivation and activation of TES, LES, and RF muscles, during ANT and POST wobble board displacements respectively.

The averaged CC functions across participants between RRA and ANT as well as between RRA and POST are shown in Figure 37. Left subplots show the averaged CC functions between RRA and ANT, and right subplots show the averaged CC functions between RRA and POST. Results are shown for Base #2 when eyes were closed (top), and Base #4 when eyes were open (bottom). A visual inspection suggests that, regardless of eye condition, RRA activation preceded ANT (Left – EC: $r = 0.33 \pm 0.09$, $\tau = -0.16 \pm 0.04$; EO: $r = 0.39 \pm 0.12$, $\tau = -0.18 \pm 0.04$), and RRA deactivation preceded POST (Right – EC: $r = -0.24 \pm 0.07$, $\tau = -0.11 \pm 0.07$; EO: $r = -0.34 \pm 0.11$, $\tau = -0.17 \pm 0.04$).

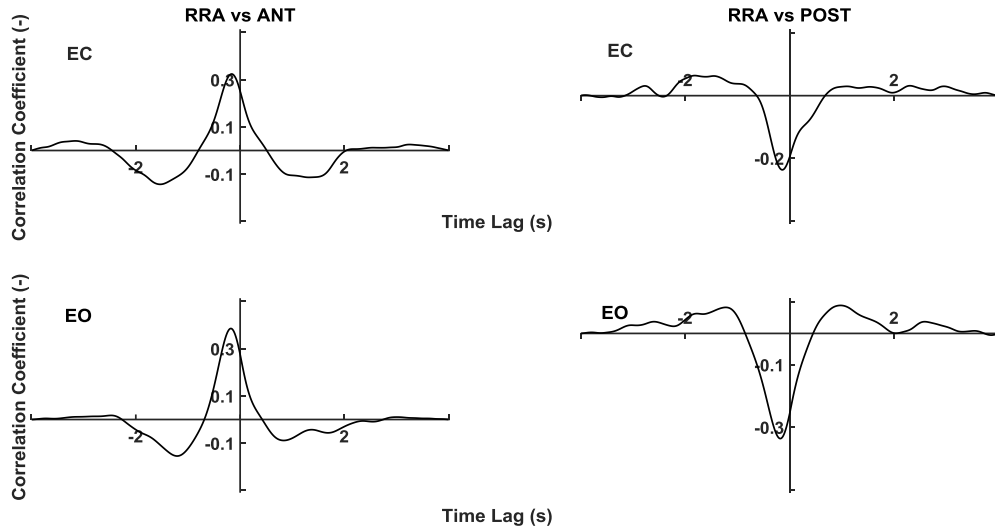


Figure 37. The averaged CC functions across participants between RRA and ANT (left); and the averaged CC functions between RRA and POST (right). Results are shown for Base #2 when eyes were closed (top), and Base #4 when eyes were open (bottom). Left: the largest peaks had a positive r and a negative time lag (EC: $r = 0.33 \pm 0.09$, $\tau = -0.16 \pm 0.04$; EO: $r = 0.39 \pm 0.12$, $\tau = -0.18 \pm 0.04$), suggesting that, regardless of eye condition, RRA activation preceded ANT; Right: the largest peaks had a negative r and a negative time lag (EC: $r = -0.24 \pm 0.07$, $\tau = -0.11 \pm 0.07$; EO: $r = -0.34 \pm 0.11$, $\tau = -0.17 \pm 0.04$), suggesting that, regardless of eye condition, RRA deactivation preceded POST.

Figure 38 shows the averaged CC functions across participants between LRA and ANT (left), and between LRA and POST (right). Results are shown for Base #2 when eyes were closed (top), and Base #4 when eyes were open (bottom). A visual inspection suggests that, regardless of eye condition, LRA activation preceded ANT (Left – EC: $r = 0.30 \pm 0.09$, $\tau = -0.14 \pm 0.04$; EO: $r = 0.40 \pm 0.14$, $\tau = -0.18 \pm 0.05$), and LRA deactivation preceded POST (Right – EC: $r = -0.24 \pm 0.07$, $\tau = -0.16 \pm 0.06$; EO: $r = -0.30 \pm 0.06$, $\tau = -0.17 \pm 0.05$).

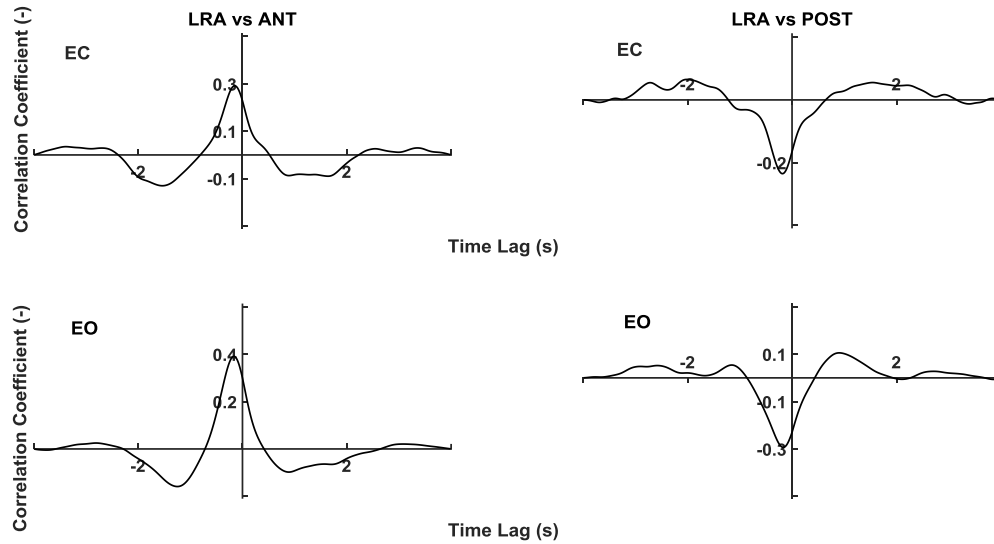


Figure 38. The averaged CC functions across participants between LRA and ANT (left); and the averaged CC functions between LRA and POST (right). Results are shown for Base #2 when eyes were closed (top), and Base #4 when eyes were open (bottom). Left: the largest peaks had a positive r and a negative time lag (EC: $r = 0.30 \pm 0.09$, $\tau = -0.14 \pm 0.04$; EO: $r = 0.40 \pm 0.14$, $\tau = -0.18 \pm 0.05$), suggesting that, regardless of eye condition, LRA activation preceded ANT; Right: the largest peaks had a negative r and a negative time lag (EC: $r = -0.24 \pm 0.07$, $\tau = -0.16 \pm 0.06$; EO: $r = -0.30 \pm 0.06$, $\tau = -0.17 \pm 0.05$), suggesting that, regardless of eye condition, LRA deactivation preceded POST.

Figure 39 shows the averaged CC functions across participants between RTES and ANT (left), and between RTES and POST (right). Results are shown for Base #2 when eyes were closed (top), and Base #4 when eyes were open (bottom). A visual inspection suggests that, regardless of eye condition, RTES deactivation preceded ANT (Left – EC: $r = -0.21 \pm 0.06$, $\tau = -0.45 \pm 0.41$; EO: $r = -0.29 \pm 0.07$, $\tau = -0.19 \pm 0.10$), and RTES activation preceded POST (Right – EC: $r = 0.27 \pm 0.06$, $\tau = -0.17 \pm 0.09$; EO: $r = 0.31 \pm 0.10$, $\tau = -0.20 \pm 0.09$).

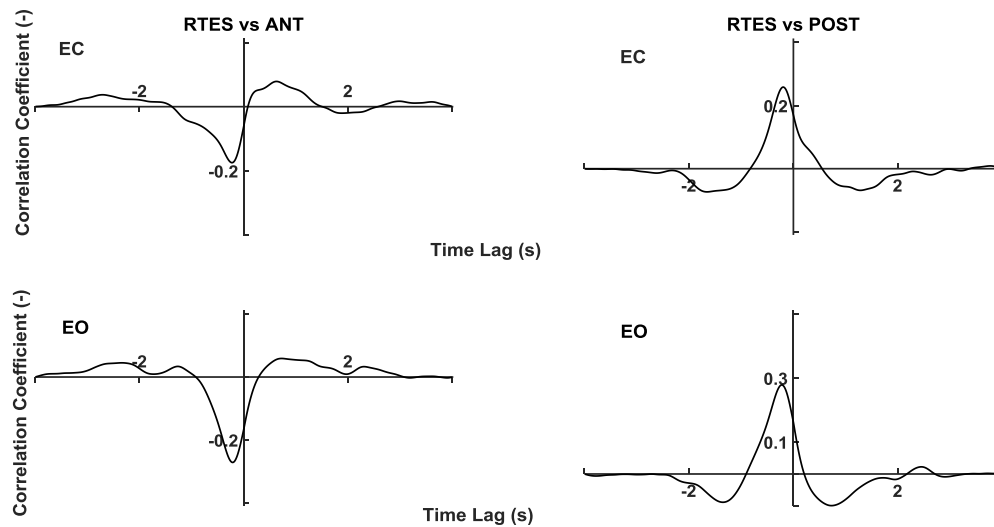


Figure 39. The averaged CC functions across participants between RTES and ANT (left); and the averaged CC functions between RTES and POST (right). Results are shown for Base #2 when eyes were closed (top), and Base #4 when eyes were open (bottom). Left: the largest peaks had a negative r and a negative time lag (EC: $r = -0.21 \pm 0.06$, $\tau = -0.45 \pm 0.41$; EO: $r = -0.29 \pm 0.07$, $\tau = -0.19 \pm 0.10$), suggesting that, regardless of eye condition, RTES deactivation preceded ANT; Right: the largest peaks had a positive r and a negative time lag (EC: $r = 0.27 \pm 0.06$, $\tau = -0.17 \pm 0.09$; EO: $r = 0.31 \pm 0.10$, $\tau = -0.20 \pm 0.09$), suggesting that, regardless of eye condition, RTES activation preceded POST.

Figure 40 shows the averaged CC functions across participants between LTES and ANT (left), and between LTES and POST (right). Results are shown for Base #2 when eyes were closed (top), and Base #4 when eyes were open (bottom). A visual inspection suggests that, regardless of eye condition, LTES deactivation preceded ANT (Left – EC: $r = -0.23 \pm 0.06$, $\tau = -0.39 \pm 0.25$; EO: $r = -0.28 \pm 0.08$, $\tau = -0.24 \pm 0.06$), and LTES activation preceded POST (Right – EC: $r = 0.26 \pm 0.09$, $\tau = -0.25 \pm 0.08$; EO: $r = 0.29 \pm 0.10$, $\tau = -0.25 \pm 0.08$).

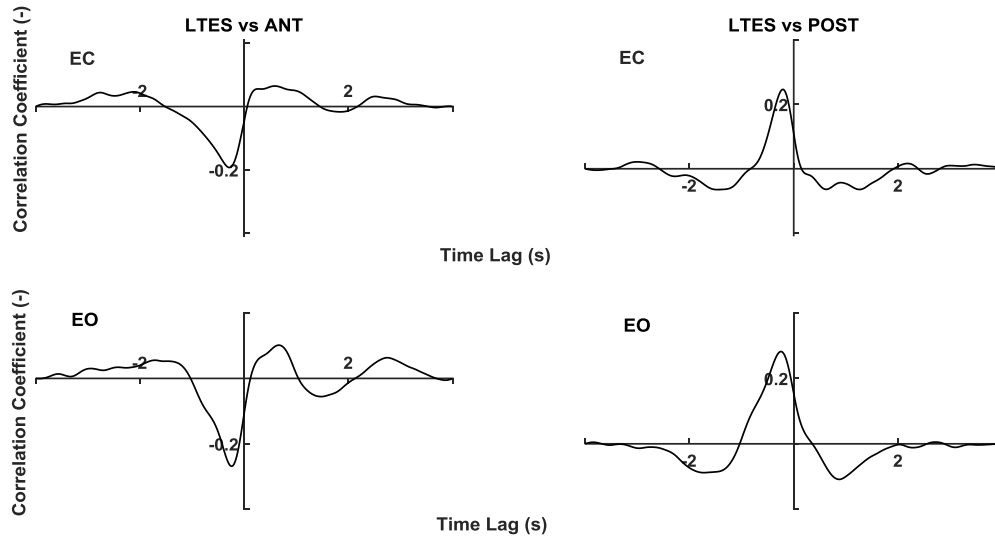


Figure 40. The averaged CC functions across participants between LTES and ANT (left); and the averaged CC functions between LTES and POST (right). Results are shown for Base #2 when eyes were closed (top), and Base #4 when eyes were open (bottom). Left: the largest peaks had a negative r and a negative time lag (EC: $r = -0.23 \pm 0.06$, $\tau = -0.39 \pm 0.25$; EO: $r = -0.28 \pm 0.08$, $\tau = -0.24 \pm 0.06$), suggesting that, regardless of eye condition, LTES deactivation preceded ANT; Right: the largest peaks had a positive r and a negative time lag (EC: $r = 0.26 \pm 0.09$, $\tau = -0.25 \pm 0.08$; EO: $r = 0.29 \pm 0.10$, $\tau = -0.25 \pm 0.08$), suggesting that, regardless of eye condition, LTES activation preceded POST.

Figure 41 shows the averaged CC functions across participants between RLES and ANT (left), and between RLES and POST (right). Results are shown for Base #2 when eyes were closed (top), and Base #4 when eyes were open (bottom). A visual inspection suggests that, regardless of eye condition, RLES deactivation preceded ANT (Left – EC: $r = -0.31 \pm 0.09$, $\tau = -0.29 \pm 0.05$; EO: $r = -0.31 \pm 0.07$, $\tau = -0.22 \pm 0.10$), and RLES activation preceded POST (Right – EC: $r = 0.23 \pm 0.09$, $\tau = -0.24 \pm 0.08$; EO: $r = 0.27 \pm 0.09$, $\tau = -0.23 \pm 0.07$).

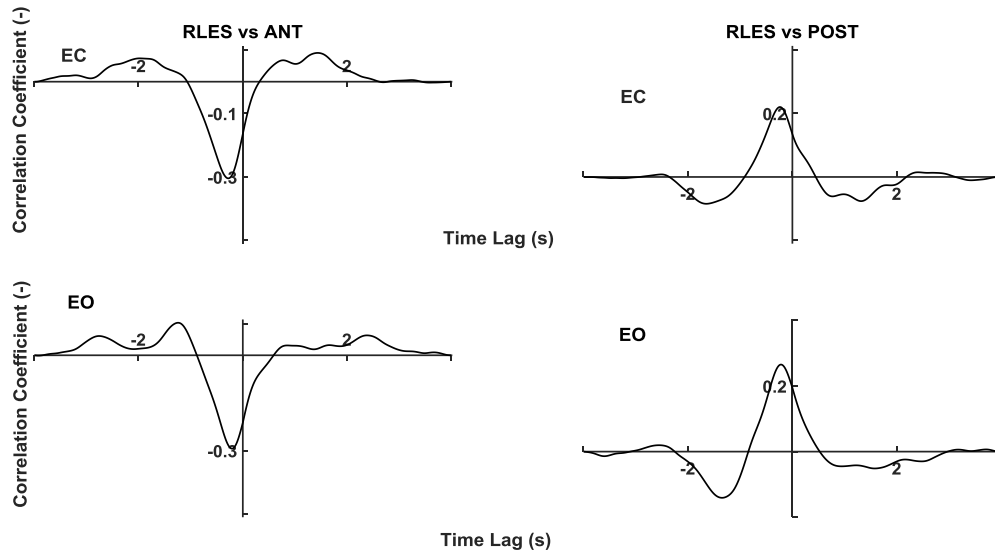


Figure 41. The averaged CC functions across participants between RLES and ANT (left); and the averaged CC functions between RLES and POST (right). Results are shown for Base #2 when eyes were closed (top), and Base #4 when eyes were open (bottom). Left: the largest peaks had a negative r and a negative time lag (EC: $r = -0.31 \pm 0.09$, $\tau = -0.29 \pm 0.05$; EO: $r = -0.31 \pm 0.07$, $\tau = -0.22 \pm 0.10$), suggesting that, regardless of eye condition, RLES deactivation preceded ANT; Right: the largest peaks had a positive r and a negative time lag (EC: $r = 0.23 \pm 0.09$, $\tau = -0.24 \pm 0.08$; EO: $r = 0.27 \pm 0.09$, $\tau = -0.23 \pm 0.07$), suggesting that, regardless of eye condition, RLES activation preceded POST.

Figure 42 shows the averaged CC functions across participants between LLES and ANT (left), and between LLES and POST (right). Results are shown for Base #2 when eyes were closed (top), and Base #4 when eyes were open (bottom). A visual inspection suggests that, regardless of eye condition, LLES deactivation preceded ANT (Left – EC: $r = -0.31 \pm 0.09$, $\tau = -0.25 \pm 0.08$; EO: $r = -0.27 \pm 0.09$, $\tau = -0.16 \pm 0.07$), and LLES activation preceded POST (Right – EC: $r = 0.28 \pm 0.10$, $\tau = -0.17 \pm 0.16$; EO: $r = 0.28 \pm 0.09$, $\tau = -0.18 \pm 0.11$).

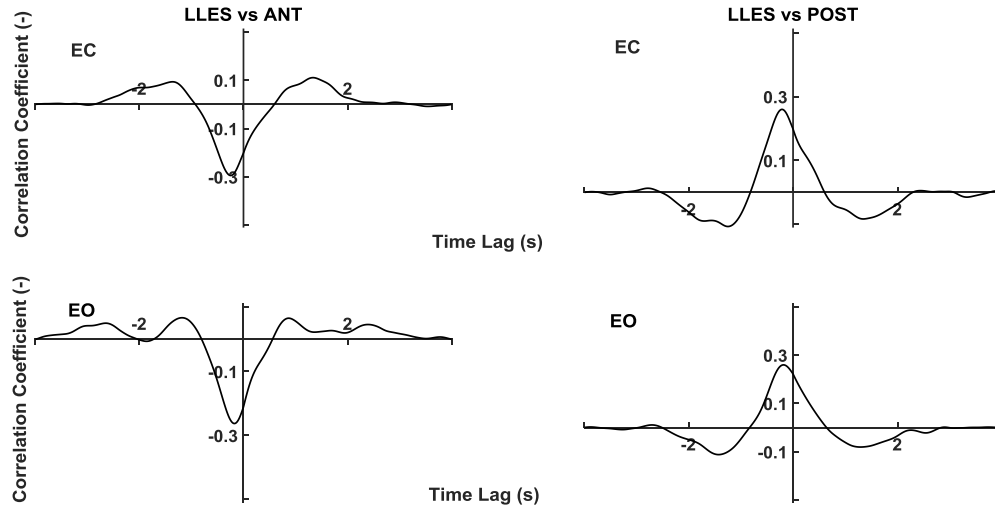


Figure 42. The averaged CC functions across participants between LLES and ANT (left); and the averaged CC functions between LLES and POST (right). Results are shown for Base #2 when eyes were closed (top), and Base #4 when eyes were open (bottom). Left: the largest peaks had a negative r and a negative time lag (EC: $r = -0.31 \pm 0.09$, $\tau = -0.25 \pm 0.08$; EO: $r = -0.27 \pm 0.09$, $\tau = -0.16 \pm 0.07$), suggesting that, regardless of eye condition, RLES deactivation preceded ANT; Right: the largest peaks had a positive r and a negative time lag (EC: $r = 0.28 \pm 0.10$, $\tau = -0.17 \pm 0.16$; EO: $r = 0.28 \pm 0.09$, $\tau = -0.18 \pm 0.11$), suggesting that, regardless of eye condition, RLES activation preceded POST.

Figure 43 shows the averaged CC functions across participants between RBF and ANT (left), and between RBF and POST (right). Results are shown for Base #2 when eyes were closed (top), and Base #4 when eyes were open (bottom). A visual inspection suggests that, regardless of eye condition, RBF activation preceded ANT (Left – EC: $r = 0.54 \pm 0.11$, $\tau = -0.19 \pm 0.04$; EO: $r = 0.47 \pm 0.12$, $\tau = -0.18 \pm 0.05$), and RBF deactivation preceded POST (Right – EC: $r = -0.46 \pm 0.16$, $\tau = -0.18 \pm 0.07$; EO: $r = -0.38 \pm 0.17$, $\tau = -0.20 \pm 0.06$).

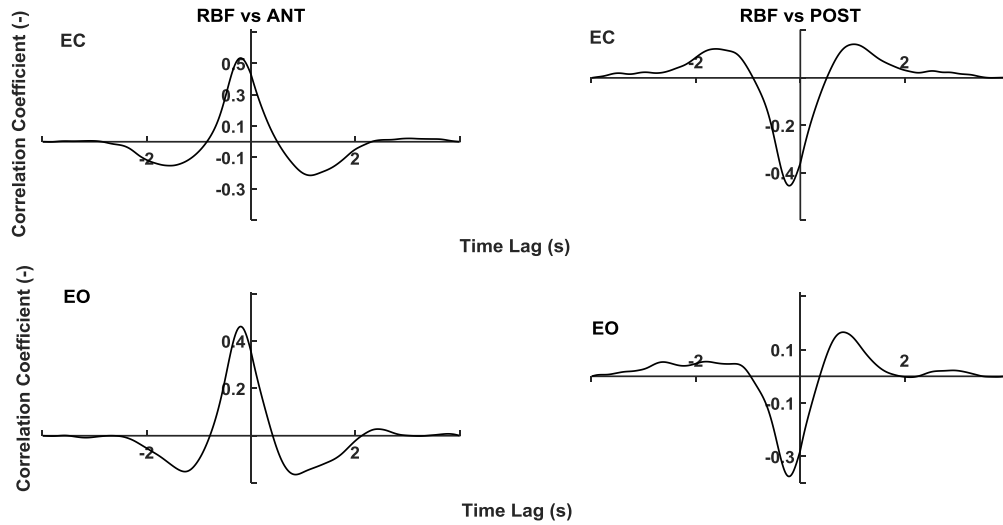


Figure 43. The averaged CC functions across participants between RBF and ANT (left); and the averaged CC functions between RBF and POST (right). Results are shown for Base #2 when eyes were closed (top), and Base #4 when eyes were open (bottom). Left: the largest peaks had a positive r and a negative time lag (EC: $r = 0.54 \pm 0.11$, $\tau = -0.19 \pm 0.04$; EO: $r = 0.47 \pm 0.12$, $\tau = -0.18 \pm 0.05$), suggesting that, regardless of eye condition, RBF activation preceded ANT; Right: the largest peaks had a negative r and a negative time lag (EC: $r = -0.46 \pm 0.16$, $\tau = -0.18 \pm 0.07$; EO: $r = -0.38 \pm 0.17$, $\tau = -0.20 \pm 0.06$), suggesting that, regardless of eye condition, RBF deactivation preceded POST.

Figure 44 shows the averaged CC functions across participants between LBF and ANT (left), and between LBF and POST (right). Results are shown for Base #2 when eyes were closed (top), and Base #4 when eyes were open (bottom). A visual inspection suggests that, regardless of eye condition, LBF activation preceded ANT (Left – EC: $r = 0.53 \pm 0.12$, $\tau = -0.18 \pm 0.06$; EO: $r = 0.52 \pm 0.11$, $\tau = -0.18 \pm 0.06$), and LBF deactivation preceded POST (Right – EC: $r = -0.45 \pm 0.13$, $\tau = -0.19 \pm 0.07$; EO: $r = -0.43 \pm 0.16$, $\tau = -0.19 \pm 0.09$).

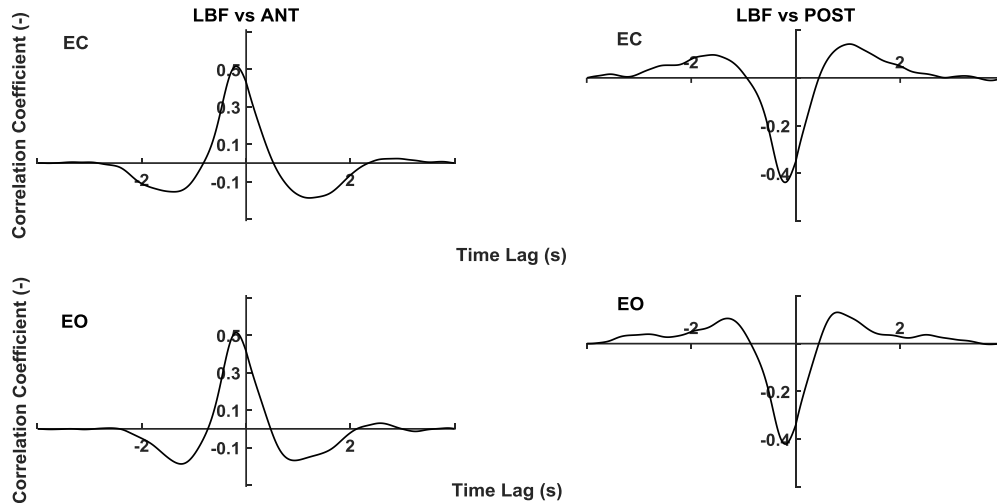


Figure 44. The averaged CC functions across participants between LBF and ANT (left); and the averaged CC functions between LBF and POST (right). Results are shown for Base #2 when eyes were closed (top), and Base #4 when eyes were open (bottom). Left: the largest peaks had a positive r and a negative time lag (EC: $r = 0.53 \pm 0.12$, $\tau = -0.18 \pm 0.06$; EO: $r = 0.52 \pm 0.11$, $\tau = -0.18 \pm 0.06$), suggesting that, regardless of eye condition, RBF activation preceded ANT; Right: the largest peaks had a negative r and a negative time lag (EC: $r = -0.45 \pm 0.13$, $\tau = -0.19 \pm 0.07$; EO: $r = -0.43 \pm 0.16$, $\tau = -0.19 \pm 0.09$), suggesting that, regardless of eye condition, RBF deactivation preceded POST.

Figure 45 shows the averaged CC functions across participants between RRF and ANT (left), and between RRF and POST (right). Results are shown for Base #2 when eyes were closed (top), and Base #4 when eyes were open (bottom). A visual inspection suggests that, regardless of eye condition, RRF deactivation preceded ANT (Left – EC: $r = -0.35 \pm 0.10$, $\tau = -0.21 \pm 0.10$; EO: $r = -0.41 \pm 0.15$, $\tau = -0.20 \pm 0.09$), and RRF activation preceded POST (Right – EC: $r = 0.39 \pm 0.15$, $\tau = -0.22 \pm 0.08$; EO: $r = 0.44 \pm 0.14$, $\tau = -0.18 \pm 0.08$).

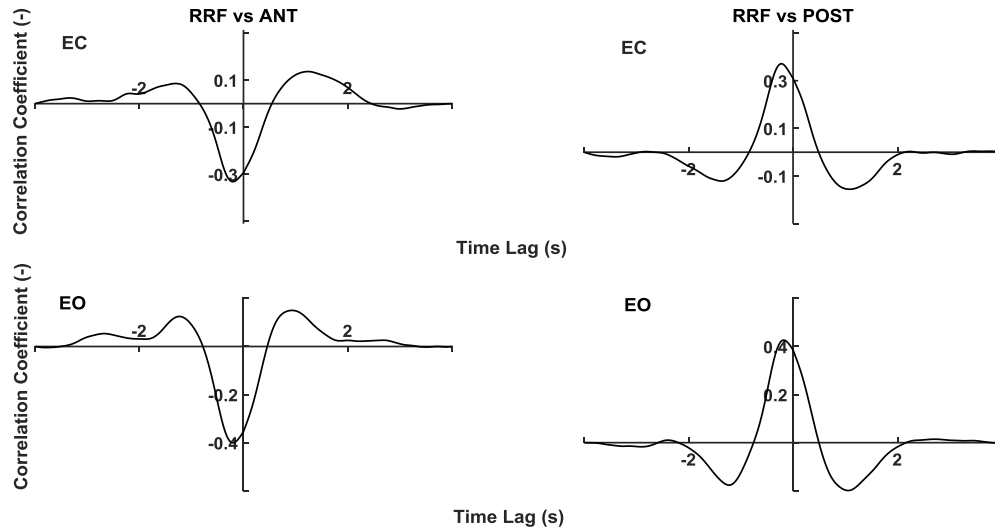


Figure 45. The averaged CC functions across participants between RRF and ANT (left); and the averaged CC functions between RRF and POST (right). Results are shown for Base #2 when eyes were closed (top), and Base #4 when eyes were open (bottom). Left: the largest peaks had a negative r and a negative time lag (EC: $r = -0.35 \pm 0.10$, $\tau = -0.21 \pm 0.10$; EO: $r = -0.41 \pm 0.15$, $\tau = -0.20 \pm 0.09$), suggesting that, regardless of eye condition, RRF deactivation preceded ANT; Right: the largest peaks had a positive r and a negative time lag (EC: $r = 0.39 \pm 0.15$, $\tau = -0.22 \pm 0.08$; EO: $r = 0.44 \pm 0.14$, $\tau = -0.18 \pm 0.08$), suggesting that, regardless of eye condition, RRF activation preceded POST.

Figure 46 shows the averaged CC functions across participants between LRF and ANT (left), and between LRF and POST (right). The results are shown for Base #2 when eyes were closed (top), and Base #4 when eyes were opened (bottom). A visual inspection suggests that regardless of eyes condition, LRF deactivation preceded ANT (Left – EC: $r = -0.40 \pm 0.14$, $\tau = -0.25 \pm 0.17$; EO: $r = -0.39 \pm 0.18$, $\tau = -0.17 \pm 0.12$) and LRF activation preceded POST (Right – EC: $r = 0.49 \pm 0.14$, $\tau = -0.18 \pm 0.09$; EO: $r = 0.47 \pm 0.15$, $\tau = -0.17 \pm 0.07$).

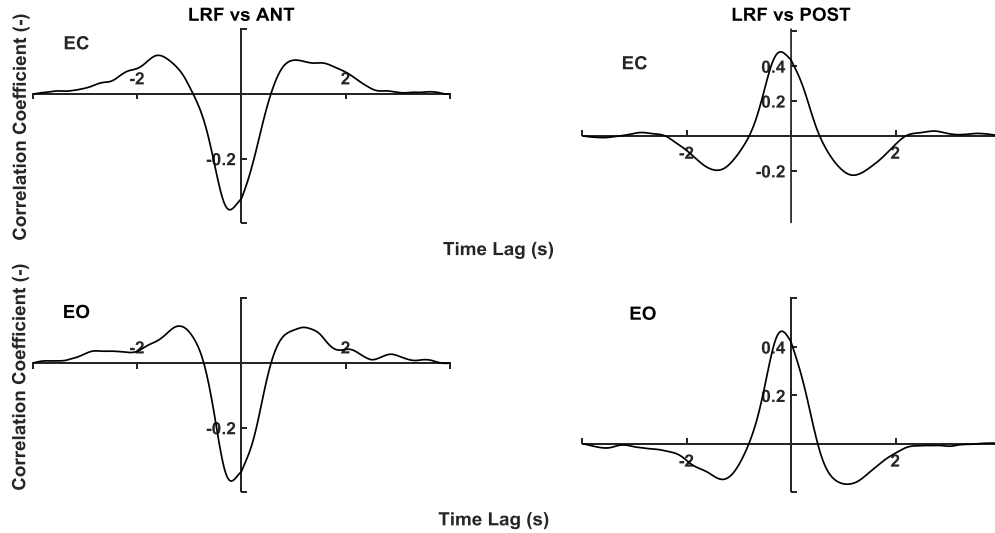


Figure 46. The averaged CC functions across participants between LRF and ANT (left); and the averaged CC functions between LRF and POST (right). Results are shown for Base #2 when eyes were closed (top), and Base #4 when eyes were open (bottom). Left: the largest peaks had a negative r and a negative time lag (EC: $r = -0.40 \pm 0.14$, $\tau = -0.25 \pm 0.17$; EO: $r = -0.39 \pm 0.18$, $\tau = -0.17 \pm 0.12$), suggesting that, regardless of eye condition, LRF deactivation preceded ANT; Right: the largest peaks had a positive r and a negative time lag (EC: $r = 0.49 \pm 0.14$, $\tau = -0.18 \pm 0.09$; EO: $r = 0.47 \pm 0.15$, $\tau = -0.17 \pm 0.07$), suggesting that, regardless of eye condition, LRF activation preceded POST.

The group-ensemble correlation coefficient (r) and time lag (τ) values (mean \pm SD) under Base #2/EC and Base #4/EO conditions for ANT and POST are shown in Table 18.

Table 18. Correlation coefficient and time lag values for ANT and POST under Base #2/EC and Base #4/EO conditions for the following muscles: right rectus abdominis, left rectus abdominis, right thoracic erector spinae, left thoracic erector spinae, right lumbar erector spinae, left lumbar erector spinae, right biceps femoris, left biceps femoris, right rectus femoris, and left rectus femoris. All values are presented as mean \pm SD.

Muscle	Anterior				Posterior			
	B #2, EC		B #4, EO		B #2, EC		B #4, EO	
	r (-)	τ (s)						
RRA	0.33 \pm 0.09	-0.16 \pm 0.04	0.39 \pm 0.12	-0.18 \pm 0.04	-0.24 \pm 0.07	-0.11 \pm 0.07	-0.34 \pm 0.11	-0.17 \pm 0.04
LRA	0.30 \pm 0.09	-0.14 \pm 0.04	0.40 \pm 0.14	-0.18 \pm 0.05	-0.24 \pm 0.07	-0.16 \pm 0.06	-0.30 \pm 0.06	-0.17 \pm 0.05
RTES	-0.21 \pm 0.06	-0.45 \pm 0.41	-0.29 \pm 0.07	-0.19 \pm 0.10	0.27 \pm 0.06	-0.17 \pm 0.09	0.31 \pm 0.10	-0.20 \pm 0.09
LTES	-0.23 \pm 0.06	-0.39 \pm 0.25	-0.28 \pm 0.08	-0.24 \pm 0.06	0.26 \pm 0.09	-0.25 \pm 0.08	0.29 \pm 0.10	-0.25 \pm 0.08
RLES	-0.31 \pm 0.09	-0.29 \pm 0.05	-0.31 \pm 0.07	-0.22 \pm 0.10	0.23 \pm 0.09	-0.24 \pm 0.08	0.27 \pm 0.09	-0.23 \pm 0.07
LLES	-0.31 \pm 0.09	-0.25 \pm 0.08	-0.27 \pm 0.09	-0.16 \pm 0.07	0.28 \pm 0.10	-0.17 \pm 0.16	0.28 \pm 0.09	-0.18 \pm 0.11
RBF	0.54 \pm 0.11	-0.19 \pm 0.04	0.47 \pm 0.12	-0.18 \pm 0.05	-0.46 \pm 0.16	-0.18 \pm 0.07	-0.38 \pm 0.17	-0.20 \pm 0.06
LBF	0.53 \pm 0.12	-0.18 \pm 0.06	0.52 \pm 0.11	-0.18 \pm 0.06	-0.45 \pm 0.13	-0.19 \pm 0.07	-0.43 \pm 0.16	-0.19 \pm 0.09
RRF	-0.35 \pm 0.10	-0.21 \pm 0.10	-0.41 \pm 0.15	-0.20 \pm 0.09	0.39 \pm 0.15	-0.22 \pm 0.08	0.44 \pm 0.14	0.18 \pm 0.08
LRF	-0.40 \pm 0.14	-0.25 \pm 0.17	-0.39 \pm 0.18	-0.17 \pm 0.12	0.49 \pm 0.14	-0.18 \pm 0.09	0.47 \pm 0.15	0.17 \pm 0.07

5.4.3.2 Medial-Lateral Wobble Board Displacements

The CC results show that, in general, LEFT and RIGHT correlated with ExO only. The activation and deactivation of RExO preceded RIGHT and LEFT, respectively (Figure 47; left). Moreover, the deactivation and activation of LExO preceded RIGHT and LEFT, respectively (Figure 47; right).

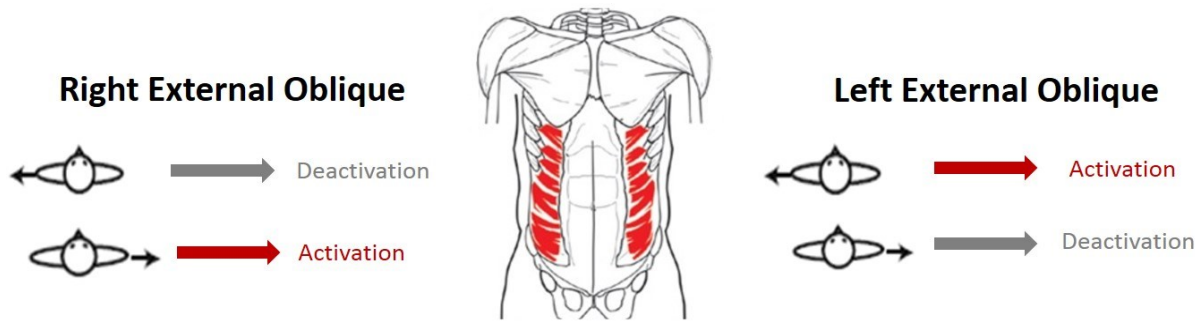


Figure 47. A schematic summary of findings during medial-lateral wobble board displacements [268]. The CC results indicate the activation and deactivation of RExO during RIGHT and LEFT wobble board displacements, respectively. Moreover, they indicate the deactivation and activation of LExO during RIGHT and LEFT wobble board displacements, respectively.

Figure 48 shows the averaged CC functions across participants between RExO and LEFT (left), and between RExO and RIGHT (right). The results are shown for Base #2 when eyes were closed (top), and Base #4 when eyes were open (bottom). A visual inspection suggests that, regardless of eye condition, RExO deactivation preceded LEFT (Left – EC: $r = -0.42 \pm 0.13$, $\tau = -0.19 \pm 0.09$; EO: $r = -0.50 \pm 0.14$, $\tau = -0.16 \pm 0.08$), and RExO activation preceded RIGHT (Right – EC: $r = 0.43 \pm 0.16$, $\tau = -0.17 \pm 0.09$; EO: $r = 0.55 \pm 0.17$, $\tau = -0.17 \pm 0.05$).

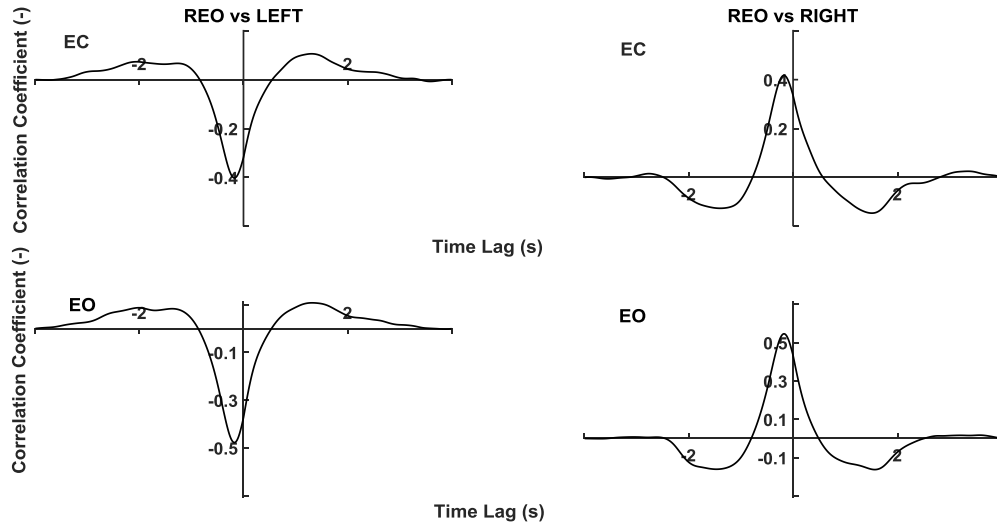


Figure 48. The averaged CC functions across participants between RExO and LEFT (left); and the averaged CC functions between RExO and RIGHT (right). Results are shown for Base #2 when eyes were closed (top), and Base #4 when eyes were open (bottom). Left: the largest peaks had a negative r and a negative time lag (EC: $r = -0.42 \pm 0.13$, $\tau = -0.19 \pm 0.09$; EO: $r = -0.50 \pm 0.14$, $\tau = -0.16 \pm 0.08$), suggesting that, regardless of eye condition, RExO deactivation preceded LEFT; Right: the largest peaks had a positive r and a negative time lag (EC: $r = 0.43 \pm 0.16$, $\tau = -0.17 \pm 0.09$; EO: $r = 0.55 \pm 0.17$, $\tau = -0.17 \pm 0.05$), suggesting that, regardless of eye condition, RExO activation preceded RIGHT.

Figure 49 shows the averaged CC functions across participants between LExO and LEFT (left), and between LExO and RIGHT (right). Results are shown for Base #2 when eyes were closed (top), and Base #4 when eyes were open (bottom). A visual inspection suggests that, regardless of eye condition, LExO activation preceded LEFT (Left – EC: $r = 0.46 \pm 0.16$, $\tau = -0.18 \pm 0.06$; EO: $r = 0.61 \pm 0.12$, $\tau = -0.18 \pm 0.04$), and LExO deactivation preceded RIGHT (Right – EC: $r = -0.38 \pm 0.15$, $\tau = -0.19 \pm 0.04$; EO: $r = -0.55 \pm 0.10$, $\tau = -0.16 \pm 0.06$).

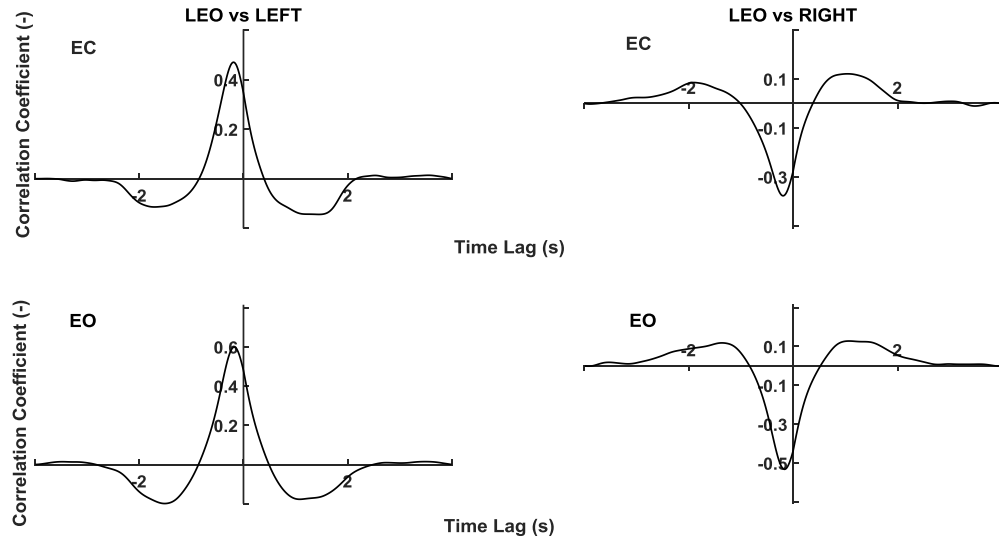


Figure 49. The averaged CC functions across participants between LExO and LEFT (left); and the averaged CC functions between LExO and RIGHT (right). Results are shown for Base #2 when eyes were closed (top), and Base #4 when eyes were open (bottom). Left: the largest peaks had a positive r and a negative time lag (EC: $r = 0.46 \pm 0.16$, $\tau = -0.18 \pm 0.06$; EO: $r = 0.61 \pm 0.12$, $\tau = -0.18 \pm 0.04$), suggesting that, regardless of eye condition, LExO activation preceded LEFT; Right: the largest peaks had a negative r and a negative time lag (EC: $r = -0.38 \pm 0.15$, $\tau = -0.19 \pm 0.04$; EO: $r = -0.55 \pm 0.10$, $\tau = -0.16 \pm 0.06$), suggesting that, regardless of eye condition, LExO deactivation preceded RIGHT.

The group-ensemble correlation coefficient (r) and time lag (τ) values (mean \pm SD) for LEFT and RIGHT under Base #2/EC and Base #4/EO conditions are shown in Table 19.

Table 19. Correlation coefficient and time lag values for LEFT and RIGHT under Base #2/EC and Base #4/EO conditions for RExO and LExO. All values are presented as mean \pm SD.

Muscle	Left				Right			
	B #2, EC		B #4, EO		B #2, EC		B #4, EO	
	r (-)	τ (s)						
REO	-0.42 ± 0.13	-0.19 ± 0.09	-0.50 ± 0.14	-0.16 ± 0.08	0.43 ± 0.16	-0.17 ± 0.09	0.55 ± 0.17	-0.17 ± 0.05
LEO	0.46 ± 0.16	-0.18 ± 0.06	0.61 ± 0.12	-0.18 ± 0.04	-0.38 ± 0.15	-0.19 ± 0.04	-0.55 ± 0.10	-0.16 ± 0.06

Chapter 6

6 Discussion

The main goal of this study was to obtain a more comprehensive, quantitative understanding of the neuromechanical mechanisms of dynamic sitting control during continuous multi-directional perturbations. In what follows, we elaborate on the validity of the applied methodology to quantify postural control during sitting. Furthermore, we characterize the role of seat instability level and the presence of visual information in stabilizing the body. Finally, we discuss spatial and temporal determinants of dynamic sitting control and use them to propose the presence of a postural adjustment strategy that is CNS-based and utilized to stabilize the wobble board.

6.1 Adequacy of Using Wobble Board Kinematics to Quantify Postural Control During Unstable Sitting

As previously mentioned, three types of measures may be used to quantify postural proficiency: COP measures [93], [94], [96], [104], [105], [107]; trunk kinematics measures [90], [92], [93], [106], [225], [229] and/or wobble board kinematics measures [89], [90], [92], [95], [225], [229]. Prieto et al. [262] and others [93], [94], [96], [104], [105], [107], [263] described or utilized the most common method for computing a range of posturographic measures (such as time-domain and frequency-domain measures), which is based on the displacement of the COP measured via a force plate. However, several studies followed the procedure applied by Prieto et al. to compute posturographic measures using angular kinematics instead of COP trajectories [92], [226]. More specifically, *these studies have applied trunk kinematics to quantify postural steadiness.*

At the same time, it has been suggested that, during dynamic sitting, not only trunk kinematics, but also wobble board kinematics capture information similar to the COP [226]. In fact, Lariviere et al. [226] showed that, during unstable sitting, *support surface tilt angles and COP displacements are highly correlated.* Although wobble board kinematics measures may not completely reflect the

information captured by trunk kinematics, *wobble board and trunk kinematics have been shown to be correlated* as well [229]. While Freddolini et al. [89], [90], [225] used wobble board kinematics to quantify postural control for the lower limbs, Lee et al. [95] used them for the trunk. Moreover, in several studies, the kinematic trajectories of the wobble board have been applied to characterize postural control during unstable sitting [89], [90], [92], [95], [225], [229]. Based on all considerations above, we chose to use wobble board kinematics – and specifically wobble board kinematics measures as well as the correlation between trunk muscle activity and wobble board kinematics – to characterize postural control during unstable sitting.

6.2 Postural Control Effort and Output are Affected by Seat Instability Level

The results on postural steadiness in accordance with the approach by Prieto et al. [262] revealed that the time-domain measures were significantly larger when increasing seat instability level (i.e., from Base #1 to Base #2 under eyes closed condition, and from Base #3 to Base #4 under eyes open condition). Although there is no universal consensus regarding the interpretation of these measures [269], [270], it has been suggested in the literature that distance measures are associated with postural stability performance (i.e., the stabilization outcome) [271]–[273], whereas velocity measures are associated with the underlying control demand (i.e., the degree of neuromuscular activity required to achieve stability) [271]–[273]. However, it should be noted that these studies used COP measures as obtained via a force plate, whereas the present study reports on angular kinematic measures obtained via optical motion capture. Nevertheless, using the logic presented in the literature, our results suggest that, by increasing task difficulty, stability performance is reduced (due to an increase in MA and RMSA measures), and the need for postural adjustments is increased (due to an increase in MV and RMSV measures).

These findings are consistent with the outcomes published by Cholewicki et al. [94] who reported that postural stability performance is reduced in AP and ML directions when task difficulty increases. Radebold et al. [105] and Silfies et al. [104] also showed that, by increasing seat instability level, stability performance decreases in both the AP and ML directions. In the former study, the study sample included both non-disabled individuals and those with LBP, whereas, in

the latter study, only non-disabled individuals participated. In terms of velocity measures, our results are in agreement with the findings of Oomen et al. [229] who demonstrated that the wobble board velocity increases when task difficulty increases. Moreover, as expected, our results demonstrate that the RANGE measure increased significantly when the degree of seat instability increased. This increase in angular displacement range is presumably a consequence of the increase in the velocity measures that reflects a larger control demand when stabilizing wobble board bases of smaller diameter [222], [229].

Our findings also demonstrate that the CFREQ measure significantly decreased in AP, ML, and TM when moving from Base #1 to Base #2 for the eyes closed condition. It has been reported that CFREQ is inversely proportional to and, hence, an indirect measure of the moment of inertia of a dynamic system and the time for that system to return to equilibrium position [272]. Systems with a larger moments of inertia are more sluggish and require more time to return to their initial position [271]–[274], which suggests that these systems may be less stable [91]. Our findings suggest that moving from an easier to a more difficult wobble board base may increase the effective moment of inertia of the trunk and wobble board system (a decrease in CFREQ measure), implying that the system is less stable when a more difficult wobble board base is used. This is not surprising, however, given the discussed time-domain evidence that postural stability performance decreases when the task difficulty is increased.

6.3 Visual Input Improves Stability During Unstable Seated Balance

The effect of visual input was investigated by comparing posturographic measures (i.e., time- and frequency-domain measures) between eyes open and eyes closed conditions when participants were balancing on Base #2. As expected, all time-domain measures, except for RMSA in TD, were significantly larger when eyes were closed. This indicates that stability performance is reduced (due to an increase in MA and RMSA measures) and the degree of postural adjustments increased (due to an increase in MV and RMSV measures) when visual input was lacking. It also implies a larger range in wobble board displacement when the eyes are closed (indicated by an increase in the RANGE measure) [271]–[273]. These time-domain findings on the influence of vision are

fully in line with those on the influence of seat instability level, indicating that increasing seat instability has a similar effect on dynamic balance control and output as eliminating visual input.

The visual, proprioceptive, and vestibular systems are three major sensory systems that have been shown to contribute to the sensorimotor control of upper body stability [96], [104], [105], [222], [275]: the visual system captures information regarding the spatial orientation and motion of the head and trunk [104], [276]; the proprioceptive system provides information regarding the orientation and motion of the various body segments with respect to each other [276]; and the vestibular system measures information regarding head orientation and motion in space [276]. Knowledge on the spatial and intersegmental orientation of the body as acquired by these sensory modalities has been shown to be essential for postural control and head stability once passed on to the CNS [277]. By eliminating visual input, a reduced level of information is available to the neuromuscular control system, resulting in a stronger reliance on the proprioceptive and vestibular systems [276]. Previous studies have shown that, in response to perturbations during sitting, participants rely more heavily on visual and proprioceptive inputs to stabilize the head and trunk [278], [279]. Our results suggest that the accuracy and precision of postural control can not be fully compensated by the proprioceptive and vestibular systems, and that the output of the postural control system is reduced when the eyes are closed [104]. However, further investigation is required to confirm these relations.

Our results are in line with the findings of Silfies et al. [104] who also reported that stability performance decreases with eyes closed. Moreover, our results are consistent with those of Andreopoulou et al. [222] who found that wobble board sway increased in the ML direction when eyes are closed. Our findings also demonstrate that, for the eyes open condition, FREQD was significantly larger in the AP and ML directions than for the eyes closed condition. It has been suggested for upright standing and quasi-static sitting measured via a force plate that FREQD may be related to trunk stiffness, with a decrease in trunk stiffness presumably increasing FREQD [271]–[273], [280]. Furthermore, Collins and De Luca [281] suggested that visual input may reduce trunk stiffness during static standing. Taken together, these findings may explain why FREQD decreased when eyes were closed: with the lack of visual input, trunk stiffness presumably increased and, consequently, FREQD decreased. Note that such increase in trunk stiffness may be

caused by a larger degree of co-contraction of agonist and antagonist muscles [16], [27] in comparison to the eyes open condition.

In addition to *dynamic sitting*, several studies have investigated the effect of eye condition on *quiet sitting*. Vette et al. [263] examined sitting balance of non-disabled participants, sitting directly on a force plate without a footrest, and reported that none of the time-domain measures were significantly different with the lack of visual input. Similarly, Serra-Ano et al. [282] and Maaswinkel et al. [283] showed that the lack of vision had no significant effect on time-domain measures in non-disabled individuals during quiet sitting. Moreover, Radebold et al. [105] and Andreopoulou et al. [222] found that, during unstable sitting, postural stability performance reduces in the absence of visual input; however, this dependency was not present for quiet sitting. In the study conducted by Radebold et al. [105], the performance of non-disabled individuals was compared with that of individuals suffering under LBP. Meanwhile, in the study by Andreopoulou et al. [222], only non-disabled individuals participated. Findings from all of the above studies suggest that, during dynamic sitting, vision has a more significant role in stabilizing the human body than during quiet sitting, and that a lack of visual input reduces postural stability for dynamic sitting only.

6.4 How Does the Human Body Control Upright Sitting While Balancing on a Wobble Board?

6.4.1 Correlation Between Muscle Activation/Deactivation and Wobble Board Motion Confirms the *Presence* of Active Control

Stability is defined as the ability of a system to return to an equilibrium position after an external or internal perturbation [1]. For quiet sitting and gentle perturbations, a tonic activation of muscles may be sufficient to achieve stability of the trunk [16], [169]. For large perturbations, however, neurally-driven, direction-specific activation of the muscles is essential for maintaining trunk stability [1]. In this context, the results of this study showed that, independent of muscle and base, correlations between muscle activity and wobble board displacement exist. This suggests that, during unstable sitting, phasic muscle activation is required to stabilize the trunk, with this phasic

activation being indicative of active control (i.e., control that originates in the CNS and is neurally-driven) [52], [284]–[287]. It should be noted that we are not questioning the existence and contribution of passive control to dynamic sitting (i.e., stabilization due to intrinsic mechanical properties of the spine, joints, and connective tissue as well as due to intraabdominal pressure); however, our results strongly suggest that active control is involved in maintaining stability during unstable sitting.

Overall, the outcomes of this study indicate that the activity of the trunk and upper leg muscles are correlated with wobble board motion. Moreover, it can be seen that, generally, the degree of correlation increased with increasing degree of seat instability (see Figure 35). This suggests that, when task difficulty increased, wobble board displacement and/or phasic trunk and upper leg muscle activation/deactivation increased – and this irrespective of eye condition. On the one hand, an increase in wobble board displacement with task difficulty agrees with our posturographic findings above, which is also consistent with previous studies on postural sway during dynamic sitting [94], [104], [105]. On the other hand, Oomen et al. [229] reported that, during dynamic sitting, muscle activation increases when task difficulty increases. Taken together, these previous studies support our conclusion that most likely both – wobble board displacement and phasic muscle activation/deactivation – increased when seat instability level increased.

6.4.2 Spatial Configuration of Trunk and Upper Leg Muscles is a *Key Influencer* of Active Control

Our findings also provide strong evidence for the existence of a direction-specific activation or deactivation of the trunk and upper leg muscles. Several studies have investigated the muscle response to perturbations during sitting. Zedka et al. [51] investigated responses of the trunk muscles to perturbations in the AP and ML directions during sitting and reported that trunk muscles respond to perturbations in a direction-specific manner. Moreover, Preuss and Fung [53], investigating the response of the trunk muscles to multidirectional perturbations in eight directions during both sitting and standing, reported that the direction of the perturbation influences the activity of the trunk muscles. Masani et al. [52] also applied perturbation forces in eight different directions during sitting, demonstrating that the muscle response depended on the pulling direction. Our results agree with these studies in the fact that, for each direction of the perturbation

(i.e., each direction of the wobble board displacement), certain muscles got intermittently activated. This directional dependency of the muscles may be explained by their geometry and anatomical placement [288]. Since the fibers of the RA and ES muscles run vertically down the trunk [48], they are more likely to get activated in the sagittal plane [52]. Conversely, since the fibers of ExO cross the trunk diagonally and transversely [48], they cover a wider range than RA and ES, and this across the sagittal and frontal planes. Therefore, also the range of action of ExO may be wider than of RA and ES [52].

Co-activation (i.e., contraction of a group of muscles) [51], [90], [229], [289], [290] and reciprocal activation (i.e., contraction of an agonist muscle while its antagonist relaxes) [229], [290], [291] of the muscles have been reported in several studies. Based on the task, the CNS chooses the appropriate muscle recruitment strategy to stabilize the body [224], [292]. The results of this study suggest that the CNS uses co-activation and reciprocal activation of muscles to stabilize the body during dynamic sitting: RA and BF got activated (deactivated) shortly before the wobble board tilted forward (backward); ES and RF got activated (deactivated) shortly before the wobble board tilted backward (forward); RExO got activated (deactivated) shortly before the wobble board tilted to the right (left); and LExO got activated (deactivated) shortly before the wobble board tilted to the left (right). Using co-activation and reciprocal activation of the muscles in this spatial and temporal configuration suggests that the CNS may implement a control strategy for stabilizing the wobble board that, while common across muscles, is differentially executed based on the muscles' anatomical placement.

6.4.3 Temporal and Spatial Determinants of Trunk and Upper Leg Muscle Activation/Deactivation Provide Insights into the Underlying *Type* of Active Control

Our results showed that RA and BF activation or deactivation preceded wobble board motion by approximately 200 ms; ES and RF activation preceded wobble board motion by approximately 250 and 200 ms, respectively; ES and RF deactivation preceded wobble board motion by approximately 300 and 200 ms, respectively; and RExO and LExO activation or deactivation preceded wobble board motion by approximately 200 ms. These time delays between muscle activation/deactivation and wobble board motion are in line with the studies by Gatev al. [284]

and Masani et al. [287] who reported that, during quiet standing, EMG activity preceded COP displacement by approximately 250 to 300 ms and 250 ms, respectively. Gatev et al. [284] concluded that the CNS anticipates changes in body position based on position and velocity measurements by the proprioceptive and vestibular systems [284], [286], [293] and activates the muscles in advance to stabilize the body. Masani et al. [286], [287] supported this interpretation by means of simulation studies, concluding that the body velocity information must play a significant role in modulating the muscle activity in such an anticipatory manner. In their as well as our cases, the described temporal relations capture the time interval from the time the EMG signal is generated to the time a moment is generated (i.e., neuromusculoskeletal torque generation delay) [294] to cause or counter the measured motion or ground reaction. In the literature, the neuromusculoskeletal torque generation delay (oftentimes also called electromechanical delay – a term more appropriately used for the delay between muscle fiber activation and muscle fiber force generation [3]) has been reported to be in the range between 200 to 380 ms for the ankle joint [294], which is also in line with our findings for the trunk-wobble board interface. As will be explored below, these temporal features, along with our results on the spatial determinants of muscle activation, suggest that the CNS modulates muscle activity in an anticipatory manner to break, or dampen, the upcoming wobble board motion via stiffness control.

Visual observations during the experiments suggest that, during unstable sitting on the wobble board, trunk movement was small in comparison to wobble board movement, and that the participants balanced on the wobble board while keeping their trunk in a relatively stable position. Mechanically speaking, the wobble board was smaller, lighter, and of smaller inertia compared to the trunk and experienced the highest degree of instability at the wobble board-stool interface. As such, it is reasonable to assume that the primary goal of the dynamic system was to stabilize the wobble board – and that stabilizing the trunk relative to the wobble board was only a secondary, yet interconnected goal. Note that this mechanical assessment agrees with our visual assessment during the experiments.

In parallel to these considerations on mechanical stabilization of the trunk and wobble board system, our results indicate that RA and BF, as well as ES and RF, are spatially correlated with anterior-posterior wobble board displacement. Our findings showed that RA and BF activation

preceded ANT, suggesting that these muscles got activated in advance of, but mostly simultaneously with anterior wobble board motion. Based on the velocity information of the body and wobble board as obtained from sensory systems (see above) [287], [295]–[297], the CNS can proactively contract RA and BF to break, or dampen, the forward wobble board displacement. If considered alone, the activation of RA may cause a backward wobble board moment when the trunk is assumed to be stable (see above); accordingly, if considered alone, the activation of BF may cause a forward wobble board moment when the trunk is assumed to be stable (see above). However, as both these muscles are co-contracted, they may serve as agonist and antagonist muscles relative to the sagittal plane motion of the wobble board, resulting in an increase of stiffness at the trunk-wobble board interface. Such increase in stiffness then breaks the upcoming wobble board movement in the anterior direction. Moreover, it can be speculated that the net moment generated by RA may be greater than that by BF, which counters the upcoming wobble board movement even further. However, further investigations into the relative moment contributions of RA and BF are required to confirm this.

Similar to the above, our results also showed that ES and RF activation preceded POST, suggesting that these muscles got activated in advance of, but mostly simultaneously with wobble board motion, to break, or dampen, wobble board motion in the posterior direction. If considered alone, the activation of ES may cause a forward wobble board moment when the trunk is assumed to be stable (see above); accordingly, if considered alone, the activation of RF may cause a backward wobble moment when the trunk is assumed to be stable (see above). However, as both these muscles are co-contracted, they again may serve as agonist and antagonist muscles relative to the sagittal plane motion of the wobble board, resulting in an increase of stiffness at the trunk-wobble board interface. Such increase in stiffness then breaks the upcoming wobble board movement in the posterior direction. Moreover, it can be speculated that the net moment generated by ES may be greater than that by RF, which counters the upcoming wobble board movement even further. Again, further investigations into the relative moment contributions of ES and RF are required to confirm this.

Moreover, among all muscles being studied, only RExO and LExO were spatially correlated with medial-lateral wobble board displacement. RExO (LExO) activation preceded RIGHT (LEFT),

suggesting that the CNS proactively contracted RExO (LExO) to break, or dampen, the upcoming RIGHT (LEFT) wobble board movement via a LEFT moment. Several reasons may exist why the ExO muscles were not paired with an antagonist muscle to increase stiffness in the frontal plane, as was observed for the sagittal plane: (1) the activation of other muscles studied in the present study did not result in a sufficiently strong correlation with wobble board movement; (2) the muscle or muscles that could exhibit such behavior in the frontal plane were not studied; and/or (3) wobble board stabilization in the frontal plane is not a result of effective stiffness modulation, but a pure result of agonist, i.e., in this case of RExO (RIGHT) and LExO (LEFT) activation.

6.5 Limitations of This Thesis Research

This study was subject to some limitations. The first limitation of this study was the use of surface electrodes to record EMG. The electrical cross-talk from the heart and/or a nearby muscle is one of the main concerns when using surface electrodes. The second limitation of this study was that the markers were placed on the t-shirt and shorts instead of the skin. While errors may occur due to relative movement between the skin and either the t-shirt or the shorts, these errors were minimized by using tightly fitting garments. Moreover, marker misplacement may induce error, since the identification of anatomical landmarks depends on the level of expertise of the researcher. However, these errors were minimized by practicing both the marker placement and experimental protocol. Time constraints in executing the experimental protocol (due to ethical reasons and fatigue concerns) represented another limitation of this study: While the reliability of the posturographic measures requires many trials of the same condition, only four trials were performed per condition due to time constraints; however, it should be noted that other studies have used a similar number of trials in their work [107], [224], [225], [228], [231]. Although many previous studies have used manual exercises for eliciting trunk and leg MVCs [145], [158], [161], [241], [243], [245], the lack of use of an appropriate apparatus to restrict body movement during MVC exercises could be viewed as another limitation of this study. Finally, several aspects of this study could be improved: More time could have been dedicated to train the participants for MVC exercises to ensure that true MVCs are elicited, and to further allow them to familiarize themselves with the wobble board to reduce a potential effect of learning. However, increasing respective times would also lead to an increase in muscular and attentional fatigue.

Chapter 7

7 Conclusions

For individuals with SCI, one of the top priorities is to improve trunk control and, consequently, their quality of life. To enhance existing therapies or develop bio-inspired assistive technologies that can facilitate trunk stability in these individuals, a more comprehensive, quantitative understanding of the neuromechanical mechanisms of dynamic sitting control in non-disabled individuals is needed.

The first objective of this study was to quantify the effect of varying levels of wobble board instability as well as of visual information elimination on postural efficiency during continuous, multi-directional perturbations. To the best of our knowledge, no study to date has used wobble board kinematic measures to quantify the effect of different seat instability levels on postural control during unstable sitting. Our findings suggest that postural stability is reduced when task difficulty is increased. Moreover, our results revealed that visual input significantly improves postural control. Although several studies investigated the effect of visual input on unstable sitting during multi-directional perturbations, their studies used COP measures to quantify postural proficiency, whereas, in our study, wobble board kinematic measures were used. Our outcomes suggest that the wobble board could be used, along with posturographic measures, as a stand-alone tool for quantitatively assessing dynamic balance – without the need for a costly force plate. To facilitate this, an inexpensive inertial measurement unit could be integrated into the wobble board to measure the wobble board's planar or three-dimensional kinematics in real-time. More work would be needed, however, to validate the sensor's measurements against a gold-standard motion capture system as was used in this study. Our results also demonstrate that visual information plays a significant role in stabilizing the body during dynamic sitting and that eliminating visual information during the balancing task has a similar effect on stabilization control and output as increasing seat instability level.

The second objective of this study was to quantify the temporal and spatial relationship between muscle activity and wobble board motion during continuous multi-directional perturbations. Our findings suggest that muscle activity and wobble board motion are, in fact, correlated, proving that active control is needed during the dynamic balancing task. More specifically, all muscles being studied (abdominal muscles, back muscles, and upper leg muscles) were spatially correlated with wobble board motion except for LD, which suggests that LD may not be a primary contributor to stabilizing the body during unstable sitting. These results have important implications for therapeutic rehabilitation programs that target an individual's muscle strength for the purpose of improving trunk stability and upper body control. In this context, we have also shown that the CNS modulates phasic muscle activation and deactivation to break, or dampen, the upcoming wobble board motion. This suggests that the primary goal of the dynamic system was to stabilize the wobble board – and that stabilizing the trunk relative to the wobble board was only a secondary, yet interconnected goal. Note that this interpretation also agrees with our visual observations during the experiments.

While the phasic activation/deactivation of the involved muscles is indicative of active control as described above, its spatial configuration suggests that it is particularly utilized by the CNS to increase the effective stiffness between the human body and the wobble board. The observed control strategy – the use of phasic muscle activity for the purpose of stiffness control – is characteristic and quite unique for the wobble board task and was consistently found across different muscles (RA, ES, BF, RF) and movement directions (ANT, POST). For the frontal plane (ML direction), this stiffness strategy was, however, not observed as only the ExO muscles were used agonistically to break, or dampen, the imminent movement. More work is needed to determine whether other muscles that were not studied in this work may serve as antagonists in the ML direction, allowing us to prove or dispute the use of stiffness control in the frontal plane.

In addition to the spatial insights, the temporal features of muscle activation demonstrate that the muscles, using the stiffness control approach described above, were activated *prior* to wobble board motion. These findings are in line with previous studies for quiet standing that have demonstrated in both experimental and simulation work that the CNS is able to use the velocity information of the various sensory modalities to generate a motor command *in advance* of an

imminent displacement. The time difference between muscle activation and displacement may be needed – in our as well as the previous studies – to compensate for the neuromusculoskeletal torque generation delay between muscle activation and moment generation, which can be quite long (up to 300 ms and longer). If this strategy is, in fact, at work for our experimental paradigm, it demonstrates that the CNS uses this velocity-based approach not only for quiet standing, but also for other postural tasks.

As demonstrated above, our work has made significant contributions to our fundamental understanding of human balance control in general and of wobble board stabilization more specifically. The gained knowledge may be beneficial for enhancing existing therapies for facilitating upper body stability and for developing advanced, bio-inspired assistive technologies for individuals with complete or incomplete SCI that effectively recruit target muscles in dependence of body kinematics.

7.1 Recommendations for Future Work

In the fundamental domain, future work could focus on using posturographic measures to characterize postural control during unstable sitting (wobble board) in comparison to quiet sitting. Moreover, it would be of interest to assess the trunk and pelvis kinematics during wobble board use and to characterize their role in body and wobble board stabilization. Finally, the role of other muscles, i.e., that were not studied in this work, in ML stabilization should be explored.

In the rehabilitative domain, future work could focus on integrating a validated inertial measurement unit into the wobble board, allowing it to be used as a quantitative assessment tool for those individuals that cannot be assessed in a standing posture. As this work demonstrates, the kinematic measurements of the wobble board along with posturographic measures could distinguish between different levels of balance proficiency in dependence of seat instability level and the availability of visual information. Finally, a training protocol could be developed to examine the effect of muscle strengthening on postural proficiency on and off the wobble board.

In the assistive technology domain, our insights can be of assistance in the design of closed-loop FES control schemes that can elicit muscle activation patterns based on trunk kinematics in non-disabled individuals. In particular, the use of stiffness control that is based on phasic activation of both agonist and antagonist muscles may be a promising approach for trunk stabilization. As such, it could complement low-level, tonic muscle activation levels that have been found to increase trunk stiffness during non-disabled, quiet sitting. While previous studies have shown that trunk and wobble board kinematics are correlated, more work is needed to quantify their relationship prior to the development of such technologies.

8 References

- [1] K. M. Moorhouse and K. P. Granata, "Role of reflex dynamics in spinal stability: intrinsic muscle stiffness alone is insufficient for stability," *J. Biomech.*, vol. 40, no. 5, pp. 1058–1065, 2007.
- [2] H. A. M. Seelen, Y. J. M. Potten, A. Huson, F. Spaans, and J. P. H. Reulen, "Impaired balance control in paraplegic subjects," *J. Electromyogr. Kinesiol.*, vol. 7, no. 2, pp. 149–160, 1997.
- [3] D. A. Winter, *Biomechanics and motor control of human movement*, 3rd ed. New Jersey: John Wiley & Sons, 2005.
- [4] G. K. Hyun and J. B. Dingwell, "A direct comparison of local dynamic stability during unperturbed standing and walking," *Exp. Brain Res.*, vol. 172, no. 1, pp. 35–48, 2006.
- [5] C. M. Bono, D. D. Cardenas, F. S. Frost, M. C. Hammond, L. B. Lindholm, I. Perakash, S. A. Stiens, and R. M. Woolsey, *spinal cord medicine: principles and practice*, 2nd ed. 2010.
- [6] C. L. Chen, K. T. Yeung, L. I. Bih, C. H. Wang, M. I. Chen, and J. C. Chien, "The relationship between sitting stability and functional performance in patients with paraplegia," *Arch. Phys. Med. Rehabil.*, vol. 84, no. 9, pp. 1276–1281, 2003.
- [7] Y. J. M. Potten, H. A. M. Seelen, J. Drukker, J. P. H. Reulen, and M. R. Drost, "Postural muscle responses in the spinal cord injured persons during forward reaching," *Ergonomics*, vol. 42, no. 9, pp. 1200–1215, 1999.
- [8] D. A. Hobson and R. E. Tooms, "Seated lumbar/pelvic alignment a comparison between spinal cord-injured and noninjured groups," *Spine (Phila. Pa. 1976)*, vol. 17, no. 3, 1992.
- [9] N. Wu, "Quantifying multi-directional trunk stiffness during sitting with and without functional electrical stimulation: able-bodied subjects," university of Toronto, 2011.
- [10] R. Chen, B. Kayser, S. Yan, and P. T. Macklem, "Twitch transdiaphragmatic pressure depends critically on thoracoabdominal configuration," *J. Appl. Physiol.*, vol. 88, no. 1, pp. 54–60, 2000.
- [11] N. Hart, I. Laffont, A. Perez De La Sota, M. Lejaille, G. Macadou, M. I. Polkey, P. Denys, and F. Lofaso, "Respiratory effects of combined truncal and abdominal support in patients with spinal cord injury," *Arch. Phys. Med. Rehabil.*, vol. 86, no. 7, pp. 1447–1451, 2005.
- [12] E. M. Gutierrez, M. Alm, C. Hultling, and H. Saraste, "Measuring seating pressure, area, and asymmetry in persons with spinal cord injury," *Eur. Spine J.*, vol. 13, no. 4, pp. 374–379, 2004.
- [13] I. Bolin, P. Bodin, and M. Kreuter, "Sitting position - posture and performance in C5 - C6

- tetraplegia.,” *Spinal Cord*, vol. 38, no. 7, pp. 425–434, 2000.
- [14] K. a. M. Samuelsson, H. Tropp, and B. Gerdle, “Shoulder pain and its consequences in paraplegic spinal cord-injured, wheelchair users,” *Spinal Cord*, vol. 42, no. 1, pp. 41–46, 2004.
- [15] M. Alm, E. Gutierrez, C. Hultling, and H. Saraste, “Clinical evaluation of seating in persons with complete thoracic spinal cord injury,” *Spinal Cord*, vol. 41, no. 10, pp. 563–571, 2003.
- [16] A. H. Vette, K. Masani, N. Wu, and M. R. Popovic, “Multidirectional quantification of trunk stiffness and damping during unloaded natural sitting,” *Med. Eng. Phys.*, vol. 36, no. 1, pp. 102–109, 2014.
- [17] K. D. Anderson, “Targeting recovery: priorities of the spinal cord-injured population,” *J. Neurotrauma*, vol. 21, no. 10, pp. 1371–1383, 2004.
- [18] Y. J. M. Janssen-Potten, H. A. Seelen, J. Drukker, and J. P. Reulen, “Chair configuration and balance control in persons with spinal cord injury,” *Arch Phys Med Rehabil*, vol. 81, no. 4, pp. 401–408, 2000.
- [19] Y. J. Janssen-Potten, H. A. Seelen, J. Drukker, F. Spaans, and M. R. Drost, “The effect of footrests on sitting balance in paraplegic subjects,” *Arch. Phys. Med. Rehabil.*, vol. 83, pp. 642–648, 2002.
- [20] J. Reft and Z. Hasan, “Trajectories of target reaching arm movements in individuals with spinal cord injury: effect of external trunk support,” *Spinal Cord*, vol. 40, pp. 186–191, 2002.
- [21] R. Aissaoui, C. Boucher, D. Bourbonnais, M. Lacoste, and J. Dansereau, “Effect of seat cushion on dynamic stability in sitting during a reaching task in wheelchair users with paraplegia,” *Arch. Phys. Med. Rehabil.*, vol. 82, no. 2, pp. 274–281, 2001.
- [22] T. E. Johnston, R. R. Betz, B. T. Smith, B. J. Benda, M. J. Mulcahey, R. Davis, T. P. Houdayer, M. A. Pontari, A. Barriskill, and G. H. Creasey, “Implantable FES system for upright mobility and bladder and bowel function for individuals with spinal cord injury,” *Spinal Cord*, vol. 43, no. 12, pp. 713–723, 2005.
- [23] M. R. Popovic, T. Keller, I. P. I. Papas, V. Dietz, and M. Morari, “Surface-stimulation technology for grasping and walking neuroprostheses,” *IEEE Eng. Med. Biol.*, vol. 20, no. 1, pp. 82–93, 2001.
- [24] J. Quintern, “Application of functional electrical stimulation in paraplegic patients,” *Neuro Rehabil.*, vol. 10, pp. 205–250, 1998.
- [25] J. R. Buckett, P. H. Peckham, G. B. Thrope, S. D. Braswell, and M. W. Keith, “A flexible, portable system for neuromuscular stimulation in the paralyzed upper extremity,” *IEEE Trans. Biomed. Eng.*, vol. 35, no. 11, 1988.

- [26] M. R. Popovic and T. A. Thrasher, “Neuroprostheses,” *Encycl. Biomater. Biomed. Eng.*, vol. 2, pp. 1056–1065, 2004.
- [27] A. H. Vette, N. Wu, K. Masani, and M. R. Popovic, “Functional electrical stimulation increases multidirectional trunk stiffness and damping in able-bodied individuals during sitting,” *Med. Eng. Phys.*, vol. 37, pp. 777–782, 2015.
- [28] A. H. Vette, K. Masani, and M. R. Popovic, “Implementation of a physiologically identified PD feedback controller for regulating the active ankle torque during quiet stance,” *IEEE Trans. Neural Syst. Rehabil. Eng.*, vol. 15, no. 1, pp. 235–243, 2007.
- [29] C. H. Ho, R. J. Triolo, A. L. Elias, K. L. Kilgore, A. F. DiMarco, K. Bogie, A. H. Vette, M. L. Audu, R. Kobetic, S. R. Chang, K. M. Chan, S. Dukelow, D. J. Bourbeau, S. W. Brose, K. J. Gustafson, Z. H. T. Kiss, and V. K. Mushahwar, “Functional electrical stimulation and spinal cord injury,” *Phys. Med. Rehabil. Clin. N. Am.*, vol. 25, no. 3, pp. 631–654, 2014.
- [30] M. Vanoncini, W. Holderbaum, and B. Andrews, “Development and experimental identification of a biomechanical model of the trunk for functional electrical stimulation control in paraplegia,” *Int. Neuromodulation Soc.*, vol. 11, no. 4, pp. 315–324, 2008.
- [31] T. A. Thrasher, V. W. Sin, K. Masani, A. H. Vette, B. C. Craven, and M. R. Popovic, “Response of the trunk to multidirectional perturbation during unsupported sitting,” *J. Appl. Biomech.*, vol. 26, pp. 332–340, 2010.
- [32] A. H. Vette, K. Masani, K. Nakazawa, and M. R. Popovic, “Neural-mechanical feedback control scheme generates physiological ankle torque fluctuation during quiet stance,” *IEEE Trans. Neural Syst. Rehabil. Eng.*, vol. 18, no. 1, pp. 86–95, 2010.
- [33] R. Claudino, E. C. C. dos Santos, and M. J. Santos, “Compensatory but not anticipatory adjustments are altered in older adults during lateral postural perturbations,” *Clin. Neurophysiol.*, vol. 124, no. 8, pp. 1628–1637, 2013.
- [34] N. Kanekar and A. S. Aruin, “The effect of aging on anticipatory postural control,” *Exp. Brain Res.*, vol. 232, no. 4, pp. 1127–1136, 2014.
- [35] A. S. Aruin, N. Kanekar, Y. J. Lee, and M. Ganesan, “Enhancement of anticipatory postural adjustments in older adults as a result of a single session of ball throwing exercise,” *Exp. Brain Res.*, vol. 233, pp. 649–655, 2015.
- [36] R. Tisserand, T. Robert, P. Chabaud, P. Livet, M. Bonnefoy, and L. Chèze, “Comparison between investigations of induced stepping postural responses and voluntary steps to better detect community-dwelling elderly fallers,” *Neurophysiol. Clin.*, vol. 45, no. 4–5, pp. 269–284, 2015.
- [37] Y. J. Lee and A. S. Aruin, “Three components of postural control associated with pushing in symmetrical and asymmetrical stance,” *Exp. Brain Res.*, vol. 228, no. 3, pp. 341–351, 2013.

- [38] A. G. Cresswell, L. Oddsson, and A. Thorstensson, "The Influence of Sudden Perturbations on Trunk Muscle Activity and Intra-Abdominal Pressure while Standing," *Exp Brain Res.*, vol. 98, no. 1994, pp. 336–341, 1994.
- [39] S. Grillner, J. Nilsson, and A. Thorstensson, "Intra-abdominal pressure changes during natural movements in man," *Acta Physiol Scand*, vol. 103, no. 3, pp. 275–283, 1978.
- [40] I. D. Loram and M. Lakie, "Human balancing of an inverted pendulum: position control by small, ballistic-like, throw and catch movements," *J. Physiol.*, vol. 540, no. 3, pp. 1111–1124, 2002.
- [41] A. E. Patla, M. G. Ishac, and D. A. Winter, "Anticipatory control of center of mass and joint stability during voluntary arm movement from a standing posture: Interplay between active and passive control," *Exp. Brain Res.*, vol. 143, no. 3, pp. 318–327, 2002.
- [42] S. M. McGill, "Electromyographic activity of the abdominal and low back musculature during the generation of isometric and dynamic axial trunk torque: implications for lumbar mechanics," *J. Orthop. Res.*, vol. 9, no. 1, pp. 91–103, 1991.
- [43] J. K. F. Ng, V. Kippers, M. Parnianpour, and C. A. Richardson, "EMG activity normalization for trunk muscles in subjects with and without back pain," *Med. Sci. Sports Exerc.*, vol. 34, no. 7, pp. 1082–1086, 2002.
- [44] P. B. O'Sullivan, K. M. Grahamslaw, M. Kendell, S. C. Lapenskie, N. E. Moller, and K. V Richards, "The effect of different standing and sitting postures on trunk muscle activity in a pain-free population," *Spine (Phila. Pa. 1976).*, vol. 27, no. 11, pp. 1238–1244, 2002.
- [45] G. J. Lehman and S. M. McGill, "Spinal manipulation causes variable spine kinematic and trunk muscle electromyographic responses," *Clin. Biomech.*, vol. 16, pp. 293–299, 2001.
- [46] F. J. Vera-Garcia, S. H. M. Brown, J. R. Gray, and S. M. McGill, "Effects of different levels of torso coactivation on trunk muscular and kinematic responses to posteriorly applied sudden loads," *Clin. Biomech.*, vol. 21, no. 5, pp. 443–455, 2006.
- [47] J. Cholewicki and S. M. McGill, "Mechanical stability of the in viva lumbar spine: implications for injury and chronic low back pain," *Clin. Biomech.*, vol. 11, no. 1, pp. 1–15, 1996.
- [48] F. P. Kendall, E. McCreary, and P. G. Provance, *Muscles, testing and function: with posture and pain*, 4th ed. Baltimore, Md: Lippincott Williams & Wilkins, 1993.
- [49] P. De Lava, "Adjustments to Zatsiorsky-Seluyanov's segment inertia parameters," *J. Biomech.*, vol. 29, no. 9, pp. 1223–1230, 1996.
- [50] D. J. Pearsall, J. G. Reid, and L. A. Livingston, "Segmental inertial parameters of the human trunk as determined from computed tomography," *Ann. Biomed. Eng.*, vol. 24, no. 2, pp. 198–210, 1996.

- [51] M. Zedka, S. Kumar, and Y. Narayan, “Electromyographic response of the trunk muscles to postural perturbation in sitting subjects,” *J. Electromyogr. Kinesiol.*, vol. 8, no. 1, pp. 3–10, 1998.
- [52] K. Masani, V. W. Sin, A. H. Vette, T. Adam Thrasher, N. Kawashima, A. Morris, R. Preuss, and M. R. Popovic, “Postural reactions of the trunk muscles to multi-directional perturbations in sitting,” *Clin. Biomech.*, vol. 24, no. 2, pp. 176–182, 2009.
- [53] R. Preuss and J. Fung, “Musculature and biomechanics of the trunk in the maintenance of upright posture,” *J. Electromyogr. Kinesiol.*, vol. 18, no. 5, pp. 815–828, 2008.
- [54] M. J. Winters and L.-Y. S. Woo, *Multiple muscle systems: biomechanics and movement organization*. springer-verlag, 1990.
- [55] N. Farahpour, S. Ghasemi, P. Allard, and M. S. Saba, “Electromyographic responses of erector spinae and lower limb’s muscles to dynamic postural perturbations in patients with adolescent idiopathic scoliosis,” *J. Electromyogr. Kinesiol.*, vol. 24, no. 5, pp. 645–651, 2014.
- [56] H. S. Jung, S. Y. Kang, J. H. Park, H. S. Cynn, and H. S. Jeon, “EMG activity and force during prone hip extension in individuals with lumbar segmental instability,” *Man. Ther.*, vol. 20, pp. 1–5, 2014.
- [57] M. C. Kim, S. K. Han, and S. K. Kim, “Changes in the range of motion of the hip joint and the muscle activity of the rectus femoris and biceps femoris of stroke patients during obstacles crossing on the ground and underwater,” *J. Phys. Ther. Sci.*, vol. 26, no. 8, pp. 1143–1146, 2014.
- [58] J. S. Oh, “Effects of pelvic belt on hip extensor muscle EMG activity during prone hip extension in females with chronic back pain,” *J. Phys. Ther. Sci.*, vol. 26, no. 7, pp. 1023–1024, 2014.
- [59] C. Y. Song, H. Y. Huang, S. C. Chen, J. J. Lin, and A. H. Chang, “Effects of femoral rotational taping on pain, lower extremity kinematics, and muscle activation in female patients with patellofemoral pain,” *J. Sci. Med. Sport*, vol. 18, no. 4, pp. 388–393, 2014.
- [60] H. R. Kuhnen, M. M. Rybar, T. Onushko, S. K. Hunter, B. D. Schmit, and A. S. Hyngstrom, “The stroke-related effects on maximal dynamic hip flexor fatigability and functional implications,” *Int. J. Cancer*, no. 414, pp. 1–23, 2013.
- [61] T. Jiroumaru, T. Kurihara, and T. Isaka, “Measurement of muscle length-related electromyography activity of the hip flexor muscles to determine individual muscle contributions to the hip flexion torque,” *Springerplus*, vol. 3, no. 1, p. 624, 2014.
- [62] K. P. Granata, K. F. Orishimo, and A. H. Sanford, “Trunk muscle coactivation in preparation for sudden load,” *J. Electromyogr. Kinesiol.*, vol. 11, pp. 247–254, 2001.
- [63] K. P. Granata, G. P. Slota, and S. E. Wilson, “Influence of Fatigue in Neuromuscular

- Control of Spinal Stability Kevin,” *Hum Factors*, vol. 46, no. 1, pp. 81–91, 2004.
- [64] P. J. Lee, E. L. Rogers, and K. P. Granata, “Active trunk stiffness increases with co-contraction,” *J. Electromyogr. Kinesiol.*, vol. 16, pp. 51–57, 2006.
- [65] J. Cholewicki, A. P. D. Simons, and A. Radebold, “Effects of external trunk loads on lumbar spine stability,” *J. Biomech.*, vol. 33, pp. 1377–1385, 2000.
- [66] M. G. Gardner-Morse and I. A. F. Stokes, “Trunk stiffness increases with steady-state effort,” *J. Biomech.*, vol. 34, pp. 457–463, 2001.
- [67] J. Chiang, J. R. Potvin, and S. R. Krajcarski, “The in vivo dynamic response of the spine to perturbations causing rapid flexion: effects of pre-load and step input magnitude,” *Clin. Biomech.*, no. 14, pp. 54–62, 1999.
- [68] M. L. McMulkin, J. C. Woldstad, and R. E. Hughes, “Torso loading via a harness method activates trunk muscles less than a hand loading method,” *J. Biomech.*, vol. 31, pp. 391–395, 1998.
- [69] K. P. Granata, G. P. Slota, and B. C. Bennett, “Paraspinal muscle reflex dynamics,” *J. Biomech.*, vol. 37, pp. 241–247, 2004.
- [70] J. S. Thomas, S. A. Lavender, D. M. Corcos, and G. B. J. Andersson, “Trunk kinematics and trunk muscle activity during a rapidly applied load,” *J. Electromyogr. Kinesiol.*, vol. 8, pp. 215–225, 1998.
- [71] K. L. C. Davidson and C. L. Hubley-Kozey, “Trunk muscle responses to demands of an exercise progression to improve dynamic spinal stability,” *Arch. Phys. Med. Rehabil.*, vol. 86, pp. 216–223, 2005.
- [72] P. W. Marshall and B. A. Murphy, “Core stability exercises on and off a Swiss ball,” *Arch. Phys. Med. Rehabil.*, vol. 86, no. 2, pp. 242–249, 2005.
- [73] K. P. Granata, P. E. Lee, and T. C. Franklin, “Co-contraction recruitment and spinal load during isometric trunk flexion and extension,” *Clin. Biomech.*, vol. 20, pp. 1029–1037, 2005.
- [74] J. H. Van Dieën, J. Cholewicki, and A. Radebold, “Trunk muscle recruitment patterns in patients with low back pain enhance the stability of the lumbar spine,” *Spine (Phila. Pa. 1976)*, vol. 28, no. 8, pp. 834–841, 2003.
- [75] S. R. Krajcarski, J. Chiang, and J. R. Potvin, “The in vivo dynamic response of the human spine to rapid lateral bend perturbation: effects of preload and step input magnitude,” *Clin. Biomech.*, vol. 26, no. 13, pp. 54–62, 1999.
- [76] P. W. Hodges, A. G. Cresswell, and A. Thorstensson, “Perturbed upper limb movements cause short-latency postural responses in trunk muscles,” *Exp. Brain Res.*, vol. 138, pp. 243–250, 2001.

- [77] W. S. Marras, K. G. Davis, and K. P. Granata, "Trunk muscle activities during asymmetric twisting motions," *J. Electromyogr. Kinesiol.*, vol. 8, pp. 247–256, 1998.
- [78] J. K. F. Ng, M. Parnianpour, C. A. Richardson, and K. Vaughan, "Functional roles of abdominal and back muscles during isometric axial rotation of the trunk," *J. Orthop. Res.*, vol. 19, pp. 463–471, 2001.
- [79] G. A. Mirka, D. Kelaher, A. Baker, A. Harrison, and J. Davis, "Selective activation of the external oblique musculature during axial torque production," *Clin. Biomech.*, vol. 12, no. 3, pp. 172–180, 1997.
- [80] W. S. Marras and K. P. Granata, "A biomechanical assessment and model of axial twisting in the thoracolumbar spine," *Spine (Phila. Pa. 1976)*, vol. 20, no. 13, pp. 1440–1451, 1995.
- [81] A. Torén and K. Öberg, "Maximum isometric trunk muscle strength and activity at trunk axial rotation during sitting," *Appl. Ergon.*, vol. 30, pp. 515–525, 1999.
- [82] A. L. Adkin, J. S. Frank, M. G. Carpenter, and G. W. Peysar, "Fear of falling modifies anticipatory postural control," *Exp. Brain Res.*, vol. 143, no. 2, pp. 160–170, 2002.
- [83] K. P. Granata and S. E. Wilson, "Trunk posture and spinal stability," *Clin. Biomech.*, vol. 16, pp. 650–659, 2001.
- [84] D. H. K. Chow, A. C. S. Cheng, A. D. Holmes, and J. H. Evans, "The effects of release height on center of pressure and trunk muscle response following sudden release of stoop lifting tasks," *Appl. Ergon.*, vol. 34, pp. 611–619, 2003.
- [85] W. S. Marras and K. P. Granata, "Spine loading during trunk lateral bending motions," *J. Biomech.*, vol. 30, no. 7, pp. 697–703, 1997.
- [86] A. Aruin and T. Shiratori, "Anticipatory postural adjustments while sitting: the effects of different leg supports," *Exp. Brain Res.*, vol. 151, pp. 46–53, 2003.
- [87] K. P. Granata and K. F. Orishimo, "Response of trunk muscle coactivation to changes in spinal stability," *J. Biomech.*, vol. 34, pp. 1117–1123, 2001.
- [88] G. L. Moseley, P. W. Hodges, and S. C. Gandevia, "External perturbation of the trunk in standing humans differentially activates components of the medial back muscles," *J. Physiol.*, vol. 547, no. Pt 2, pp. 581–587, 2003.
- [89] M. Freddolini, S. Strike, and R. Y. W. Lee, "Stiffness properties of the trunk in people with low back pain," *Hum. Mov. Sci.*, vol. 36, pp. 70–79, 2014.
- [90] M. Freddolini, S. Strike, and R. Y. W. Lee, "The role of trunk muscles in sitting balance control in people with low back pain," *J. Electromyogr. Kinesiol.*, vol. 24, pp. 947–953, 2014.
- [91] M. Milosevic, K. Masani, M. J. Kuipers, H. Rouhani, M. C. Verrier, K. M. V McConville,

- and M. R. Popovic, "Trunk control impairment is responsible for postural instability during quiet sitting in individuals with cervical spinal cord injury," *Clin. Biomech.*, vol. 30, no. 5, pp. 507–512, 2015.
- [92] C. Lariviere, D. H. Gagnon, and H. Mecheri, "Trunk postural control in unstable sitting: effect of sex and low back pain status," *Clin. Biomech.*, vol. 30, no. 9, pp. 933–939, 2015.
- [93] N. W. Willigenburg, I. Kingma, and J. H. Van Dieen, "Center of pressure trajectories, trunk kinematics and trunk muscle activation during unstable sitting in low back pain patients," *Gait Posture*, vol. 38, no. 4, pp. 625–630, 2013.
- [94] J. Cholewicki, G. K. Polzhofer, and A. Radebold, "Postural control of trunk during unstable sitting," *J. Biomech.*, vol. 33, no. 12, pp. 1733–1737, 2000.
- [95] H. Lee, K. P. Granata, and M. L. Madigan, "Effects of trunk exertion force and direction on postural control of the trunk during unstable sitting," *Clin. Biomech.*, vol. 23, no. 5, pp. 505–509, 2008.
- [96] W. Sung, M. Abraham, C. Plastaras, and S. P. Silfies, "Trunk motor control deficits in acute and subacute low back pain are not associated with pain or fear of movement," *Spine J.*, vol. 15, no. 8, pp. 1772–1782, 2015.
- [97] N. Kavcic, S. Grenier, and S. M. McGill, "Quantifying tissue loads and spine stability while performing commonly prescribed low back stabilization exercises," *Spine (Phila. Pa. 1976)*, vol. 29, no. 20, pp. 2319–2329, 2004.
- [98] N. Kavcic, S. Grenier, and S. M. McGill, "Determining the stabilizing role of individual torso muscles during rehabilitation exercises," *Spine (Phila. Pa. 1976)*, vol. 29, no. 11, pp. 1254–1265, 2004.
- [99] J. P. Arokoski, T. Valta, O. Airaksinen, and M. Kankaanpaa, "Back and abdominal muscle function during stabilization exercises," *Arch. Phys. Med. Rehabil.*, vol. 82, no. 8, pp. 1089–1098, 2001.
- [100] J. P. Arokoski, T. Valta, M. Kankaanpaa, and O. Airaksinen, "Activation of lumbar paraspinal and abdominal muscles during therapeutic exercises in chronic low back pain patients," *Arch. Phys. Med. Rehabil.*, vol. 85, pp. 823–832, 2004.
- [101] D. G. Behm, A. M. Leonard, W. B. Young, W. A. C. Bonsey, and S. N. Mackinnon, "Trunk muscle electromyographic activity with unstable and unilateral exercises," *J. Strength Cond. Res.*, vol. 19, no. 1, pp. 193–201, 2005.
- [102] G. M. Karst and G. M. Willett, "Effects of specific exercise instructions on abdominal muscle activity during trunk curl exercises," *J. Orthop. Sports Phys. Ther.*, vol. 34, no. 1, pp. 4–12, 2004.
- [103] G. M. Souza, L. L. Baker, and C. M. Powers, "Electromyographic activity of selected trunk muscles during dynamic spine stabilization exercises," *Arch. Phys. Med. Rehabil.*, vol. 82,

- no. 11, pp. 1551–1557, 2001.
- [104] S. P. Silfies, J. Cholewicki, and A. Radebold, “The effects of visual input on postural control of the lumbar spine in unstable sitting,” *Hum. Mov. Sci.*, vol. 22, no. 3, pp. 237–252, 2003.
- [105] A. Radebold, J. Cholewicki, G. K. Polzhofer, and H. S. Greene, “Impaired postural control of the lumbar spine is associated with delayed muscle response times in patients with chronic idiopathic low back pain,” *Spine (Phila. Pa. 1976)*., vol. 26, no. 7, pp. 724–730, 2001.
- [106] U. Van Daele, F. Hagman, S. Truijen, P. Vorlat, B. Van Gheluwe, and P. Vaes, “Differences in balance strategies between nonspecific chronic low back pain patients and healthy control subjects during unstable sitting,” *Spine (Phila. Pa. 1976)*., vol. 34, no. 11, pp. 1233–1238, 2009.
- [107] J. H. Van Dieën, L. L. J. Koppes, and J. W. R. Twisk, “Low back pain history and postural sway in unstable sitting,” *Spine (Phila. Pa. 1976)*., vol. 35, no. 7, pp. 812–817, 2010.
- [108] A. M. Sherwood, M. R. Dimitrijevic, and W. Barry McKay, “Evidence of subclinical brain influence in clinically complete spinal cord injury: discomplete SCI,” *J. Neurol. Sci.*, vol. 110, no. 1–2, pp. 90–98, 1992.
- [109] G. Creasy, J. Wilberger, and W. Young, “International standards for neurological and functional classification of spinal cord injury,” *Spinal Cord*, vol. 35, no. 5, pp. 266–274, 1997.
- [110] A. Gorgey and G. Dudley, “Skeletal muscle atrophy and increased intramuscular fat after incomplete spinal cord injury,” *Spinal Cord*, vol. 45, pp. 304–309, 2007.
- [111] Z. Dennis, *Posture sitting, standing, chair design & exercise*. Charles C Thomas Pub Ltd, 1988.
- [112] H. A. Seelen, “Compensatory muscle activity for sitting posture during upper extremity task performance in paraplegic persons,” *Scand J Rehabil Med*, vol. 7, pp. 149–160, 1997.
- [113] H. A. Seelen, Y. J. Potten, J. J. Adam, J. Drukker, F. Spaans, and A. Huson, “Postural motor programming in paraplegic patients during rehabilitation,” *Ergonomics*, vol. 41, no. 3, pp. 302–16, 1998.
- [114] S. M. McGill, S. Grenier, N. Kavcic, and J. Cholewicki, “Coordination of muscle activity to assure stability of the lumbar spine,” *J. Electromyogr. Kinesiol.*, vol. 13, pp. 353–359, 2003.
- [115] V. J. Basmajian and C. J. DeLuca, *Muscles alive: their functions revealed by electromyography*, 5th ed. Baltimore: Williams & Wilkins, 1985.
- [116] V. Wai Hang Sin, “Muscle recruitment patterns during sitting,” University of Toronto, 2007.

- [117] J. D. M. Drake and J. P. Callaghan, "Elimination of electrocardiogram contamination from electromyogram signals: An evaluation of currently used removal techniques," *J. Electromyogr. Kinesiol.*, vol. 16, no. 2, pp. 175–187, 2006.
- [118] T. R. Allen, R. L. Brookham, A. C. Cudlip, and C. R. Dickerson, "Comparing surface and indwelling electromyographic signals of the supraspinatus and infraspinatus muscles during submaximal axial humeral rotation," *J. Electromyogr. Kinesiol.*, vol. 23, no. 6, pp. 1343–1349, 2013.
- [119] G. L. Soderberg and L. M. Knutson, "A guide for use and interpretation of kinesiological electromyographic data," *Phys. Ther.*, vol. 80, no. 5, pp. 485–498, 2000.
- [120] E. A. Clancy, E. L. Morin, and R. Merletti, "Sampling, noise-reduction and amplitude estimation issues in surface electromyography," *J. Electromyogr. Kinesiol.*, vol. 12, pp. 1–16, 2002.
- [121] G. L. Soderberg and T. M. Cook, "Electromyography in biomechanics," *Phys. Ther.*, vol. 64, no. 12, pp. 1813–1820, 1984.
- [122] D. Abejon and C. A. Feler, "Is impedance a parameter to be taken into account in spinal cord stimulation?," *Pain Physician*, vol. 10, no. 4, pp. 533–40, 2007.
- [123] W. Dankaerts, P. B. O'sullivan, A. F. Burnett, L. M. Straker, and L. A. Danneels, "Reliability of EMG measurements for trunk muscles during maximal and sub-maximal voluntary isometric contractions in healthy controls and CLBP patients," *J. Electromyogr. Kinesiol.*, vol. 14, pp. 333–342, 2004.
- [124] A. Burden, "How should we normalize electromyograms obtained from healthy participants? What we have learned from over 25years of research," *J. Electromyogr. Kinesiol.*, vol. 20, no. 6, pp. 1023–1035, 2010.
- [125] D. Staudenmann, I. Kingma, D. F. Stegeman, and J. H. Van Dieen, "Towards optimal multi-channel EMG electrode configurations in muscle force estimation: a high density EMG study," *J. Electromyogr. Kinesiol.*, vol. 15, no. 1, pp. 1–11, 2005.
- [126] D. Staudenmann, J. R. Potvin, I. Kingma, D. F. Stegeman, and J. H. Van Dieen, "Effects of EMG processing on biomechanical models of muscle joint systems: Sensitivity of trunk muscle moments, spinal forces, and stability," *J. Biomech.*, vol. 40, no. 4, pp. 900–909, 2007.
- [127] M. S. Redfern, R. E. Hughes, and D. B. Chaffin, "High-pass filtering to remove electrocardiographic interference from torso EMG recordings," *Clin. Biomech.*, vol. 8, no. 1, pp. 44–48, 1993.
- [128] J. C. E. Van Der Burg, I. Kingma, and J. H. Van Dieën, "Is the trunk movement more perturbed after an asymmetric than after a symmetric perturbation during lifting?," *J. Biomech.*, vol. 37, no. 7, pp. 1071–1077, 2004.

- [129] D. Gagnon, C. Larivière, and P. Loisel, “Comparative ability of EMG, optimization, and hybrid modelling approaches to predict trunk muscle forces and lumbar spine loading during dynamic sagittal plane lifting,” *Clin. Biomech.*, vol. 16, no. 5, pp. 359–372, 2001.
- [130] J. R. Potvin and S. H. M. Brown, “Less is more: high pass filtering, to remove up to 99% of the surface EMG signal power, improves EMG-based biceps brachii muscle force estimates,” *J. Electromyogr. Kinesiol.*, vol. 14, no. 3, pp. 389–399, 2004.
- [131] Y. Albertus-Kajee, R. Tucker, W. Derman, R. P. Lamberts, and M. I. Lambert, “Alternative methods of normalising EMG during running,” *J. Electromyogr. Kinesiol.*, vol. 21, no. 4, pp. 579–586, 2011.
- [132] T. Rantalainen, A. Kłodowski, and H. Piitulainen, “Effect of innervation zones in estimating biceps brachii force-EMG relationship during isometric contraction,” *J. Electromyogr. Kinesiol.*, vol. 22, no. 1, pp. 80–87, 2012.
- [133] M. D. Mitchell, M. B. Yarossi, D. N. Pierce, E. L. Garbarini, and G. F. Forrest, “Reliability of surface EMG as an assessment tool for trunk activity and potential to determine neurorecovery in SCI,” *Spinal Cord*, vol. 53, no. 5, pp. 368–74, 2015.
- [134] C. Larivi, D. Gagnon, and P. Loisel, “The comparison of trunk muscles EMG activation between subjects with and without chronic low back pain during flexion-extension and lateral bending tasks,” *J. Electromyogr. Kinesiol.*, vol. 10, pp. 79–91, 2000.
- [135] J. Cholewicki and J. J. VanVliet Iv, “Relative contribution of trunk muscles to the stability of the lumbar spine during isometric exertions,” *Clin. Biomech.*, vol. 17, no. 2, pp. 99–105, 2002.
- [136] P. Dolan, I. Kingma, M. P. De Looze, J. H. Van Dieen, H. M. Toussaint, C. T. Baten, and M. A. Adams, “An EMG technique for measuring spinal loading during asymmetric lifting,” *Clin. Biomech.*, vol. 16 Suppl, no. 1, 2001.
- [137] B. Laursen, B. R. Jensen, G. Németh, and G. Sjøgaard, “A model predicting individual shoulder muscle forces based on relationship between electromyographic and 3D external forces in static position,” *J. Biomech.*, vol. 31, no. 8, pp. 731–739, 1998.
- [138] P. Madeleine, P. Bajaj, K. Sjøgaard, and L. Arendt-Nielsen, “Mechanomyography and electromyography force relationships during concentric, isometric and eccentric contractions,” *J. Electromyogr. Kinesiol.*, vol. 11, no. 2, pp. 113–121, 2001.
- [139] G. Kamen and G. E. Caldwell, “Physiology and interpretation of the electromyogram,” *J. Clin. Neurophysiol.*, vol. 13, no. 5, pp. 366–384, 1996.
- [140] S. M. McGill, N. S. Kavcic, and E. Harvey, “Sitting on a chair or an exercise ball: Various perspectives to guide decision making,” *Clin. Biomech.*, vol. 21, no. 4, pp. 353–360, 2006.
- [141] J. R. Potvin, R. W. Norman, and S. M. McGill, “Mechanically corrected EMG for the continuous estimation of erector spinae muscle loading during repetitive lifting,” *Eur. J.*

- Appl. Physiol.*, no. 74, pp. 119–132, 1996.
- [142] A. M. Burden, M. Trew, and V. Baltzopoulos, “Normalisation of gait EMGs: a re-examination,” *J. Electromyogr. Kinesiol.*, vol. 13, no. 6, pp. 519–532, 2003.
- [143] A. Burden and R. Bartlett, “Normalisation of EMG amplitude: an evaluation and comparison of old and new methods,” *Med. Eng. Phys.*, vol. 21, no. 4, pp. 247–257, 1999.
- [144] C. Disselhorst-Klug, T. Schmitz-Rode, and G. Rau, “Surface electromyography and muscle force: Limits in sEMG-force relationship and new approaches for applications,” *Clin. Biomech.*, vol. 24, no. 3, pp. 225–235, 2009.
- [145] F. J. Vera-Garcia, J. M. Moreside, and S. M. McGill, “MVC techniques to normalize trunk muscle EMG in healthy women,” *J. Electromyogr. Kinesiol.*, vol. 20, pp. 10–16, 2010.
- [146] J. Cholewicki, J. Van Dieen, A. S. Lee, and P. N. Reeves, “A comparison of a maximum exertion method and a model-based, sub-maximum exertion method for normalizing trunk EMG,” *J. Electromyogr. Kinesiol.*, vol. 21, pp. 767–773, 2011.
- [147] D. Staudenmann, K. Roeleveld, D. F. Stegeman, and J. H. Van Dieen, “Methodological aspects of SEMG recordings for force estimation - A tutorial and review,” *J. Electromyogr. Kinesiol.*, vol. 20, no. 3, pp. 375–387, 2010.
- [148] J. S. Dufour, W. S. Marras, and G. G. Knapik, “An EMG-assisted model calibration technique that does not require MVCs,” *J. Electromyogr. Kinesiol.*, vol. 23, no. 3, pp. 608–613, 2013.
- [149] A. S. Pollock, B. R. Durward, and P. J. Rowe, “What is balance?,” *Clin. Rehabil.*, vol. 14, pp. 402–406, 2000.
- [150] C. Frigo and P. Crenna, “Multichannel SEMG in clinical gait analysis: A review and state-of-the-art,” *Clin. Biomech.*, vol. 24, no. 3, pp. 236–245, 2009.
- [151] J. K. F. Ng, C. A. Richardson, M. Parnianpour, and V. Kippers, “EMG activity of trunk muscles and torque output during isometric axial rotation exertion: A comparison between back pain patients and matched controls,” *J. Orthop. Res.*, vol. 20, pp. 112–121, 2002.
- [152] G. Hirsch, G. Beach, C. Cooke, M. Menard, and S. Locke, “Relationship between performance on lumbar dynamometry and Waddell score in a population with low-back pain,” *Spine (Phila. Pa. 1976)*, vol. 16, no. 9, pp. 1039–1043, 1991.
- [153] J. S. Thomas, C. R. France, D. Sha, and N. Vander Wiele, “The influence of pain-related fear on peak muscle activity and force generation during maximal isometric trunk exertions,” *Spine (Phila. Pa. 1976)*, vol. 33, no. 11, pp. E342-8, 2008.
- [154] C. Nordander, J. Willner, G. Å. Hansson, B. Larsson, J. Unge, L. Granquist, and S. Skerfving, “Influence of the subcutaneous fat layer, as measured by ultrasound, skinfold calipers and BMI, on the EMG amplitude,” *Eur. J. Appl. Physiol.*, vol. 89, no. 6, pp. 514–

519, 2003.

- [155] B. A. Alkner, P. A. Tesch, and H. E. Berg, “Quadriceps EMG/force relationship in knee extension and leg press,” *Med. Sci. Sport. Exerc.*, vol. 32, no. 2, pp. 459–63, 2000.
- [156] S. Y. Chiou, Y. F. Shih, L. W. Chou, A. H. McGregor, and P. H. Strutton, “Impaired neural drive in patients with low back pain,” *Eur. J. Pain*, vol. 18, no. 6, pp. 794–802, 2014.
- [157] J. E. Kawamoto, S. J. Aboodarda, and D. G. Behm, “Effect of differing intensities of fatiguing dynamic contractions on contralateral homologous muscle performance,” *J. Sport. Sci. Med.*, vol. 13, pp. 836–845, 2014.
- [158] N. Cordeiro, N. Cortes, O. Fernandes, A. Diniz, and P. Pezarat-Correia, “Dynamic knee stability and ballistic knee movement after ACL reconstruction: an application on instep soccer kick,” *Knee Surg. Sports Traumatol. Arthrosc.*, vol. 23, pp. 1100–1106, 2014.
- [159] T. Miura and K. Sakuraba, “Properties of force output and spectral EMG in young patients with nonspecific low back pain during isometric trunk extension,” *J. Phys. Ther. Sci.*, vol. 26, pp. 323–9, 2014.
- [160] K. Masumoto, T. Shono, S. ichiro Takasugi, N. Hotta, K. Fujishima, and Y. Iwamoto, “Age-related differences in muscle activity, stride frequency and heart rate response during walking in water,” *J. Electromyogr. Kinesiol.*, vol. 17, no. 5, pp. 596–604, 2007.
- [161] L. R. Frost, M. E. Gerling, J. L. Markic, and S. H. M. Brown, “Exploring the effect of repeated-day familiarization on the ability to generate reliable maximum voluntary muscle activation,” *J. Electromyogr. Kinesiol.*, vol. 22, pp. 886–892, 2012.
- [162] S. Jin and G. A. Mirka, “The effect of a lower extremity kinematic constraint on lifting biomechanics,” *Appl. Ergon.*, vol. 42, no. 6, pp. 867–872, 2011.
- [163] E. Rejc, S. Lazzer, G. Antonutto, M. Isola, and P. E. Di Prampero, “Bilateral deficit and EMG activity during explosive lower limb contractions against different overloads,” *Eur. J. Appl. Physiol.*, vol. 108, pp. 157–165, 2010.
- [164] G. T. Allison, P. Godfrey, and G. Robinson, “EMG signal amplitude assessment during abdominal bracing and hollowing,” *J. Electromyogr. Kinesiol.*, vol. 8, no. 1, pp. 51–57, 1998.
- [165] D. M. Urquhart, P. W. Hodges, and I. H. Story, “Postural activity of the abdominal muscles varies between regions of these muscles and between body positions,” *Gait Posture*, vol. 22, pp. 295–301, 2005.
- [166] S. Micera, G. Vannozzi, A. M. Sabatini, and P. Dario, “Improving detection of muscle activation intervals,” *IEEE Eng. Med. Biol.*, vol. 20, pp. 38–46, 2001.
- [167] P. W. Hodges and B. H. Bui, “A comparison of computer-based methods for the determination of onset of muscle contraction using electromyography,”

- Electroencephalogr. Clin. Neurophysiol.*, vol. 101, pp. 511–519, 1996.
- [168] G. Morey-Klapsing, A. Arampatzis, and G. P. Brüggemann, “Choosing EMG parameters: Comparison of different onset determination algorithms and EMG integrals in a joint stability study,” *Clin. Biomech.*, vol. 19, no. 2, pp. 196–201, 2004.
- [169] I. A. F. Stokes, M. Gardner-Morse, S. M. Henry, and G. J. Badger, “Decrease in trunk muscular response to perturbation with preactivation of lumbar spinal musculature,” *Spine (Phila. Pa. 1976)*, vol. 25, no. 15, pp. 1957–1964, 2000.
- [170] G. Severini, S. Conforto, M. Schmid, and T. D’Alessio, “Novel formulation of a double threshold algorithm for the estimation of muscle activation intervals designed for variable SNR environments,” *J. Electromyogr. Kinesiol.*, vol. 22, no. 6, pp. 878–885, 2012.
- [171] P. Banato, T. D’Alessio, and M. Knaflitz, “A statistical method for the measurement of muscle activation intervals from surface myoelectric signal during gait,” *IEEE Trans. Biomed. Eng.*, vol. 45, no. 3, pp. 287–299, 1998.
- [172] D. Farina, R. Merletti, and R. M. Enoka, “The extraction of neural strategies from the surface EMG: an update,” *J. Appl. Physiol.*, vol. 96, pp. 1486–1495, 2004.
- [173] K. S. Turker, “Electromyography: some methodological problems and issues,” *Phys. Ther.*, vol. 37, pp. 698–710, 1993.
- [174] L. C. Brereton and S. M. McGill, “Frequency response of spine extensors during rapid isometric contractions: Effects of muscle length and tension,” *J. Electromyogr. Kinesiol.*, vol. 8, no. 4, pp. 227–232, 1998.
- [175] G. T. Allison, “Trunk muscle onset detection technique for EMG signals with ECG artefact,” *J. Electromyogr. Kinesiol.*, vol. 13, no. 3, pp. 209–216, 2003.
- [176] A. M. J. Bull, F. H. Berkshire, and A. A. Amis, “Accuracy of an electromagnetic measurement device and application to the measurement and description of knee joint motion,” *Proc. Instn Mech Engrs*, vol. 212, pp. 347–355, 1998.
- [177] K. N. An, M. C. Jacobsen, L. J. Berglund, and E. Y. S. Chao, “Application of a magnetic tracking device to kinesiological studies,” *J. Biomech.*, vol. 21, no. 7, pp. 613–620, 1988.
- [178] M. J. Percy and R. J. Hindle, “New method for the non-invasive three-dimensional measurement of human back movement,” *Clin. Biomech.*, vol. 4, pp. 73–79, 1989.
- [179] R. H. Brown, A. H. Burstein, C. L. Nash, and C. C. Schock, “Spinal analysis using a three-dimensional radiographic technique,” *J. Biomech.*, vol. 9, no. 6, pp. 353–365, 1976.
- [180] A. Leardini, F. Biagi, C. Belvedere, and M. G. Benedetti, “Quantitative comparison of current models for trunk motion in human movement analysis,” *Clin. Biomech.*, vol. 24, no. 7, pp. 542–550, 2009.

- [181] A. Cappozzo, U. Della Croce, A. Leardini, and L. Chiari, "Human movement analysis using stereophotogrammetry. Part 1: theoretical background," *Gait Posture*, vol. 21, no. 2, pp. 186–196, 2005.
- [182] P. B. Shull, W. Jirattigalachote, M. A. Hunt, M. R. Cutkosky, and S. L. Delp, "Quantified self and human movement: a review on the clinical impact of wearable sensing and feedback for gait analysis and intervention," *Gait Posture*, vol. 40, no. 1, pp. 11–19, 2014.
- [183] A. Salarian, H. Russmann, F. J. G. Vingerhoets, C. Dehollain, Y. Blanc, P. R. Burkhard, and K. Aminian, "Gait assessment in Parkinson's disease: toward an ambulatory system for long-term monitoring," *IEEE Trans. Biomed. Eng.*, vol. 51, no. 8, pp. 1434–1443, 2004.
- [184] A. M. Sabatini, "Quaternion-based strap-down integration method for applications of inertial sensing to gait analysis," *Med. Biol. Eng. Comput.*, vol. 43, 2005.
- [185] J. R. Rebula, L. V Ojeda, P. G. Adamczyk, and A. D. Kuo, "Measurement of foot placement and its variability with inertial sensors," *Gait Posture*, vol. 38, no. 4, pp. 974–980, 2013.
- [186] J. K. Lee and E. J. Park, "3D spinal motion analysis during staircase walking using an ambulatory inertial and magnetic sensing system," *Med. Biol. Eng. Comput.*, vol. 49, pp. 755–764, 2011.
- [187] H. Dejnabadi, B. M. Jolles, E. Casanova, P. Fua, and K. Aminian, "Estimation and visualization of sagittal kinematics of lower limbs orientation using body-fixed sensors," *IEEE Trans. Biomed. Eng.*, vol. 53, no. 7, pp. 1385–1393, 2006.
- [188] A. Schmitz, M. Ye, R. Shapiro, R. Yang, and B. Noehren, "Accuracy and repeatability of joint angles measured using a single camera markerless motion capture system," *J. Biomech.*, vol. 47, no. 2, pp. 587–591, 2014.
- [189] A. Schmitz, M. Ye, G. Boggess, R. Shapiro, R. Yang, and B. Noehren, "The measurement of in vivo joint angles during a squat using a single camera markerless motion capture system as compared to a marker based system," *Gait Posture*, vol. 41, pp. 694–698, 2015.
- [190] S. Corazza, L. Mündermann, A. M. Chaudhari, T. Demattio, C. Cobelli, and T. P. Andriacchi, "A markerless motion capture system to study musculoskeletal biomechanics: Visual hull and simulated annealing approach," *Ann. Biomed. Eng.*, vol. 34, no. 6, pp. 1019–1029, 2006.
- [191] R. Huiskes, J. Kremers, A. DE Lange, H. J. Woltring, G. Selvik, and T. J. G. Van Rens, "Analytical stereophotogrammetric determination of three-dimensional knee-joint geometry," *J. Biomech.*, vol. 18, no. 8, pp. 559–570, 1985.
- [192] G. Selvik, P. Alberius, and A. S. Aronson, "A roentgen stereophotogrammetric system. Construction, calibration and technical accuracy," *Acta Radiol Diagn*, vol. 24, no. 4, pp. 343–52, 1983.
- [193] P. Allard, I. A. F. Stokes, and J.-P. Blanchi, *Three dimensional analysis of human*

- movement*. Champaign, IL: Human Kinetics Publishers, 1995.
- [194] W. P. Stevens, “Reconstruction of three-dimensional anatomical landmark coordinates using video-based stereophotogrammetry,” *J. Anat.*, vol. 191, pp. 277–284, 1997.
- [195] L. Chiari, U. Della Croce, A. Leardini, and A. Cappozzo, “Human movement analysis using stereophotogrammetry. Part 2: instrumental errors,” *Gait Posture*, vol. 21, no. 2, pp. 197–211, 2005.
- [196] C. Wong, Z. Q. Zhang, B. Lo, and G. Z. Yang, “Wearable sensing for solid biomechanics: a review,” *IEEE Sens. J.*, vol. 15, no. 5, pp. 2747–2760, 2015.
- [197] W. Zijlstra and K. Aminian, “Mobility assessment in older people: new possibilities and challenges,” *Eur. J. Ageing*, vol. 4, pp. 3–12, 2007.
- [198] T. C. Nguyen and R. Baker, “Two methods of calculating thorax kinematics in children with myelomeningocele,” *Clin. Biomech.*, vol. 19, no. 10, pp. 1060–1065, 2004.
- [199] K. D. Taylor, F. M. Mottier, D. W. Simmons, W. Cohen, R. J. Pavlak, D. P. Cornell, and G. B. Hankins, “An automated motion measurement system for clinical gait analysis,” *J. Biomech.*, vol. 15, no. 7, pp. 505–516, 1982.
- [200] G. Ferrigno, N. A. Borghese, and A. Pedotti, “Pattern recognition in 3D automatic human motion analysis,” *ISPRS J. Photogramm. Remote Sens.*, vol. 45, pp. 227–246, 1990.
- [201] N. I. Durlach and A. S. Mavor, *Virtual reality: scientific and technological challenges*. Washington, D.C: National Academy Press, 1995.
- [202] J. E. Visser, M. G. Carpenter, H. van der Kooij, and B. R. Bloem, “The clinical utility of posturography,” *Clin. Neurophysiol.*, vol. 119, pp. 2424–2436, 2008.
- [203] M. Ferrarin, M. Rizzone, L. Lopiano, M. Recalcati, and A. Pedotti, “Effects of subthalamic nucleus stimulation and L-dopa in trunk kinematics of patients with Parkinson’s disease,” *Gait Posture*, vol. 19, no. 2, pp. 164–171, 2004.
- [204] M. Ferrarin, L. Lopiano, M. Rizzone, M. Lanotte, B. Bergamasco, M. Recalcati, and A. Pedotti, “Quantitative analysis of gait in Parkinson’s disease: a pilot study on the effects of bilateral sub-thalamic stimulation,” *Gait Posture*, vol. 16, pp. 135–148, 2002.
- [205] G. Wu, F. C. T. Van Der Helm, H. E. J. Veeger, M. Makhsous, P. Van Roy, C. Anglin, J. Nagels, A. R. Karduna, K. McQuade, X. Wang, F. W. Werner, and B. Buchholz, “ISB recommendation on definitions of joint coordinate systems of various joints for the reporting of human joint motion - Part II: Shoulder, elbow, wrist and hand,” *J. Biomech.*, vol. 38, no. 5, pp. 981–992, 2005.
- [206] C. Frigo, R. Carabalona, M. Dalla Mura, and S. Negrini, “The upper body segmental movements during walking by young females,” *Clin. Biomech.*, vol. 18, no. 5, pp. 419–425, 2003.

- [207] S. Fantozzi, M. G. Benedetti, A. Leardini, S. A. Banks, A. Cappello, D. Assirelli, and F. Catani, "Fluoroscopic and gait analysis of the functional performance in stair ascent of total knee replacement designs," *Gait Posture*, vol. 17, pp. 225–234, 2003.
- [208] A. Cappozzo, F. Catani, U. Della Croce, and A. Leardini, "Position and orientation in space of bones during movement: anatomical frame definition and determination," *Clin. Biomech.*, vol. 10, no. 4, pp. 171–178, 1995.
- [209] H. Furnée, *Three-dimensional analysis of human locomotion*, Allard, Pa. New York: Wiley, 1997.
- [210] S. Ayatollahzadeh, "Human trunk multi-segment kinematics : sensitivity to experimental errors," University of Toronto, 2014.
- [211] C. Fortin, S. Nadeau, and H. Labelle, "Inter-trial and test-retest reliability of kinematic and kinetic gait parameters among subjects with adolescent idiopathic scoliosis," *Eur. Spine J.*, vol. 17, no. 2, pp. 204–216, 2008.
- [212] A. H. Vette, T. Yoshida, T. A. Thrasher, K. Masani, and M. R. Popovic, "A complete, non-lumped, and verifiable set of upper body segment parameters for three-dimensional dynamic modeling," *Med. Eng. Phys.*, vol. 33, pp. 70–79, 2011.
- [213] A. H. Vette, T. Yoshida, T. A. Thrasher, K. Masani, and M. R. Popovic, "A comprehensive three-dimensional dynamic model of the human head and trunk for estimating lumbar and cervical joint torques and forces from upper body kinematics," *Med. Eng. Phys.*, vol. 34, no. 5, pp. 640–649, 2012.
- [214] M. P. Kadaba, H. K. Ramakrishnan, and M. E. Wootten, "Measurement of lower extremity kinematics during level walking," *J. Orthop. Res.*, vol. 8, pp. 383–392, 1990.
- [215] C. J. Craig, *Introduction to robotics: mechanics and control*, 3rd ed. New Jersey: Pearson, 2005.
- [216] G. K. Cole, B. M. Nigg, J. L. Ronsky, and M. R. Yeadon, "Application of the joint coordinate system to three-dimensional joint attitude and movement representation: a standardization proposal," *J. Biomech. Eng.*, vol. 115, no. 4A, pp. 344–349, 1993.
- [217] F. Gazzani, "Comparative assessment of two algorithms for calibrating stereophotogrammetric systems," *J. Biomech.*, vol. 26, no. 12, pp. 1449–1454, 1993.
- [218] A. Leardini, A. Chiari, U. Della Croce, and A. Cappozzo, "Human movement analysis using stereophotogrammetry part 3. Soft tissue artifact assessment and compensation," *Gait Posture*, vol. 21, no. 2, pp. 212–225, 2005.
- [219] U. Della Croce, A. Leardini, L. Chiari, and A. Cappozzo, "Human movement analysis using stereophotogrammetry Part 4: Assessment of anatomical landmark misplacement and its effects on joint kinematics," *Gait Posture*, vol. 21, no. 2, pp. 226–237, 2005.

- [220] A. Cappozzo, F. Catani, U. Della Croce, and A. Leardini, "Position and orientation in space of bone during movement: anatomical frame definition and determination," *Clin. Biomech.*, vol. 10, no. 4, pp. 171–178, 1995.
- [221] M. Rabuffetti, G. Baroni, M. Ferrarin, G. Ferrigno, and A. Pedotti, "Self-marking of anatomical landmarks for on-orbit experimental motion analysis compared to expert direct-marking," *Hum. Mov. Sci.*, vol. 21, pp. 439–455, 2002.
- [222] G. Andreopoulou, E. Maaswinkel, L. E. Cofré Lizama, and J. H. Van Dieën, "Effects of support surface stability on feedback control of trunk posture," *Exp. Brain Res.*, vol. 233, no. 4, pp. 1079–1087, 2015.
- [223] D. Barbado, J. Moreside, and F. J. Vera-Garcia, "Reliability and repetition effect of the center of pressure and kinematics parameters that characterize trunk postural control during unstable sitting test," *Am. Acad. Phys. Med. Rehabil.*, pp. 1–12, 2016.
- [224] J. Cholewicki, N. P. Reeves, V. Q. Everding, and D. C. Morrisette, "Lumbosacral orthoses reduce trunk muscle activity in a postural control task," *J. Biomech.*, vol. 40, pp. 1731–1736, 2007.
- [225] M. Freddolini, S. Strike, and R. Lee, "Dynamic stability of the trunk during unstable sitting in people with low back pain," *Spine (Phila. Pa. 1976)*, vol. 39, no. 10, pp. 785–790, 2014.
- [226] C. Larivière, H. Mecheri, A. Shahvarpour, D. Gagnon, and A. Shirazi-Adl, "Criterion validity and between-day reliability of an inertial-sensor-based trunk postural stability test during unstable sitting," *J. Electromyogr. Kinesiol.*, vol. 23, no. 4, pp. 899–907, 2013.
- [227] H. Lee and K. P. Granata, "Process stationarity and reliability of trunk postural stability," *Clin. Biomech.*, vol. 23, no. 6, pp. 735–742, 2008.
- [228] F. Munoz, A. I. Rouboa, and P. R. Rougier, "The balance control effects on sitting posture induced by lumbosacral orthosis wear vary depending on the level of stability," *Appl. Ergon.*, vol. 44, pp. 511–516, 2013.
- [229] N. M. C. W. Oomen, N. P. Reeves, M. C. Priess, and J. H. Van Dieën, "Trunk muscle coactivation is tuned to changes in task dynamics to improve responsiveness in a seated balance task," *J. Electromyogr. Kinesiol.*, vol. 25, no. 5, pp. 765–772, 2015.
- [230] R. A. Preuss, S. G. Grenier, and S. M. McGill, "Postural control of the lumbar spine in unstable sitting," *Arch. Phys. Med. Rehabil.*, vol. 86, no. 12, pp. 2309–2315, 2005.
- [231] N. P. Reeves, V. Q. Everding, J. Cholewicki, and D. C. Morrisette, "The effects of trunk stiffness on postural control during unstable seated balance," *Exp. Brain Res.*, vol. 174, no. 4, pp. 694–700, 2006.
- [232] A. Shahvarpour, A. Shirazi-Adl, and C. Larivière, "Active-passive biodynamics of the human trunk when seated on a wobble chair," *J. Biomech.*, vol. 49, no. 6, pp. 939–945, 2016.

- [233] G. P. Slota, K. P. Granata, and M. L. Madigan, "Effects of seated whole-body vibration on postural control of the trunk during unstable seated balance," *Clin. Biomech.*, vol. 23, no. 4, pp. 381–386, 2008.
- [234] M. L. Tanaka, M. A. Nussbaum, and S. D. Ross, "Evaluation of the threshold of stability for the human spine," *J. Biomech.*, vol. 42, no. 8, pp. 1017–1022, 2009.
- [235] M. L. Tanaka, S. D. Ross, and M. A. Nussbaum, "Mathematical modeling and simulation of seated stability," *J. Biomech.*, vol. 43, no. 5, pp. 906–912, 2010.
- [236] J. C. E. van der Burg, E. E. H. van Wegen, M. B. Rietberg, G. Kwakkel, and J. H. Van Dieën, "Postural control of the trunk during unstable sitting in Parkinson's disease," *Park. Relat. Disord.*, vol. 12, no. 8, pp. 492–498, 2006.
- [237] M. J. Vezina and C. L. Hubley-Kozey, "Muscle activation in therapeutic exercises to improve trunk stability," *Arch. Phys. Med. Rehabil.*, vol. 81, no. 10, pp. 1370–1379, 2000.
- [238] S. H. M. Brown and J. R. Potvin, "Constraining spine stability levels in an optimization model leads to the prediction of trunk muscle cocontraction and improved spine compression force estimates," *J. Biomech.*, vol. 38, pp. 745–754, 2005.
- [239] J. P. Callaghan, J. L. Gunning, and S. M. McGill, "The relationship between lumbar spine load and muscle activity during extensor exercises," *Phys. Ther.*, vol. 78, no. 1, pp. 8–18, 1998.
- [240] S. A. Lavender, Y. H. Tsuang, G. B. Andersson, A. Hafezi, and C. C. Shin, "Trunk muscle cocontraction: the effects of moment direction and moment magnitude," *J. Orthop. Res.*, vol. 10, pp. 691–700, 1992.
- [241] S. McGill, J. Andersen, and J. Cannon, "Muscle activity and spine load during anterior chain whole body linkage exercises: the body saw, hanging leg raise and walkout from a push-up," *J. Sports Sci.*, vol. 33, no. 4, pp. 419–426, 2015.
- [242] B. M. Meyers and P. J. Keir, "Trunk muscle response to lifting unbalanced loads with and without knowledge of centre of mass," *Clin. Biomech.*, vol. 18, no. 8, pp. 712–720, 2003.
- [243] D. Czaprowski, A. Afeltowicz, A. Gebicka, P. Pawlowska, A. Kedra, C. Barrios, and M. Hadala, "Abdominal muscle EMG-activity during bridge exercises on stable and unstable surfaces," *Phys. Ther. Sport*, vol. 15, pp. 162–168, 2014.
- [244] E. Bressel, D. G. Dolny, and M. Gibbons, "Trunk muscle activity during exercises performed on land and in water," *Med. Sci. Sports Exerc.*, vol. 43, pp. 1927–1932, 2011.
- [245] S. Atkins, "Electromyographic response of global abdominal stabilizers in response to stable- and unstable-base isometric exercise," *J. Strength Cond. Res.*, vol. 29, pp. 1609–1615, 2014.
- [246] S. H. M. Brown, M. L. Haumann, and J. R. Potvin, "The responses of leg and trunk muscles

- to sudden unloading of the hands: Implications for balance and spine stability,” *Clin. Biomech.*, vol. 18, pp. 812–820, 2003.
- [247] H. Hassanlouei, L. Arendt-Nielsen, U. G. Kersting, and D. Falla, “Effect of exercise-induced fatigue on postural control of the knee,” *J. Electromyogr. Kinesiol.*, vol. 22, pp. 342–347, 2012.
- [248] B. S. Hassan, S. Mockett, and M. Doherty, “Static postural sway, proprioception, and maximal voluntary quadriceps contraction in patients with knee osteoarthritis and normal control subjects,” *Ann. Rheum. Dis.*, vol. 60, pp. 612–618, 2001.
- [249] R. L. Cromwell, T. k Aadland-Monahan, A. T. Nelson, S. Stern-Sylvestre, and B. Seder, “Sagittal plane analysis of head,neck,and trunk kinematics and electromyographic activity during locomotion,” *J. Orthop. Sport. Phys. Ther.*, vol. 31, no. 5, pp. 255–262, 2001.
- [250] M. W. Olson, “Trunk extensor fatigue influences trunk muscle activities during walking gait,” *J. Electromyogr. Kinesiol.*, vol. 20, no. 1, pp. 17–24, 2010.
- [251] T. Eason, C. R. Gavel, K. A. Hawley, S. S. Galen, and M. H. Malek, “Reliability of the log-transformed EMG amplitude-power output relationship for incremental knee-extensor ergometry,” *Muscle and Nerve*, vol. 52, no. 3, pp. 428–434, 2015.
- [252] C. Giroux, G. Guilhem, A. Couturier, D. Chollet, and G. Rabita, “Is muscle coordination affected by loading condition in ballistic movements?,” *J. Electromyogr. Kinesiol.*, vol. 25, no. 1, pp. 69–76, 2015.
- [253] R. van den tillar, V. Anderson, and A. H. Saeterbakken, “Comparison of muscle activation and performance during 6 rm, two-legged free-weight squats,” *Kinesiol. Slov.*, vol. 20, no. 2, pp. 5–16, 2014.
- [254] A. Saito, K. Watanabe, and H. Akima, “Coordination among thigh muscles including the vastus intermedius and adductor magnus at different cycling intensities,” *Hum. Mov. Sci.*, vol. 40, no. 2015, pp. 14–23, 2015.
- [255] G. Paz, M. Maia, F. Santiago, V. Lima, and H. Miranda, “Muscle activity of the erector spinae during pilates isometric exercises on and off Swiss Ball,” *J. Sports Med. Phys. Fitness*, vol. 54, no. 5, pp. 507–515, 2014.
- [256] K. P. Granata and W. S. Marras, “An EMG-assisted model of loads on the lumbar spine during asymmetric trunk extensions,” *J. Biomech.*, vol. 26, no. 12, pp. 1429–1438, 1993.
- [257] P. Moin, *Fundamentals of engineering numerical analysis*, 2nd ed. Cambridge, 2010.
- [258] J. Nilsson, M. Panizza, and M. Hallett, “Principles of digital sampling of a physiologic signal,” *Electroencephalogr. Clin. Neurophysiol.*, vol. 89, no. 5, pp. 349–358, 1993.
- [259] C. Angeloni, P. O. Riley, and D. E. Krebs, “Frequency content of whole body gait kinematic data,” *IEEE Trans. Rehabil. Eng.*, vol. 2, no. 1, pp. 40–46, 1994.

- [260] G. E. Robertson, G. Caldwell, J. Hamill, G. Kamen, and S. N. Whittlesey, *Research methods in biomechanics*. Champaign: Human Kinetics, 2004.
- [261] N. R. Crawford, G. T. Yamaguchi, and C. A. Dickman, “Methods for determining spinal flexion/extension, lateral bending, and axial rotation from marker coordinate data: analysis and refinement,” *Hum. Mov. Sci.*, vol. 15, pp. 55–78, 1996.
- [262] T. E. Prieto, J. B. Myklebust, R. G. Hoffmann, E. G. Lovett, and B. M. Myklebust, “Measures of postural steadiness: Differences between healthy young and elderly adults,” *IEEE Trans. Biomed. Eng.*, vol. 43, no. 9, pp. 956–966, 1996.
- [263] A. H. Vette, K. Masani, V. Sin, and M. R. Popovic, “Posturographic measures in healthy young adults during quiet sitting in comparison with quiet standing,” *Med. Eng. Phys.*, vol. 32, pp. 32–38, 2010.
- [264] G. E. P. Box, G. M. Jenkins, and G. C. Reinsel, *Time series analysis: forecasting and control*, 3rd ed. Englewood Cliffs, NJ, 1994.
- [265] T. Soderstrom and P. Stoica, *System Identification*. Prentice Hall, 1989.
- [266] “Rectus femoris.” [Online]. Available: <http://www.markgiubarelli.com/yoga-anatomy/rectus-femoris/>. [Accessed: 02-Jun-2017].
- [267] “Biceps femoris – long head.” [Online]. Available: <http://www.markgiubarelli.com/yoga-anatomy/biceps-femoris-long-head/>. [Accessed: 02-Jun-2017].
- [268] “Chair supported thoracic, lumbar & hip active sidebends,” 2017. [Online]. Available: <http://www.safe-stretch.info/chair-sidebend/>. [Accessed: 05-Jun-2017].
- [269] N. Genthon, N. Vuillerme, J. P. Monnet, C. Petit, and P. Rougier, “Biomechanical assessment of the sitting posture maintenance in patients with stroke,” *Clin. Biomech.*, vol. 22, no. 9, pp. 1024–1029, 2007.
- [270] O. Shirado, M. Kawase, A. Minami, and T. E. Strax, “Quantitative evaluation of long sitting in paraplegic patients with spinal cord injury,” *Arch. Phys. Med. Rehabil.*, vol. 85, no. 8, pp. 1251–1256, 2004.
- [271] M. Grangeon, D. Gagnon, C. Gauthier, G. Jacquemin, K. Masani, and M. R. Popovic, “Effects of upper limb positions and weight support roles on quasi-static seated postural stability in individuals with spinal cord injury,” *Gait Posture*, vol. 36, no. 3, pp. 572–579, 2012.
- [272] M. Grangeon, D. Gagnon, C. Duclos, C. Gauthier, C. Larivière, and P. Gourdou, “Characterizing postural stability in a quasi-static sitting position among individuals with sensorimotor impairments following spinal cord injury,” *J. Bioeng. Biomed. Sci.*, vol. 3, no. 1, pp. 1–10, 2013.
- [273] M. Grangeon, C. Gauthier, C. Duclos, J. F. Lemay, and D. Gagnon, “Unsupported eyes

- closed sitting and quiet standing share postural control strategies in healthy individuals,” *Motor Control*, pp. 10–24, 2014.
- [274] R. A. Schmidt and T. D. Lee, *Motor control and learning: a behavioral emphasis*, Fifth. 2011.
- [275] H. Forsberg and H. Hirschfeld, “Postural adjustments in sitting humans following external perturbations: muscle activity and kinematics,” *Exp. Brain Res.*, pp. 515–527, 1994.
- [276] M. Cenciarini, P. J. Loughlin, P. J. Sparto, and M. S. Redfern, “Stiffness and damping in postural control increase with age,” *IEEE Trans. Biomed. Eng.*, vol. 57, no. 2, pp. 267–275, 2010.
- [277] J. S. Blouin, M. Descarreaux, A. Bélanger-Gravel, M. Simoneau, and N. Teasdale, “Attenuation of human neck muscle activity following repeated imposed trunk-forward linear acceleration,” *Exp. Brain Res.*, vol. 150, no. 4, pp. 458–464, 2003.
- [278] J. H. J. Allum, M. Gresty, E. Keshner, and C. Shupert, “The control of head movements during human balance corrections,” *J. Vestib. Res.*, vol. 7, 1997.
- [279] N. Vibert, H. G. MacDougall, C. de Waele, D. P. D. Gilchrist, A. M. Burgess, A. Sidis, A. Migliaccio, I. S. Curthoys, and P. P. Vidal, “Variability in the control of head movements in seated humans: A link with whiplash injuries?,” *J. Physiol.*, vol. 532, no. 3, pp. 851–868, 2001.
- [280] C. Maurer and R. J. Peterka, “A new interpretation of spontaneous sway measures based on a simple model of human postural control,” *Journal of Neurophysiology*, 2005. .
- [281] J. J. Collins and C. J. De Luca, “The effects of visual input on open-loop and closed-loop postural control mechanisms,” *Exp. Brain Res.*, vol. 103, no. 1, pp. 151–163, 1995.
- [282] P. Serra-Añó, L. López-Bueno, X. García-Massó, M. T. Pellicer-Chenoll, and L.-M. González, “Postural control mechanisms in healthy adults in sitting and standing positions,” *Percept. Mot. Skills*, vol. 121, no. 1, pp. 119–34, 2015.
- [283] E. Maaswinkel, H. E. J. Veeger, and J. H. Dieen, “Interactions of touch feedback with muscle vibration and galvanic vestibular stimulation in the control of trunk posture,” *Gait Posture*, vol. 39, no. 2, pp. 745–749, 2014.
- [284] P. Gatev, S. Thomas, T. Kepple, and M. Hallett, “Feedforward ankle strategy of balance during quiet stance in adults,” *J. Physiol.*, vol. 514, no. 3, pp. 915–928, 1999.
- [285] R. Fitzpatrick, D. Burke, and S. C. Gandevia, “Loop gain of reflexes controlling human standing measured with the use of postural and vestibular disturbances,” *J. Neurophysiol.*, vol. 76, no. 6, pp. 3994–4008, 1996.
- [286] K. Masani, M. R. Popovic, K. Nakazawa, M. Kouzaki, and D. Nozaki, “Importance of body sway velocity information in controlling ankle extensor activities during quiet stance,” *J.*

- Neurophysiol.*, vol. 90, no. 6, pp. 3774–3782, 2003.
- [287] K. Masani, A. H. Vette, and M. R. Popovic, “Controlling balance during quiet standing: Proportional and derivative controller generates preceding motor command to body sway position observed in experiments,” *Gait Posture*, vol. 23, no. 2, pp. 164–172, 2006.
- [288] I. A. F. Stokes and M. Gardner-Morse, “Quantitative anatomy of the lumbar musculature,” *J. Biomech.*, vol. 32, no. 3, pp. 311–316, 1999.
- [289] A. S. Ali, K. A. Rowen, and J. F. Iles, “Vestibular actions on back and lower limb muscles during postural tasks in man,” *J. Physiol.*, vol. 546, no. 2, pp. 615–624, 2003.
- [290] B. Chen, Y. J. Lee, and A. S. Aruin, “Anticipatory and compensatory postural adjustments in conditions of body asymmetry induced by holding an object,” *Exp. Brain Res.*, vol. 233, no. 11, pp. 3087–3096, 2015.
- [291] M. J. Santos, N. Kanekar, and A. S. Aruin, “The role of anticipatory postural adjustments in compensatory control of posture: 1. Electromyographic analysis,” *J. Electromyogr. Kinesiol.*, vol. 20, no. 3, pp. 388–397, 2010.
- [292] D. W. Franklin and T. E. Milner, “Adaptive control of stiffness to stabilize hand position with large loads,” *Exp. Brain Res.*, vol. 152, no. 2, pp. 211–220, 2003.
- [293] J. Jeka, T. Kiemel, R. Creath, F. Horak, and R. Peterka, “Controlling human upright posture: velocity information is more accurate than position or acceleration,” *J. Neurophysiol.*, vol. 92, no. 4, pp. 2368–2379, 2004.
- [294] K. Masani, A. H. Vette, N. Kawashima, and M. R. Popovic, “Neuromusculoskeletal torque-generation process has a large destabilizing effect on the control mechanism of quiet standing,” *J. Neurophysiol.*, vol. 100, no. 3, pp. 1465–1475, 2008.
- [295] J. J. Jeka, G. Schoner, T. Dijkstra, P. Ribeiro, and J. R. Lackner, “Coupling of fingertip somatosensory information to head and body sway,” *Exp. Brain Res.*, vol. 113, no. 3, pp. 475–483, 1997.
- [296] H. Esteky and H. D. Schwark, “Responses of rapidly adapting neurons in cat primary somatosensory cortex to constant-velocity mechanical stimulation,” *J. Neurophysiol.*, vol. 72, no. 5, pp. 2269–2279, 1994.
- [297] T. M. H. Dijkstra, G. Schöner, M. A. Giese, and C. C. A. M. Gielen, “Frequency dependence of the action-perception cycle for postural control in a moving visual environment: relative phase dynamics,” *Biol. Cybern.*, vol. 71, no. 6, pp. 489–501, 1994.

9 Appendices

9.1 Appendix A – Figures for Validation of Time Synchronization Procedure

Figures 1 to 15 show the acquired signals in stacked plots for participants 1 to 5. The first plot shows the push button signal in the EMG system; the second, the push button signal in the Mocap system; the third, the raw EMG signal; and the fourth, the angle of the wobble board.

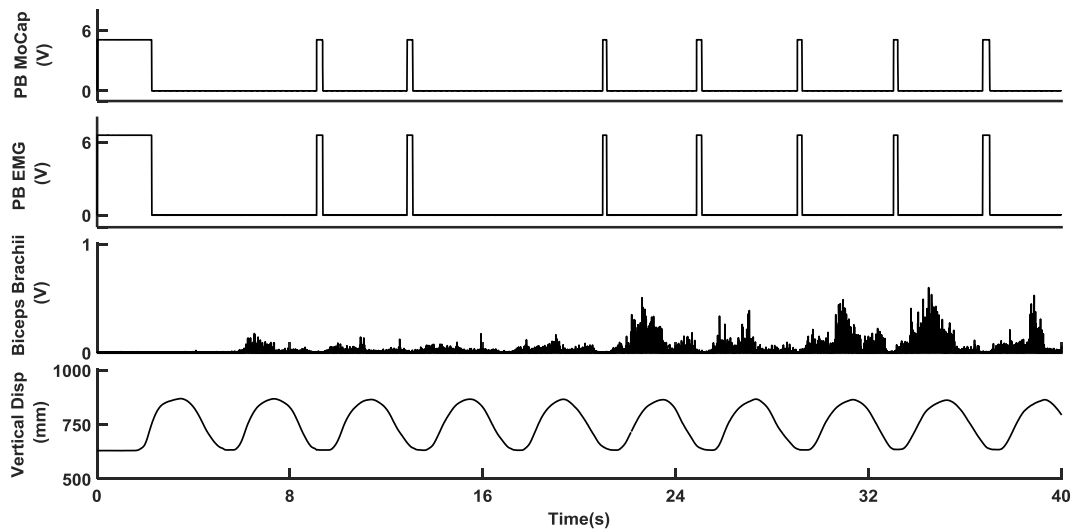


Figure 1. Experimental data from the first trial of Participant # 1.

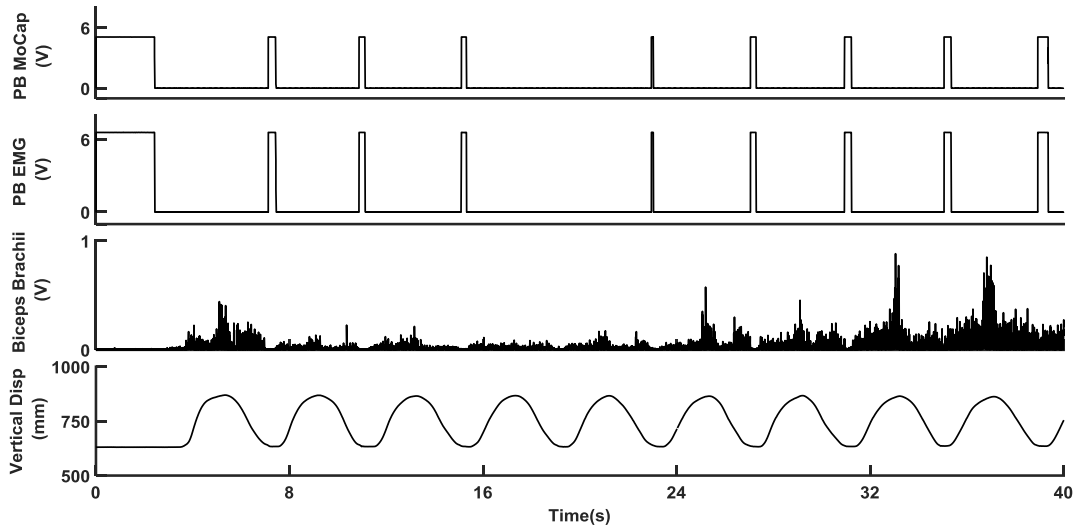


Figure 2. Experimental data from the second trial of Participant # 1.

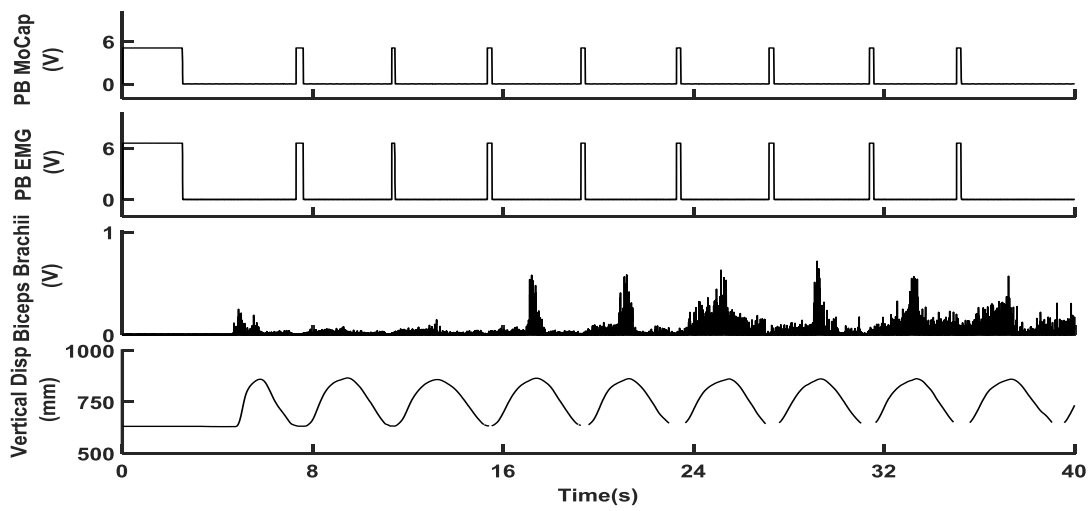


Figure 3. Experimental data from the third trial of Participant # 1.

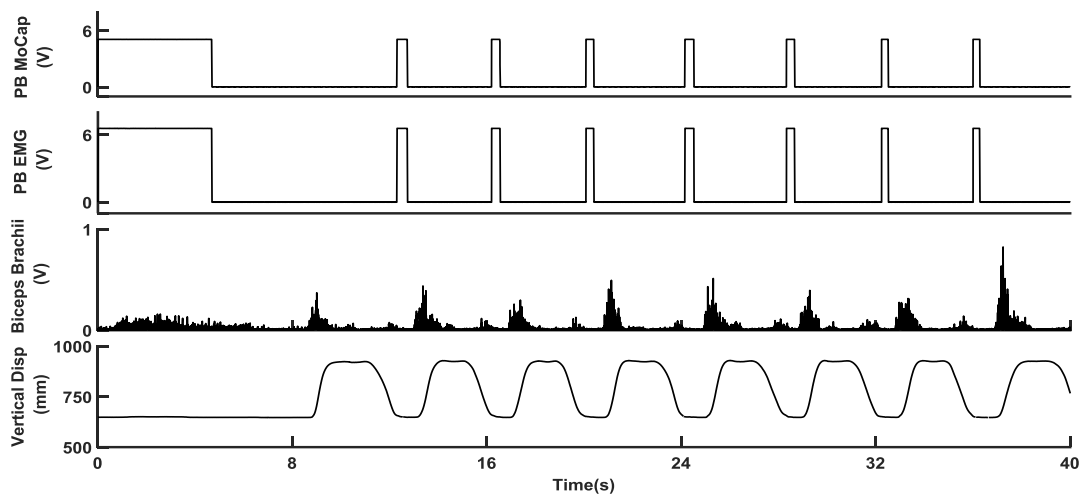


Figure 4. Experimental data from the first trial of Participant # 2.

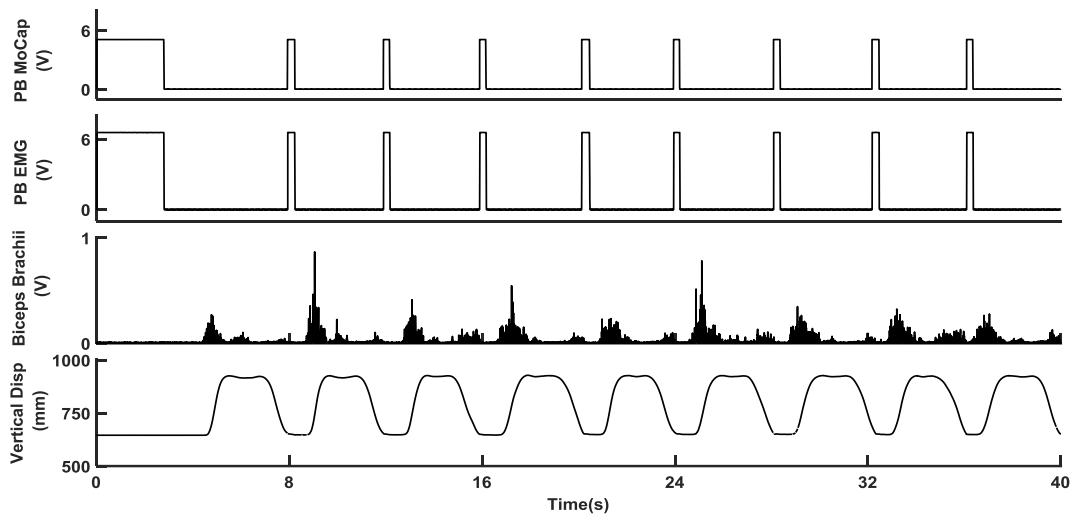


Figure 5. Experimental data from the second trial of Participant # 2.

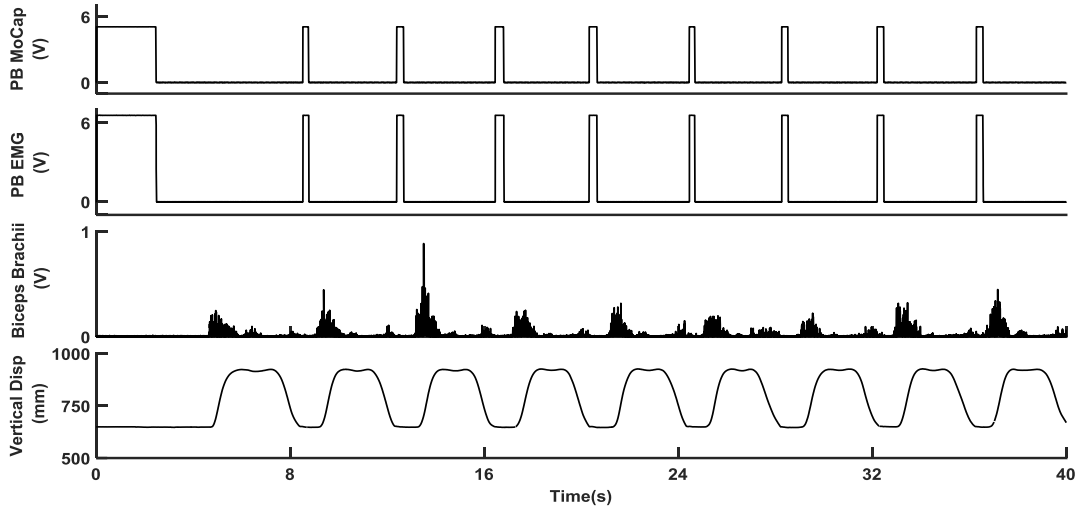


Figure 6. Experimental data from the third trial of Participant # 2.

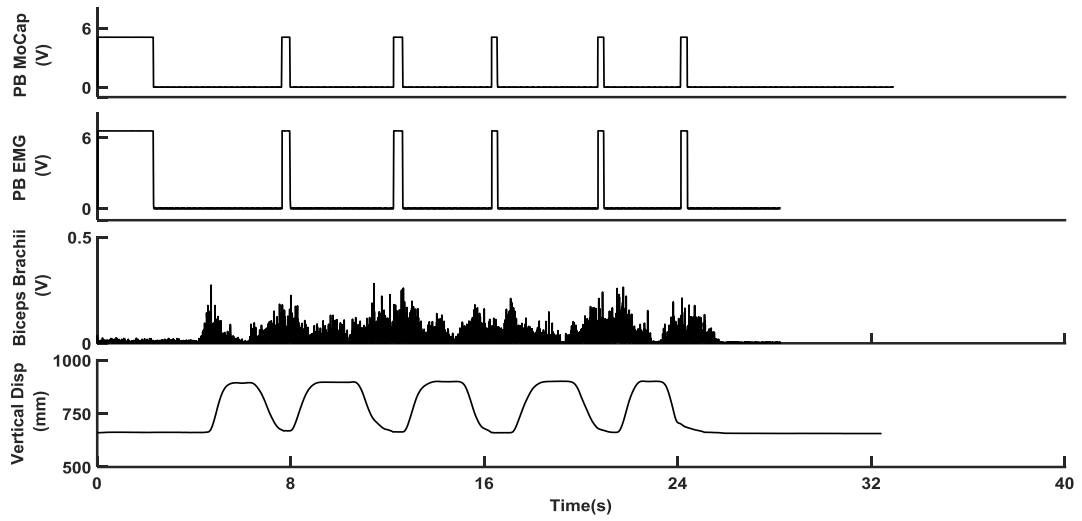


Figure 7. Experimental data from the first trial of Participant # 3.

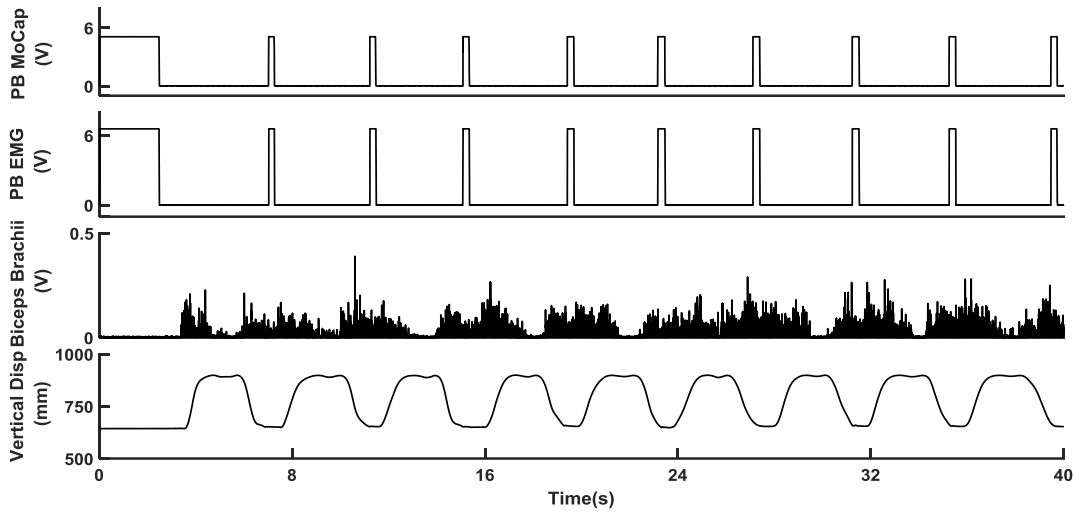


Figure 8. Experimental data from the second trial of Participant # 3.

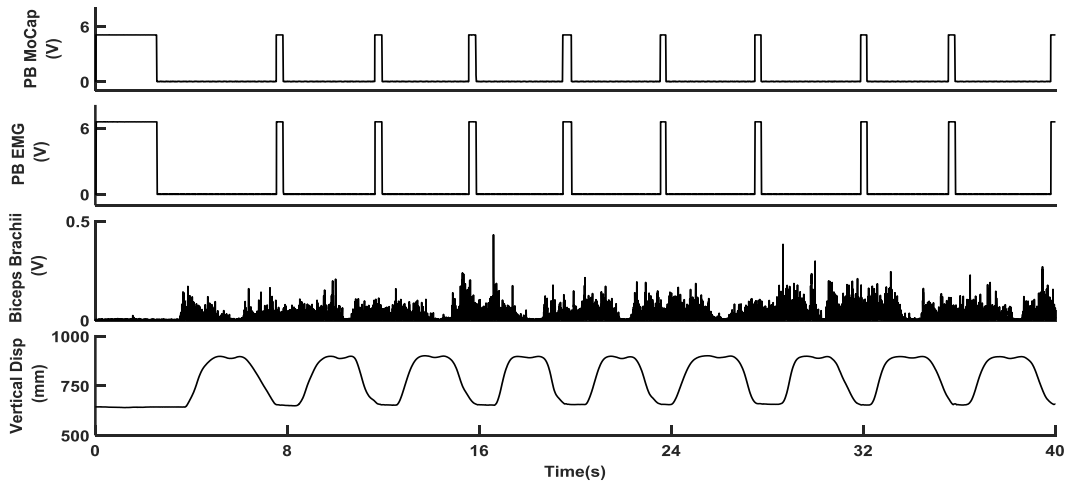


Figure 9. Experimental data from the third trial of Participant # 3.

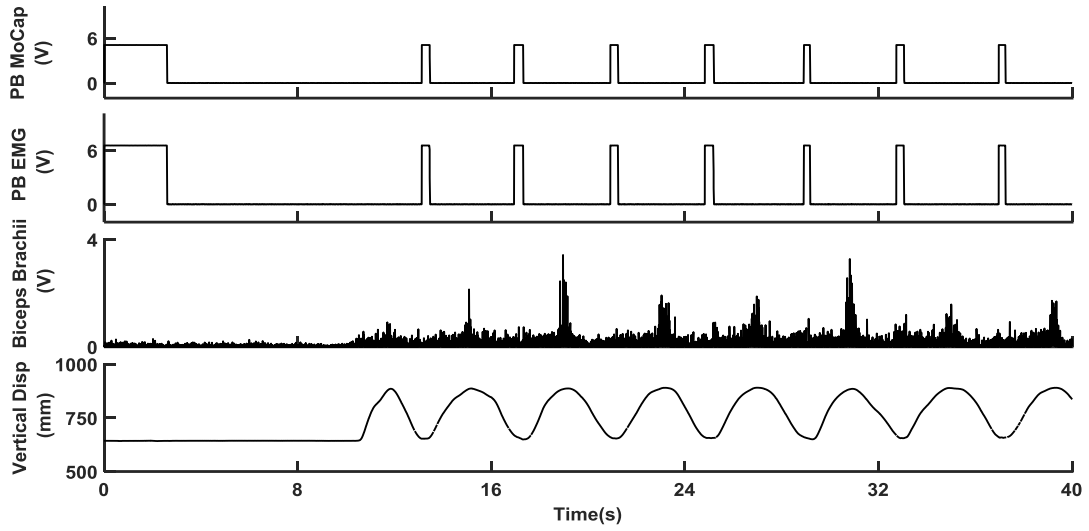


Figure 10. Experimental data from the first trial of Participant # 4.

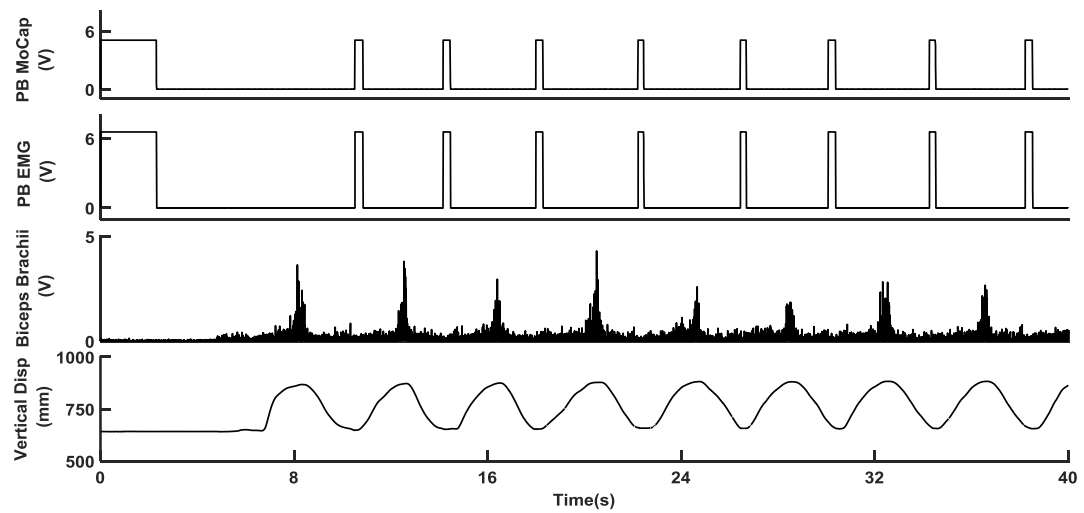


Figure 11. Experimental data from the second trial of Participant # 4.

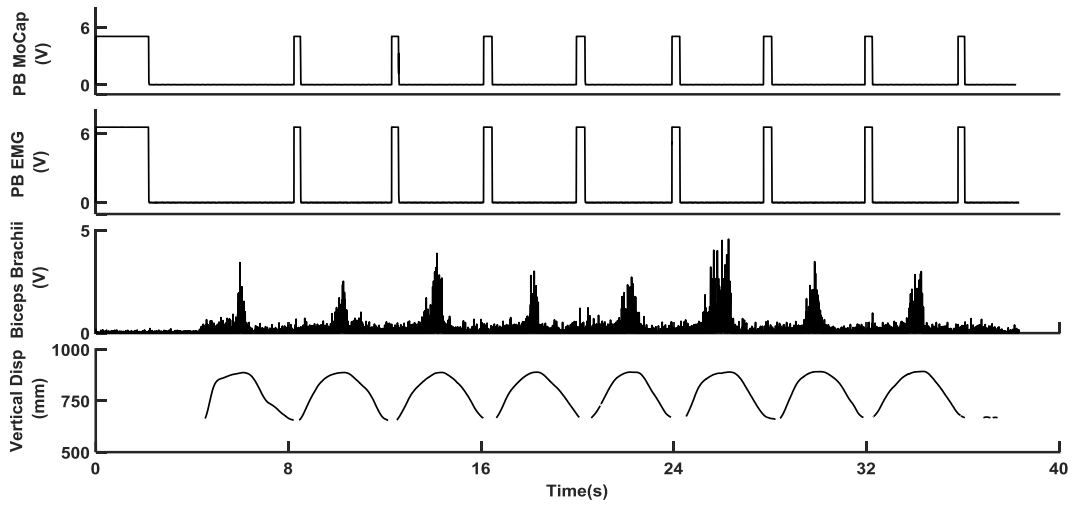


Figure 12. Experimental data from the third trial of Participant # 4.

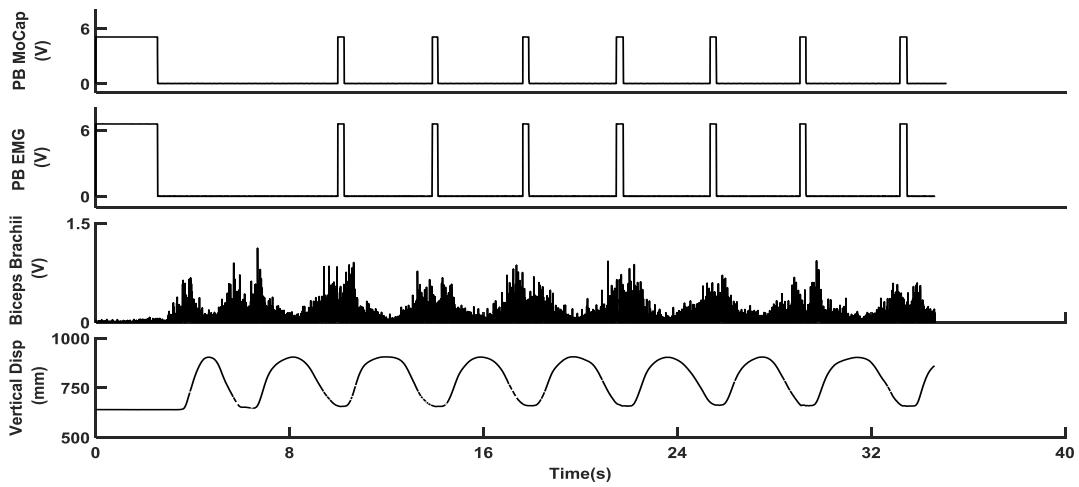


Figure 13. Experimental data from the first trial of Participant # 5.

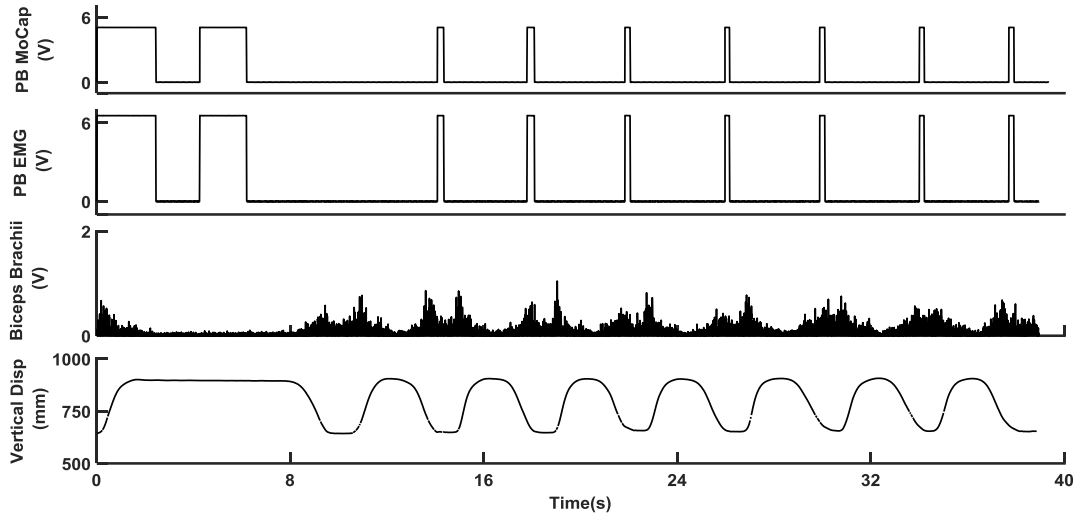


Figure 14. Experimental data from the second trial of Participant # 5.

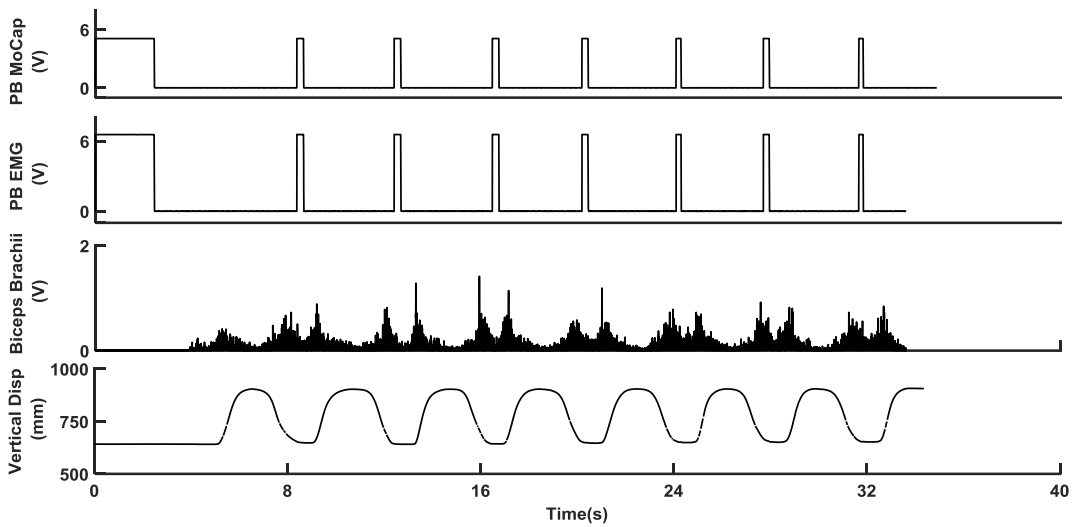


Figure 15. Experimental data from the third trial of Participant # 5.

9.2 Appendix B – MVC Values Obtained via Four Different Calculation Methods

Respective MVC values for Participant #1 (mean \pm SD for 3 trials), obtained via the four different calculation methods are shown in Tables 1 to 6.

Table 1. The MVC values of the two exercises for the right rectus abdominis for each participant. All values are presented as mean \pm SD across three trials.

Participant #	RRA							
	Exercise #1 (all in mV)				Exercise #2 (all in mV)			
	Method 1	Method 2	Method 3	Method 4	Method 1	Method 2	Method 3	Method 4
1	578 \pm 162	102 \pm 8	91 \pm 8	92 \pm 8	1506 \pm 291	375 \pm 14	322 \pm 26	333 \pm 11
2	595 \pm 50	170 \pm 23	144 \pm 24	150 \pm 25	512 \pm 50	162 \pm 20	140 \pm 10	149 \pm 15
3	1690 \pm 144	494 \pm 37	421 \pm 7	435 \pm 7	1150 \pm 199	329 \pm 32	264 \pm 29	284 \pm 17
4	268 \pm 8	80 \pm 13	67 \pm 9	71 \pm 9	415 \pm 14	134 \pm 6	110 \pm 3	116 \pm 4
5	483 \pm 581	48 \pm 3	42 \pm 1	42 \pm 1	95 \pm 6	32 \pm 4	27 \pm 2	28 \pm 3
6	818 \pm 89	239 \pm 44	167 \pm 26	197 \pm 21	418 \pm 45	112 \pm 7	93 \pm 8	95 \pm 7

Table 2. The MVC values of the two exercises for the left rectus abdominis for each participant. All values are presented as mean \pm SD across three trials.

Participant #	LRA							
	Exercise #1 (all in mV)				Exercise #2 (all in mV)			
	Method 1	Method 2	Method 3	Method 4	Method 1	Method 2	Method 3	Method 4
1	522 \pm 46	123 \pm 6	112 \pm 10	113 \pm 11	625 \pm 12	134 \pm 9	122 \pm 3	125 \pm 3
2	230 \pm 42	76 \pm 14	61 \pm 13	64 \pm 10	189 \pm 18	57 \pm 4	49 \pm 5	53 \pm 6
3	456 \pm 117	112 \pm 6	97 \pm 5	100 \pm 6	1265 \pm 117	333 \pm 27	272 \pm 13	285 \pm 27
4	283 \pm 23	66	56 \pm 4	57 \pm 5	279 \pm 51	100 \pm 25	83 \pm 13	85 \pm 15
5	169 \pm 13	48 \pm 3	42 \pm 2	44 \pm 1	105 \pm 9	32 \pm 2	26 \pm 1	27 \pm 1
6	792 \pm 296	182 \pm 21	143 \pm 28	153 \pm 18	317 \pm 6	73 \pm 3	63 \pm 3	67 \pm 2

Table 3. The MVC values of the two exercises for the right external oblique for each participant. All values are presented as mean \pm SD across three trials.

Participant #	RExO							
	Exercise #1 (all in mV)				Exercise #2 (all in mV)			
	Method 1	Method 2	Method 3	Method 4	Method 1	Method 2	Method 3	Method 4
1	815 \pm 28	218 \pm 18	194 \pm 13	197 \pm 16	601 \pm 152	155 \pm 29	132 \pm 22	143 \pm 32
2	617 \pm 101	171 \pm 19	144 \pm 17	147 \pm 16	320 \pm 63	97 \pm 16	82 \pm 17	86 \pm 13
3	555 \pm 146	153 \pm 40	142 \pm 37	143 \pm 36	688 \pm 214	199 \pm 52	175 \pm 45	179 \pm 47
4	327 \pm 42	92 \pm 8	77 \pm 6	81 \pm 6	168 \pm 64	55 \pm 19	41 \pm 14	47 \pm 18
5	259 \pm 31	357 \pm 479	71 \pm 2	72 \pm 2	296 \pm 6	97 \pm 15	79 \pm 11	82 \pm 8
6	702 \pm 220	218 \pm 99	175 \pm 71	187 \pm 75	648 \pm 124	170 \pm 12	153 \pm 9	155 \pm 9

Table 4. The MVC values of the two exercises for the left external oblique for each participant. All values are presented as mean \pm SD across three trials.

Participant #	LExO							
	Exercise #1 (all in mV)				Exercise #2 (all in mV)			
	Method 1	Method 2	Method 3	Method 4	Method 1	Method 2	Method 3	Method 4
1	-	-	-	-	-	-	-	-
2	595 \pm 88	158 \pm 7	141 \pm 6	146 \pm 2	582 \pm 49	174 \pm 11	152 \pm 3	155 \pm 6
3	431 \pm 77	133 \pm 46	102 \pm 36	333 \pm 351	846 \pm 123	230 \pm 12	197 \pm 7	207 \pm 6
4	433 \pm 40	142 \pm 5	121 \pm 8	122 \pm 8	163 \pm 21	53 \pm 5	46 \pm 3	46 \pm 4
5	-	-	-	-	-	-	-	-
6	595 \pm 34	170 \pm 22	148 \pm 21	156 \pm 19	562 \pm 49	158 \pm 19	141 \pm 21	145 \pm 20

Table 5. The MVC values of the two exercises for the right latissimus dorsi for each participant. All values are presented as mean \pm SD across three trials.

Participant #	RLD							
	Exercise #1 (all in mV)				Exercise #2 (all in mV)			
	Method 1	Method 2	Method 3	Method 4	Method 1	Method 2	Method 3	Method 4
1	597 \pm 92	149 \pm 34	132 \pm 26	134 \pm 25	301 \pm 57	60 \pm 8	52 \pm 9	55 \pm 9
2	486 \pm 70	124 \pm 28	99 \pm 9	101 \pm 8	172 \pm 23	46 \pm 2	38 \pm 5	39 \pm 4
3	726 \pm 87	164 \pm 18	138 \pm 20	139 \pm 20	556 \pm 123	111 \pm 24	104 \pm 21	106 \pm 22
4	181 \pm 24	51 \pm 4	45 \pm 5	46 \pm 5	83 \pm 9	22 \pm 3	20 \pm 3	20 \pm 3
5	449 \pm 69	106 \pm 7	97 \pm 6	97 \pm 7	198 \pm 44	48 \pm 15	38 \pm 9	43 \pm 11
6	647 \pm 60	149 \pm 19	124 \pm 19	135 \pm 13	142 \pm 43	29 \pm 10	26 \pm 10	27 \pm 10

Table 6. The MVC values of the two exercises for the left latissimus dorsi for each participant. All values are presented as mean \pm SD across three trials.

Participant #	LLD							
	Exercise #1 (all in mV)				Exercise #2 (all in mV)			
	Method 1	Method 2	Method 3	Method 4	Method 1	Method 2	Method 3	Method 4
1	670 \pm 62	136 \pm 11	107 \pm 28	113 \pm 20	304 \pm 32	71 \pm 12	59 \pm 10	62 \pm 12
2	359 \pm 56	90 \pm 9	80 \pm 6	82 \pm 7	84 \pm 65	32 \pm 4	28 \pm 3	29 \pm 4
3	771 \pm 168	175 \pm 15	134 \pm 28	144 \pm 24	672 \pm 150	155 \pm 19	139 \pm 14	142 \pm 13
4	267 \pm 35	81 \pm 10	71 \pm 13	73 \pm 11	81 \pm 2	24 \pm 2	21 \pm 2	21 \pm 2
5	352 \pm 16	84 \pm 4	69 \pm 6	76 \pm 4	191 \pm 60	53 \pm 31	41 \pm 19	44 \pm 20
6	414 \pm 8	114 \pm 14	105 \pm 11	106 \pm 11	143 \pm 39	35 \pm 10	31 \pm 10	32 \pm 9

9.3 Appendix C – Health Screening Form

APPENDIX 2a: HEALTH SCREENING FORM (H)

Use of Stochastic Resonance for Improving Postural Control in the Elderly and Individuals Post-Stroke

This questionnaire asks some questions about your health status. This information is used to guide us with your entry into the study. Specific medical conditions that will not allow you to participate in this study include any neurological or musculoskeletal conditions, or any injury/pain that makes the participation uncomfortable.

Participant ID: _____ Collector Initials: _____

Date: _____

DEMOGRAPHIC INFORMATION (self-report / direct measurement):

Age: _____ years Weight: _____ kg

Sex: _____ Height: _____ cm

Dominant Hand: _____ Dominant Leg: _____

For Females: Pregnant _____ Nursing _____

SELF REPORT CHECKLIST:

Past Health Problems:

- | | | |
|--|--|---|
| <input type="checkbox"/> Stroke | <input type="checkbox"/> Migraine/Frequent Headaches | <input type="checkbox"/> Heart Murmur |
| <input type="checkbox"/> Traumatic Brain Injury | <input type="checkbox"/> Seizures or Epilepsy | <input type="checkbox"/> High/Low Blood Pressure |
| <input type="checkbox"/> Concussion | <input type="checkbox"/> Chronic Joint Pain | <input type="checkbox"/> High Cholesterol |
| <input type="checkbox"/> Brain Tumor | <input type="checkbox"/> Chronic Muscle Pain | <input type="checkbox"/> Congenital Heart Disease |
| <input type="checkbox"/> Amyotrophic Lateral Sclerosis | <input type="checkbox"/> Back Injuries | <input type="checkbox"/> Disease of the Arteries |
| <input type="checkbox"/> Cerebral Palsy | <input type="checkbox"/> Low Back Pain | <input type="checkbox"/> Rheumatic Fever |
| <input type="checkbox"/> Multiple Sclerosis | <input type="checkbox"/> Swollen/Stiff Joints | <input type="checkbox"/> Emphysema, Pneumonia, Asthma, Bronchitis |
| <input type="checkbox"/> Parkinson's Disease | <input type="checkbox"/> Bone Disease | <input type="checkbox"/> Diabetes |
| <input type="checkbox"/> Peripheral Nerve Injuries | <input type="checkbox"/> Osteoarthritis | <input type="checkbox"/> Ulcers |
| <input type="checkbox"/> Spina Bifida | <input type="checkbox"/> Rheumatoid Arthritis | <input type="checkbox"/> Kidney or Liver Disease |
| <input type="checkbox"/> Spinal Cord Injuries | <input type="checkbox"/> Repetitive Strain Injury | |
| <input type="checkbox"/> Loss of Consciousness | <input type="checkbox"/> Fibromyalgia | |
| <input type="checkbox"/> Bleeding Disorders | <input type="checkbox"/> Heart Attack | |

Present Health:

List current problems:

- 1.
- 2.
- 3.
- 4.

List medications taken now or in last 3 months:

- 1.
- 2.
- 3.
- 4.

List Symptoms:

- | | |
|---|---|
| <input type="checkbox"/> Fatigue | <input type="checkbox"/> Shortness of breath |
| <input type="checkbox"/> Numbness/tingling of arms/legs/face | <input type="checkbox"/> Joint/muscle pain |
| <input type="checkbox"/> Loss of / trouble understanding speech | <input type="checkbox"/> Back pain/injury |
| <input type="checkbox"/> Loss of / double vision | <input type="checkbox"/> Leg pain/injury |
| <input type="checkbox"/> Dizziness | <input type="checkbox"/> Irregular heart beat |
| <input type="checkbox"/> Loss of coordination/balance | <input type="checkbox"/> Chest pain/pressure |
| <input type="checkbox"/> Severe/unusual headache | <input type="checkbox"/> Persistent cough |
| <input type="checkbox"/> Memory problems | <input type="checkbox"/> Wheezing |
| <input type="checkbox"/> Vertigo | |

Current Physical Training Status:

You consider your physical training status to be: High Average Low

List the types of physical activities that you do on a regular basis:

Habits:

Smoking: Never Ex-smoker Regular Average # cigarettes/day []

9.4 Appendix D – Consent Form

Albert H. Vette, Ph.D.

Assistant Professor
Department of Mechanical Engineering
10-326 Donadeo Innovation Centre for Engineering
9211 116 Street NW
University of Alberta

Research Scientist
Glenrose Rehabilitation Hospital
10230 111 Avenue NW
Edmonton, Alberta
T5G 0B7



Phone: 780-492-1534
Email: albert.vette@ualberta.ca

PARTICIPANT CONSENT FORM (H)

Title of Study:

Use of Stochastic Resonance for Improving Postural Control in the Elderly and Individuals Post-Stroke

Principal Investigator:

Dr. Albert Vette
Department of Mechanical Engineering
10-326 Donadeo Innovation Centre for Engineering
9211 116 Street NW
University of Alberta
Edmonton, Alberta T6G 1H9

Phone: 780-492-1534
Email: albert.vette@ualberta.ca

Why am I being asked to take part in this research study?

You are being invited to take part in a research study. Before you make a decision, one of the researchers will go over this form with you. You are encouraged to ask questions if you feel anything needs to be made clearer. You will be given a copy of this form for your records.

Elderly people and people with stroke fall more often than healthy young people. Consequences of falling can be serious. Increased risk of falling can also lead to reduced activity. There are different reasons for a high risk of falling in the elderly and post-stroke. They include environmental hazards, balance problems and medication use. To avoid falls, it is critical to use our senses such as touch and vision effectively.

A signal that contains no specific information is called noise. If applied to the body, it can improve the detection and transmission of weak sensory signals. Recently, this sensory noise

has been used to improve standing balance. However, our understanding of sensory noise and its effect on fall risk is limited. One goal is to better understand the effect of sensory noise on sensory detection and motor activity. Another goal is to test whether sensory noise can improve postural tasks related to falling. If so, sensory noise may be used for reducing postural problems in the elderly and post-stroke.

You are asked to participate in this study as part of a healthy comparison group. This will allow us to compare the performance of healthy people and people with stroke.

What is the reason for doing the study?

We would like to gain a better understanding of how sensory noise affects balance control. There are three sub-studies associated with this study. You are asked to participate in Sub-Study #2. In this sub-study, we would like to quantify upright posture during unstable sitting. Improved upright posture via sensory noise may reduce fall risk.

What will I be asked to do?

The session will take about 3 hours and will take place at the Syncrude Centre for Motion and Balance (SCMB), Glenrose Rehabilitation Hospital (see letterhead for address). Note that information on free parking and on directions to and within the hospital will be given to you today.

All of the data is completely confidential. At no time will your name or other identifying information be directly associated with it.

You are asked to sit on an unstable wobble board (part 1) and quietly on a stool (part 2). Your task is to balance your upper body in an upright position as good as you can. In order to prevent falls, a researcher will always stand close by. The researcher will assist you in recovering upright posture if needed.

You will be asked to complete balancing trials for different levels of difficulty, using different wobble boards. Half of the trials will be performed with eyes open, half of them with eyes closed. Each trial will not be longer than 60 seconds.

Patches will be attached to your trunk. These patches will measure the muscle activity during the study. Before the patches will be attached, that area of the skin will be cleaned. We will use mildly abrasive cream or a shaver and alcohol wipes for cleaning. In addition, you will wear reflective markers that record the motion of the trunk.

What are the risks and discomforts?

Participants may feel generally tired from the testing session. Some participants may experience slight discomfort when cleaning the skin for patch attachment. If participants have

sensitive skin, they may develop a slight temporary reddening. This would be caused by the adhesive used to affix the patches.

It is not possible to know all of the risks that may happen in a study, but the researchers have taken all reasonable safeguards to minimize any known risks to a study participant.

What are the benefits to me?

You may benefit by learning about experimental procedures used in neuroscience and biomechanics research. However, you may not get any direct benefit from being in this research study. This study may help other people who have balance problems in the future.

Do I have to take part in the study?

Being in this study is your choice. If you decide to be in the study, you can change your mind and stop being in the study at any time, and it will in no way affect your relationship to the University of Alberta or the Glenrose Rehabilitation Hospital.

We will ask you to complete a medical history form. Please note that you do not have to answer any questions that you are not comfortable with.

In case you decide to withdraw your participation, experimental testing will stop immediately. Note that the data recorded up to that point will be discarded and not used in subsequent analyses.

Data can be withdrawn from the study as long as obtained results have not been published.

Will my information be kept private?

During the study we will be collecting data about you. We will do everything we can to make sure that this data is kept private. No data relating to this study that includes your name will be released outside of the researcher's office or published by the researchers. Sometimes, by law, we may have to release your information with your name so we cannot guarantee absolute privacy. However, we will make every legal effort to make sure that your information is kept private.

After the study is done, we will still need to securely store your data that was collected as part of the study. At the University of Alberta, we keep data stored for a minimum of 5 years after the end of the study.

What if I have questions?

If you have any questions about the research now or later, please contact Albert Vette at 780-492-1534 or by email at albert.vette@ualberta.ca.

If you have any questions regarding your rights as a research participant, you may contact the Health Research Ethics Board at 780-492-2615. This office has no affiliation with the study investigators.

There are no conflicts of interest associated with this study.

Albert H. Vette, Ph.D.

Assistant Professor
Department of Mechanical Engineering
10-326 Donadeo Innovation Centre for Engineering
9211 116 Street NW
Edmonton, Alberta T6G 1H9

Research Scientist
Glenrose Rehabilitation Hospital
10230 111 Avenue NW
Edmonton, Alberta
T5G 0B7



Phone: 780-492-1534
Email: albert.vette@ualberta.ca

CONSENT

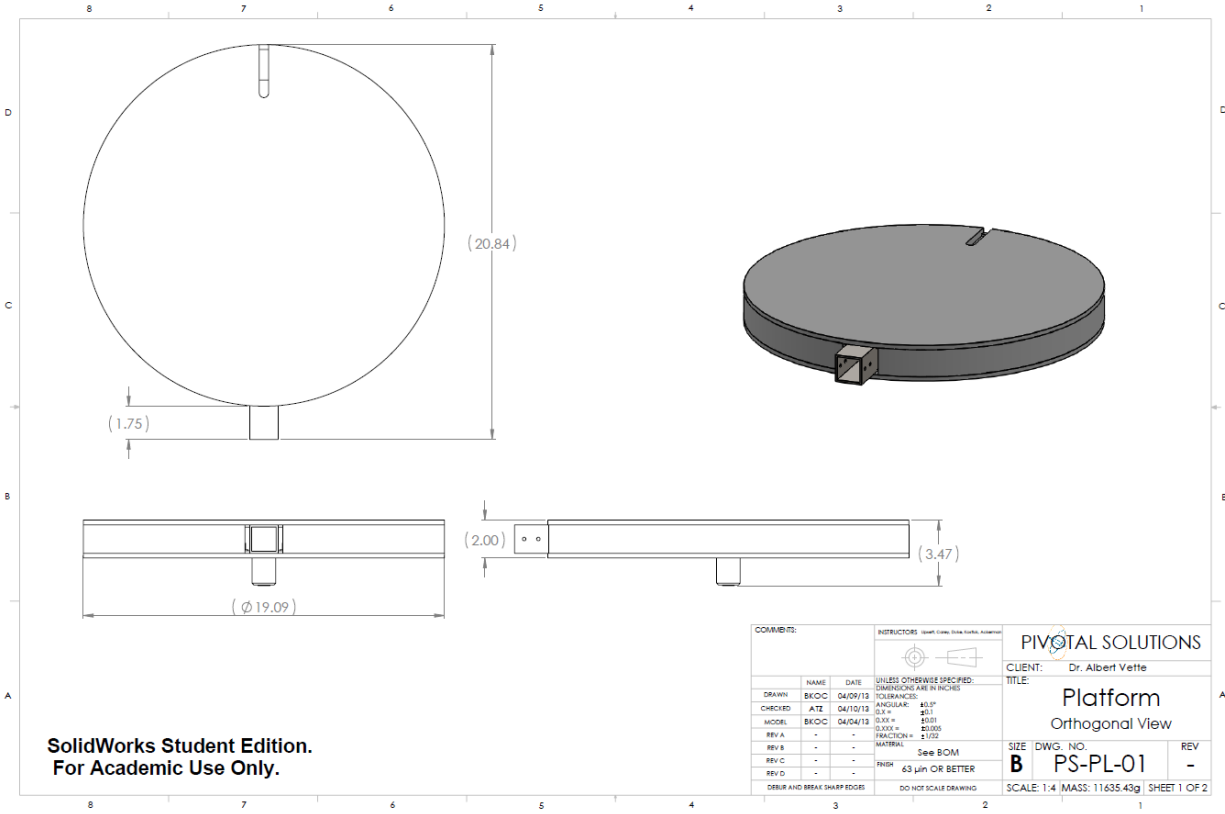
Title of Study: Use of Stochastic Resonance for Improving Postural Control in the Elderly and Individuals Post-Stroke

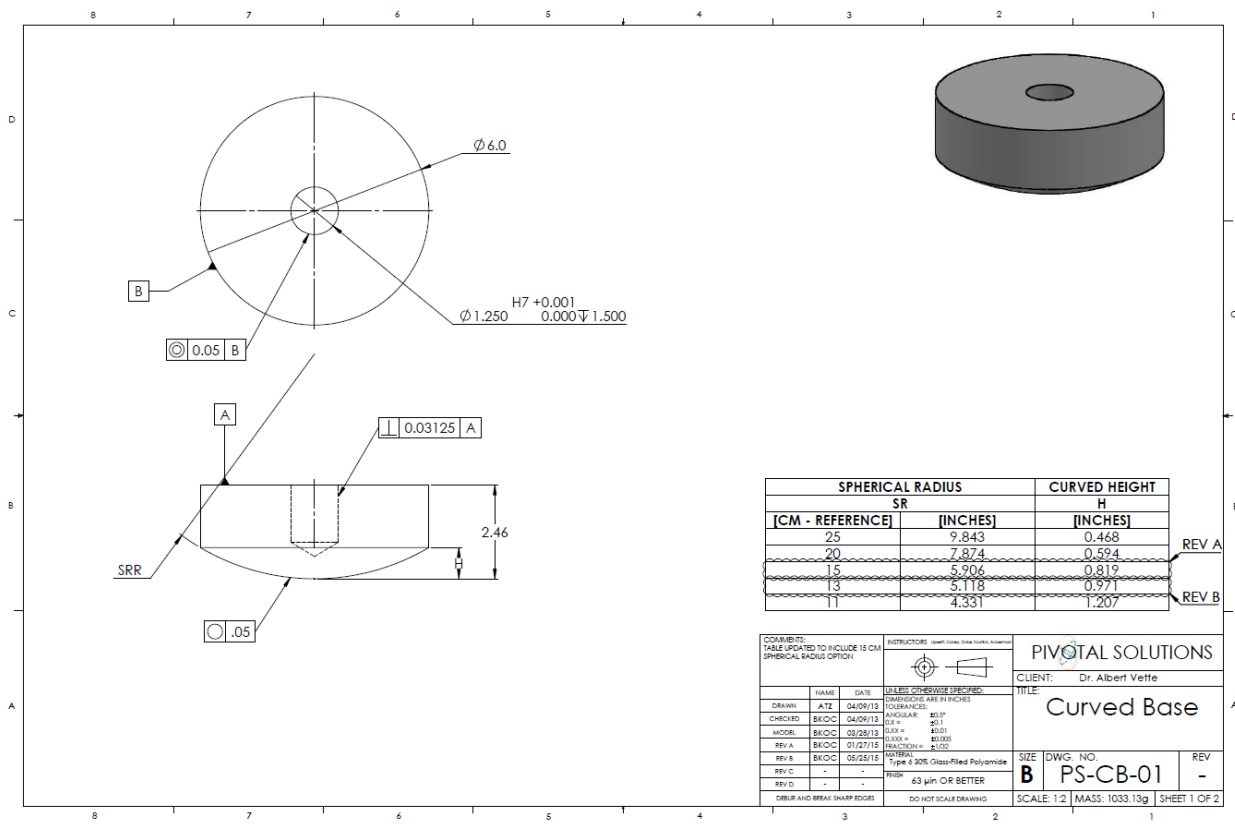
Principal Investigator: Albert Vette, Ph.D.

Phone Number: 780-492-1534

	<u>Yes</u>	<u>No</u>
Do you understand that you have been asked to be in a research study?	<input type="checkbox"/>	<input type="checkbox"/>
Have you read and received a copy of the attached Information Sheet?	<input type="checkbox"/>	<input type="checkbox"/>
Do you understand the benefits and risks involved in taking part in this research study?	<input type="checkbox"/>	<input type="checkbox"/>
Have you had an opportunity to ask questions and discuss this study?	<input type="checkbox"/>	<input type="checkbox"/>
Do you understand that you are free to leave the study at any time, without having to give a reason and without affecting your relationship with the University of Alberta and the Glenrose Rehabilitation Hospital	<input type="checkbox"/>	<input type="checkbox"/>
Has the issue of confidentiality been explained to you?	<input type="checkbox"/>	<input type="checkbox"/>
Do you understand who will have access to your study records?	<input type="checkbox"/>	<input type="checkbox"/>
Who explained this study to you? _____		
I agree to take part in this study:		
Signature of Research Participant _____		
(Printed Name) _____		
Date: _____		

9.5 Appendix E – Wobble Board and Bases Drawings





SPHERICAL RADIUS		CURVED HEIGHT
SR		H
[CM - REFERENCE]	[INCHES]	[INCHES]
25	9.843	0.468
20	7.874	0.594
15	5.906	0.819
13	5.118	0.971
11	4.331	1.207

COMMENTS:
TABLE UPDATED TO INCLUDE 15 CM SPHERICAL RADIUS OPTION

INSTRUCTIONS: (Insert Glass Base Under Assembly)

PIVOTAL SOLUTIONS
CLIENT: Dr. Albert Vette

TITLE: Curved Base

DATE	NAME	DATE	DESCRIPTION	SIZE	DWG. NO.	REV
04/09/12	ATZ	04/09/12	INITIALS	B	PS-CB-01	-
04/09/12	EKOC	04/09/12	ANGULAR: 85.0°			
03/28/12	EKOC	03/28/12	TOLERANCES: 0.01			
01/27/12	EKOC	01/27/12	FINISH: 63 μin OR BETTER			
05/26/12	EKOC	05/26/12	NOTES: Type 0 30% Glass-Filled Polyamide			
-	-	-	DO NOT SCALE DRAWING			

SCALE: 1:2 | MASS: 1033.13g | SHEET 1 OF 2

9.6 Appendix F – Group-Ensemble Average Levels of Muscle Activity for Each Participant

The average levels of muscle activity (%EMG) for all muscles and all conditions for each participant are shown in Tables 1 to 15.

Table 1. Average values of the normalized EMG activity for Participant # 1 for all muscles and conditions. Values are presented as mean \pm SD. All values are given as a percentage of MVC (%).

Participant # 1	B #1, EC		B #2, EC		B #2, EO		B #3, EO		B #4, EO	
	mean	SD								
RRA (%)	1.17	0.27	1.37	0.42	1.16	0.28	1.78	0.70	3.10	3.13
RExO (%)	1.65	0.61	3.35	2.07	1.43	0.50	4.35	2.08	4.76	3.98
RTES (%)	2.51	0.48	3.41	1.93	1.74	0.42	3.58	2.11	5.39	2.25
RLES (%)	1.59	0.36	1.37	0.58	1.22	0.28	1.39	0.51	2.53	2.06
RLD (%)	7.60	3.10	11.56	3.37	4.24	1.95	11.42	3.91	11.82	4.82
RRF (%)	1.74	1.28	1.29	0.62	1.23	0.30	2.23	1.41	3.88	3.03
RBF (%)	1.60	0.40	1.98	0.97	1.09	0.30	2.00	1.10	2.96	2.43
LRA (%)	1.91	0.33	2.11	0.53	1.92	0.34	2.42	0.68	3.76	3.16
LExO (%)	0.77	0.56	2.07	1.85	0.67	0.20	2.96	3.14	3.99	5.09
LTES (%)	6.25	1.17	6.39	2.04	3.90	0.81	5.19	2.04	6.46	2.73
LLES (%)	2.81	0.88	1.54	0.44	1.97	0.53	1.34	0.34	2.06	1.25
LLD (%)	5.66	2.20	7.73	2.23	4.38	1.73	7.53	2.86	7.52	3.07
LRF (%)	8.10	1.72	10.41	3.19	9.37	2.37	10.15	2.96	15.99	6.97
LBF (%)	1.67	0.97	2.15	1.00	0.94	0.34	2.98	1.69	2.48	1.57

Table 2. Average values of the normalized EMG activity for Participant # 2 for all muscles and conditions. Values are presented as mean \pm SD. All values are given as a percentage of MVC (%).

Participant # 2	B #1, EC		B #2, EC		B #2, EO		B #3, EC		B #3, EO		B #4, EO		B #5, EO	
	mean	SD	mean	SD	mean	SD	mean	SD	mean	SD	mean	SD	mean	SD
RRA (%)	4.78	1.19	5.24	2.20	4.53	1.50	22.81	17.83	8.13	4.98	15.52	5.95	28.95	20.44
RExO (%)	6.06	2.23	10.13	4.04	5.39	2.37	21.00	11.59	9.78	4.87	15.08	6.86	21.02	10.35
RTES (%)	5.07	0.72	8.25	1.67	8.33	1.41	8.01	3.82	6.65	1.72	6.54	2.06	7.07	3.00
RLES (%)	1.86	0.16	2.19	0.32	2.10	0.36	2.80	0.94	2.20	0.58	2.20	0.43	3.06	1.03
RLD (%)	12.43	1.85	16.89	4.34	14.74	3.54	23.78	11.76	14.14	3.77	18.25	6.34	20.29	8.07
RRF (%)	3.31	0.32	3.31	0.37	3.30	0.24	4.68	2.86	3.16	0.36	3.49	0.60	4.23	1.25
RBF (%)	1.95	0.74	1.51	0.45	2.64	0.59	2.99	1.78	2.21	0.68	2.22	0.83	3.10	2.03
LRA (%)	4.33	1.14	4.00	1.59	4.29	1.83	13.51	5.67	9.98	10.11	10.25	3.29	19.70	12.21
LExO (%)	4.72	1.52	5.07	3.50	5.22	3.10	11.63	8.26	7.09	4.36	8.56	4.94	15.24	9.35
LTES (%)	6.14	0.74	6.31	1.44	8.41	1.55	8.98	3.00	8.90	2.41	8.09	2.13	11.58	5.00
LLES (%)	2.27	0.17	2.53	0.40	2.34	0.96	3.38	1.48	2.47	1.03	2.27	0.54	3.80	2.34
LLD (%)	27.67	4.32	24.69	6.17	30.01	7.96	41.58	14.79	41.51	15.76	34.10	12.04	57.87	36.45
LRF (%)	2.47	0.17	2.52	0.30	2.47	0.19	2.97	0.55	2.66	0.35	2.53	0.21	3.08	0.73
LBF (%)	1.97	0.58	1.85	0.75	1.66	0.34	3.95	2.13	1.80	0.69	2.36	0.75	3.18	2.10

Table 3. Average values of the normalized EMG activity for Participant # 3 for all muscles and conditions. Values are presented as mean \pm SD. All values are given as a percentage of MVC (%).

Participant # 3	B #1, EC		B #2, EC		B #3, EC		B #3, EO		B #4, EO		B #5, EO	
	mean	SD										
RRA (%)	3.52	1.19	4.20	2.16	7.85	4.85	3.08	1.13	4.11	2.39	5.88	3.74
RExO (%)	4.17	1.79	5.19	2.05	9.26	5.71	3.87	2.13	4.76	4.41	6.48	6.04
RTES (%)	2.23	0.61	2.96	1.24	4.52	3.12	2.08	0.83	3.82	1.98	5.14	3.23
RLES (%)	1.63	0.16	1.73	0.36	2.41	1.10	1.69	0.21	2.11	0.57	2.34	1.11
RLD (%)	1.26	0.52	1.72	1.23	3.12	3.70	1.51	0.96	2.35	1.41	3.49	2.64
RRF (%)	9.39	2.38	5.49	2.05	7.48	5.92	4.55	1.40	6.19	2.74	6.65	3.43
RBF (%)	0.82	0.29	1.19	0.64	3.16	4.06	1.04	0.63	2.07	2.89	4.43	4.54
LRA (%)	5.61	1.37	5.76	2.88	11.34	5.18	5.20	1.33	6.93	4.13	8.61	4.47
LExO (%)	5.26	2.47	2.81	1.72	7.50	4.92	3.83	1.58	6.11	4.58	6.28	5.17
LTES (%)	5.79	1.57	5.01	2.36	5.24	2.33	3.35	1.48	4.96	2.43	5.71	2.43
LLES (%)	1.06	0.14	1.13	0.20	1.58	0.61	1.11	0.12	1.38	0.42	1.44	0.40
LLD (%)	2.71	0.85	2.26	1.22	2.21	1.14	1.32	0.48	1.85	0.89	2.52	1.34
LRF (%)	8.02	3.27	3.38	2.63	7.94	8.58	5.48	2.47	7.73	4.58	6.63	5.01
LBF (%)	0.60	0.07	1.09	0.78	1.65	1.88	0.67	0.33	1.04	1.45	1.68	1.97

Table 4. Average values of the normalized EMG activity for Participant # 4 for all muscles and conditions. Values are presented as mean \pm SD. All values are given as a percentage of MVC (%).

Participant # 4	B #1, EC		B #2, EC		B #2, EO		B #3, EO		B #4, EO	
	mean	SD								
RRA (%)	4.84	0.46	4.94	0.59	5.08	0.57	4.93	0.49	6.03	2.52
RExO (%)	2.69	1.08	2.36	1.16	1.13	0.22	1.50	0.66	3.20	3.11
RTES (%)	4.16	0.94	3.99	0.73	4.47	0.98	4.51	1.11	5.61	2.57
RLES (%)	1.56	0.24	1.99	0.90	2.93	0.81	2.48	0.67	3.88	1.94
RLD (%)	3.82	2.01	3.92	1.65	2.85	0.63	4.20	1.84	5.82	3.39
RRF (%)	4.20	2.59	3.40	1.11	4.75	1.39	7.80	3.50	16.24	10.09
RBF (%)	4.06	1.93	3.37	1.30	2.84	2.43	2.93	3.71	5.97	15.27
LRA (%)	5.80	0.52	5.87	0.55	5.79	0.60	5.86	0.59	6.86	1.89
LExO (%)	6.87	1.79	5.92	1.59	5.02	0.74	5.71	1.66	13.95	12.56
LTES (%)	5.86	1.81	5.96	2.03	6.17	1.86	7.08	4.17	15.44	15.55
LLES (%)	2.34	1.11	2.46	1.30	2.55	0.55	2.84	0.98	5.13	3.30
LLD (%)	1.81	0.65	1.58	0.32	1.54	0.31	1.61	0.41	2.42	1.11
LRF (%)	4.33	1.88	2.86	1.37	4.16	1.73	7.73	5.45	20.44	19.65
LBF (%)	1.03	0.16	1.07	0.41	0.95	0.07	1.00	0.11	1.44	1.11

Table 5. Average values of the normalized EMG activity for Participant # 5 for all muscles and conditions. Values are presented as mean \pm SD. All values are given as a percentage of MVC (%).

Participant # 5	B #1, EC		B #2, EC		B #2, EO		B #3, EO		B #4, EO		B #5, EO	
	mean	SD										
RRA (%)	7.94	1.48	9.06	1.60	9.09	1.56	8.99	1.54	9.01	2.02	10.70	4.68
RExO (%)	11.94	2.77	13.26	3.13	12.07	2.74	12.57	2.73	11.95	3.18	13.92	5.90
RTES (%)	1.23	0.38	1.22	0.39	1.31	0.35	1.33	0.32	1.81	0.59	2.71	1.37
RLES (%)	4.06	0.67	4.12	0.73	3.75	0.55	4.21	0.65	4.50	0.72	5.21	1.36
RLD (%)	6.53	3.84	4.80	2.32	6.68	3.70	6.01	2.30	8.13	3.37	11.74	4.69
RRF (%)	2.35	0.83	2.55	0.91	2.13	0.64	2.01	0.52	4.21	1.92	8.93	8.54
RBF (%)	1.69	0.98	1.56	0.73	1.08	0.18	1.26	0.44	1.83	1.15	3.30	2.93
LRA (%)	8.50	1.62	9.73	1.60	9.28	1.49	9.58	1.60	10.88	4.08	11.88	5.23
LExO (%)	13.48	3.01	14.52	3.60	13.50	2.90	13.61	3.02	12.51	3.30	14.49	5.60
LTES (%)	1.42	0.37	1.39	0.35	1.17	0.30	1.15	0.31	1.44	0.44	2.32	1.34
LLES (%)	2.35	0.35	2.61	0.45	2.40	0.36	2.63	0.42	2.77	0.47	3.24	0.85
LLD (%)	12.00	3.45	11.84	3.21	9.81	3.10	7.94	2.09	8.76	3.17	13.36	5.59
LRF (%)	2.57	1.01	3.53	1.56	2.51	0.75	3.08	1.22	4.69	1.71	7.30	3.80
LBF (%)	0.89	0.21	1.03	0.28	0.78	0.13	0.69	0.10	0.99	0.36	2.20	2.18

Table 6. Average values of the normalized EMG activity for Participant # 6 for all muscles and conditions. Values are presented as mean \pm SD. All values are given as a percentage of MVC (%).

Participant # 6	B #1, EC		B #2, EC		B #2, EO		B #3, EO		B #4, EO	
	mean	SD								
RRA (%)	2.54	0.92	4.21	1.59	2.71	0.80	2.60	0.68	4.81	1.76
RExO (%)	2.04	1.03	2.73	1.00	2.98	0.91	2.82	0.95	4.70	1.99
RTES (%)	5.30	1.05	4.79	1.16	3.39	1.11	4.47	1.08	4.86	1.42
RLES (%)	0.92	0.16	0.97	0.19	0.91	0.19	0.93	0.19	1.03	0.26
RLD (%)	7.81	1.97	7.54	2.35	4.12	1.83	6.16	1.58	6.46	2.79
RRF (%)	0.91	0.07	0.97	0.15	1.02	0.13	0.98	0.17	1.42	0.77
RBF (%)	1.40	0.39	1.17	0.58	0.90	0.39	0.44	0.14	0.49	0.25
LRA (%)	2.50	0.88	3.67	1.06	2.54	0.57	2.50	0.55	4.23	1.74
LExO (%)	1.55	0.90	1.63	0.68	2.08	0.59	2.11	0.78	3.04	1.86
LTES (%)	7.19	1.46	6.11	1.67	3.18	1.55	4.17	1.71	3.42	1.42
LLES (%)	1.23	0.23	1.37	0.46	1.21	0.24	1.15	0.23	1.35	0.52
LLD (%)	4.30	1.81	3.23	0.82	1.27	0.51	1.66	0.62	1.95	1.16
LRF (%)	2.20	0.38	2.76	0.71	2.40	0.43	2.47	0.64	2.99	1.06
LBF (%)	1.63	1.18	0.90	0.66	0.47	0.09	0.54	0.17	0.58	0.40

Table 7. Average values of the normalized EMG activity for Participant # 7 for all muscles and conditions. Values are presented as mean \pm SD. All values are given as a percentage of MVC (%).

Participant # 7	B #1, EC		B #2, EC		B #2, EO		B #3, EO		B #4, EO	
	mean	SD								
RRA (%)	6.27	0.71	6.23	0.66	6.06	0.64	6.20	0.67	6.32	0.76
RExO (%)	0.86	0.21	0.93	0.29	0.72	0.09	0.89	0.42	1.10	0.57
RTES (%)	6.81	1.16	7.05	1.32	6.28	0.93	7.71	2.06	8.27	2.27
RLES (%)	2.83	0.47	4.60	1.11	2.98	0.43	3.83	1.51	4.00	1.40
RLD (%)	7.17	2.18	8.41	2.16	6.36	1.30	8.77	1.53	10.35	2.55
RRF (%)	1.98	0.16	2.34	0.45	2.20	0.28	2.00	0.40	2.74	0.65
RBF (%)	0.53	0.25	0.78	0.49	0.57	0.34	0.55	0.20	0.70	0.40
LRA (%)	4.06	0.39	4.09	0.37	4.03	0.37	4.12	0.39	4.15	0.55
LExO (%)	2.43	1.41	2.01	1.15	1.57	0.52	2.66	1.40	4.30	2.39
LTES (%)	5.27	0.99	5.39	1.30	4.38	0.74	5.31	1.17	6.52	2.08
LLES (%)	2.80	0.71	4.34	0.92	3.29	0.64	3.90	0.87	3.43	1.26
LLD (%)	2.99	0.53	3.09	0.65	2.73	0.55	3.10	0.67	3.59	0.95
LRF (%)	3.51	0.46	2.27	0.44	3.83	0.76	3.63	1.27	4.35	1.74
LBF (%)	0.34	0.02	0.42	0.37	0.35	0.02	0.37	0.05	0.47	0.57

Table 8. Average values of the normalized EMG activity for Participant # 8 for all muscles and conditions. Values are presented as mean \pm SD. All values are given as a percentage of MVC (%).

Participant # 8	B #1, EC		B #2, EC		B #3, EC		B #3, EO		B #4, EO		B #5, EO	
	mean	SD										
RRA (%)	3.38	0.65	3.82	0.83	6.46	2.43	4.06	0.73	3.75	0.80	4.49	1.36
RExO (%)	3.27	1.40	4.13	1.83	7.50	3.54	4.43	1.21	2.85	1.71	4.34	2.61
RTES (%)	2.54	0.92	5.20	3.26	8.60	3.75	3.13	1.82	3.17	1.34	9.19	3.39
RLES (%)	1.90	0.23	2.02	0.29	2.62	0.84	2.14	0.28	2.13	0.30	2.37	0.42
RLD (%)	7.11	2.15	9.28	4.02	7.16	3.56	4.94	3.17	7.16	3.80	6.52	3.25
RRF (%)	1.50	0.23	1.93	0.71	3.54	1.87	2.08	0.82	2.97	1.76	3.26	1.71
RBF (%)	3.73	2.31	2.63	1.91	1.90	2.15	6.77	1.87	5.45	3.39	1.65	1.12
LRA (%)	4.96	2.23	5.12	1.20	8.08	2.71	6.49	1.96	5.33	1.46	5.94	1.59
LExO (%)	3.15	1.17	5.20	2.06	9.74	5.90	8.00	2.01	5.07	2.46	6.93	4.54
LTES (%)	2.41	1.24	5.67	2.08	9.05	4.29	2.23	0.87	2.42	0.80	8.36	3.28
LLES (%)	1.47	0.29	1.63	0.32	2.26	0.84	1.69	0.25	1.70	0.32	2.10	0.59
LLD (%)	2.67	1.39	2.30	1.90	2.79	1.55	4.02	2.33	3.68	1.51	3.80	2.66
LRF (%)	0.91	0.16	1.35	0.63	2.76	1.71	2.07	0.91	3.63	1.93	3.56	1.80
LBF (%)	1.79	0.85	1.12	0.63	1.48	1.04	0.90	0.25	0.82	0.10	1.01	0.38

Table 9. Average values of the normalized EMG activity for Participant # 9 for all muscles and conditions. Values are presented as mean \pm SD. All values are given as a percentage of MVC (%).

Participant # 9	B #1, EC		B #2, EC		B #2, EO		B #3, EO		B #4, EO	
	mean	SD								
RRA (%)	1.89	0.56	2.17	0.74	1.77	0.34	3.54	2.36	4.60	3.48
RExO (%)	2.01	0.83	2.41	1.02	1.76	0.75	4.79	2.79	10.06	6.44
RTES (%)	0.63	0.14	0.60	0.14	0.59	0.12	0.66	0.30	0.88	0.54
RLES (%)	4.16	1.44	4.53	1.17	4.18	0.99	5.02	1.49	6.95	4.50
RLD (%)	3.45	1.18	3.04	1.07	2.73	1.03	3.38	0.93	4.82	2.71
RRF (%)	1.08	0.73	2.64	1.60	0.82	0.49	0.95	0.50	2.32	1.70
RBF (%)	1.13	0.62	0.68	0.29	1.25	0.50	0.88	0.72	1.28	1.35
LRA (%)	1.05	0.20	1.12	0.34	1.03	0.20	1.98	2.05	2.21	1.45
LExO (%)	2.34	1.20	4.60	1.56	1.42	0.70	8.15	3.75	10.20	7.81
LTES (%)	6.79	1.59	7.24	2.21	4.98	1.60	8.75	2.76	8.48	3.34
LLES (%)	1.26	0.40	1.17	0.34	1.05	0.25	1.30	0.54	1.72	1.28
LLD (%)	1.78	0.55	1.82	0.85	1.48	0.51	2.33	0.84	3.16	1.78
LRF (%)	0.81	0.36	1.86	1.04	0.63	0.11	1.04	0.49	1.78	1.97
LBF (%)	0.73	0.46	0.79	0.47	0.61	0.21	2.15	1.71	2.11	1.61

Table 10. Average values of the normalized EMG activity for Participant # 10 for all muscles and conditions. Values are presented as mean \pm SD. All values are given as a percentage of MVC (%).

Participant # 10	B #1, EC		B #2, EC		B #2, EO		B #3, EO		B #4, EO	
	mean	SD								
RRA (%)	6.41	1.06	7.63	1.24	2.55	0.66	5.24	1.13	7.21	1.71
RExO (%)	7.53	1.74	8.49	1.92	3.03	0.81	5.47	2.16	8.53	2.53
RTES (%)	2.42	0.49	2.90	1.26	3.59	0.68	2.54	0.59	3.00	0.67
RLES (%)	1.05	0.14	1.05	0.13	1.06	0.21	1.06	0.24	1.05	0.18
RLD (%)	4.58	1.56	3.91	1.35	5.90	1.80	4.46	1.86	5.08	1.52
RRF (%)	9.54	2.46	9.41	4.02	8.90	1.85	6.83	2.12	9.16	3.34
RBF (%)	0.98	1.11	2.50	4.73	0.94	1.56	0.97	0.93	1.34	2.36
LRA (%)	2.22	0.48	3.08	0.57	1.59	0.32	2.86	0.97	2.59	0.56
LExO (%)	3.20	0.98	4.63	1.48	1.72	0.59	4.71	2.51	4.13	1.95
LTES (%)	2.93	0.92	2.95	0.90	2.77	1.00	2.98	0.92	3.11	0.92
LLES (%)	1.10	0.20	1.11	0.17	1.11	0.16	1.17	0.33	1.15	0.34
LLD (%)	1.34	0.55	1.34	0.54	1.36	0.59	1.39	0.54	1.45	0.54
LRF (%)	2.12	0.54	3.19	1.67	4.26	1.38	3.52	1.49	2.35	1.42
LBF (%)	1.23	0.32	0.79	0.14	0.70	0.07	0.91	0.40	0.98	0.41

Table 11. Average values of the normalized EMG activity for Participant # 11 for all muscles and conditions. Values are presented as mean \pm SD. All values are given as a percentage of MVC (%).

Participant # 11	B #1, EC		B #2, EC		B #2, EO		B #3, EO		B #4, EO	
	mean	SD	mean	SD	mean	SD	mean	SD	mean	SD
RRA (%)	17.12	2.98	19.02	3.67	14.19	2.31	16.25	2.88	18.25	5.03
RExO (%)	12.95	3.05	16.16	3.53	19.39	4.79	19.13	4.55	21.47	6.28
RTES (%)	1.27	0.31	1.88	0.79	1.34	0.30	1.53	0.53	2.22	0.82
RLES (%)	3.01	0.49	3.36	0.66	2.78	0.38	3.02	0.56	4.11	1.10
RLD (%)	2.63	0.75	3.98	1.61	1.87	0.74	2.51	1.30	4.34	1.84
RRF (%)	17.82	8.31	16.65	8.05	17.93	5.87	23.77	7.55	28.32	12.17
RBF (%)	0.72	0.17	0.60	0.21	0.68	0.12	28.08	10.81	0.81	0.26
LRA (%)	19.42	4.03	20.12	4.83	14.42	2.98	18.33	3.81	19.15	6.10
LExO (%)	11.75	2.53	12.00	2.94	11.75	3.24	13.79	3.07	16.34	5.15
LTES (%)	2.30	0.60	2.39	1.24	2.27	0.55	1.79	0.68	3.43	1.87
LLES (%)	3.00	0.56	3.33	0.73	2.58	0.42	2.95	0.54	3.93	0.92
LLD (%)	2.83	0.78	2.68	1.22	2.57	0.57	1.71	0.88	3.51	1.63
LRF (%)	13.41	4.59	12.08	5.62	11.57	4.34	12.43	4.97	13.29	6.26
LBF (%)	1.20	0.40	1.44	0.68	0.95	0.09	1.14	0.37	1.24	0.56

Table 12. Average values of the normalized EMG activity for Participant # 12 for all muscles and conditions. Values are presented as mean \pm SD. All values are given as a percentage of MVC (%).

Participant # 12	B #1, EC		B #2, EC		B #2, EO		B #3, EO		B #4, EO	
	mean	SD								
RRA (%)	2.56	5.21	2.07	0.71	1.99	1.45	2.64	1.89	2.97	3.09
RExO (%)	5.14	1.91	7.67	3.01	2.63	1.17	9.38	3.15	8.51	8.38
RTES (%)	4.81	1.42	5.29	1.91	4.13	1.33	3.36	1.54	7.48	5.36
RLES (%)	1.02	0.32	1.04	0.18	0.98	0.35	1.05	0.23	1.55	1.08
RLD (%)	4.07	2.90	5.11	2.63	1.98	0.97	2.53	2.15	6.77	8.91
RRF (%)	5.33	2.69	7.91	4.45	4.59	3.37	6.38	3.71	10.37	8.05
RBF (%)	0.58	0.33	0.64	0.18	0.50	0.08	0.65	0.25	1.14	1.89
LRA (%)	1.29	1.01	1.29	0.46	1.18	0.36	1.78	1.01	2.33	2.58
LExO (%)	4.43	1.82	4.00	1.89	3.04	1.51	5.57	2.06	8.32	6.84
LTES (%)	3.11	0.86	2.35	0.70	4.87	0.92	2.10	0.63	5.13	2.41
LLES (%)	1.14	0.26	1.23	0.28	1.20	0.31	1.18	0.32	2.06	1.58
LLD (%)	3.37	6.19	2.47	0.73	3.15	2.86	2.61	1.59	5.36	3.56
LRF (%)	2.58	1.24	3.74	2.18	2.35	1.62	2.46	1.12	4.35	2.97
LBF (%)	0.48	0.20	0.64	0.64	0.44	0.10	0.51	0.21	2.17	3.58

Table 13. Average values of the normalized EMG activity for Participant # 13 for all muscles and conditions. Values are presented as mean \pm SD. All values are given as a percentage of MVC (%).

Participant # 13	B #1, EC		B #2, EC		B #2, EO		B #3, EO		B #4, EO	
	mean	SD								
RRA (%)	13.61	2.42	18.94	3.09	8.34	1.16	10.71	2.71	16.38	6.61
RExO (%)	11.37	3.34	13.23	3.41	5.63	2.18	8.82	3.30	10.77	5.50
RTES (%)	6.41	1.05	7.62	1.54	8.22	1.40	6.22	1.05	6.67	2.80
RLES (%)	3.36	0.34	3.43	0.35	3.35	0.34	3.25	0.38	3.52	1.56
RLD (%)	3.09	1.30	3.34	1.04	4.43	1.60	3.02	0.59	3.38	1.08
RRF (%)	10.43	2.78	11.49	4.46	10.17	7.38	14.05	7.85	12.55	6.13
RBF (%)	2.72	1.22	2.07	0.96	1.23	0.20	1.29	0.39	1.98	1.15
LRA (%)	17.24	3.03	25.56	4.82	9.14	1.82	14.36	4.82	20.76	9.45
LExO (%)	8.40	2.03	10.88	2.77	5.94	1.95	9.25	2.71	8.96	4.63
LTES (%)	7.01	1.48	6.81	1.45	8.83	1.74	6.90	1.51	6.89	1.57
LLES (%)	3.49	0.35	3.59	0.61	3.48	0.30	3.33	0.61	4.28	2.20
LLD (%)	4.10	1.44	4.47	1.58	3.80	1.38	4.03	1.55	4.74	1.81
LRF (%)	4.65	0.91	5.41	1.90	5.98	5.17	7.36	4.68	7.31	5.61
LBF (%)	5.36	2.19	4.18	3.05	2.33	1.12	1.74	1.24	3.18	2.96

Table 14. Average values of the normalized EMG activity for Participant # 14 for all muscles and conditions. Values are presented as mean \pm SD. All values are given as a percentage of MVC (%).

Participant # 14	B #1, EC		B #2, EC		B #2, EO		B #3, EO		B #4, EO	
	mean	SD								
RRA (%)	4.89	0.87	6.59	2.05	4.62	0.88	6.55	2.11	6.81	2.22
RExO (%)	2.17	0.58	4.10	4.33	2.81	0.86	4.61	3.54	4.84	4.84
RTES (%)	2.92	0.66	4.55	2.04	2.54	0.52	3.75	2.11	3.98	2.12
RLES (%)	2.39	0.38	3.33	1.06	2.12	0.26	2.61	0.66	2.86	0.62
RLD (%)	6.06	1.38	10.62	5.88	5.85	1.52	8.19	3.67	8.97	4.62
RRF (%)	2.97	0.68	4.08	1.47	2.51	0.37	3.36	1.50	3.28	1.08
RBF (%)	5.24	2.08	10.52	6.02	1.80	0.86	10.51	6.11	7.15	5.71
LRA (%)	6.15	1.87	8.53	3.86	6.79	2.13	9.02	3.87	9.16	3.32
LExO (%)	4.24	1.32	5.79	3.60	3.14	1.05	6.56	7.06	6.34	2.62
LTES (%)	3.83	0.86	5.76	1.57	3.51	0.65	5.29	1.95	5.09	1.27
LLES (%)	2.13	0.44	3.14	1.03	1.68	0.18	2.37	0.93	2.43	0.61
LLD (%)	5.44	1.12	8.30	2.30	4.95	1.39	7.22	2.84	7.51	1.66
LRF (%)	3.41	1.11	4.80	4.60	4.10	1.81	2.87	1.36	3.90	1.87
LBF (%)	1.98	0.51	5.85	4.54	1.45	0.10	4.69	5.41	3.89	2.90

Table 15. Average values of the normalized EMG activity for Participant # 15 for all muscles and conditions. Values are presented as mean \pm SD. All values are given as a percentage of MVC (%).

Participant # 15	B #1, EC		B #2, EC		B #2, EO		B #3, EO		B #4, EO	
	mean	SD								
RRA (%)	6.24	0.59	6.33	2.95	7.10	0.74	8.26	1.78	8.46	5.90
RExO (%)	6.82	1.80	7.95	3.76	6.09	1.86	10.01	5.31	11.29	7.64
RTES (%)	5.83	1.49	7.81	2.76	5.88	1.48	5.84	1.51	9.94	6.19
RLES (%)	3.81	0.63	3.97	0.99	4.16	0.76	4.64	0.89	4.72	1.68
RLD (%)	6.16	1.64	8.14	3.16	5.73	1.19	6.33	1.43	10.08	5.34
RRF (%)	2.47	0.92	2.31	0.93	4.19	2.18	3.40	1.84	2.59	1.64
RBF (%)	1.11	0.60	1.45	1.17	1.21	0.80	2.68	1.83	4.05	2.34
LRA (%)	5.46	0.55	5.40	2.16	6.50	0.71	6.96	2.59	7.39	4.39
LExO (%)	10.60	3.83	10.91	6.08	10.39	3.80	15.88	7.78	18.04	11.34
LTES (%)	6.82	2.59	9.35	4.04	8.83	3.45	9.19	4.30	13.94	6.70
LLES (%)	3.13	1.18	3.35	1.78	3.56	1.05	4.35	1.83	4.38	2.21
LLD (%)	3.32	0.92	4.24	2.47	3.55	1.01	5.23	3.36	9.42	7.18
LRF (%)	2.97	1.60	2.19	0.81	2.76	1.48	2.34	0.85	2.64	2.25
LBF (%)	0.97	0.38	1.35	0.81	1.23	0.65	2.17	1.34	3.25	2.44

9.7 Appendix G – Group-Ensemble Posturographic Measures for Each Participant

The mean angle (MA); the root mean square amplitude of the angle (RMSA); the mean of the absolute angular velocity (MV); the root mean square amplitude of the angular velocity (RMSV); the range (RANGE); the centroidal frequency (CFREQ); and the frequency dispersion (FREQD) for all conditions and each participant are shown in Tables 1 to 15.

Table 1. Analysis of the AP, ML, TM, and TD fluctuations. Posturographic measures were calculated for Base #1 and #2 under EC condition. Shown are the mean \pm SD for Participant #1.

Participant # 1	B #1, EC		B #2, EC		B #2, EO		B #3, EO		B #4, EO	
	mean	SD	mean	SD	mean	SD	mean	SD	mean	SD
MA (AP) (deg)	1.10	0.32	1.52	0.36	1.22	0.38	1.76	0.58	3.26	0.56
MA (ML) (deg)	0.85	0.11	1.47	0.50	0.72	0.16	2.36	1.05	3.28	0.58
MA (TD) (deg)	9.26	2.44	13.77	6.02	7.42	1.77	23.17	11.54	44.29	5.25
MA (TM) (deg)	1.08	0.33	1.49	0.29	1.19	0.30	1.62	0.52	2.85	0.33
RMSA (AP) (deg)	1.36	0.35	1.89	0.40	1.44	0.38	2.20	0.59	4.02	0.68
RMSA (ML) (deg)	1.08	0.15	1.88	0.54	0.92	0.19	2.87	1.22	4.30	0.49
RMSA (TD) (deg)	11.62	2.98	17.58	7.30	9.49	2.18	28.51	15.08	55.02	7.51
RMSA (TM) (deg)	1.32	0.36	1.85	0.32	1.42	0.30	2.02	0.58	3.49	0.35
MV (AP) (deg/s)	2.97	0.32	4.00	0.28	1.83	0.24	4.40	0.98	7.30	0.75
MV (ML) (deg/s)	2.28	0.39	3.33	0.43	1.56	0.20	4.30	1.45	6.52	1.72
MV (TD) (deg/s)	24.34	7.56	33.35	8.68	15.46	3.12	52.17	36.85	117.30	45.16
MV (TM) (deg/s)	2.96	0.19	3.95	0.25	1.84	0.21	4.27	1.03	7.06	1.10
RMSV (AP) (deg/s)	3.90	0.38	5.35	0.38	2.36	0.29	5.88	1.41	9.23	0.97
RMSV (ML) (deg/s)	2.97	0.48	4.33	0.44	2.06	0.28	5.49	1.70	8.70	2.34
RMSV (TD) (deg/s)	32.48	10.16	48.23	13.60	23.41	7.41	319.06	542.01	858.85	602.27
RMSV (TM) (deg/s)	3.90	0.24	5.25	0.27	2.34	0.26	5.71	1.42	9.14	1.38
RANGE (AP) (deg)	7.09	1.44	9.58	1.90	6.19	1.00	11.64	1.44	19.10	1.91
RANGE (ML) (deg)	5.61	0.81	10.08	1.28	4.79	0.96	13.06	4.37	22.19	0.77
RANGE (TD) (deg)	61.01	16.62	110.81	50.15	53.85	10.80	171.37	125.33	316.91	81.76
RANGE (TM) (deg)	6.54	1.33	9.18	1.23	6.12	0.83	10.58	2.37	14.41	0.70
CFREQ (AP) (Hz)	0.58	0.08	0.52	0.03	0.40	0.05	0.57	0.11	0.53	0.07
CFREQ (ML) (Hz)	0.54	0.05	0.45	0.07	0.42	0.06	0.41	0.07	0.41	0.04
CFREQ (TD) (Hz)	0.55	0.05	0.54	0.13	0.44	0.08	0.80	0.60	0.96	0.61
CFREQ (TM) (Hz)	0.59	0.08	0.53	0.04	0.39	0.04	0.56	0.08	0.57	0.05
FREQD (AP) (-)	0.51	0.03	0.54	0.04	0.57	0.05	0.58	0.03	0.57	0.05
FREQD (ML) (-)	0.51	0.07	0.52	0.02	0.53	0.04	0.59	0.05	0.58	0.03
FREQD (TD) (-)	0.55	0.06	0.57	0.04	0.55	0.04	0.65	0.09	0.70	0.06
FREQD (TM) (-)	0.49	0.04	0.54	0.03	0.58	0.05	0.58	0.04	0.61	0.06

Table 2. Analysis of the AP, ML, TM, and TD fluctuations. Posturographic measures were calculated for Base #1 and #2 under EC condition. Shown are the mean \pm SD for Participant #2.

Participant # 2	B #1, EC		B #2, EC		B #3, EC		B #3, EO		B #4, EO		B #5, EO	
	mean	SD	mean	SD	SD	mean	SD	mean	mean	SD	mean	SD
MA (AP) (deg)	0.54	0.19	1.15	0.23	3.06	0.45	1.36	0.28	1.21	0.17	2.79	0.64
MA (ML) (deg)	0.29	0.05	0.95	0.08	2.72	0.27	1.02	0.36	1.03	0.12	2.22	0.34
MA (TD) (deg)	2.88	0.94	14.56	4.34	27.28	4.98	8.58	2.95	6.61	0.83	20.37	5.19
MA (TM) (deg)	0.53	0.18	1.22	0.19	2.60	0.19	1.32	0.32	1.20	0.15	2.60	0.59
RMSA (AP) (deg)	0.73	0.27	1.48	0.29	3.89	0.61	1.72	0.37	1.56	0.30	3.54	0.64
RMSA (ML) (deg)	0.37	0.08	1.30	0.17	3.43	0.52	1.33	0.46	1.33	0.15	2.91	0.43
RMSA (TD) (deg)	3.70	1.33	18.81	5.73	40.04	8.60	11.10	4.00	8.47	0.64	29.85	7.52
RMSA (TM) (deg)	0.71	0.27	1.52	0.20	3.22	0.29	1.67	0.40	1.54	0.29	3.28	0.71
MV (AP) (deg/s)	1.30	0.41	2.89	0.25	7.02	1.06	3.57	0.81	3.23	0.54	7.37	0.56
MV (ML) (deg/s)	0.76	0.28	2.19	0.25	6.57	0.41	2.96	1.11	3.12	0.32	6.55	0.79
MV (TD) (deg/s)	7.56	3.27	35.91	11.63	87.39	12.42	25.29	12.79	19.36	1.43	63.79	14.14
MV (TM) (deg/s)	1.27	0.39	2.81	0.07	7.00	0.93	3.50	0.84	3.28	0.49	7.76	0.81
RMSV (AP) (deg/s)	1.81	0.70	3.73	0.39	9.36	1.25	4.78	1.06	4.31	0.60	9.60	0.76
RMSV (ML) (deg/s)	1.05	0.39	3.00	0.42	8.75	0.75	4.03	1.59	4.38	0.48	8.93	1.27
RMSV (TD) (deg/s)	10.14	4.42	51.75	16.04	884.57	171.95	36.18	19.81	27.84	2.40	319.57	263.29
RMSV (TM) (deg/s)	1.75	0.66	3.65	0.13	9.31	1.01	4.70	1.13	4.39	0.50	10.14	0.92
RANGE (AP) (deg)	4.18	1.67	7.58	1.35	19.25	3.28	8.96	2.61	8.40	2.33	18.59	3.38
RANGE (ML) (deg)	2.06	0.59	7.93	1.61	18.26	4.15	8.29	2.88	7.51	0.72	17.33	3.22
RANGE (TD) (deg)	19.65	8.10	113.03	23.74	355.59	6.53	66.24	30.96	51.25	5.73	248.36	97.08
RANGE (TM) (deg)	4.10	1.54	7.43	1.02	14.96	1.58	8.61	2.39	7.91	2.34	17.18	4.33
CFREQ (AP) (Hz)	0.54	0.07	0.52	0.07	0.49	0.09	0.59	0.06	0.60	0.10	0.55	0.07
CFREQ (ML) (Hz)	0.56	0.07	0.47	0.03	0.51	0.06	0.54	0.08	0.56	0.03	0.56	0.08
CFREQ (TD) (Hz)	0.56	0.08	0.56	0.06	1.52	0.39	0.60	0.10	0.56	0.05	0.65	0.10
CFREQ (TM) (Hz)	0.54	0.08	0.52	0.09	0.56	0.09	0.59	0.06	0.60	0.11	0.60	0.09
FREQD (AP) (-)	0.63	0.05	0.63	0.05	0.57	0.04	0.60	0.05	0.60	0.05	0.60	0.02
FREQD (ML) (-)	0.54	0.04	0.62	0.05	0.59	0.08	0.59	0.02	0.56	0.03	0.62	0.03
FREQD (TD) (-)	0.56	0.05	0.65	0.03	0.67	0.06	0.59	0.03	0.56	0.02	0.66	0.04
FREQD (TM) (-)	0.63	0.05	0.61	0.06	0.58	0.05	0.60	0.05	0.60	0.06	0.61	0.02

Table 3. Analysis of the AP, ML, TM, and TD fluctuations. Posturographic measures were calculated for Base #1 and #2 under EC condition. Shown are the mean \pm SD for Participant #3.

Participant # 3	B #1, EC		B #2, EC		B #3, EC		B #3, EO		B #4, EO		B #5, EO	
	mean	SD	mean	SD	mean	SD	mean	SD	mean	SD	mean	SD
MA (AP) (deg)	0.74	0.13	1.14	0.13	2.08	0.85	0.80	0.21	1.70	0.49	2.12	0.51
MA (ML) (deg)	0.61	0.07	0.96	0.23	2.28	0.36	0.95	0.07	2.21	0.28	2.98	0.61
MA (TD) (deg)	21.82	5.08	69.47	47.41	96.52	19.17	91.77	9.21	120.01	4.01	65.84	7.40
MA (TM) (deg)	0.61	0.04	1.00	0.09	2.13	0.92	0.70	0.03	1.54	0.32	2.28	0.29
RMSA (AP) (deg)	0.98	0.17	1.40	0.17	2.78	1.07	1.01	0.25	2.20	0.65	2.73	0.59
RMSA (ML) (deg)	0.79	0.07	1.17	0.23	3.03	0.52	1.30	0.08	2.84	0.43	3.74	0.59
RMSA (TD) (deg)	33.66	8.49	86.37	52.03	108.41	15.67	111.34	11.42	130.72	3.19	79.73	8.38
RMSA (TM) (deg)	0.79	0.07	1.22	0.12	2.64	1.18	0.95	0.11	1.95	0.41	2.79	0.25
MV (AP) (deg/s)	1.78	0.44	2.11	0.32	4.21	0.83	1.31	0.05	3.11	0.45	3.96	0.59
MV (ML) (deg/s)	2.05	0.36	2.60	0.37	5.98	1.29	2.05	0.42	5.56	0.86	7.01	0.52
MV (TD) (deg/s)	72.83	16.21	186.87	110.63	318.05	59.92	215.04	73.80	317.14	67.88	238.18	32.30
MV (TM) (deg/s)	1.93	0.46	2.33	0.41	5.39	0.95	1.85	0.17	3.88	0.53	5.79	0.45
RMSV (AP) (deg/s)	2.31	0.56	2.73	0.47	5.77	1.59	1.70	0.10	4.12	0.52	5.12	0.76
RMSV (ML) (deg/s)	2.65	0.46	3.28	0.43	7.96	1.80	2.90	0.79	7.32	1.19	9.13	0.61
RMSV (TD) (deg/s)	712.49	420.62	1857.62	1076.85	2545.49	430.55	2168.92	667.36	2771.90	383.52	1970.43	305.32
RMSV (TM) (deg/s)	2.51	0.60	3.00	0.51	7.39	1.47	2.60	0.40	5.28	0.64	7.57	0.69
RANGE (AP) (deg)	5.42	1.28	6.66	1.05	14.31	4.04	5.13	1.09	11.05	3.33	14.66	3.02
RANGE (ML) (deg)	4.29	0.37	5.58	0.38	17.05	3.50	8.00	2.63	16.35	2.61	18.95	1.76
RANGE (TD) (deg)	302.57	108.65	359.19	1.55	359.65	0.45	359.90	0.05	359.77	0.16	359.27	0.37
RANGE (TM) (deg)	4.00	0.59	5.60	0.60	10.83	3.80	5.47	1.68	9.48	1.77	11.58	0.87
CFREQ (AP) (Hz)	0.44	0.08	0.39	0.04	0.41	0.04	0.42	0.07	0.45	0.05	0.41	0.02
CFREQ (ML) (Hz)	0.58	0.05	0.50	0.03	0.54	0.07	0.48	0.12	0.52	0.02	0.52	0.04
CFREQ (TD) (Hz)	0.78	0.32	1.09	0.12	1.35	0.13	1.11	0.25	1.21	0.07	1.38	0.29
CFREQ (TM) (Hz)	0.56	0.09	0.48	0.04	0.51	0.11	0.55	0.09	0.59	0.06	0.53	0.04
FREQD (AP) (-)	0.59	0.05	0.58	0.04	0.59	0.02	0.59	0.04	0.60	0.02	0.59	0.02
FREQD (ML) (-)	0.56	0.04	0.57	0.02	0.60	0.06	0.63	0.04	0.59	0.02	0.62	0.03
FREQD (TD) (-)	0.69	0.06	0.75	0.03	0.69	0.02	0.74	0.02	0.73	0.01	0.72	0.04
FREQD (TM) (-)	0.59	0.04	0.61	0.02	0.64	0.04	0.63	0.03	0.63	0.02	0.64	0.04

Table 4. Analysis of the AP, ML, TM, and TD fluctuations. Posturographic measures were calculated for Base #1 and #2 under EC condition. Shown are the mean \pm SD for Participant #4.

Participant # 4	B #1, EC		B #2, EC		B #2, EO		B #3, EO		B #4, EO	
	mean	SD	mean	SD	mean	SD	mean	SD	mean	SD
MA (AP) (deg)	0.98	0.32	1.28	0.11	1.17	0.39	1.36	0.18	2.84	0.69
MA (ML) (deg)	0.73	0.32	1.01	0.26	0.74	0.12	1.33	0.24	3.35	1.08
MA (TD) (deg)	57.33	55.33	26.10	13.06	38.73	14.55	87.41	29.38	87.07	6.13
MA (TM) (deg)	0.82	0.24	1.22	0.06	0.85	0.22	1.38	0.37	2.33	0.52
RMSA (AP) (deg)	1.25	0.44	1.61	0.09	1.44	0.48	1.82	0.30	3.75	0.85
RMSA (ML) (deg)	0.96	0.49	1.26	0.32	0.93	0.16	1.83	0.31	4.20	1.35
RMSA (TD) (deg)	66.46	62.48	33.43	16.91	52.33	21.79	104.77	26.96	101.60	5.78
RMSA (TM) (deg)	1.01	0.26	1.53	0.08	1.08	0.29	1.71	0.45	2.93	0.70
MV (AP) (deg/s)	2.16	0.27	2.28	0.25	2.01	0.19	2.37	0.20	5.71	1.03
MV (ML) (deg/s)	2.33	0.81	2.44	0.52	1.68	0.30	3.21	0.48	7.89	2.45
MV (TD) (deg/s)	206.29	237.99	62.29	31.23	104.41	47.76	269.05	86.44	242.70	52.36
MV (TM) (deg/s)	2.37	0.54	2.48	0.46	1.84	0.29	3.03	0.46	6.75	1.93
RMSV (AP) (deg/s)	2.76	0.36	3.06	0.23	2.69	0.27	3.06	0.27	7.65	1.40
RMSV (ML) (deg/s)	3.08	1.02	3.26	0.64	2.17	0.39	4.36	0.64	10.63	3.56
RMSV (TD) (deg/s)	1516.55	1814.14	220.78	296.43	949.93	719.82	2453.06	612.83	2160.89	288.72
RMSV (TM) (deg/s)	3.07	0.78	3.29	0.52	2.46	0.47	4.03	0.54	9.23	2.73
RANGE (AP) (deg)	5.81	1.77	7.12	0.49	6.84	2.56	9.18	1.72	21.06	6.75
RANGE (ML) (deg)	5.60	3.22	6.34	2.01	4.58	0.88	10.75	0.89	21.11	5.89
RANGE (TD) (deg)	212.43	170.46	193.29	111.00	303.52	111.64	359.85	0.10	359.72	0.20
RANGE (TM) (deg)	4.95	1.09	6.76	0.76	5.47	1.85	7.94	1.96	13.92	3.17
CFREQ (AP) (Hz)	0.50	0.10	0.43	0.04	0.50	0.04	0.39	0.06	0.41	0.04
CFREQ (ML) (Hz)	0.62	0.14	0.50	0.05	0.47	0.05	0.44	0.06	0.47	0.08
CFREQ (TD) (Hz)	0.90	0.39	0.56	0.05	1.00	0.35	1.28	0.21	1.11	0.16
CFREQ (TM) (Hz)	0.59	0.13	0.46	0.05	0.50	0.01	0.47	0.02	0.57	0.11
FREQD (AP) (-)	0.54	0.07	0.56	0.05	0.60	0.02	0.57	0.04	0.56	0.03
FREQD (ML) (-)	0.50	0.06	0.53	0.04	0.53	0.04	0.57	0.04	0.56	0.01
FREQD (TD) (-)	0.62	0.13	0.61	0.05	0.68	0.04	0.70	0.06	0.73	0.03
FREQD (TM) (-)	0.54	0.06	0.59	0.04	0.57	0.02	0.61	0.05	0.62	0.02

Table 5. Analysis of the AP, ML, TM, and TD fluctuations. Posturographic measures were calculated for Base #1 and #2 under EC condition. Shown are the mean \pm SD for Participant #5.

Participant # 5	B #1, EC		B #2, EC		B #2, EO		B #3, EO		B #4, EO		B #5, EO	
	mean	SD										
MA (AP) (deg)	0.43	0.06	0.61	0.09	0.42	0.09	0.40	0.10	0.75	0.12	1.41	0.50
MA (ML) (deg)	0.49	0.11	0.77	0.16	0.39	0.07	0.55	0.04	0.98	0.29	2.30	0.77
MA (TD) (deg)	105.99	26.96	102.72	28.19	117.14	19.83	107.91	29.43	96.80	28.54	115.28	14.83
MA (TM) (deg)	0.37	0.06	0.58	0.12	0.30	0.04	0.44	0.09	0.74	0.16	1.47	0.50
RMSA (AP) (deg)	0.52	0.07	0.78	0.13	0.52	0.10	0.51	0.15	0.95	0.15	1.87	0.68
RMSA (ML) (deg)	0.61	0.13	1.02	0.17	0.50	0.09	0.75	0.05	1.30	0.42	2.99	0.93
RMSA (TD) (deg)	121.70	19.69	114.89	24.32	128.06	17.36	118.89	22.81	114.69	18.68	123.81	13.49
RMSA (TM) (deg)	0.45	0.08	0.73	0.13	0.38	0.05	0.60	0.11	0.97	0.24	1.94	0.71
MV (AP) (deg/s)	1.32	0.16	1.81	0.17	0.85	0.12	0.98	0.07	2.01	0.42	3.98	1.33
MV (ML) (deg/s)	1.78	0.38	2.52	0.21	1.07	0.17	1.90	0.19	3.31	0.64	6.07	1.74
MV (TD) (deg/s)	441.18	92.49	403.37	57.77	346.78	72.99	445.51	58.25	377.70	102.98	377.24	79.57
MV (TM) (deg/s)	1.57	0.18	2.25	0.20	0.97	0.17	1.47	0.33	2.65	0.50	5.22	1.70
RMSV (AP) (deg/s)	1.65	0.21	2.27	0.20	1.11	0.18	1.27	0.12	2.62	0.56	5.40	1.76
RMSV (ML) (deg/s)	2.25	0.45	3.35	0.38	1.39	0.25	2.68	0.47	4.35	0.80	7.77	2.11
RMSV (TD) (deg/s)	3306.59	508.24	2974.83	509.94	2891.23	476.58	3192.34	345.00	2988.38	504.08	2953.24	539.70
RMSV (TM) (deg/s)	1.99	0.22	2.94	0.31	1.29	0.25	2.12	0.60	3.54	0.77	6.75	1.92
RANGE (AP) (deg)	2.47	0.16	3.88	0.97	2.69	0.29	2.66	0.98	5.22	0.90	10.61	4.22
RANGE (ML) (deg)	3.12	0.23	6.07	1.22	2.89	0.66	4.55	1.30	7.58	2.41	16.94	4.34
RANGE (TD) (deg)	359.87	0.11	359.71	0.36	359.82	0.12	359.83	0.14	359.86	0.08	359.87	0.07
RANGE (TM) (deg)	2.17	0.16	3.84	0.55	2.02	0.35	3.14	0.57	5.12	1.24	10.83	4.06
CFREQ (AP) (Hz)	0.54	0.03	0.57	0.06	0.53	0.09	0.56	0.03	0.57	0.02	0.54	0.04
CFREQ (ML) (Hz)	0.64	0.10	0.58	0.11	0.51	0.03	0.64	0.09	0.64	0.09	0.52	0.05
CFREQ (TD) (Hz)	1.39	0.05	1.37	0.15	1.28	0.16	1.42	0.11	1.32	0.05	1.21	0.18
CFREQ (TM) (Hz)	0.74	0.11	0.70	0.12	0.65	0.05	0.69	0.23	0.74	0.05	0.70	0.11
FREQD (AP) (-)	0.58	0.04	0.59	0.04	0.63	0.03	0.59	0.03	0.53	0.03	0.53	0.06
FREQD (ML) (-)	0.53	0.04	0.55	0.04	0.59	0.02	0.60	0.04	0.57	0.04	0.64	0.02
FREQD (TD) (-)	0.68	0.03	0.70	0.04	0.71	0.04	0.68	0.02	0.72	0.03	0.76	0.03
FREQD (TM) (-)	0.57	0.02	0.62	0.04	0.61	0.02	0.66	0.03	0.59	0.06	0.60	0.02

Table 6. Analysis of the AP, ML, TM, and TD fluctuations. Posturographic measures were calculated for Base #1 and #2 under EC condition. Shown are the mean \pm SD for Participant #6.

Participant # 6	B #1, EC		B #2, EC		B #2, EO		B #3, EO		B #4, EO	
	mean	SD	mean	SD	mean	SD	mean	SD	mean	SD
MA (AP) (deg)	0.59	0.13	1.08	0.17	0.72	0.16	1.14	0.33	1.50	0.28
MA (ML) (deg)	0.32	0.06	0.74	0.13	0.32	0.11	0.66	0.21	1.21	0.36
MA (TD) (deg)	5.58	1.00	9.72	1.36	8.97	4.59	15.05	10.57	31.52	16.45
MA (TM) (deg)	0.56	0.13	1.05	0.16	0.66	0.12	1.16	0.40	1.41	0.19
RMSA (AP) (deg)	0.77	0.15	1.34	0.20	0.91	0.21	1.38	0.30	1.90	0.36
RMSA (ML) (deg)	0.41	0.06	0.94	0.17	0.43	0.13	0.86	0.25	1.68	0.50
RMSA (TD) (deg)	7.41	2.09	12.41	1.37	11.25	4.95	22.11	18.33	46.02	23.55
RMSA (TM) (deg)	0.72	0.14	1.32	0.18	0.83	0.16	1.40	0.39	1.81	0.26
MV (AP) (deg/s)	1.49	0.34	2.25	0.22	0.84	0.07	1.58	0.17	2.35	0.86
MV (ML) (deg/s)	0.95	0.26	1.97	0.46	0.59	0.02	1.32	0.29	2.60	0.85
MV (TD) (deg/s)	16.17	7.56	25.25	4.11	12.22	2.18	42.60	39.23	101.05	82.14
MV (TM) (deg/s)	1.43	0.34	2.30	0.24	0.85	0.08	1.58	0.25	2.43	0.78
RMSV (AP) (deg/s)	2.05	0.49	3.07	0.30	1.13	0.11	2.07	0.24	3.17	1.21
RMSV (ML) (deg/s)	1.33	0.29	2.68	0.75	0.89	0.12	1.84	0.36	3.72	1.46
RMSV (TD) (deg/s)	26.09	17.62	35.62	6.88	18.71	2.61	304.48	540.60	847.16	919.78
RMSV (TM) (deg/s)	1.97	0.47	3.11	0.39	1.17	0.13	2.11	0.34	3.35	1.27
RANGE (AP) (deg)	4.15	0.84	7.20	1.20	4.10	0.81	5.99	0.54	9.19	1.88
RANGE (ML) (deg)	2.45	0.24	5.14	1.14	2.35	0.60	4.77	1.26	10.26	3.26
RANGE (TD) (deg)	49.74	36.13	78.79	20.99	55.96	15.08	140.92	146.52	265.45	129.42
RANGE (TM) (deg)	3.78	0.74	7.30	0.74	3.77	0.72	6.19	0.99	8.35	1.32
CFREQ (AP) (Hz)	0.51	0.12	0.45	0.03	0.35	0.04	0.36	0.04	0.38	0.06
CFREQ (ML) (Hz)	0.59	0.03	0.54	0.11	0.52	0.11	0.42	0.05	0.45	0.07
CFREQ (TD) (Hz)	0.56	0.08	0.56	0.12	0.42	0.08	0.65	0.35	0.86	0.54
CFREQ (TM) (Hz)	0.52	0.12	0.46	0.04	0.39	0.06	0.36	0.04	0.39	0.08
FREQD (AP) (-)	0.56	0.08	0.59	0.03	0.58	0.05	0.60	0.03	0.56	0.02
FREQD (ML) (-)	0.58	0.02	0.56	0.04	0.62	0.03	0.57	0.04	0.60	0.03
FREQD (TD) (-)	0.62	0.03	0.56	0.05	0.62	0.07	0.63	0.08	0.65	0.05
FREQD (TM) (-)	0.55	0.07	0.59	0.03	0.60	0.05	0.60	0.02	0.63	0.05

Table 7. Analysis of the AP, ML, TM, and TD fluctuations. Posturographic measures were calculated for Base #1 and #2 under EC condition. Shown are the mean \pm SD for Participant #7.

Participant # 7	B #1, EC		B #2, EC		B #2, EO		B #3, EO		B #4, EO	
	mean	SD	mean	SD	mean	SD	mean	SD	mean	SD
MA (AP) (deg)	0.47	0.12	1.18	0.41	0.27	0.09	0.62	0.21	1.71	0.84
MA (ML) (deg)	0.42	0.04	0.71	0.23	0.23	0.06	0.71	0.42	1.09	0.13
MA (TD) (deg)	21.92	7.66	32.31	9.60	13.06	4.83	32.84	22.37	78.92	18.51
MA (TM) (deg)	0.41	0.04	0.91	0.26	0.25	0.04	0.83	0.50	1.56	0.78
RMSA (AP) (deg)	0.58	0.12	1.55	0.57	0.33	0.09	0.89	0.49	2.22	1.06
RMSA (ML) (deg)	0.54	0.05	0.94	0.32	0.27	0.06	0.89	0.54	1.61	0.22
RMSA (TD) (deg)	30.90	12.92	46.63	12.09	16.16	4.82	58.71	33.93	99.73	14.94
RMSA (TM) (deg)	0.51	0.03	1.12	0.27	0.29	0.04	1.07	0.67	2.01	0.94
MV (AP) (deg/s)	0.94	0.25	1.95	0.32	0.45	0.07	1.12	0.38	2.33	0.52
MV (ML) (deg/s)	1.31	0.30	1.66	0.55	0.35	0.03	1.21	0.67	2.65	0.71
MV (TD) (deg/s)	65.21	45.14	83.01	22.23	22.34	3.02	89.73	77.72	202.91	51.43
MV (TM) (deg/s)	1.24	0.33	1.85	0.44	0.39	0.05	1.35	0.66	2.56	0.35
RMSV (AP) (deg/s)	1.26	0.34	2.58	0.41	0.62	0.12	1.61	0.59	3.31	0.93
RMSV (ML) (deg/s)	1.85	0.36	2.28	0.74	0.51	0.07	1.65	0.95	3.88	1.56
RMSV (TD) (deg/s)	495.27	523.55	814.06	519.58	32.77	4.57	1164.75	962.42	2041.48	221.29
RMSV (TM) (deg/s)	1.71	0.38	2.46	0.57	0.56	0.11	1.89	0.97	3.65	0.75
RANGE (AP) (deg)	2.65	0.48	7.81	2.44	1.57	0.46	4.86	3.23	10.72	3.75
RANGE (ML) (deg)	3.21	0.64	5.14	1.99	1.19	0.10	4.41	3.16	10.95	1.26
RANGE (TD) (deg)	231.49	148.37	315.36	83.02	74.76	12.71	299.73	119.84	359.81	0.12
RANGE (TM) (deg)	2.93	0.37	5.39	0.82	1.34	0.26	4.94	3.23	9.47	1.98
CFREQ (AP) (Hz)	0.47	0.10	0.42	0.05	0.49	0.15	0.42	0.05	0.37	0.03
CFREQ (ML) (Hz)	0.62	0.06	0.46	0.03	0.47	0.04	0.48	0.08	0.45	0.06
CFREQ (TD) (Hz)	1.04	0.60	0.99	0.38	0.51	0.17	0.89	0.33	1.06	0.12
CFREQ (TM) (Hz)	0.60	0.09	0.46	0.03	0.47	0.05	0.45	0.08	0.44	0.05
FREQD (AP) (-)	0.59	0.03	0.60	0.04	0.58	0.03	0.64	0.03	0.57	0.01
FREQD (ML) (-)	0.45	0.07	0.58	0.02	0.62	0.01	0.60	0.02	0.52	0.06
FREQD (TD) (-)	0.62	0.03	0.72	0.05	0.56	0.04	0.74	0.03	0.74	0.03
FREQD (TM) (-)	0.50	0.10	0.60	0.03	0.63	0.02	0.62	0.02	0.60	0.03

Table 8. Analysis of the AP, ML, TM, and TD fluctuations. Posturographic measures were calculated for Base #1 and #2 under EC condition. Shown are the mean \pm SD for Participant #8.

Participant # 8	B #1, EC		B #2, EC		B #3, EC		B #3, EO		B #4, EO		B #5, EO	
	mean	SD	mean	SD	mean	SD	mean	SD	mean	SD	mean	SD
MA (AP) (deg)	0.69	0.14	0.99	0.16	1.38	0.17	0.54	0.06	0.83	0.26	1.13	0.30
MA (ML) (deg)	0.42	0.12	0.90	0.16	1.58	0.34	0.71	0.11	1.08	0.25	1.67	0.27
MA (TD) (deg)	5.19	0.68	21.47	7.23	55.97	29.53	9.99	1.88	22.88	4.01	34.13	18.23
MA (TM) (deg)	0.68	0.15	0.96	0.24	1.43	0.25	0.56	0.07	0.93	0.23	1.18	0.24
RMSA (AP) (deg)	0.88	0.21	1.23	0.19	1.80	0.18	0.69	0.10	1.06	0.31	1.46	0.32
RMSA (ML) (deg)	0.55	0.14	1.16	0.24	2.13	0.50	0.96	0.17	1.52	0.29	2.20	0.29
RMSA (TD) (deg)	6.69	0.54	29.50	10.47	68.38	33.30	12.99	2.57	30.61	4.81	43.39	20.53
RMSA (TM) (deg)	0.87	0.22	1.19	0.24	1.82	0.36	0.74	0.13	1.24	0.23	1.50	0.28
MV (AP) (deg/s)	1.37	0.18	2.43	0.51	4.55	0.77	1.30	0.21	1.77	0.30	3.18	0.68
MV (ML) (deg/s)	1.39	0.27	2.41	0.20	5.38	1.06	1.96	0.30	2.85	0.63	5.36	0.90
MV (TD) (deg/s)	16.51	1.54	71.18	35.97	250.31	161.28	27.17	4.69	63.44	15.81	117.82	78.77
MV (TM) (deg/s)	1.39	0.20	2.39	0.43	5.22	1.01	1.42	0.22	2.19	0.33	4.10	0.85
RMSV (AP) (deg/s)	1.77	0.26	3.29	0.83	6.25	1.39	1.74	0.36	2.31	0.40	4.13	0.82
RMSV (ML) (deg/s)	1.86	0.29	3.24	0.25	7.63	1.93	2.63	0.30	3.94	0.78	7.21	1.16
RMSV (TD) (deg/s)	22.47	1.11	423.41	391.03	1589.16	1212.72	36.76	5.65	228.52	274.86	660.18	757.70
RMSV (TM) (deg/s)	1.80	0.29	3.26	0.84	7.33	1.83	1.93	0.39	3.03	0.44	5.66	1.00
RANGE (AP) (deg)	4.41	1.14	6.71	1.64	10.09	1.58	3.88	1.03	6.13	1.70	8.50	0.79
RANGE (ML) (deg)	2.97	0.48	6.11	0.79	13.74	4.97	6.06	1.15	10.04	2.29	12.78	2.21
RANGE (TD) (deg)	36.00	4.57	242.38	97.05	320.00	78.45	72.52	12.66	220.82	84.75	261.64	109.20
RANGE (TM) (deg)	4.38	1.22	6.53	1.33	9.61	2.14	4.08	0.97	7.36	1.39	8.79	2.06
CFREQ (AP) (Hz)	0.47	0.02	0.52	0.06	0.62	0.10	0.49	0.07	0.48	0.08	0.56	0.07
CFREQ (ML) (Hz)	0.61	0.07	0.54	0.05	0.61	0.10	0.54	0.08	0.52	0.08	0.61	0.03
CFREQ (TD) (Hz)	0.61	0.05	0.95	0.22	1.01	0.28	0.55	0.09	0.58	0.07	0.89	0.27
CFREQ (TM) (Hz)	0.48	0.02	0.56	0.07	0.76	0.12	0.51	0.05	0.52	0.04	0.69	0.04
FREQD (AP) (-)	0.57	0.03	0.56	0.04	0.55	0.03	0.55	0.07	0.59	0.05	0.57	0.05
FREQD (ML) (-)	0.53	0.03	0.57	0.03	0.56	0.05	0.58	0.03	0.58	0.05	0.58	0.05
FREQD (TD) (-)	0.57	0.01	0.66	0.04	0.69	0.06	0.57	0.04	0.64	0.04	0.66	0.05
FREQD (TM) (-)	0.56	0.03	0.59	0.03	0.60	0.05	0.58	0.05	0.63	0.05	0.62	0.02

Table 9. Analysis of the AP, ML, TM, and TD fluctuations. Posturographic measures were calculated for Base #1 and #2 under EC condition. Shown are the mean \pm SD for Participant #9.

Participant # 9	B #1, EC		B #2, EC		B #2, EO		B #3, EO		B #4, EO	
	mean	SD								
MA (AP) (deg)	1.04	0.35	1.43	0.37	1.22	0.27	2.34	0.28	3.42	1.16
MA (ML) (deg)	0.72	0.16	1.28	0.21	0.64	0.11	1.92	0.65	3.51	1.64
MA (TD) (deg)	46.42	24.46	37.69	9.13	25.71	5.57	59.40	22.53	73.58	12.64
MA (TM) (deg)	0.70	0.07	1.27	0.25	1.06	0.43	1.94	0.37	2.46	1.07
RMSA (AP) (deg)	1.31	0.44	1.81	0.37	1.53	0.34	2.91	0.16	4.21	1.48
RMSA (ML) (deg)	0.90	0.20	1.71	0.28	0.84	0.15	2.50	0.79	4.40	1.77
RMSA (TD) (deg)	58.93	28.75	51.64	10.09	36.30	5.37	73.29	22.92	91.30	7.47
RMSA (TM) (deg)	0.88	0.09	1.63	0.33	1.33	0.52	2.35	0.45	3.05	1.22
MV (AP) (deg/s)	2.42	0.95	3.14	0.40	1.55	0.25	4.35	0.81	5.96	2.50
MV (ML) (deg/s)	2.28	0.83	3.34	0.33	1.58	0.12	3.92	1.02	6.18	2.26
MV (TD) (deg/s)	146.98	111.66	118.01	33.69	55.14	14.95	151.09	54.08	172.63	33.64
MV (TM) (deg/s)	2.38	0.89	3.37	0.27	1.57	0.15	4.24	0.97	6.06	1.94
RMSV (AP) (deg/s)	3.22	1.28	4.13	0.54	2.07	0.36	5.90	1.15	8.01	3.52
RMSV (ML) (deg/s)	2.93	1.15	4.50	0.36	2.29	0.34	5.37	1.44	8.43	2.85
RMSV (TD) (deg/s)	1056.80	903.61	1006.99	286.48	257.28	351.10	1219.22	778.26	1726.91	378.54
RMSV (TM) (deg/s)	3.07	1.16	4.45	0.32	2.11	0.21	5.80	1.41	8.19	2.47
RANGE (AP) (deg)	6.69	2.01	9.87	1.95	6.77	1.47	15.39	1.80	19.93	6.84
RANGE (ML) (deg)	4.88	1.66	10.22	1.57	5.21	1.02	12.66	3.86	20.45	5.33
RANGE (TD) (deg)	319.41	74.64	356.44	2.29	230.11	86.30	333.91	51.59	359.46	0.76
RANGE (TM) (deg)	4.48	0.78	8.60	2.20	6.03	2.06	10.59	2.32	12.91	2.64
CFREQ (AP) (Hz)	0.51	0.13	0.46	0.04	0.36	0.07	0.46	0.06	0.42	0.05
CFREQ (ML) (Hz)	0.56	0.10	0.48	0.07	0.57	0.11	0.50	0.06	0.43	0.09
CFREQ (TD) (Hz)	0.79	0.30	1.04	0.34	0.67	0.21	1.12	0.40	1.11	0.29
CFREQ (TM) (Hz)	0.64	0.21	0.48	0.08	0.40	0.11	0.49	0.05	0.60	0.09
FREQD (AP) (-)	0.50	0.05	0.55	0.05	0.59	0.03	0.52	0.06	0.52	0.04
FREQD (ML) (-)	0.51	0.06	0.52	0.03	0.58	0.03	0.58	0.02	0.55	0.05
FREQD (TD) (-)	0.67	0.04	0.70	0.04	0.65	0.08	0.69	0.04	0.74	0.06
FREQD (TM) (-)	0.56	0.02	0.56	0.01	0.59	0.03	0.57	0.03	0.56	0.04

Table 10. Analysis of the AP, ML, TM, and TD fluctuations. Posturographic measures were calculated for Base #1 and #2 under EC condition. Shown are the mean \pm SD for Participant #10.

Participant # 10	B #1, EC		B #2, EC		B #2, EO		B #3, EO		B #4, EO	
	mean	SD	mean	SD	mean	SD	mean	SD	mean	SD
MA (AP) (deg)	0.48	0.04	0.82	0.09	0.52	0.09	0.90	0.21	1.12	0.21
MA (ML) (deg)	0.34	0.04	0.67	0.09	0.45	0.15	0.75	0.06	0.98	0.18
MA (TD) (deg)	7.47	1.63	17.87	8.25	15.91	8.12	10.42	1.55	10.75	3.02
MA (TM) (deg)	0.46	0.04	0.78	0.08	0.51	0.10	0.89	0.21	1.05	0.23
RMSA (AP) (deg)	0.61	0.05	1.06	0.13	0.66	0.11	1.13	0.23	1.40	0.27
RMSA (ML) (deg)	0.45	0.07	0.84	0.13	0.58	0.21	0.95	0.05	1.24	0.23
RMSA (TD) (deg)	10.56	2.67	24.27	11.81	21.37	11.52	13.27	2.00	14.85	5.26
RMSA (TM) (deg)	0.58	0.05	1.00	0.11	0.65	0.14	1.10	0.22	1.33	0.29
MV (AP) (deg/s)	1.18	0.29	1.74	0.23	1.30	0.13	2.01	0.11	2.39	0.27
MV (ML) (deg/s)	0.82	0.15	1.58	0.13	1.10	0.26	2.29	0.19	2.59	0.29
MV (TD) (deg/s)	17.74	4.42	43.17	20.94	43.39	21.39	31.49	4.27	31.45	14.66
MV (TM) (deg/s)	1.18	0.28	1.74	0.15	1.31	0.16	2.04	0.19	2.38	0.21
RMSV (AP) (deg/s)	1.50	0.34	2.22	0.33	1.73	0.19	2.69	0.17	3.09	0.36
RMSV (ML) (deg/s)	1.10	0.17	2.10	0.16	1.49	0.35	3.07	0.15	3.38	0.39
RMSV (TD) (deg/s)	24.83	5.51	70.32	40.38	69.18	40.09	44.20	6.53	179.71	294.42
RMSV (TM) (deg/s)	1.51	0.34	2.24	0.22	1.75	0.22	2.71	0.27	3.14	0.32
RANGE (AP) (deg)	3.01	0.28	5.61	0.94	3.50	0.78	5.49	1.04	7.29	1.55
RANGE (ML) (deg)	2.89	0.59	4.29	1.05	2.94	1.04	5.52	0.08	6.49	1.82
RANGE (TD) (deg)	70.45	24.35	148.07	80.14	138.27	83.58	74.60	4.65	130.50	135.52
RANGE (TM) (deg)	2.93	0.31	5.28	0.68	3.40	0.85	5.22	0.95	7.13	1.47
CFREQ (AP) (Hz)	0.49	0.05	0.42	0.06	0.57	0.10	0.51	0.04	0.45	0.06
CFREQ (ML) (Hz)	0.46	0.04	0.45	0.03	0.53	0.09	0.58	0.05	0.54	0.06
CFREQ (TD) (Hz)	0.45	0.03	0.47	0.04	0.67	0.12	0.60	0.06	0.78	0.52
CFREQ (TM) (Hz)	0.52	0.07	0.44	0.05	0.57	0.12	0.53	0.05	0.48	0.05
FREQD (AP) (-)	0.59	0.04	0.56	0.03	0.62	0.02	0.56	0.05	0.57	0.03
FREQD (ML) (-)	0.61	0.01	0.60	0.03	0.62	0.01	0.56	0.04	0.60	0.03
FREQD (TD) (-)	0.61	0.01	0.62	0.03	0.62	0.03	0.56	0.05	0.59	0.02
FREQD (TM) (-)	0.59	0.04	0.57	0.03	0.64	0.02	0.57	0.04	0.57	0.04

Table 11. Analysis of the AP, ML, TM, and TD fluctuations. Posturographic measures were calculated for Base #1 and #2 under EC condition. Shown are the mean \pm SD for Participant #11.

Participant # 11	B #1, EC		B #2, EC		B #2, EO		B #3, EO		B #4, EO	
	mean	SD	mean	SD	mean	SD	mean	SD	mean	SD
MA (AP) (deg)	0.69	0.15	0.84	0.14	0.44	0.17	0.66	0.21	1.02	0.23
MA (ML) (deg)	0.57	0.07	0.94	0.21	0.66	0.16	0.86	0.21	2.04	0.46
MA (TD) (deg)	20.82	7.17	28.91	21.88	21.93	13.44	98.78	25.54	114.94	26.67
MA (TM) (deg)	0.60	0.15	0.83	0.09	0.58	0.28	0.65	0.18	1.30	0.28
RMSA (AP) (deg)	0.84	0.19	1.02	0.17	0.55	0.21	0.81	0.24	1.30	0.29
RMSA (ML) (deg)	0.77	0.08	1.25	0.30	0.78	0.17	1.23	0.31	2.67	0.49
RMSA (TD) (deg)	27.56	11.91	39.67	33.60	29.26	16.66	109.64	21.91	124.96	19.78
RMSA (TM) (deg)	0.77	0.17	1.04	0.12	0.69	0.29	0.92	0.28	1.69	0.28
MV (AP) (deg/s)	1.20	0.11	1.58	0.34	0.71	0.06	1.02	0.18	2.12	0.44
MV (ML) (deg/s)	1.47	0.39	2.09	0.75	0.98	0.15	1.77	0.32	4.41	0.52
MV (TD) (deg/s)	42.41	19.01	82.70	92.24	54.37	38.32	259.67	69.69	276.48	84.19
MV (TM) (deg/s)	1.46	0.29	1.98	0.69	0.89	0.12	1.46	0.24	3.30	0.37
RMSV (AP) (deg/s)	1.54	0.19	2.08	0.48	0.95	0.10	1.36	0.28	2.87	0.43
RMSV (ML) (deg/s)	1.98	0.48	2.75	0.95	1.28	0.23	2.44	0.58	5.90	0.64
RMSV (TD) (deg/s)	197.99	304.25	608.39	1105.97	484.05	570.86	2335.95	489.49	2561.90	562.73
RMSV (TM) (deg/s)	1.92	0.36	2.61	0.97	1.15	0.15	2.07	0.38	4.66	0.55
RANGE (AP) (deg)	4.02	1.22	4.87	0.64	2.78	0.97	4.00	1.03	6.36	1.45
RANGE (ML) (deg)	4.25	0.40	6.47	2.29	3.33	0.55	7.40	1.77	15.15	1.52
RANGE (TD) (deg)	174.23	123.75	194.23	121.95	212.26	163.57	359.65	0.21	359.70	0.50
RANGE (TM) (deg)	3.91	0.95	5.19	0.95	3.09	0.78	5.21	1.79	9.13	0.91
CFREQ (AP) (Hz)	0.40	0.05	0.42	0.04	0.39	0.07	0.38	0.03	0.45	0.01
CFREQ (ML) (Hz)	0.53	0.11	0.42	0.06	0.41	0.10	0.45	0.10	0.44	0.06
CFREQ (TD) (Hz)	0.57	0.27	0.60	0.31	0.74	0.52	1.14	0.12	1.17	0.17
CFREQ (TM) (Hz)	0.54	0.16	0.47	0.07	0.39	0.08	0.53	0.11	0.53	0.09
FREQD (AP) (-)	0.54	0.03	0.55	0.03	0.57	0.02	0.57	0.05	0.50	0.02
FREQD (ML) (-)	0.52	0.04	0.53	0.02	0.60	0.03	0.59	0.04	0.56	0.03
FREQD (TD) (-)	0.59	0.11	0.62	0.10	0.65	0.06	0.75	0.04	0.73	0.03
FREQD (TM) (-)	0.55	0.05	0.55	0.02	0.58	0.04	0.63	0.02	0.60	0.05

Table 12. Analysis of the AP, ML, TM, and TD fluctuations. Posturographic measures were calculated for Base #1 and #2 under EC condition. Shown are the mean \pm SD for Participant #12.

Participant # 12	B #1, EC		B #2, EC		B #2, EO		B #3, EO		B #4, EO	
	mean	SD	mean	SD	mean	SD	mean	SD	mean	SD
MA (AP) (deg)	0.52	0.04	1.08	0.22	0.60	0.35	1.10	0.56	1.82	0.98
MA (ML) (deg)	0.44	0.11	1.37	0.30	0.36	0.19	0.81	0.28	2.63	1.41
MA (TD) (deg)	53.80	38.26	128.33	22.58	37.13	42.68	108.77	38.48	122.23	11.64
MA (TM) (deg)	0.45	0.11	1.04	0.16	0.59	0.41	1.01	0.49	1.96	1.05
RMSA (AP) (deg)	0.65	0.05	1.38	0.26	0.77	0.48	1.44	0.73	2.34	1.27
RMSA (ML) (deg)	0.56	0.12	1.73	0.40	0.48	0.28	1.18	0.44	3.42	1.77
RMSA (TD) (deg)	70.39	45.85	135.82	17.24	48.91	54.32	117.35	35.21	130.58	7.85
RMSA (TM) (deg)	0.56	0.13	1.29	0.17	0.78	0.58	1.33	0.63	2.43	1.23
MV (AP) (deg/s)	1.27	0.28	2.45	0.36	0.85	0.18	1.29	0.36	4.49	2.16
MV (ML) (deg/s)	1.13	0.33	3.07	0.78	0.70	0.28	1.60	0.78	5.55	1.47
MV (TD) (deg/s)	150.80	98.18	278.77	17.38	88.29	89.10	236.31	138.30	372.07	82.59
MV (TM) (deg/s)	1.24	0.28	2.86	0.37	0.79	0.25	1.49	0.52	5.12	1.58
RMSV (AP) (deg/s)	1.65	0.36	3.27	0.60	1.12	0.29	1.80	0.49	6.11	3.06
RMSV (ML) (deg/s)	1.52	0.43	4.11	1.00	0.98	0.43	2.40	1.07	7.32	1.64
RMSV (TD) (deg/s)	1426.31	1144.88	2643.57	248.96	912.89	1212.34	2208.45	1149.38	3045.62	426.58
RMSV (TM) (deg/s)	1.66	0.33	3.87	0.63	1.06	0.38	2.17	0.71	6.96	2.05
RANGE (AP) (deg)	3.39	0.91	7.83	2.23	3.44	1.98	6.66	2.93	12.64	6.91
RANGE (ML) (deg)	3.23	0.62	9.05	2.46	2.49	1.49	6.73	2.56	17.44	7.59
RANGE (TD) (deg)	302.03	115.63	359.87	0.07	229.54	152.19	359.79	0.22	359.95	0.06
RANGE (TM) (deg)	3.07	0.93	6.49	0.70	3.59	2.62	6.12	2.92	10.95	3.25
CFREQ (AP) (Hz)	0.45	0.05	0.45	0.05	0.45	0.05	0.38	0.11	0.51	0.06
CFREQ (ML) (Hz)	0.46	0.06	0.43	0.02	0.53	0.04	0.48	0.09	0.48	0.06
CFREQ (TD) (Hz)	1.03	0.39	1.03	0.09	0.77	0.25	0.97	0.33	1.13	0.15
CFREQ (TM) (Hz)	0.52	0.08	0.55	0.05	0.44	0.06	0.43	0.12	0.57	0.08
FREQD (AP) (-)	0.54	0.04	0.55	0.02	0.62	0.03	0.56	0.02	0.54	0.04
FREQD (ML) (-)	0.52	0.04	0.56	0.02	0.62	0.05	0.57	0.02	0.61	0.02
FREQD (TD) (-)	0.70	0.09	0.77	0.03	0.69	0.07	0.73	0.04	0.76	0.02
FREQD (TM) (-)	0.54	0.02	0.55	0.03	0.63	0.02	0.61	0.02	0.63	0.04

Table 13. Analysis of the AP, ML, TM, and TD fluctuations. Posturographic measures were calculated for Base #1 and #2 under EC condition. Shown are the mean \pm SD for Participant #13.

Participant # 13	B #1, EC		B #2, EC		B #2, EO		B #3, EO		B #4, EO	
	mean	SD	mean	SD	mean	SD	mean	SD	mean	SD
MA (AP) (deg)	0.53	0.08	1.24	0.07	0.65	0.14	1.23	0.16	2.33	0.26
MA (ML) (deg)	0.60	0.04	1.02	0.15	0.67	0.19	1.37	0.21	2.17	0.24
MA (TD) (deg)	10.61	2.89	37.80	24.42	19.99	5.31	83.81	22.91	71.27	15.17
MA (TM) (deg)	0.59	0.10	1.08	0.16	0.67	0.19	1.34	0.15	1.76	0.25
RMSA (AP) (deg)	0.69	0.10	1.50	0.08	0.85	0.25	1.54	0.20	2.95	0.30
RMSA (ML) (deg)	0.76	0.08	1.25	0.18	0.90	0.23	1.92	0.29	2.84	0.35
RMSA (TD) (deg)	13.48	3.49	50.44	29.81	39.73	19.65	102.81	27.96	89.65	14.84
RMSA (TM) (deg)	0.75	0.12	1.31	0.19	0.87	0.22	1.68	0.15	2.25	0.27
MV (AP) (deg/s)	0.98	0.14	1.67	0.02	1.24	0.29	2.28	0.62	3.84	0.30
MV (ML) (deg/s)	1.14	0.27	1.75	0.30	1.60	0.37	2.59	0.39	4.99	0.73
MV (TD) (deg/s)	20.48	3.00	78.43	48.18	65.90	30.78	192.69	69.51	193.98	41.40
MV (TM) (deg/s)	1.06	0.19	1.86	0.20	1.43	0.26	2.83	0.52	4.47	0.39
RMSV (AP) (deg/s)	1.28	0.18	2.18	0.06	1.73	0.35	2.94	0.76	4.95	0.54
RMSV (ML) (deg/s)	1.54	0.39	2.37	0.42	2.28	0.44	3.65	0.53	6.83	0.88
RMSV (TD) (deg/s)	28.60	4.00	862.91	655.37	902.61	697.83	1957.40	773.91	1883.37	280.08
RMSV (TM) (deg/s)	1.40	0.28	2.44	0.28	1.94	0.29	3.78	0.70	5.95	0.49
RANGE (AP) (deg)	3.78	0.47	6.63	0.51	4.52	1.75	7.24	0.88	13.92	2.07
RANGE (ML) (deg)	4.09	0.73	5.62	0.23	5.77	1.56	10.49	1.55	16.25	1.75
RANGE (TD) (deg)	76.15	14.63	298.06	107.88	291.08	131.43	359.65	0.34	359.80	0.11
RANGE (TM) (deg)	3.84	0.72	6.07	1.25	4.67	0.96	7.63	0.40	11.59	0.77
CFREQ (AP) (Hz)	0.37	0.04	0.34	0.02	0.43	0.05	0.39	0.03	0.38	0.04
CFREQ (ML) (Hz)	0.39	0.06	0.40	0.06	0.54	0.08	0.42	0.04	0.48	0.05
CFREQ (TD) (Hz)	0.40	0.04	0.90	0.31	0.89	0.49	1.15	0.22	1.30	0.10
CFREQ (TM) (Hz)	0.38	0.07	0.41	0.06	0.51	0.06	0.46	0.05	0.53	0.06
FREQD (AP) (-)	0.58	0.06	0.55	0.03	0.60	0.05	0.55	0.04	0.54	0.02
FREQD (ML) (-)	0.57	0.02	0.58	0.02	0.53	0.04	0.58	0.04	0.58	0.05
FREQD (TD) (-)	0.59	0.04	0.76	0.04	0.69	0.07	0.76	0.01	0.71	0.01
FREQD (TM) (-)	0.58	0.04	0.59	0.03	0.57	0.04	0.59	0.05	0.61	0.04

Table 14. Analysis of the AP, ML, TM, and TD fluctuations. Posturographic measures were calculated for Base #1 and #2 under EC condition. Shown are the mean \pm SD for Participant #14.

Participant # 14	B #1, EC		B #2, EC		B #2, EO		B #3, EO		B #4, EO	
	mean	SD	mean	SD	mean	SD	mean	SD	mean	SD
MA (AP) (deg)	0.88	0.28	1.94	0.16	0.92	0.19	1.73	1.11	2.29	0.52
MA (ML) (deg)	0.73	0.11	2.17	0.46	0.58	0.11	1.83	0.81	1.79	0.30
MA (TD) (deg)	7.29	3.73	24.50	7.04	7.47	2.26	18.26	16.58	30.34	11.59
MA (TM) (deg)	0.91	0.27	2.10	0.11	0.85	0.17	1.58	0.84	1.85	0.26
RMSA (AP) (deg)	1.10	0.35	2.35	0.16	1.11	0.19	2.09	1.26	2.82	0.54
RMSA (ML) (deg)	0.91	0.15	2.84	0.64	0.73	0.16	2.45	1.07	2.32	0.37
RMSA (TD) (deg)	9.31	5.13	29.09	7.68	9.22	2.41	26.93	27.10	41.52	16.33
RMSA (TM) (deg)	1.14	0.34	2.56	0.21	1.04	0.17	1.93	1.00	2.27	0.28
MV (AP) (deg/s)	1.39	0.19	3.05	0.47	0.79	0.02	2.54	1.18	3.57	0.51
MV (ML) (deg/s)	1.36	0.14	3.41	0.73	0.80	0.08	2.93	0.97	3.95	0.82
MV (TD) (deg/s)	13.85	7.25	35.97	4.07	8.56	2.56	39.65	43.81	69.75	42.82
MV (TM) (deg/s)	1.44	0.23	3.46	0.70	0.81	0.06	2.67	1.21	3.78	0.55
RMSV (AP) (deg/s)	1.83	0.19	4.19	0.81	1.04	0.05	3.42	1.75	4.63	0.67
RMSV (ML) (deg/s)	1.80	0.18	4.68	0.98	1.05	0.07	4.04	1.58	5.38	1.15
RMSV (TD) (deg/s)	18.66	10.22	54.47	9.56	11.37	2.99	326.12	532.37	450.24	680.85
RMSV (TM) (deg/s)	1.90	0.24	4.64	0.88	1.06	0.09	3.57	1.73	4.95	0.67
RANGE (AP) (deg)	5.35	1.51	10.78	2.41	4.80	0.44	10.84	6.74	13.64	0.81
RANGE (ML) (deg)	4.57	0.87	15.04	3.93	3.67	0.81	12.83	5.17	12.73	2.14
RANGE (TD) (deg)	47.66	28.41	133.62	33.31	39.35	7.14	160.55	171.81	246.28	78.08
RANGE (TM) (deg)	5.52	1.47	11.51	2.78	4.37	0.57	8.92	4.51	11.10	1.27
CFREQ (AP) (Hz)	0.38	0.07	0.39	0.08	0.28	0.03	0.43	0.05	0.39	0.08
CFREQ (ML) (Hz)	0.41	0.02	0.36	0.04	0.36	0.04	0.35	0.03	0.43	0.05
CFREQ (TD) (Hz)	0.44	0.02	0.42	0.02	0.33	0.04	0.54	0.30	0.73	0.29
CFREQ (TM) (Hz)	0.36	0.05	0.37	0.03	0.29	0.03	0.43	0.05	0.44	0.05
FREQD (AP) (-)	0.55	0.03	0.57	0.03	0.51	0.03	0.57	0.02	0.56	0.05
FREQD (ML) (-)	0.54	0.04	0.56	0.02	0.56	0.05	0.53	0.02	0.55	0.02
FREQD (TD) (-)	0.55	0.03	0.60	0.04	0.55	0.03	0.60	0.09	0.68	0.06
FREQD (TM) (-)	0.55	0.04	0.57	0.01	0.52	0.04	0.57	0.04	0.57	0.02

Table 15. Analysis of the AP, ML, TM, and TD fluctuations. Posturographic measures were calculated for Base #1 and #2 under EC condition. Shown are the mean \pm SD for Participant #15.

Participant # 15	B #1, EC		B #2, EC		B #2, EO		B #3, EO		B #4, EO	
	mean	SD	mean	SD	mean	SD	mean	SD	mean	SD
MA (AP) (deg)	0.84	0.13	2.40	0.21	0.87	0.12	1.94	0.99	3.53	1.31
MA (ML) (deg)	0.67	0.07	2.54	0.39	0.80	0.03	2.16	1.03	4.19	1.53
MA (TD) (deg)	8.94	1.80	30.09	19.12	7.96	0.41	30.73	14.08	39.58	17.11
MA (TM) (deg)	0.82	0.13	2.51	0.33	0.87	0.13	1.71	0.46	2.76	0.60
RMSA (AP) (deg)	1.06	0.20	2.97	0.24	1.17	0.20	2.46	1.23	4.65	1.74
RMSA (ML) (deg)	0.85	0.10	3.36	0.57	1.02	0.08	3.12	1.58	5.61	1.63
RMSA (TD) (deg)	11.33	2.57	39.02	22.35	10.12	0.72	42.28	20.55	54.01	22.55
RMSA (TM) (deg)	1.04	0.21	3.12	0.50	1.17	0.20	2.29	0.69	3.46	0.65
MV (AP) (deg/s)	2.11	0.55	4.32	0.50	1.85	0.12	3.28	0.77	6.53	2.10
MV (ML) (deg/s)	2.06	0.59	4.23	0.40	1.58	0.18	3.96	1.58	6.49	1.57
MV (TD) (deg/s)	26.17	5.96	73.24	55.14	16.05	2.27	66.79	31.11	79.03	35.68
MV (TM) (deg/s)	2.10	0.53	4.27	0.71	1.89	0.13	3.77	0.88	5.72	1.57
RMSV (AP) (deg/s)	2.70	0.77	5.54	0.69	2.46	0.24	4.15	0.89	8.85	2.70
RMSV (ML) (deg/s)	2.62	0.85	5.49	0.47	2.18	0.23	5.15	1.98	8.51	1.84
RMSV (TD) (deg/s)	33.18	8.63	563.37	655.04	23.28	2.59	650.05	516.91	692.73	476.02
RMSV (TM) (deg/s)	2.71	0.76	5.58	0.90	2.53	0.26	4.98	1.18	7.58	1.88
RANGE (AP) (deg)	5.71	1.89	14.63	1.63	6.77	1.32	12.11	4.80	23.22	7.62
RANGE (ML) (deg)	4.48	1.06	17.59	3.67	5.21	0.98	16.64	9.06	25.41	2.89
RANGE (TD) (deg)	60.62	16.08	264.40	109.43	52.43	8.50	288.19	110.19	297.19	121.69
RANGE (TM) (deg)	5.69	2.05	14.89	2.67	6.79	1.32	11.68	3.43	14.74	1.56
CFREQ (AP) (Hz)	0.51	0.06	0.38	0.04	0.48	0.04	0.40	0.05	0.37	0.02
CFREQ (ML) (Hz)	0.58	0.11	0.36	0.06	0.44	0.04	0.45	0.14	0.32	0.02
CFREQ (TD) (Hz)	0.57	0.15	0.80	0.39	0.47	0.07	0.86	0.28	0.65	0.37
CFREQ (TM) (Hz)	0.52	0.06	0.38	0.07	0.48	0.04	0.45	0.09	0.40	0.05
FREQD (AP) (-)	0.54	0.06	0.56	0.01	0.58	0.04	0.54	0.04	0.54	0.04
FREQD (ML) (-)	0.56	0.04	0.54	0.03	0.54	0.08	0.52	0.04	0.55	0.04
FREQD (TD) (-)	0.57	0.02	0.66	0.11	0.56	0.08	0.70	0.11	0.69	0.11
FREQD (TM) (-)	0.54	0.06	0.55	0.02	0.57	0.03	0.58	0.06	0.59	0.04

9.8 Appendix H – Number of Participants for Calculating the Group-Ensemble CC Functions

The number of participants that were used to calculate the group-ensemble CC functions (across participants) is shown in Tables 1 to 8.

Table 1. The number of participants that were used to calculate the group-ensemble CC functions (across participants) for AP direction. The results are shown for: RA, BF, RF, ES with B #2, EC and B #4, EO.

Muscle	Anterior		Posterior	
	B #2, EC	B #4, EO	B #2, EC	B #4, EO
RRA	6 out of 15	12 out of 15	4 out of 15	7 out of 15
LRA	5 out of 15	11 out of 15	3 out of 15	8 out of 15
RBF	13 out of 15	13 out of 15	14 out of 15	12 out of 15
LBF	15 out of 15			
RRF	11 out of 15	11 out of 15	13 out of 15	13 out of 15
LRF	10 out of 15	12 out of 15	10 out of 15	11 out of 15
RTES	6 out of 15	5 out of 15	8 out of 15	9 out of 15
LTES	8 out of 15	4 out of 15	5 out of 15	8 out of 15
RLES	8 out of 15	7 out of 15	10 out of 15	10 out of 15
LLES	8 out of 15	9 out of 15	8 out of 15	9 out of 15

Table 2. The number of participants that were used to calculate the group-ensemble CC functions (across participants) for RA and AP direction. The results are shown for: B #1, EC; B #3, EC; B #2, EO; B #3, EO; and B #5, EO.

Condition	Anterior		Posterior	
	RRA	LRA	RRA	LRA
B #1, EC	3 out of 15	no correlation	no correlation	no correlation
B #3, EC	3 out of 3	2 out of 3	3 out of 3	2 out of 3
B #2, EO	no correlation	no correlation	no correlation	no correlation
B #3, EO	6 out of 15	4 out of 15	5 out of 15	3 out of 15
B #5, EO	3 out of 4	3 out of 4	2 out of 4	3 out of 4

Table 3. The number of participants that were used to calculate the group-ensemble CC functions (across participants) for BF and AP direction. The results are shown for: B #1, EC; B #3, EC; B #2, EO; B #3, EO; and B #5, EO.

Condition	Anterior		Posterior	
	RBF	LBF	RBF	LBF
B #1, EC	11 out 15	13 out of 15	10 out of 15	12 out of 15
B #3, EC	3 out of 3	3 out of 3	3 out of 3	3 out of 3
B #2, EO	9 out of 13	10 out of 13	8 out of 13	4 out of 13
B #3, EO	9 out of 15	13 out of 15	10 out of 15	9 out of 15
B #5, EO	3 out of 4	4 out of 4	3 out of 4	4 out of 4

Table 4. The number of participants that were used to calculate the group-ensemble CC functions (across participants) for RF and AP direction. The results are shown for: B #1, EC; B #3, EC; B #2, EO; B #3, EO; and B #5, EO.

Condition	Anterior		Posterior	
	RRF	LRF	RRF	LRF
B #1, EC	6 out of 15	7 out of 15	12 out of 15	9 out of 15
B #3, EC	3 out of 3	2 out of 3	3 out of 3	2 out of 3
B #2, EO	3 out of 13	4 out of 13	7 out of 13	5 out of 13
B #3, EO	6 out of 15	9 out of 15	12 out of 15	9 out of 15
B #5, EO	3 out of 4	2 out of 4	4 out of 4	2 out of 4

Table 5. The number of participants that were used to calculate the group-ensemble CC functions (across participants) for ES and anterior direction. The results are shown for: B #1, EC; B #3, EC; B #2, EO; B #3, EO; and B #5, EO.

Condition	Anterior			
	RTES	LTES	RLES	LLES
B #1, EC	5 out of 15	4 out of 15	4 out of 15	9 out of 15
B #3, EC	no correlation	no correlation	no correlation	2 out of 3
B #2, EO	4 out of 13	3 out of 13	4 out of 13	5 out of 13
B #3, EO	9 out of 15	5 out of 15	5 out of 15	5 out of 15
B #5, EO	3 out of 4	2 out of 4	3 out of 4	2 out of 4

Table 6. The number of participants that were used to calculate the group-ensemble CC functions (across participants) for ES and posterior direction. The results are shown for: B #1, EC; B #3, EC; B #2, EO; B #3, EO; and B #5, EO.

Condition	Posterior			
	RTES	LTES	RLES	LLES
B #1, EC	2 out of 15	4 out of 15	3 out of 15	2 out of 15
B #3, EC	no correlation	no correlation	no correlation	2 out of 3
B #2, EO	2 out of 15	2 out of 15	2 out of 15	no correlation
B #3, EO	3 out of 15	3 out of 15	3 out of 15	2 out of 15
B #5, EO	2 out of 4	1 out of 4	3 out of 4	3 out of 4

Table 7. The number of participants that were used to calculate the group-ensemble CC functions (across participants) for ML direction. The results are shown for: ExO with B #2, EC and B #4, EO.

Muscle	Left		Right	
	B #2, EC	B #4, EO	B #2, EC	B #4, EO
RExO	13 out of 15	14 out of 15	13 out of 15	14 out of 15
LExO	13 out of 15	13 out of 15	12 out of 15	14 out of 15

Table 8. The number of participants that were used to calculate the group-ensemble CC functions (across participants) for ExO and ML direction. The results are shown for: B #1, EC; B #3, EC; B #2, EO; B #3, EO; and B #5, EO.

Condition	Left		Right	
	RExO	LExO	RExO	LExO
B #1, EC	11 out of 15	8 out of 15	11 out of 15	10 out of 15
B #3, EC	3 out of 3			
B #2, EO	9 out of 13	7 out of 13	8 out of 13	6 out of 13
B #3, EO	12 out of 15	13 out of 15	14 out of 15	11 out of 15
B #5, EO	4 out of 4			